Improved Modelling of Piezoelectric Composites



Cameron Alexander Spalding
St. Anne's College
University of Oxford

Supervisors: Chris Breward and Jon Chapman

Thesis submitted for the degree of
Doctor of Philosophy of Mathematics

Hilary Term 2026

Acknowledgements

I am deeply grateful to my supervisors, Chris Breward and Jon Chapman, for the engaging way they brought mathematical modelling to life. Their expertise, clarity of thought, insistence on precision, challenge of assumptions, and patience were essential in keeping my work focused and on track.

I am also very grateful to Thales Group, the industrial sponsors of this thesis, for their support. I would like to thank David Hardie and Hannah Rose in the R&D department in particular, for their technical input, insights, feedback, and continued interest in this study. Time spent with them and other members of the R&D department in Somerset gave me exposure to real-world sonar applications and fabrication processes. These experiences motivated my work and provided essential background and practical context for the modelling developed in this thesis.

Additional thanks go to Luc Nguyen, whose teaching sparked my interest in functional analysis, Ben Fehrman who first introduced me to asymptotic homogenisation and my other supervisors in the Mathematics Faculty at Oxford for their inspiring teaching while I was an undergraduate. Finally, I thank my family and friends for showing interest when things were going well, and support when things were not going so well.

Abstract

Piezoelectric composites are widely preferred to monolithic piezoelectric ceramics or polymers because they offer a wider, readily tailorable range of effective electromechanical properties. However, accurate modelling of such composites remains challenging due to strong material contrasts between constituent phases, electromechanical coupling, and microscale interactions at phase interfaces. These features give rise to non-uniform local strain and electric fields that cannot be captured reliably by simplified analytical models. Consequently, the effective behaviour of piezoelectric composites is often studied using finite element methods (FEM), in which the full microstructure is explicitly resolved. While full-field FEM can compute behaviour accurately, it is computationally expensive, particularly in the context of iterative design and optimisation of composite materials.

In this thesis, we develop a two-scale asymptotic homogenisation framework for linear piezoelectric composites with periodic microstructures. The method separates the analysis into a microscale problem defined on a representative unit cell and a macroscale problem governing the effective response of the composite. Two asymptotic expansions are introduced, one for the mechanical displacement and one for the electric potential, and the coupled governing equations are solved systematically at successive orders. This procedure yields the leading-order macroscopic fields and, at the next stage, a set of coupled cell problems posed on the unit cell. These cell problems describe how the microscale arrangement of piezoelectric and passive phases distorts local strain and electric fields, including interactions at phase boundaries. The cell problems are solved numerically using FEM on the unit cell only, and the resulting solutions are averaged to obtain effective stiffness, piezoelectric coupling, and dielectric tensors, which define homogenised equations governing the macroscopic behaviour.

Having established the homogenisation framework, for selected material parameters we calculate effective coefficients using established methods, namely the Method of Mixtures, the Representative Volume Element, and the Differential Effective Medium approaches, and compare these results with those derived using our framework. We extend the model for bulk sensors and thin-layer bending actuators

through the incorporation of wave and beam theory, respectively. Our models predict quantities including voltage output, mechanical impedance, wave speed, and bending response. We show that, in contrast to leading methods, our framework can be applied irrespective of geometry or lattice structure and that, unlike full FEM simulations, it provides physical insight into microscale behaviour, which is particularly useful for design and optimisation.

Contents

1 Introduction **1**

1.1 Background 1

1.2 Benefits of piezoelectric composites over piezo-ceramics and piezo-polymers 3

1.3 Connectivity of common composites 4

1.4 Literature review 5

1.5 Objectives of thesis 9

1.6 Overview of thesis 9

1.7 Statement of Originality 10

2 Establishing the Homogenisation problem **11**

2.1 Introduction 11

2.2 Linear elasticity 11

2.3 Quasi-electrostatics 12

2.4 Coupling linear elasticity with quasi-electrostatics 13

2.5 Formulae for isotropic materials 16

2.6 Non-dimensionalisation 17

2.7 Homogenisation 20

2.7.1 Asymptotic expansions to find the cell problems 21

2.7.2 Macroscale equations and effective coefficients 30

3 Comparison of effective coefficients derived using other approaches to our results **35**

3.1 Introduction 35

3.2 Coefficients derived using the Asymptotic Homogenisation Model . . 36

3.3 Coefficients derived using the Differential Effective Medium approach 36

3.4 Coefficients derived using the Method of Mixtures approach 37

3.5 Coefficients derived using the Representative Volume Element approach 38

3.6 Comparison of the four approaches 40

4 The Limit of Small Volume Fraction of Inclusions 48
4.1 Introduction . . . 48
4.2 Mechanical cell problems . . . 50
4.2.1 Simplifying the equations . . . 50
4.2.2 Rescaling the PDEs to the inner region . . . 51
4.2.3 Solutions to cell problems . . . 53
4.2.3.1 The 11-problem . . . 53
4.2.3.1.1 The leading-order inner problem . . . 54
4.2.3.1.2 Outer limit of the leading-order inner solution . . . 56
4.2.3.1.3 First order outer solution . . . 57
4.2.3.1.4 Inner limit of the first order outer solution . . . 59
4.2.3.1.5 Second order inner solution . . . 59
4.2.3.2 The 22-problem . . . 61
4.2.3.3 The 33-problem . . . 63
4.2.3.3.1 The leading-order inner problem . . . 63
4.2.3.3.2 Outer limit of leading-order inner solution . . . 63
4.2.3.3.3 Leading-order outer solution . . . 64
4.2.3.3.4 Inner limit of first order outer solution . . . 64
4.2.3.3.5 Second order inner solution . . . 64
4.2.3.4 The 23-problem . . . 66
4.2.3.4.1 The leading-order inner problem . . . 66
4.2.3.4.2 Outer limit of the leading-order inner solution . . . 67
4.2.3.4.3 First leading-order outer solution . . . 67
4.2.3.4.4 Inner limit of first leading-order outer solution . . . 68
4.2.3.4.5 Second order inner solution . . . 68
4.2.3.5 The 13-problem . . . 70
4.2.3.6 The 12-problem . . . 71
4.2.3.6.1 The leading-order inner problem . . . 71
4.2.3.6.2 Outer limit of the leading-order inner solution . . . 72
4.2.3.6.3 First-leading-order outer solution . . . 72
4.2.3.6.4 Inner limit of the two-term outer expansion . . . 73
4.2.3.6.5 Second order inner solution . . . 74
4.3 Electrical cell problems . . . 76
4.3.1 Simplifying the equations . . . 76
4.3.2 Rescaling the PDEs in the inner region . . . 77
4.3.3 Solutions to cell problems . . . 78
4.3.3.1 The **1**-problem . . . 78

4.3.3.1.1 The leading-order inner problem 78
4.3.3.1.2 Outer limit of the leading-order inner solution 79
4.3.3.1.3 First leading-order outer solution 79
4.3.3.1.4 Inner limit of the first leading-order outer solution . . 80
4.3.3.1.5 Second order inner solution 80
4.3.3.2 The **2**-problem 81
4.3.3.3 The **3**-problem 82
4.4 Formulae for effective coefficients 83
4.4.1 Establishing the integral formulae 83
4.4.2 Low volume fraction formulae 84
4.4.2.1 Effective stiffness tensor coefficients 84
4.4.2.2 Effective electromechanical tensor coefficients 86
4.4.2.3 Effective dielectric tensor coefficients 87
4.5 Comparison of the AHM low volume fraction polynomials and the full numerical solution 87
4.6 Low Volume fraction approximations for Differential Effective Medium method 91
4.7 Low Volume fraction approximations for Method of Mixtures approach 94
4.8 Comparison between approaches 94
4.9 Conclusions 98

5 Modelling of Bulk Piezoelectric Sensors 99
5.1 Introduction 99
5.1.1 Methods for modelling Bulk Sensors 100
5.2 Modelling of Piezoelectric Sensors 101
5.2.1 Derivation of Linearised Equations of Acoustics 102
5.2.2 Equations of motion in the solid 103
5.3 Continuity and jump conditions 103
5.4 Solving physical problems 104
5.4.1 Half-space transducer 106
5.4.1.1 Wave-like solutions 106
5.4.2 Finite-thickness transducer 108
5.4.2.1 Solutions 109
5.5 Results 111
5.6 Conclusions 115

6 Modelling of Piezoelectric Beam Actuators 117
6.1 Introduction . . . 117
6.1.1 Challenges to the modelling of Beam Actuators . . . 118
6.1.2 Gap in literature . . . 118
6.2 Framework for Modelling Actuators . . . 119
6.2.1 Introduction . . . 119
6.2.1.1 Derivation of Classical Beam Theory for a homogeneous material . . . 120
6.2.2 Equations of Motion . . . 123
6.2.3 Non-Dimensionalisation . . . 126
6.2.4 Establishing the Equations of Motion using asymptotic expansions . . . 128
6.2.4.1 The $\mathcal{O}(1)$ problem . . . 130
6.2.4.2 The $\mathcal{O}(\varepsilon)$ problem . . . 131
6.2.4.3 The $\mathcal{O}(\varepsilon^2)$ problem . . . 132
6.2.4.4 The $\mathcal{O}(\varepsilon^3)$ problem . . . 134
6.2.4.5 The $\mathcal{O}(\varepsilon^4)$ problem . . . 137
6.2.4.6 Neutral Surface . . . 139
6.3 Solution to Homogenised Problem . . . 140
6.3.1 Rescaled Problem . . . 141
6.3.2 Simply Supported Beam Problem . . . 142
6.3.3 Cantilever Beam Problem . . . 147
6.4 Multilayer Beam . . . 152
6.4.1 Introduction . . . 152
6.4.2 Adjusted coefficients . . . 153
6.4.3 Mechanical cell functions of the first kind . . . 153
6.4.4 Mechanical cell functions of the second kind . . . 155
6.4.5 Cell functions driven by voltage . . . 156
6.4.6 Effective coefficients . . . 157
6.4.7 Special case: Single Layer Beam . . . 159
6.5 Comparison between results derived through AHBM and classical Euler–Bernoulli beam theory for a single beam using the homogenised material . . . 159
6.6 Re-dimensionalising homogenised equations . . . 160
6.7 Simplified homogenisation method for layered composites . . . 162
6.8 Case study of Sequential Homogenisation: The Hairbrush . . . 163
6.8.1 Results . . . 166

6.9 Case study of Sequential Homogenisation: Jungle Gym 172
6.9.1 Standard Homogenisation set-up 172
6.9.2 Sequential Homogenisation set-up 172
6.9.3 Results 173
6.10 Conclusions 176

7 Conclusions **178**
7.1 Review of thesis 178
7.2 Concluding remarks 180
7.3 Future work 181

8 Bibliography **184**

A Lagrangian formulation of piezoelectric problem **190**

B Definitions of Uniform Ellipticity **192**

C Weak formulations and numerical solutions to cell equations arising from our homogenisation model **193**

D Isotropy **197**
D.1 Mechanical isotropy 197
D.2 Piezoelectric isotropy 197
D.3 Dielectrical isotropy 197

E Symmetry relations for homogenisation of bulk materials **198**

F Cell problems for a bulk device made of a 1-3 composite **204**
F.1 Assumptions about the tensors in each phase 204
F.2 Mechanical cell problems 205
F.3 Electrical cell problems 206
F.4 Cell functions that are zero 207
F.5 Effective coefficients 207
F.5.1 Stiffness coefficients 207
F.5.2 Electromechanical coefficients 208
F.5.3 Dielectric coefficients 208

G Definitions of lattice sums **209**

H Taylor expansions of lattice sums computations **210**

I Symmetry relations for actuator problem **213**

J Solving the time-independent piezoelectric problem on the unit cell with actuator boundary conditions **217**

J.1 Case with no forcing 217

J.2 Solution to $O(\varepsilon)$ problem for time-dependent problem 220

K Cell functions for the actuator problem **222**

K.1 Mechanically driven cell functions 222

K.1.1 Cell functions of the first kind 222

K.1.1.1 Solution to vertical strain functions 223

K.1.2 Cell functions of the second kind 223

K.1.2.1 Solution to vertical strain functions 224

K.2 Cell functions driven by voltage 224

L Multilayer beam derivations **226**

L.1 Cell functions of the first kind 226

L.2 Cell functions of the second kind 228

L.3 Voltage driven cell functions 230

M Eigenvalues and eigenfunctions of the $\frac{d^4}{dx^4}$ operator **232**

M.1 Simply Supported beam 232

M.2 Cantilever beam 233

M.2.1 Properties 235

N Stability analysis for case where the forcing frequency is double the natural frequency **236**

List of Figures

1.1 Schematic of the two types of piezoelectric effects 1
1.2 Schematic showing composites with different connectivities. 4
1.3 Schematic of a 1-3 composite, a 0-3 composite and a 2-2 composite . 5

3.1 Schematic showing cross sections of geometries used by Smith & Auld and Avellaneda & Swart 40
3.2 Schematic of a 1-3 composite with cylindrical pillars in a hexagonal lattice 41
3.3 Schematic for close-packing and graph of volume fraction against inclusion radius 42
3.4 Graph showing κ_{eff} using the AHM, the DEM, the MoM and the RVE approaches 43
3.5 Graph showing μ_{eff} using the AHM, the DEM and the RVE approaches 44
3.6 Graph showing $e_{\text{eff},13}$ using the AHM, the DEM, the MoM and the RVE approaches 45
3.7 Graph showing $e_{\text{eff},33}$ using the AHM, the DEM, the MoM and the RVE approaches 46
3.8 Graph showing $\epsilon^{S}_{\text{eff},33}$ using the AHM, the DEM, the MoM and the RVE approaches 47

4.1 Schematic of piezoelectric material poled in Z-direction 49
4.2 Unit cell with cylindrical inclusion of radius $0 < r \ll 1$ 53
4.3 Material with isolated cylindrical inclusion of radius 1 53
4.4 Comparison between κ_{eff} found using FEM and the low volume fraction polynomials 88
4.5 Comparison between μ_{eff} found using FEM and the low volume fraction polynomials 89
4.6 Comparison between $-e_{\text{eff},13}$ found using FEM and the low volume fraction polynomials. 90
4.7 Comparison between $e_{\text{eff},33}$ found using FEM and the low volume fraction polynomials. 90

4.8 Comparison between effective $\epsilon^S_{\text{eff},33}$ found using FEM and the low volume fraction polynomials 91
4.9 Comparison between the low volume fraction polynomials for κ_{eff} . . 94
4.10 Comparison between the low volume fraction polynomials for μ_{eff} . . 95
4.11 Comparison between the low volume fraction polynomials for $-e_{\text{eff},13}$ 96
4.12 Comparison between the low volume fraction polynomials for $e_{\text{eff},33}$. 97
4.13 Comparison between the low volume fraction polynomials for $\epsilon^S_{\text{eff},33}$. 97

5.1 Schematic of typical sensor set-up 101
5.2 Schematic showing an half-space transducer 105
5.3 Schematic showing the finite-thickness transducer 105
5.4 Schematic of a 1-3 composite with a square lattice and square rods . 112
5.5 Schematic of a 1-3 composite with a square lattice and circular rods . 112
5.6 Schematic of a 1-3 composite with a hexagonal lattice and cylindrical rods. 112
5.7 Schematic of a 1-3 composite with a square lattice and square rods . 112
5.8 Schematic of a unit cell for a 3-3 composite 112
5.9 Schematic of a Jungle Gym sensor made up of several Jungle Gym Cells 112
5.10 Graph comparing how the voltage output coefficient V_0 varies with different lattices and inclusion shapes 113
5.11 Graph comparing how the effective wave speed c_s varies for different lattices and inclusions 114
5.12 Graph comparing how the effective mechanical impedance Z_s varies for different lattices and inclusions 115

6.1 Schematic of a beam actuator 118
6.2 Schematic of a simply supported beam 142
6.3 Graph showing a comparison of analytical and numerical solutions of the c_1 coefficient for the simply supported beam problem 147
6.4 Schematic of a Cantilever Beam 147
6.5 Graph showing a comparison of analytic and numerical solutions of the c_1 coefficient for the cantilever problem 152
6.6 Schematic of a multilayer beam comprised of homogeneous layers . . 153
6.7 Schematic of the Sequential Homogenisation recipe 162
6.8 Schematic of a 1-3-2 composite 163

6.9 Graph showing a comparison of the effective planar stiffness coefficient A_{11}^{11} under Standard and Sequential Homogenisation for a Hairbrush geometry . . . 166
6.10 Graph showing a comparison of the heights of the neutral surface $Z^{\dagger}$ under Standard and Sequential Homogenisation for a Hairbrush geometry . . . 167
6.11 Graph showing a comparison of effective flexural rigidity D_{11}^{11} under Standard and Sequential Homogenisation for a Hairbrush geometry . 168
6.12 Graph showing a comparison of effective piezoelectric stress coefficient $e_{s,11}^{3}$ under Standard and Sequential Homogenisation for a Hairbrush geometry . . . 169
6.13 Graph showing a comparison of effective piezoelectric bending moment coefficient $e_{m,11}^{3}$ under Standard and Sequential Homogenisation for a Hairbrush geometry . . . 170
6.14 Graphs showing how the natural frequency of the lowest mode of oscillations f_1 varies with the volume fraction of PZTA5 for the simply supported and cantilever beam problems for the Hairbrush geometry 171
6.15 Schematic of a Jungle Gym actuator which is one cell high . . . 172
6.16 Schematic of a Jungle Gym actuator which is infinitely many cells high 173
6.17 Graph showing a comparison of the effective planar stiffness coefficient A_{11}^{11} under Standard and Sequential Homogenisation for a Jungle Gym geometry . . . 173
6.18 Graph showing a comparison of effective flexural rigidity D_{11}^{11} under Standard and Sequential Homogenisation for a Jungle Gym geometry 174
6.19 Graph showing a comparison of the effective piezoelectric stress coefficient $e_{s,11}^{3}$ under Standard and Sequential Homogenisation for a Jungle Gym geometry . . . 175
6.20 Graphs showing how the frequency of the lowest mode of oscillation f_1 varies with the volume fraction of PZTA5 for the simply supported and cantilever beam problems for the Jungle Gym geometry . . . 176

List of Tables

1.1 Typical constitutive parameters for PZT at room temperature (stress-charge form) 5

2.1 Material parameters for Stycast and PZTA5 20

6.1 Data for actuator problem under simply supported boundary conditions 146

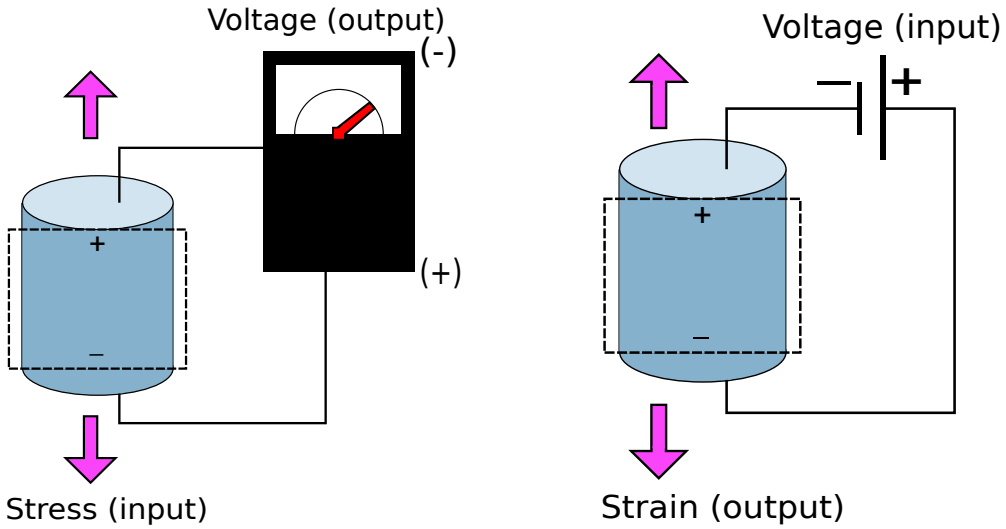
6.2 Dimensions of our cantilever beam actuator 165

Chapter 1

Introduction

1.1 Background

The piezoelectric effect was first discovered by Jacques and Pierre Curie in 1880 (see [18]) when they observed that the application of mechanical stress to quartz crystals resulted in an electrical charge, and the application of an electric field resulted in their deformation. These phenomena, illustrated in Figures (1.1a) and (1.1b) are known as the direct and inverse piezoelectric effect, respectively.



(a) Direct piezoelectric effect.

(b) Inverse piezoelectric effect.

Figure 1.1: Schematic of the two types of piezoelectric effects. Adapted from [46].

Piezoelectric effects are generated as the crystals in piezoelectric materials lack a centre of symmetry. Under the direct effect, when stress is applied, it distorts the lattice which shifts the positions of positive and negative ions in the material. The change in dipole alignment produces a net polarisation which generates an electric field and hence a potential difference. Conversely, under the inverse effect,

the imposed electrical field causes the dipoles in the lattice to reorientate themselves to align with the field, which forces the lattice to deform, producing a mechanical strain.

Piezoelectrics are important smart materials as they generate energy or movement almost instantaneously, without the need for gears or mechanical parts and are capable of producing very precise movement. They are widely used in industry, engineering, electronics, medicine, defence, and science (see [45]). Vehicles incorporate piezoelectric devices for sensing and actuation, including fuel injection, assisted parking, monitoring of tyre pressure and vibration control. In industry, ultrasonic actuators are widely used, for example for cutting, drilling, trimming, welding and cleaning, while piezoelectric sensors are used to measure force, pressure, vibration and acoustic emissions and so on. Piezoelectric Micro-Electro-Mechanical Systems (MEMS) are silicon-based devices which are used in automated manufacturing processes. In automated assembly lines, ultrasonic MEMS sensors can detect components, and identify misalignment or excessive wear of machine parts. MEMS are also widely used in consumer electronics including quartz resonators, timing oscillators, microphones and in smartphones.

In medicine, piezoelectric devices are used in ultrasound imaging probes, ultrasonic surgical tools (including scalpels to perform keyhole surgery) and micro-pumps (which deliver microscopic quantities of drugs), as well as smart health monitoring devices including implanted and wearable technology.

In defence, a wide range of sonar devices are used to navigate, monitor and detect underwater activity and threats (e.g. sea mines), as well as to map the profile of the seabed. Engineers and scientists also use sonar technology to map the ocean floor, as well as study marine life and carry out non-destructive testing of underwater structures. In science, piezoelectric actuators underpin Atomic Force and Scanning Tunnelling Microscopes, as they allow highly detailed images to be created from a tiny probe which can be positioned with atomic accuracy. Additionally, piezoelectric actuators are essential for the remote realignment of optical lenses on telescopes in space.

The electric performance of piezoelectric materials is affected by a range of factors including the driving frequency, amplitude of the applied field, electrical loading conditions, dielectric losses, as well as composition and microstructure. The key physical parameters that describe a piezoelectric material are:

i. the elastic constants (i.e., the bulk and shear moduli),

ii. the piezoelectric, or electromechanical, coefficients that describe how electrical energy is converted into mechanical energy (known as 'coupling constants') and

iii. the permittivity, or dielectric, constants which measure how easily the material polarises in response to an electric field, and therefore how much electric charge it can store.

The most common piezoelectric material is ceramic Lead Zirconate Titanate, known as PZT [38]. It has exceptionally large piezoelectric coefficients compared to other commonly used piezoelectric materials, such as quartz and polymer-based piezoelectrics, meaning a small mechanical stress produces a large electrical output, and conversely, a small electric field produces a significant deformation. PZT properties may be finely tuned by changing the ratio of zirconium to titanium or by 'doping'[1] with small amounts of other elements, as needed. Additionally, PZT is structurally, stable, and inexpensive to produce.

1.2 Benefits of composites over piezo-ceramics and piezo-polymers

Piezo-ceramics (such as pure PZT) are widely used in applications where high stiffness, very high electromechanical coupling, and strong electromechanical force are required. But they are hard, stiff, and brittle and tend to break rather than deform under large mechanical loading [38]. They also have extremely high acoustic impedance[2]. Piezo-polymers (e.g. Polyvinylidene Fluoride (PVDF)) can be used where low acoustic impedances and high flexibility are needed, such as wearable sensors. However, they have lower electromechanical coupling, lower stiffness, lower acoustic output, and higher dielectric losses than piezo-ceramics such as PZT [38], meaning they are used for specialised purposes only.

Piezoelectric composites offer a significant advance over both piezo-ceramics and piezo-polymers, since the overall properties of composites (such as stiffness, sensitivity, bandwidth, and impedance matching) may be easily engineered by fine-tuning the microstructure and composition, as required [51].

As noted by [53], the electromechanical coupling constants in piezoelectric composites can be larger than those for piezo-ceramics and piezo-polymers, and composites can provide a wide range of overall dielectric constants as well as low dielectric and mechanical losses. For medical imaging devices, piezoelectric composites have been developed which allow higher operating frequencies, and therefore a much higher resolution than piezo-ceramics or piezo-polymers. Additionally, composites

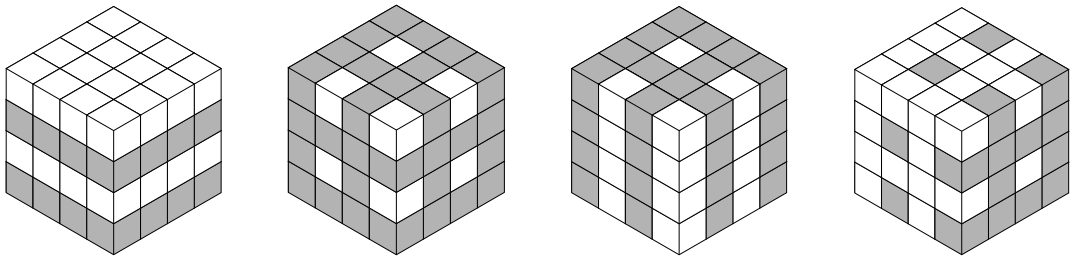
[1] Doping is the practice of adding chemicals during the fabrication process to enhance the piezoelectric properties of the composite.

[2] Acoustic impedance is the resistance to the propagation of waves through the material.

with piezoelectric fibres arranged in a parallelogram allow an electric field to be applied in one direction by deforming the composite in another direction and vice versa.

1.3 Connectivity of common composites

Composites are classified by the connectivity of each of the materials. Connectivity is defined as the number of dimensions through which the material is continuous, as illustrated by Figure 1.2. The connectivity between piezoelectric and polymer phases plays an important role in determining the effective electromechanical properties and when designing a new device, a suitable connectivity must be selected.



(a) 2-2 Composite. (b) 0-3 Composite. (c) 1-3 Composite. (d) 3-3 Composite.

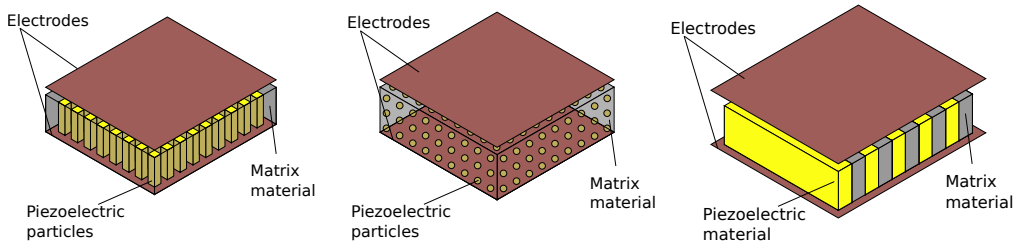
Figure 1.2: Schematic showing composites with different connectivities. Adapted from [24].

The three main connectivity classes are:

i. **1-3 composites**, where rods of piezoelectric ceramic material have been inserted into the polymer. The connectivity of the ceramic rod is 1 while the connectivity of the polymer is 3, see Figure (1.3a).

ii. **0-3 composites**, where inclusions (e.g. spheres) of ceramic material are embedded in the polymer. The connectivity of the inclusions is 0 while the connectivity of the polymer is 3, see Figure (1.3b).

iii. **2-2 composites**, where slabs of ceramic and polymer are alternated in a periodic fashion. The connectivity of both phases is 2, see Figure (1.3c).



(a) 1-3 composite (b) 0-3 composite (c) 2-2 composite

Figure 1.3: Schematic of three different types of common composites. The red plates represent the electrodes, the yellow parts represent the piezoelectric material and the grey parts represent the polymer material. These images were adapted from [30].

In Table 1.1, we outline typical values for the material parameters of PZT.

Property	**Symbol**	**Typical values**	**Units**
Elastic stiffness (constant E)	c_{11}^E	$(12\text{–}17) \times 10^{10}$	Pa
	c_{33}^E	$(10\text{–}14) \times 10^{10}$	Pa
	c_{44}^E	$(2\text{–}4) \times 10^{10}$	Pa
Piezoelectric stress coefficients	e_{31}	-5 to -7	$\mathrm{C\,m^{-2}}$
	e_{33}	12–18	$\mathrm{C\,m^{-2}}$
	e_{15}	10–15	$\mathrm{C\,m^{-2}}$
Clamped permittivity	ε_{33}^S	$(500\text{–}2000)\,\varepsilon_0$	$\mathrm{F\,m^{-1}}$
	ε_{11}^S	$(800\text{–}3000)\,\varepsilon_0$	$\mathrm{F\,m^{-1}}$
Density	ρ	7400–7800	$\mathrm{kg\,m^{-3}}$

Table 1.1: Typical constitutive parameters for PZT at room temperature (stress-charge form). Adapted from [52].

Thales, our industrial partner, is interested in piezoelectric composites as they are used in sonar devices. These devices emit a sound wave from a transmitter which is reflected by nearby objects. The reflected wave hits the detector, which sends an electronic signal. The distance between the nearby object and the transmitter can be calculated using the time taken for the transmission and reception of the sound wave. At the device level, the piezoelectric composite forms the sensing element of the sonar system operating either passively by detecting incident wave or actively by transmitting and receiving pulses, with the resulting electrical signals determining detection sensitivity and spatial separation. Thales would like to optimise these devices, and are particularly interested in 1-3 composites.

1.4 Literature review

There is extensive literature on analytical and numerical approaches to modelling

piezoelectric composites. Analytical models have played a critical role in understanding the characteristics of piezoelectric composites [24]. Our review focusses on analytical models.

As identified by [24], the literature on analytical models can be broadly grouped into six different categories, comprising of micromechanical-based models (first developed by Hashimoto [57]), Eshelby-type models (first developed by [21]) with extensions including the Mori-Tanaka approach [48], [20] and [19]), the Dilute Approximation Method [20], the Self-Consistent Approach [10], the extended Method of Mixtures approach [37] and models based on Homogenisation models including Asymptotic Homogenisation [14, 32, 39, 50, 56, 56], which is the subject of this thesis.

A key analytical approach in the context of our study was developed by Smith & Auld [53] 1991, based on the Method of Mixtures (MoM) approach. They derived formulae for the effective coefficients of a 1-3 composite of square ceramic rods aligned in the thickness mode. Under this approach, the strain and electric fields are assumed to be independent of the in-plane coordinates x and y within each phase, and are then averaged over the contributions of the constituent phases. In their paper, the volume fraction of the piezoelectric ceramic was reduced to achieve the lower acoustic impedance required for a 1-3 composite, at the cost of a reduction in electrical coupling and performance. The method uses some *ad-hoc* assumptions which are well suited to thickness-mode behaviour, where deformation occurs predominantly through the thickness (or poling) direction, and the electromechanical fields are assumed to be uniform. Their method is widely used in the design of thickness-mode transducers, although, as recognised by [53], the model does not work for in-plane or shear behaviour, which significantly limits its use for describing real-world scenarios.

In 1995 Wenwu Cao & Wenkang Qi [12] studied plane wave propagation through a finite 2-2 composite. They extended the T-Matrix (or transfer-matrix) technique, a wave-based scattering approach in which the response of a single periodic unit cell is characterised by a matrix that relates incident waves to transmitted and reflected waves, by introducing a plane-wave ansatz in which the displacement and potential fields are represented as a supposition of plane waves with unknown amplitudes. This formulation allows band structures to be predicted using only a small number of unit cells without having to rely on Floquet Theory [7] and its idealised assumption of an infinitely periodic medium. Their results show that the dispersion curves for a small number of unit cells rapidly converge to those obtained through Floquet

Theory [7]. Their paper demonstrates that accurate predictions may be made using only a few cells.

In 1998, Avellaneda & Swart [4] extended the work of Smith & Auld by developing a Differential Effective Medium (DEM) method to derive a more precise framework for evaluating the performance of 1-3 composites. This method involves calculating the effective coefficients based only on the volume fraction of the inclusions and the material parameters (i.e., the elasticity, piezoelectricity and permittivity) of the polymer and ceramic by solving a system of ODEs. Their results closely agree with Hill's Uniform Field Theory approach [34]. The DEM method built on earlier work by Hashin [31], who sought to determine the effective properties of composite materials by averaging the behaviour over a Representative Volume Element (RVE). The DEM method was also inspired by the work of Torquato [54] in 1991, which focusses on finding the effective properties of randomized heterogeneous materials that depend upon the microstructure through n-point correlation functions. Avellaneda & Swart compared results found using their method to results by Smith & Auld and by Helsing's Boundary integral method [33][3] and found that it had a closer agreement with the latter.

A different approach to finding the effective material properties of a piezoelectric composite material is to use Asymptotic Homogenisation Theory. This involves introducing microscopic variables $\boldsymbol{X}$ alongside the macroscopic variable $\boldsymbol{X}$ to capture the multiple scales behaviour of the solutions. A perturbation expansion is posed for the dependent variables. The resulting problems at each order are then solved on the unit cell at the microscale, and the geometry of the microscale and properties of the phases are systematically incorporated into expressions for the averaged material properties which are contained in a homogenous macroscopic model. In 1998, Bravo-Castillero *et. al.* [13] found explicit solutions for all effective coefficients when the connectivity is in series and also when in parallel. In 2001, Bravo-Castillero *et. al.* [25] also derived the effective properties of a 1-3 composite, by using estimates for the integrals of the cell functions. These estimates closely agree with the electromechanical coupling factor and the longitudinal wave velocity derived by Smith & Auld [53]. In 2005, Andrianov *et. al.* [3] found the effective properties of composite wires under longitudinal shear, arranged in a hexagonal lattice. In 2011, Li *et. al.* [44], building on the work of H. Berger *et. al.* [9], and Ronit Kar-Gupta *et. al.* ([40] and [41]), used the unit cell as an RVE. To determine each effective coefficient, they apply zero normal displacement (or zero potential electric field) to all but one

[3]Helsing's Boundary integral method reformulates the static elasticity equations as boundary integral equations defined only on the boundary between neighbouring phases.

edge of the unit cell and apply a unit normal displacement (or unit potential) in a suitable edge of the unit cell[4]. They then solve the cell equations using FEM and calculate the desired coefficient by integrating on the unit cell.

There is significant literature on additional approaches, including: the Finite Element Method [42], the Fourier series expansion method [11], the eigenfunction expansion-variational method [58], the Boundary Element Method [33] and the Effective field approach [1].

Experimental studies on the properties on piezoelectric composites and devices is limited. A key study by Newnham, Skinner & Cross in 1978 [51] introduced the concept of connectivity, and showed its importance on piezoelectric performance. They demonstrated experimentally that connectivity strongly governs how stress and electric fields are transmitted through piezoelectric composites, and provided measurements of electromechanical quantities including coupling coefficients, dielectric response, and resonance behaviour. Their work established that composite behaviour depends not only on constituent material properties, but also on the continuity of the piezoelectric phase and the associated load and field transfer paths.

In the 1980s, experimental studies by Gururaja and others [26–29] extended this work in the context of 1-3 composites for ultrasound transducers. They calculated theoretical predictions for a number of different piezoelectric rods of different diameters and volume fractions and reported experimental values for bandwidth, sensitivity, impedance response, and effective coupling under operating conditions and also considered impedance matching. Their work reinforced the practical importance of connectivity as well as geometry of inclusions.

The experimental study by Hashimoto and Yamaguchi in 1986 [57] is particularly significant and is repeatedly cited in the literature. For the first time, they derived the elastic, piezoelectric and dielectric constants for 1-3 multi-layered composite designed for an ultrasound transducer. The study provided an experimental picture of how stiffness, coupling, and permittivity coexist in real materials. Their work highlighted that experimental results are likely to vary from theoretical ones as effective properties are strongly influenced by fabrication quality, particularly the integrity of bonding at the ceramic–polymer interface.

Further important experimental insight was provided in by Chan in 1987 [15] and by Chan and Unsworth in 1989 [16]. In [16], a theoretical model was used to predict characteristics including velocity, dielectric response, acoustic impedance, electromechanical coupling factor and piezoelectric coefficients for a layered 1–3 com-

[4]Which direction is suitable will depend on the coefficient being determined.

posite developed for ultrasonic transducer applications. Experimental measurements carried out showed good agreement with the theoretical predictions.

In 2007, Ballas [5] provided valuable experimental insight beyond thickness-mode devices, by conducting significant experimental investigations of a real-world multilayer beam bending actuator with an integrated sensor, testing this device extensively under static and dynamic loading. Amongst other things, his work demonstrated bending deformation, frequency dependence, and damping effects on the electromechanical response of beam actuators.

It is recognised in the literature that direct experimental validation of both analytical and numerical models for piezoelectric composites and devices remains scarce [24]. The scarcity of experimental studies (and reference data) in the literature may be partially due to the challenge of fabricating fully periodic microstructures and dealing with real-world effects such as imperfect bonding and damping, which can complicate direct validation of piezoelectric composites and devices (see [57]).

1.5 Objectives of thesis

Our aim is to develop simplified mathematical models of piezoelectric composites using Asymptotic Homogenisation Theory. This method approximates a composite of two materials with a complicated microstructure, reducing it to a system that is a homogenous material, the effective material properties of which depend on the microstructure. We will develop a model which predicts the effective properties of piezoelectric composites with different microstructures, to facilitate the optimal design of such materials. Using homogenisation theory, we will determine all the effective electromechanical coefficients, i.e., the elastic stiffness constants, the piezoelectric constants, and the dielectric constants. We will use these coefficients to determine the effective behaviour of piezoelectric devices.

As part of the homogenisation process, we will derive 'cell problems', which will need to be solved by finite element methods. The solution of the cell problems will be needed to determine the effective physical parameters in the homogenised macroscale model. We aim to develop a methodology that can be applied to any type of geometry and/or spatial distribution of piezoelectric inclusions. Such a model may be used to facilitate the design of a wide range of piezoelectric devices.

1.6 Overview of thesis

In Chapter 2, we present the underpinning model for piezoelectricity and non-dimensionalise it. We describe the Asymptotic Homogenisation method for finding

the effective macroscale elastic, piezoelectric (or electromechanical), and dielectric properties along with the homogenised model that holds at the macroscale. This will involve solving relevant cell problems at the microscale using FEM.

In Chapter 3, we will calculate the effective coefficients derived using the DEM method [4], the MoM approach [53] and the RVE method [44], and compare these with results found using the recipe presented in Chapter 2. We will consider three different geometries[5], and compare and contrast the behaviour of the effective coefficients as the volume fraction of the ceramic material is increased with the equivalent results for the other three methods.

In Chapter 4, we consider the case where the volume fraction of the inclusion material is small (i.e., up to approximately 10-20% of the composite). Firstly, we will derive closed-form polynomial approximations for the effective coefficients for a 1-3 composite. We will then derive low volume fraction polynomials for the effective coefficients using the DEM and the MoM approaches. Finally, we will compare these three approximations with each other and also compare the low volume fraction polynomials with the full numerical solutions calculated using Chapter 2.

In Chapter 5, we extend our model to predict the behaviour of bulk sensors by incorporating wave theory. Firstly, we derive the solutions to a problem with an incoming pressure wave with fixed amplitude and frequency in two physical set-ups. We then explore the effect of choosing different geometries on the effective properties of the solid and the effective electrical output.

In Chapter 6, we extend our model to analyse the behaviour of thin beam actuators by incorporating beam theory. We do this by first altering the equations of motion and continuity and boundary conditions so they incorporate axial forces (which were not significant for bulk devices), and then combine the asymptotic homogenisation procedure with a small-aspect-ratio expansion. We solve two physical problems, namely the simply supported problem and the cantilever beam problem.

Finally, in Chapter 7, we summarise key aspects of our framework and discuss important findings and physical insights highlighted by our results. We conclude by suggesting possible avenues for further work to advance our approach.

1.7 Statement of Originality

Chapter 2 is independent work, but follows the general framework of asymptotic homogenisation as described for piezo-electric composites in [24], for example. The material in Chapters 3-7 is original unless otherwise stated in the text.

[5]By geometries, we mean different types of lattice structures and inclusion shapes.

Chapter 2

Establishing the Homogenisation problem

2.1 Introduction

In this chapter, we will establish the piezoelectric equations which underpin the rest of this thesis. These equations are derived by coupling the quasi-electrostatic equations[1] with the linear elasticity equation. We consider a material with two phases, a piezoelectric inclusion phase, and a non-piezoelectric matrix phase. We will state the boundary conditions that will hold at the interfaces between the two phases. Throughout the thesis, indices $i, j, k, l \in \{1, 2, 3\}$ denote spatial components, and we adopt the Einstein summation convention, whereby repeated indices are summed over (unless stated otherwise). We denote by ∇ the gradient with respect to the spatial variable $\boldsymbol{x}$, with components $(\nabla f)_i = \frac{\partial f}{\partial x^i}$, and $\nabla\cdot$ denotes the divergence.

2.2 Linear elasticity

We define the displacement vector $\boldsymbol{u}$ to be the vector that describes the displacement of the material from its original configuration. The von-Kármán strain tensor (see [35]), $\boldsymbol{S}$, is given by

$$\boldsymbol{S} = \frac{1}{2}\left[\nabla \boldsymbol{u} + (\nabla \boldsymbol{u})^{\mathrm{Tr}} + \nabla \boldsymbol{u} \colon (\nabla \boldsymbol{u})^{\mathrm{Tr}}\right], \tag{2.2.1}$$

where Tr denotes matrix transposition, and : denotes tensor contraction. In this case, the last index of $\nabla \boldsymbol{u}$ is contracted with the first index of $(\nabla \boldsymbol{u})^{\mathrm{Tr}}$, corresponding to matrix multiplication. Assuming the displacements are small, we neglect the

[1] Quasi-electrostatic equations are a special case under Maxwell's Laws where the electric field is assumed to depend on time and the magnetic field is slowly varying.

quadratic term to get

$$\boldsymbol{S} = \frac{1}{2}\left[\nabla \boldsymbol{u} + (\nabla \boldsymbol{u})^{\mathrm{Tr}}\right]. \tag{2.2.2}$$

We define $\boldsymbol{c}$ to be the stiffness tensor of rank 4, which describes how the stress is related to the strain.

The stiffness tensor $\boldsymbol{c}$ has the following symmetries

$$c_{ij}^{kl} = c_{ji}^{kl} = c_{ij}^{lk} = c_{kl}^{ij}. \tag{2.2.3}$$

By Hooke's Law (see [35]), the Cauchy stress tensor $\boldsymbol{\sigma}$ is given by

$$\boldsymbol{\sigma} = \boldsymbol{c} : \boldsymbol{S}. \tag{2.2.4}$$

In this case, the last two indices of $\boldsymbol{c}$ are contracted with both indices of $\boldsymbol{S}$. In index notation, this reads as

$$\sigma_{ij} = c_{ij}^{kl} S_{kl}. \tag{2.2.5}$$

Using (2.2.2)-(2.2.5), we deduce that

$$\sigma_{ij} = c_{ij}^{kl} S_{kl} = \frac{1}{2} c_{ij}^{kl}\left(\frac{\partial u_k}{\partial x^l} + \frac{\partial u_l}{\partial x^k}\right) = c_{ij}^{kl}\frac{\partial u_k}{\partial x^l}. \tag{2.2.6}$$

Assuming there are no body forces[2], and writing ρ as the mass density of the material, then the equation of elasticity (which is a variation of Newton's Second Law) states that

$$(\nabla \cdot \boldsymbol{\sigma}) = \rho \frac{\partial^2 \boldsymbol{u}}{\partial t^2}. \tag{2.2.7}$$

Combining (2.2.6) with (2.2.7) yields us the linearised elasticity equation, and reads

$$\rho \frac{\partial^2 \boldsymbol{u}}{\partial t^2} = \nabla \cdot (\boldsymbol{c} : \nabla \boldsymbol{u}). \tag{2.2.8}$$

2.3 Quasi-electrostatics

Quasi-electrostatics is the study of time-dependent electric fields where the magnetic field varies slowly with time. We define $\boldsymbol{E}$ to be the electric field and define $\boldsymbol{\epsilon}$ to be the free permittivity (or dielectric) tensor of our medium. The vector $\boldsymbol{\mathcal{D}}$ denotes the Dielectric displacement. The components of the dielectric displacement vector

[2]The piezoelectric effect will be introduced later as an additional strain.

$\boldsymbol{\mathcal{D}}$ are given by [4], and read as

$$\mathcal{D}_i = \epsilon_i^j E_j, \tag{2.3.1}$$

where ϵ_i^j has the symmetry

$$\epsilon_i^j = \epsilon_j^i. \tag{2.3.2}$$

We assume that there is no charge in our system and so Gauss' Law (see [4]) states that

$$\nabla \cdot \boldsymbol{\mathcal{D}} = 0. \tag{2.3.3}$$

For a slowly varying magnetic field, Faraday's Law (see [4]) states that

$$\nabla \times \boldsymbol{E} = \mathbf{0}, \tag{2.3.4}$$

which means that the electric field $\boldsymbol{E}$ is conservative, and therefore there exists a scalar potential function φ satisfying

$$\boldsymbol{E} = -\nabla\varphi. \tag{2.3.5}$$

Combining (2.3.1), (2.3.3) and (2.3.5) yields Gauss' Law, which describes how the electrical potential behaves, and reads

$$-\nabla \cdot (\boldsymbol{\epsilon} \cdot \nabla\varphi) = 0. \tag{2.3.6}$$

2.4 Coupling linear elasticity with quasi-electrostatics

Having established the equations of linear elasticity and quasi-electrostatics, we will see how the two processes couple due to direct and inverse piezoelectric effects. This will help us derive the full piezoelectric equations. We assume that the stiffness tensor $\boldsymbol{c}$ is (pseudo-)invertible, meaning there exists $\boldsymbol{s}$ satisfying the equivalent symmetries to those produced in (2.2.3) as well as the relationship

$$c_{ij}^{kl} s_{kl}^{i'j'} = \frac{1}{2}\left[\delta_i^{i'}\delta_j^{j'} + \delta_i^{j'}\delta_j^{i'}\right], \tag{2.4.1}$$

where δ represents the Kronecker delta symbol.

We want $\boldsymbol{s}$ to satisfy (2.4.1) so it can be used to 'invert' the stiffness tensor $\boldsymbol{c}$. Given such a tensor exists, it is unique (see [17]). It is called the compliance tensor.

Using the compliance tensor we rearrange (2.2.5) and use (2.3.1) to get the

following uncoupled strain-charge constitutive equations

$$S_{ij} = s_{ij}^{kl}\sigma_{kl}, \tag{2.4.2}$$

$$\mathcal{D}_i = \epsilon_i^k E_k. \tag{2.4.3}$$

For piezoelectric materials, we have to incorporate extra terms that encompass the coupling between elastic deformation and dielectric displacement. We introduce the piezoelectric strain tensor $\boldsymbol{d}$ which has the following symmetry

$$d_{ij}^k = d_{ji}^k. \tag{2.4.4}$$

The piezoelectric strain tensor describes how the strain translates into a dielectric displacement and how an electric field translates into an extra strain. Following [4] we augment (2.4.2) and (2.4.3) to include the coupling terms by writing

$$S_{ij} = s_{ij}^{kl}\sigma_{kl} + d_{ij}^k E_k, \tag{2.4.5}$$

$$\mathcal{D}_i = d_i^{kl}\sigma_{kl} + \epsilon_i^k E_k. \tag{2.4.6}$$

The $d_i^{kl}\sigma_{kl}$ term in (2.4.6) arises from the direct piezoelectric effect, while the $d_{ij}^k E_k$ term from (2.4.5) arises from the inverse piezoelectric effect. We note that $d_{ij}^k = d_k^{ij}$. The reason we are writing them differently is to indicate we are taking the tensor transpose in (2.4.6).

We wish to rearrange equations (2.4.5) and (2.4.6) to make the tensors $\boldsymbol{\sigma}$ and $\boldsymbol{\mathcal{D}}$ the subjects of the equations. Since $\boldsymbol{s}$ is (pseudo-)invertible, we can rearrange (2.4.5) to give

$$\sigma_{ij} = c_{ij}^{i'j'} S_{i'j'} - c_{ij}^{i'j'} d_{i'j'}^k E_k. \tag{2.4.7}$$

We substitute σ_{ij} from (2.4.7) into (2.4.6) to find that

$$\mathcal{D}_i = d_i^{kl} c_{kl}^{k'l'} S_{k'l'} + \left(\epsilon_i^k - d_i^{k'l'} c_{k'l'}^{i'j'} d_{i'j'}^k\right) E_k. \tag{2.4.8}$$

We define the components of the piezoelectric stress tensor $\boldsymbol{e}$ by

$$e_{ij}^k = c_{ij}^{i'j'} d_{i'j'}^k, \tag{2.4.9}$$

and define the components of the clamped permittivity tensor $\boldsymbol{\epsilon}^S$ (see [4]) by

$$\epsilon_i^{Sk} = \epsilon_i^k - d_i^{k'l'} c_{k'l'}^{i'j'} d_{i'j'}^k. \tag{2.4.10}$$

Here, the superscript S indicates that the permittivity is evaluated at constant strain. From (2.3.2) and (2.4.10), we see that $\boldsymbol{\epsilon}^S$ has the following symmetry

$$\epsilon_i^{Sj} = \epsilon_j^{Si}. \tag{2.4.11}$$

We substitute (2.4.9) and (2.4.10) into (2.4.8) to get

$$\mathcal{D}_i = e_i^{kl} S_{kl} + \epsilon_i^{Sk} E_k. \tag{2.4.12}$$

We substitute (2.4.9) into (2.4.7) to find

$$\sigma_{ij} = c_{ij}^{kl} S_{kl} - e_{ij}^k E_k. \tag{2.4.13}$$

We note that

$$e_{ij}^k = e_{ji}^k. \tag{2.4.14}$$

Using (2.4.12) and (2.4.13), the conservation laws (2.2.7) and (2.3.3) yield

$$\rho \frac{\partial^2 u_j}{\partial t^2} = \frac{\partial \sigma_{ij}}{\partial x_i} = \frac{\partial}{\partial x_i}\left(c_{ij}^{kl} S_{kl} - e_{ij}^k E_k\right), \tag{2.4.15}$$

$$0 = \frac{\partial \mathcal{D}_i}{\partial x_i} = \frac{\partial}{\partial x_i}\left(e_i^{kl} S_{kl} + \epsilon_i^{Sk} E_k\right), \tag{2.4.16}$$

respectively. We note that $e_{ij}^k = e_k^{ij}$ and once again, the reason we are writing them differently is to indicate we are taking the tensor transpose in (2.4.16).

Using (2.2.2) and (2.3.5), we re-write (2.4.12), (2.4.13), (2.4.15) and (2.4.16) as

$$\sigma_{ij} = c_{ij}^{kl} \frac{\partial u_k}{\partial x^l} + e_{ij}^k \frac{\partial \varphi}{\partial x^k}, \tag{2.4.17}$$

$$\mathcal{D}_i = e_i^{kl} \frac{\partial u_k}{\partial x^l} - \epsilon_i^{Sk} \frac{\partial \varphi}{\partial x^k}, \tag{2.4.18}$$

$$\rho \frac{\partial^2 u_j}{\partial t^2} = \frac{\partial \sigma_{ij}}{\partial x_i} = \frac{\partial}{\partial x_i}\left(c_{ij}^{kl} \frac{\partial u_k}{\partial x^l} + e_{ij}^k \frac{\partial \varphi}{\partial x^k}\right), \tag{2.4.19}$$

$$0 = \frac{\partial \mathcal{D}_i}{\partial x_i} = \frac{\partial}{\partial x_i}\left(e_i^{kl} \frac{\partial u_k}{\partial x^l} - \epsilon_i^{Sk} \frac{\partial \varphi}{\partial x^k}\right), \tag{2.4.20}$$

respectively.

Equations (2.4.19) and (2.4.20) hold in the matrix phase, with constant material properties ρ_M, $\boldsymbol{c}_M$, $\boldsymbol{e}_M$, $\boldsymbol{\epsilon}_M^S$, and in the inclusion phase, with constant material properties ρ_I, $\boldsymbol{c}_I$, $\boldsymbol{e}_I$, $\boldsymbol{\epsilon}_I^S$ where subscripts M and I denote the matrix and inclusion phases respectively. The matrix phase is not piezoelectric, and thus $\boldsymbol{e}_M = \boldsymbol{0}$. We henceforth write $\boldsymbol{e}_I = \boldsymbol{e}$ to simplify our notation.

Let $\boldsymbol{n}$ denote the unit normal of the interface between the two materials (pointing out of the inclusion). At the interfaces between the two phases (namely $\partial M \cap \partial I$,

where ∂M and ∂I are the boundaries of M and I respectively), we assume that $\boldsymbol{u}$, φ, $\boldsymbol{\sigma}\cdot\boldsymbol{n}$ and $\boldsymbol{\mathcal{D}}\cdot\boldsymbol{n}$ are all continuous[3]. Therefore the following continuity conditions apply

$$u_{M,j} = u_{I,j}, \tag{2.4.21}$$

$$\varphi_M = \varphi_I, \tag{2.4.22}$$

$$n^i\left(c^{kl}_{M,ij}\frac{\partial u_{M,k}}{\partial x^l}\right) = n^i\left(c^{kl}_{I,ij}\frac{\partial u_{I,k}}{\partial x^l} + e^k_{ij}\frac{\partial \varphi_I}{\partial x^k}\right), \tag{2.4.23}$$

$$n^i\left(-\epsilon^{Sk}_{M,i}\frac{\partial \varphi_M}{\partial x^k}\right) = n^i\left(e^{kl}_i\frac{\partial u_{I,k}}{\partial x^l} - \epsilon^{Sk}_{I,i}\frac{\partial \varphi_I}{\partial x^k}\right), \tag{2.4.24}$$

along the interface between the two phases.

2.5 Formulae for isotropic materials

Although we will usually consider isotropic materials (see §D.1-D.3), the framework we will develop in this chapter will also be applicable to non-isotropic materials. In this section, we will explore how equations (2.4.19)-(2.4.24) simplify when the materials in each phase are isotropic. We substitute (D.1.1) and (D.3.1) into (2.4.19) and (2.4.20) and we then use the fact that $\boldsymbol{c}$, $\boldsymbol{e}$ and $\boldsymbol{\epsilon}^S$ are piece-wise constant to recover the Navier form of the linearised piezoelectric equations

$$\rho\frac{\partial^2 \boldsymbol{u}}{\partial t^2} = \kappa\nabla\left(\nabla\cdot\boldsymbol{u}\right) + \mu\nabla^2\boldsymbol{u} + \nabla\cdot\left(\boldsymbol{e}\cdot\nabla\varphi\right), \tag{2.5.1}$$

$$0 = \nabla\cdot\left(\boldsymbol{e}^{\mathrm{Tr}}:\nabla\boldsymbol{u}\right) - \epsilon^S\nabla^2\varphi, \tag{2.5.2}$$

where λ and μ denote the Lamè parameters defined in §D.1 and

$$\kappa = \lambda + \mu. \tag{2.5.3}$$

The governing equations (2.5.1) and (2.5.2) hold in both the matrix phase M and the inclusion phase I, with their given material parameters. Using (D.1.1) and (D.3.1) once again, the continuity conditions (2.4.21)-(2.4.24) are re-written as

$$\boldsymbol{u}_M = \boldsymbol{u}_I, \tag{2.5.4}$$

$$\varphi_M = \varphi_I, \tag{2.5.5}$$

[3]These conditions impose the folowing: no cracks, no discontinuity of potentials (in accordance with Faraday's Law), a balance of forces (in accordance with Newton's Third Law) and no charge build up between phases (in accordance with Gauss' Law).

$$\left(\lambda_M \mathbb{1}_{\mathbf{3\times 3}} \left(\nabla \cdot \boldsymbol{u}_M\right) + \mu_M \left(\nabla \boldsymbol{u}_M + \left(\nabla \boldsymbol{u}_M\right)^{\mathrm{Tr}}\right)\right) \cdot \boldsymbol{n}$$
$$= \left(\lambda_I \mathbb{1}_{\mathbf{3\times 3}} \left(\nabla \cdot \boldsymbol{u}_I\right) + \mu_I \left(\nabla \boldsymbol{u}_I + \left(\nabla \boldsymbol{u}_I\right)^{\mathrm{Tr}}\right) + \boldsymbol{e} \cdot \nabla \varphi_I\right) \cdot \boldsymbol{n}, \quad (2.5.6)$$

$$\left(-\boldsymbol{\epsilon}_M^S \nabla \varphi_M\right) \cdot \boldsymbol{n} = \left(\boldsymbol{e}^{\mathrm{Tr}} : \nabla \boldsymbol{u}_I - \boldsymbol{\epsilon}_I^S \nabla \varphi_I\right) \cdot \boldsymbol{n}, \quad (2.5.7)$$

along the interface between the two materials, where $\mathbb{1}_{\mathbf{3\times 3}}$ is the 3×3 identity matrix.

2.6 Non-dimensionalisation

We suppose that the scale of the device is L and that the distance between the inclusions is ℓ, where $\ell \ll L$. We non-dimensionalise the governing equations (2.4.19) and (2.4.20), together with the continuity conditions (2.4.21)-(2.4.24) across the interface between both phases, using

$$\begin{aligned} &\boldsymbol{x} = L\overline{\boldsymbol{x}}, \qquad \boldsymbol{c} = c_{\mathrm{typ}}\overline{\boldsymbol{c}}, \qquad \boldsymbol{e} = e_{\mathrm{typ}}\overline{\boldsymbol{e}}, \qquad \boldsymbol{\epsilon}^S = \epsilon_{\mathrm{typ}}\overline{\boldsymbol{\epsilon}}^S, \qquad \rho = \rho_{\mathrm{typ}}\overline{\rho} \\ &\boldsymbol{u} = U\overline{\boldsymbol{u}}, \qquad \varphi = \Phi\overline{\varphi}, \qquad \boldsymbol{\sigma} = \sigma_{\mathrm{unit}}\overline{\boldsymbol{\sigma}}, \qquad \boldsymbol{\mathcal{D}} = \mathcal{D}_{\mathrm{unit}}\overline{\boldsymbol{\mathcal{D}}}, \qquad t = T\overline{t}, \end{aligned} \quad (2.6.1)$$

where we take c_{typ}, e_{typ}, ϵ_{typ} and one of U or Φ from the data, for example we might pick $\epsilon_{\mathrm{typ}} = \epsilon^S_{I,33}$, and choose an intrinsic scaling for the remaining one of U and Φ by balancing terms in the equations. We will also pick the unknown scalings T, σ_{unit}, and $\mathcal{D}_{\mathrm{unit}}$ [4], by balancing terms.

We substitute (2.6.1) into (2.4.17)-(2.4.20), to find that

$$\overline{\sigma}_{M,ij} = \left(\frac{c_{\mathrm{typ}}U}{L\sigma_{\mathrm{unit}}}\right)\overline{c}^{kl}_{M,ij}\frac{\partial \overline{u}_{M,k}}{\partial \overline{x}^l}, \quad (2.6.2)$$

$$\overline{\mathcal{D}}_{M,i} = -\left(\frac{\epsilon_{\mathrm{typ}}\Phi}{L\mathcal{D}_{\mathrm{unit}}}\right)\overline{\epsilon}^{Sk}_{M,i}\frac{\partial \overline{\varphi}_M}{\partial \overline{x}^k}, \quad (2.6.3)$$

$$\overline{\rho}_M \frac{\partial^2 \overline{u}_{M,j}}{\partial \overline{t}^2} = \left(\frac{\sigma_{\mathrm{unit}}T^2}{L\rho_{\mathrm{typ}}U}\right)\frac{\partial \overline{\sigma}_{M,ij}}{\partial \overline{x}_i} = \left(\frac{c_{\mathrm{typ}}T^2}{L^2\rho_{\mathrm{typ}}}\right)\frac{\partial}{\partial \overline{x}_i}\left(\overline{c}^{kl}_{M,ij}\frac{\partial \overline{u}_{M,k}}{\partial \overline{x}^l}\right), \quad (2.6.4)$$

$$0 = \frac{\partial \overline{\mathcal{D}}_{M,i}}{\partial \overline{x}_i} = \left(\frac{\epsilon_{\mathrm{typ}}\Phi}{L\mathcal{D}_{\mathrm{unit}}}\right)\frac{\partial}{\partial \overline{x}_i}\left(-\overline{\epsilon}^{Sk}_{M,i}\frac{\partial \overline{\varphi}_M}{\partial \overline{x}^k}\right), \quad (2.6.5)$$

[4] T, σ_{unit}, and $\mathcal{D}_{\mathrm{unit}}$ are the characteristic time, stress and dielectric displacement units, respectively.

respectively in the matrix phase, and that

$$\overline{\sigma}_{I,ij} = \left(\frac{c_{\text{typ}}U}{L\sigma_{\text{unit}}}\right)\overline{c}^{kl}_{I,ij}\frac{\partial \overline{u}_{I,k}}{\partial \overline{x}^l} + \left(\frac{e_{\text{typ}}\Phi}{L\sigma_{\text{unit}}}\right)\overline{e}^{k}_{ij}\frac{\partial \overline{\varphi}_I}{\partial \overline{x}^k}, \tag{2.6.6}$$

$$\overline{\mathcal{D}}_{I,i} = \left(\frac{e_{\text{typ}}U}{L\mathcal{D}_{\text{unit}}}\right)\overline{e}^{kl}_{i}\frac{\partial \overline{u}_{I,k}}{\partial \overline{x}^l} - \left(\frac{\epsilon_{\text{typ}}\Phi}{L\mathcal{D}_{\text{unit}}}\right)\overline{\epsilon}^{Sk}_{I,i}\frac{\partial \overline{\varphi}_I}{\partial \overline{x}^k}, \tag{2.6.7}$$

$$\overline{\rho}_I\frac{\partial^2 \overline{u}_{I,j}}{\partial \overline{t}^2} = \left(\frac{\sigma_{\text{unit}}T^2}{L\rho_{\text{typ}}U}\right)\frac{\partial \overline{\sigma}_{I,ij}}{\partial \overline{x}_i} = \frac{\partial}{\partial \overline{x}_i}\left(\left(\frac{c_{\text{typ}}T^2}{L^2\rho_{\text{typ}}}\right)\overline{c}^{kl}_{I,ij}\frac{\partial \overline{u}_{I,k}}{\partial \overline{x}^l} + \left(\frac{e_{\text{typ}}\Phi T^2}{L^2\rho_{\text{typ}}U}\right)\overline{e}^{k}_{ij}\frac{\partial \overline{\varphi}_I}{\partial \overline{x}^k}\right), \tag{2.6.8}$$

$$0 = \frac{\partial \overline{\mathcal{D}}_{I,i}}{\partial \overline{x}_i} = \frac{\partial}{\partial \overline{x}_i}\left(\left(\frac{e_{\text{typ}}U}{L\mathcal{D}_{\text{unit}}}\right)\overline{e}^{kl}_{i}\frac{\partial \overline{u}_{I,k}}{\partial \overline{x}^l} - \left(\frac{\epsilon_{\text{typ}}\Phi}{L\mathcal{D}_{\text{unit}}}\right)\overline{\epsilon}^{Sk}_{I,i}\frac{\partial \overline{\varphi}_I}{\partial \overline{x}^k}\right), \tag{2.6.9}$$

respectively in the inclusion phase. We substitute (2.6.1) into continuity conditions (2.4.21)-(2.4.24), to find that

$$\overline{u}_{M,k} = \overline{u}_{I,k}, \tag{2.6.10}$$

$$\overline{\varphi}_M = \overline{\varphi}_I, \tag{2.6.11}$$

$$\begin{aligned} n^i\overline{\sigma}_{M,ij} &= n^i\left(\left(\frac{c_{\text{typ}}U}{L\sigma_{\text{unit}}}\right)\overline{c}^{kl}_{M,ij}\frac{\partial \overline{u}_{M,k}}{\partial \overline{x}^l}\right) \\ &= n^i\overline{\sigma}_{I,ij} = n^i\left(\left(\frac{c_{\text{typ}}U}{L\sigma_{\text{unit}}}\right)\overline{c}^{kl}_{I,ij}\frac{\partial \overline{u}_{I,k}}{\partial \overline{x}^l} + \left(\frac{e_{\text{typ}}\Phi}{L\sigma_{\text{unit}}}\right)\overline{e}^{k}_{ij}\frac{\partial \overline{\varphi}_I}{\partial \overline{x}^k}\right), \end{aligned} \tag{2.6.12}$$

$$\begin{aligned} n^i\overline{\mathcal{D}}_{M,i} &= n^i\left(-\left(\frac{\epsilon_{\text{typ}}\Phi}{L\mathcal{D}_{\text{unit}}}\right)\overline{\epsilon}^{Sk}_{M,i}\frac{\partial \overline{\varphi}_M}{\partial \overline{x}^k}\right) \\ &= n^i\overline{\mathcal{D}}_{I,i} = n^i\left(\left(\frac{e_{\text{typ}}U}{L\mathcal{D}_{\text{unit}}}\right)\overline{e}^{kl}_{i}\frac{\partial \overline{u}_{I,k}}{\partial \overline{x}^l} - \left(\frac{\epsilon_{\text{typ}}\Phi}{L\mathcal{D}_{\text{unit}}}\right)\overline{\epsilon}^{Sk}_{I,i}\frac{\partial \overline{\varphi}_I}{\partial \overline{x}^k}\right), \end{aligned} \tag{2.6.13}$$

along the interfaces between the two phases. We see that there are five dimensionless parameter groups, namely

$$\frac{\rho_{\text{typ}}L^2}{T^2c_{\text{typ}}}, \qquad \frac{\sigma_{\text{unit}}L}{c_{\text{typ}}U}, \qquad \frac{e_{\text{typ}}U}{\epsilon_{\text{typ}}\Phi}, \qquad \frac{\mathcal{D}_{\text{unit}}L}{\epsilon_{\text{typ}}\Phi}, \qquad \frac{e_{\text{typ}}\Phi}{c_{\text{typ}}U}. \tag{2.6.14}$$

Given one of Φ or U, we deduce the scalar for the other by setting

$$\frac{e_{\text{typ}}\Phi}{c_{\text{typ}}U} = 1. \tag{2.6.15}$$

We determine $T, \sigma_{\text{unit}}, \mathcal{D}_{\text{unit}}$ using

$$\frac{\rho_{\text{typ}} L^2}{T^2 c_{\text{typ}}} = 1, \tag{2.6.16}$$

$$\frac{\sigma_{\text{unit}} L}{c_{\text{typ}} U} = 1, \tag{2.6.17}$$

$$\frac{\mathcal{D}_{\text{unit}} L}{\epsilon_{\text{typ}} \Phi} = 1, \tag{2.6.18}$$

respectively. Thus

$$T = \sqrt{\frac{\rho_{\text{typ}}}{c_{\text{typ}}}} L, \tag{2.6.19}$$

$$\sigma_{\text{unit}} = \frac{c_{\text{typ}} U}{L}, \tag{2.6.20}$$

$$\mathcal{D}_{\text{unit}} = \frac{\epsilon_{\text{typ}} \Phi}{L}. \tag{2.6.21}$$

One dimensionless parameter remains, namely

$$S_p = \frac{e_{\text{typ}} U}{\epsilon_{\text{typ}} \Phi} = \frac{(e_{\text{typ}})^2}{\epsilon_{\text{typ}} c_{\text{typ}}}, \tag{2.6.22}$$

which we call the coupling coefficient. Thus dropping hats, (2.6.2)-(2.6.9) read as follows

$$\sigma_{M,ij} = c^{kl}_{M,ij} \frac{\partial u_{M,k}}{\partial x^l}, \tag{2.6.23}$$

$$\mathcal{D}_{M,i} = -\epsilon^{Sk}_{M,i} \frac{\partial \varphi_M}{\partial x^k}, \tag{2.6.24}$$

$$\rho_M \frac{\partial^2 u_{M,j}}{\partial t^2} = \frac{\partial \sigma_{M,ij}}{\partial x_i} = \frac{\partial}{\partial x_i} \left(c^{kl}_{M,ij} \frac{\partial u_{M,k}}{\partial x^l} \right), \tag{2.6.25}$$

$$0 = \frac{\partial \mathcal{D}_{M,i}}{\partial x_i} = \frac{\partial}{\partial x_i} \left(-\epsilon^{Sk}_{M,i} \frac{\partial \varphi_M}{\partial x^k} \right), \tag{2.6.26}$$

in the matrix phase, and

$$\sigma_{I,ij} = c^{kl}_{I,ij} \frac{\partial u_{I,k}}{\partial x^l} + e^k_{ij} \frac{\partial \varphi_I}{\partial x^k}, \tag{2.6.27}$$

$$\mathcal{D}_{I,i} = S_p e^{kl}_i \frac{\partial u_{I,k}}{\partial x^l} - \epsilon^{Sk}_{I,i} \frac{\partial \varphi_I}{\partial x^k}, \tag{2.6.28}$$

$$\rho_I \frac{\partial^2 u_{I,j}}{\partial t^2} = \frac{\partial \sigma_{I,ij}}{\partial x_i} = \frac{\partial}{\partial x_i} \left(c^{kl}_{I,ij} \frac{\partial u_{I,k}}{\partial x^l} + e^k_{ij} \frac{\partial \varphi_I}{\partial x^k} \right), \tag{2.6.29}$$

$$0 = \frac{\partial \mathcal{D}_{I,i}}{\partial x_i} = \frac{\partial}{\partial x_i} \left(S_p e^{kl}_i \frac{\partial u_{I,k}}{\partial x^l} - \epsilon^{Sk}_{I,i} \frac{\partial \varphi_I}{\partial x^k} \right), \tag{2.6.30}$$

in the inclusion phase, while continuity conditions (2.4.21)-(2.4.24) reduce to

$$u_{M,k} = u_{I,k}, \tag{2.6.31}$$

$$\varphi_M = \varphi_I, \tag{2.6.32}$$

$$n^i \sigma_{M,ij} = n^i \left(c^{kl}_{M,ij} \frac{\partial u_{M,k}}{\partial x^l} \right) = n^i \sigma_{I,ij} = n^i \left(c^{kl}_{I,ij} \frac{\partial u_{I,k}}{\partial x^l} + e^k_{ij} \frac{\partial \varphi_I}{\partial x^k} \right), \tag{2.6.33}$$

$$n^i \mathcal{D}_{M,i} = n^i \left(-\epsilon^{Sk}_{M,i} \frac{\partial \varphi_M}{\partial x^k} \right) = n^i \mathcal{D}_{I,i} = n^i \left(S_p e^{kl}_i \frac{\partial u_{I,k}}{\partial x^l} - \epsilon^{Sk}_{I,i} \frac{\partial \varphi_I}{\partial x^k} \right), \tag{2.6.34}$$

along the boundary of the interface between the two phases.

In the rest of this thesis, we will use the data contained in Table 2.1. We also choose $c_{\text{typ}} = \kappa_I = 97.2$ GPa, $e_{\text{typ}} = e_{33} = 19.3$ Cm^{-2} and $\epsilon_{\text{typ}} = \epsilon_{33} = 1700\epsilon_0$, where ϵ_0 is the permittivity of free space.

Material	Stycast	PZTA5
Type	Polymer matrix	Ceramic inclusion
λ (GPa)	5.1	74.6
μ (GPa)	3.3	22.6
κ (GPa)	8.4	97.2
e_{13} (Cm^{-2})	0	-5.3
e_{33} (Cm^{-2})	0	19.3
e_{51} (Cm^{-2})	0	0
ϵ_{33} (ϵ_0)	4	1700
ρ (kg/m^3)	1590	7750

Table 2.1: Material parameters for a polymer matrix and piezoelectric inclusion. Source: [4].

We calculate that for these materials, $S_p \approx 0.25$.

To close the model, we must combine (2.6.25), (2.6.26), (2.6.29), (2.6.30) and interface conditions (2.6.31)-(2.6.34) with initial conditions and macroscopic boundary conditions. These will depend on the particular scenario in question and we will return to these boundary conditions in Chapters 5 and 6.

2.7 Homogenisation

We now exploit the difference in size between the device length L and the distance between the inclusions ℓ, assuming that

$$\varepsilon = \frac{\ell}{L} \ll 1. \tag{2.7.1}$$

2.7.1 Asymptotic expansions to find the cell problems

In the device, $\boldsymbol{u}$ and φ satisfy equations (2.6.23)-(2.6.30) along with continuity conditions (2.6.31)-(2.6.34). We introduce the microscopic variable $\boldsymbol{X} = \frac{\boldsymbol{x}}{\varepsilon}$ and assume that all dependent variables vary with $\boldsymbol{x}$ and $\boldsymbol{X}$ independently. We assume regular asymptotic expansions in ε for $\boldsymbol{u}$ and φ. Such expansions are a standard assumption in classical homogenisation theory for periodic structures (see [8]).

$$\boldsymbol{u} = \boldsymbol{u}(t,\, \boldsymbol{x},\ \boldsymbol{X}) \sim \sum_{m=0}^{\infty} \boldsymbol{u}_{(m)}(t,\, \boldsymbol{x},\ \boldsymbol{X})\varepsilon^m, \tag{2.7.2}$$

$$\varphi = \varphi(t,\, \boldsymbol{x},\ \boldsymbol{X}) \sim \sum_{m=0}^{\infty} \varphi_{(m)}(t,\, \boldsymbol{x},\ \boldsymbol{X})\varepsilon^m. \tag{2.7.3}$$

We impose periodicity in $\boldsymbol{X}$ with period 1 where any non-periodic variation in $\boldsymbol{u}$ and φ is accounted for through the macroscopic variable $\boldsymbol{x}$. Due to this assumption we can restrict the domain of the microscopic variable $\boldsymbol{X}$ to be the unit torus $\Gamma = \mathbb{T}^3 = \mathbb{R}^3/\mathbb{Z}^3$, i.e. the unit cube $[0,1]^3$, with periodic boundary conditions imposed on opposite faces. This allows us to focus on the region around one inclusion. We denote $u_{(m)k}$ to mean the k^{th} entry of $\boldsymbol{u}_{(m)}$. Since $\boldsymbol{x}$ and $\boldsymbol{X}$ are being treated as independent variables, in accordance with the chain rule, the derivatives in the system defined in equations (2.6.23)-(2.6.34) are altered in the form

$$\frac{\partial}{\partial x_i} \to \frac{\partial}{\partial x_i} + \frac{1}{\varepsilon}\frac{\partial}{\partial X_i}. \tag{2.7.4}$$

We define $\Gamma_I = \Gamma \cap I$ and $\Gamma_M = \Gamma \cap M$. Using (2.7.4), equations (2.6.25) and (2.6.26) in the matrix phase yield

$$\begin{aligned}
\rho_M \frac{\partial^2 u_{M,j}}{\partial t^2} &= \frac{\partial \sigma_{M,ij}}{\partial x_i} + \varepsilon^{-1}\frac{\partial \sigma_{M,ij}}{\partial X_i} \\
&= \left(\frac{\partial}{\partial x_i} + \varepsilon^{-1}\frac{\partial}{\partial X_i}\right)\left(c^{kl}_{M,ij}\left(\frac{\partial u_{M,k}}{\partial x^l} + \varepsilon^{-1}\frac{\partial u_{M,k}}{\partial X^l}\right)\right), \qquad (2.7.5) \\
0 &= \frac{\partial \mathcal{D}_{M,i}}{\partial x_i} + \varepsilon^{-1}\frac{\partial \mathcal{D}_{M,i}}{\partial X_i} \\
&= \left(\frac{\partial}{\partial x_i} + \varepsilon^{-1}\frac{\partial}{\partial X_i}\right)\left(-\epsilon^{Sk}_{M,i}\left(\frac{\partial \varphi_M}{\partial x^k} + \varepsilon^{-1}\frac{\partial \varphi_M}{\partial X^k}\right)\right), \qquad (2.7.6)
\end{aligned}$$

while in the inclusion phase, equations (2.6.29) and (2.6.30) yield

$$\begin{aligned}\rho_I \frac{\partial^2 u_{I,j}}{\partial t^2} &= \frac{\partial \sigma_{I,ij}}{\partial x_i} + \varepsilon^{-1}\frac{\partial \sigma_{I,ij}}{\partial X_i} \\ &= \left(\frac{\partial}{\partial x_i} + \varepsilon^{-1}\frac{\partial}{\partial X_i}\right)\left(c^{kl}_{I,ij}\left(\frac{\partial u_{I,k}}{\partial x^l} + \varepsilon^{-1}\frac{\partial u_{I,k}}{\partial X^l}\right) + e^k_{ij}\left(\frac{\partial \varphi_I}{\partial x^k} + \varepsilon^{-1}\frac{\partial \varphi_I}{\partial X^k}\right)\right),\end{aligned} \tag{2.7.7}$$

$$\begin{aligned}0 &= \frac{\partial \mathcal{D}_{I,i}}{\partial x_i} + \varepsilon^{-1}\frac{\partial \mathcal{D}_{I,i}}{\partial X_i} \\ &= \left(\frac{\partial}{\partial x_i} + \varepsilon^{-1}\frac{\partial}{\partial X_i}\right)\left(S_p e^{kl}_i\left(\frac{\partial u_{I,k}}{\partial x^l} + \varepsilon^{-1}\frac{\partial u_{I,k}}{\partial X^l}\right) - \epsilon^{Sk}_{I,i}\left(\frac{\partial \varphi_I}{\partial x^k} + \varepsilon^{-1}\frac{\partial \varphi_I}{\partial X^k}\right)\right).\end{aligned} \tag{2.7.8}$$

The continuity conditions (2.6.31)-(2.6.34) hold on the boundary $\partial\Gamma_I \cap \partial\Gamma_M$, and read

$$u_{M,k} = u_{I,k}, \tag{2.7.9}$$

$$\varphi_M = \varphi_I, \tag{2.7.10}$$

$$\begin{aligned}n^i \sigma_{M,ij} &= n^i\left(c^{kl}_{M,ij}\left(\frac{\partial u_{M,k}}{\partial x^l} + \varepsilon^{-1}\frac{\partial u_{M,k}}{\partial X^l}\right)\right) \\ &= n^i \sigma_{I,ij} = n^i\left(c^{kl}_{I,ij}\left(\frac{\partial u_{I,k}}{\partial x^l} + \varepsilon^{-1}\frac{\partial u_{I,k}}{\partial X^l}\right) + e^k_{ij}\left(\frac{\partial \varphi_I}{\partial x^k} + \varepsilon^{-1}\frac{\partial \varphi_I}{\partial X^k}\right)\right),\end{aligned} \tag{2.7.11}$$

$$\begin{aligned}n^i \mathcal{D}_{M,i} &= n^i\left(-\epsilon^{Sk}_{M,i}\left(\frac{\partial \varphi_M}{\partial x^k} + \varepsilon^{-1}\frac{\partial \varphi_M}{\partial X^k}\right)\right) \\ &= n^i \mathcal{D}_{I,i} = n^i\left(S_p e^{kl}_i\left(\frac{\partial u_{I,k}}{\partial x^l} + \varepsilon^{-1}\frac{\partial u_{I,k}}{\partial X^l}\right) - \epsilon^{Sk}_{I,i}\left(\frac{\partial \varphi_I}{\partial x^k} + \varepsilon^{-1}\frac{\partial \varphi_I}{\partial X^k}\right)\right),\end{aligned} \tag{2.7.12}$$

We collect together terms involving similar powers of ε in (2.7.5) and (2.7.6) and then multiply both equations by ε^2 to get

$$\begin{aligned}&\varepsilon^2 \rho_M \frac{\partial^2 u_{M,j}}{\partial t^2} = \varepsilon^2 \frac{\partial \sigma_{M,ij}}{\partial x_i} + \varepsilon \frac{\partial \sigma_{M,ij}}{\partial X_i} = \left[\frac{\partial}{\partial X_i}\left(c^{kl}_{M,ij}\frac{\partial u_{M,k}}{\partial X^l}\right)\right] \\ &+ \varepsilon\left[\frac{\partial}{\partial X_i}\left(c^{kl}_{M,ij}\frac{\partial u_{M,k}}{\partial x^l}\right) + \frac{\partial}{\partial x_i}\left(c^{kl}_{M,ij}\frac{\partial u_{M,k}}{\partial X^l}\right)\right] + \varepsilon^2\left[\frac{\partial}{\partial x_i}\left(c^{kl}_{M,ij}\frac{\partial u_{M,k}}{\partial x^l}\right)\right],\end{aligned} \tag{2.7.13}$$

$$0 = \varepsilon^2 \frac{\partial \mathcal{D}_{M,i}}{\partial x_i} + \varepsilon \frac{\partial \mathcal{D}_{M,i}}{\partial X_i} = \left[\frac{\partial}{\partial X_i} \left(-\epsilon^{Sk}_{M,i} \frac{\partial \varphi_M}{\partial X^k} \right) \right]$$
$$+ \varepsilon \left[\frac{\partial}{\partial X_i} \left(-\epsilon^{Sk}_{M,i} \frac{\partial \varphi_M}{\partial x^k} \right) + \frac{\partial}{\partial x_i} \left(-\epsilon^{Sk}_{M,i} \frac{\partial \varphi_M}{\partial X^k} \right) \right] + \varepsilon^2 \left[\frac{\partial}{\partial x_i} \left(-\epsilon^{Sk}_{M,i} \frac{\partial \varphi_M}{\partial x^k} \right) \right], \quad (2.7.14)$$

in the matrix phase. We repeat the process for (2.7.7) and (2.7.8) to give

$$\varepsilon^2 \rho_I \frac{\partial^2 u_{I,j}}{\partial t^2} = \varepsilon^2 \frac{\partial \sigma_{I,ij}}{\partial x_i} + \varepsilon \frac{\partial \sigma_{I,ij}}{\partial X_i} = \left[\frac{\partial}{\partial X_i} \left(c^{kl}_{I,ij} \frac{\partial u_{I,k}}{\partial X^l} + e^k_{ij} \frac{\partial \varphi_I}{\partial X^k} \right) \right]$$
$$+ \varepsilon \left[\frac{\partial}{\partial X_i} \left(c^{kl}_{I,ij} \frac{\partial u_{I,k}}{\partial x^l} + e^k_{ij} \frac{\partial \varphi_I}{\partial x^k} \right) + \frac{\partial}{\partial x_i} \left(c^{kl}_{I,ij} \frac{\partial u_{I,k}}{\partial X^l} + e^k_{ij} \frac{\partial \varphi_I}{\partial X^k} \right) \right]$$
$$+ \varepsilon^2 \left[\frac{\partial}{\partial x_i} \left(c^{kl}_{I,ij} \frac{\partial u_{I,k}}{\partial x^l} + e^k_{ij} \frac{\partial \varphi_I}{\partial x^k} \right) \right], \quad (2.7.15)$$

$$0 = \varepsilon^2 \frac{\partial \mathcal{D}_{I,i}}{\partial x_i} + \varepsilon \frac{\partial \mathcal{D}_{I,i}}{\partial X_i} = \left[\frac{\partial}{\partial X_i} \left(S_p e^{kl}_i \frac{\partial u_{I,k}}{\partial X^l} - \epsilon^{Sk}_{I,i} \frac{\partial \varphi_I}{\partial X^k} \right) \right]$$
$$+ \varepsilon \left[\frac{\partial}{\partial X_i} \left(S_p e^{kl}_i \frac{\partial u_{I,k}}{\partial x^l} - \epsilon^{Sk}_{I,i} \frac{\partial \varphi_I}{\partial x^k} \right) + \frac{\partial}{\partial x_i} \left(S_p e^{kl}_i \frac{\partial u_{I,k}}{\partial X^l} - \epsilon^{Sk}_{I,i} \frac{\partial \varphi_I}{\partial X^k} \right) \right]$$
$$+ \varepsilon^2 \left[\frac{\partial}{\partial x_i} \left(S_p e^{kl}_i \frac{\partial u_{I,k}}{\partial x^l} - \epsilon^{Sk}_{I,i} \frac{\partial \varphi_I}{\partial x^k} \right) \right], \quad (2.7.16)$$

in the inclusion phase. Similarly (2.7.9)-(2.7.12) yield

$$u_{M,k} = u_{I,k}, \quad (2.7.17)$$
$$\varphi_M = \varphi_I, \quad (2.7.18)$$

$$\varepsilon n^i \sigma_{M,ij} = n^i \left(c^{kl}_{M,ij} \frac{\partial u_{M,k}}{\partial X^l} \right) + \varepsilon n^i \left(c^{kl}_{M,ij} \frac{\partial u_{M,k}}{\partial x^l} \right)$$
$$= \varepsilon n^i \sigma_{I,ij} = n^i \left(c^{kl}_{I,ij} \frac{\partial u_{I,k}}{\partial X^l} + e^k_{ij} \frac{\partial \varphi_I}{\partial X^k} \right) + \varepsilon n^i \left(c^{kl}_{I,ij} \frac{\partial u_{I,k}}{\partial x^l} + e^k_{ij} \frac{\partial \varphi_I}{\partial x^k} \right), \quad (2.7.19)$$

$$\varepsilon n^i \mathcal{D}_{M,i} = n^i \left(-\epsilon^{Sk}_{M,i} \frac{\partial \varphi_M}{\partial X^k} \right) + \varepsilon n^i \left(-\epsilon^{Sk}_{M,i} \frac{\partial \varphi_M}{\partial x^k} \right)$$
$$= \varepsilon n^i \mathcal{D}_{I,i} = n^i \left(S_p e^{kl}_i \frac{\partial u_{I,k}}{\partial X^l} - \epsilon^{Sk}_{I,i} \frac{\partial \varphi_I}{\partial X^k} \right) + \varepsilon n^i \left(S_p e^{kl}_i \frac{\partial u_{I,k}}{\partial x^l} - \epsilon^{Sk}_{I,i} \frac{\partial \varphi_I}{\partial x^k} \right), \quad (2.7.20)$$

along the boundary of the interface between the two phases.

We expand the dependent variables as asymptotic series of the forms given in

(2.7.2) and (2.7.3). The leading-order versions of (2.7.13) and (2.7.14) are

$$\frac{\partial}{\partial X_i}\left(c^{kl}_{M,ij}\frac{\partial u_{M,(0)k}}{\partial X^l}\right) = 0_j, \tag{2.7.21}$$

$$\frac{\partial}{\partial X_i}\left(-\epsilon^{Sk}_{M,i}\frac{\partial \varphi_{M,(0)}}{\partial X^k}\right) = 0, \tag{2.7.22}$$

in the matrix phase, where 0_j is the j^{th} component of the zero-vector. The leading-order versions of (2.7.15) and (2.7.16) are

$$\frac{\partial}{\partial X_i}\left(c^{kl}_{I,ij}\frac{\partial u_{I,(0)k}}{\partial X^l} + e^{k}_{ij}\frac{\partial \varphi_{I,(0)}}{\partial X^k}\right) = 0_j, \tag{2.7.23}$$

$$\frac{\partial}{\partial X_i}\left(S_p e^{kl}_{i}\frac{\partial u_{I,(0)k}}{\partial X^l} - \epsilon^{Sk}_{I,i}\frac{\partial \varphi_{I,(0)}}{\partial X^k}\right) = 0, \tag{2.7.24}$$

in the inclusion phase, while the leading-order versions of (2.7.17)-(2.7.20) are

$$u_{M,(0)k} = u_{I,(0)k}, \tag{2.7.25}$$

$$\varphi_{M,(0)} = \varphi_{I,(0)}, \tag{2.7.26}$$

$$n^i\left(c^{kl}_{M,ij}\frac{\partial u_{M,(0)k}}{\partial X^l}\right) = n^i\left(c^{kl}_{I,ij}\frac{\partial u_{I,(0)k}}{\partial X^l} + e^{k}_{ij}\frac{\partial \varphi_{I,(0)}}{\partial X^k}\right), \tag{2.7.27}$$

$$n^i\left(-\epsilon^{Sk}_{M,i}\frac{\partial \varphi_{M,(0)}}{\partial X^k}\right) = n^i\left(S_p e^{kl}_{i}\frac{\partial u_{I,(0)k}}{\partial X^l} - \epsilon^{Sk}_{I,i}\frac{\partial \varphi_{I,(0)}}{\partial X^k}\right), \tag{2.7.28}$$

along the boundary of the interface between the two phases. Using (2.7.21)-(2.7.24), which hold pointwise in the matrix and inclusion phases, we deduce the following identity

$$\begin{aligned}
-\iiint_{\Gamma_M}\frac{\partial}{\partial X_i}\left(c^{kl}_{M,ij}\frac{\partial u_{M,(0)k}}{\partial X^l}\right)u^j_{M,(0)}\mathrm{d}V \\
+\frac{1}{S_p}\iiint_{\Gamma_M}\frac{\partial}{\partial X_i}\left(-\epsilon^{Sk}_{M,i}\frac{\partial \varphi_{M,(0)}}{\partial X^k}\right)\varphi_{M,(0)}\mathrm{d}V \\
-\iiint_{\Gamma_I}\frac{\partial}{\partial X_i}\left(c^{kl}_{I,ij}\frac{\partial u_{I,(0)k}}{\partial X^l} + e^{k}_{ij}\frac{\partial \varphi_{I,(0)}}{\partial X^k}\right)u^j_{I,(0)}\mathrm{d}V \\
+\frac{1}{S_p}\iiint_{\Gamma_I}\frac{\partial}{\partial X_i}\left(S_p e^{kl}_{i}\frac{\partial u_{I,(0)k}}{\partial X^l} - \epsilon^{Sk}_{I,i}\frac{\partial \varphi_{I,(0)}}{\partial X^k}\right)\varphi_{I,(0)}\mathrm{d}V = 0.
\end{aligned} \tag{2.7.29}$$

Here $\mathrm{d}V$ denotes integrating with respect to the microscopic variable $\boldsymbol{X}$. Using the Divergence Theorem along with continuity conditions (2.7.25)-(2.7.28), equation

(2.7.29) simplifies to

$$\iiint_{\Gamma_M}\left(c^{kl}_{M,ij}\frac{\partial u_{M,(0)k}}{\partial X^l}\frac{\partial u^j_{M,(0)}}{\partial X_i}+\frac{1}{S_p}\epsilon^{Sk}_{M,i}\frac{\partial\varphi_{M,(0)}}{\partial X^k}\frac{\partial\varphi_{M,(0)}}{\partial X_i}\right)\mathrm{d}V$$
$$+\iiint_{\Gamma_I}\left(c^{kl}_{I,ij}\frac{\partial u_{I,(0)k}}{\partial X^l}\frac{\partial u^j_{I,(0)}}{\partial X_i}+\frac{1}{S_p}\epsilon^{Sk}_{I,i}\frac{\partial\varphi_{I,(0)}}{\partial X^k}\frac{\partial\varphi_{I,(0)}}{\partial X_i}\right)\mathrm{d}V=0. \quad (2.7.30)$$

We use inequalities (B.0.1) and (B.0.3) established in Appendix B to deduce that

$$\Lambda_1\left[\iiint_{\mathbb{T}^3}\sum_{ij}\left|\frac{\left(\nabla_{\boldsymbol{X}}\boldsymbol{u}_{(0)}\right)_{ij}+\left(\nabla_{\boldsymbol{X}}\boldsymbol{u}_{(0)}\right)_{ji}}{2}\right|^2\mathrm{d}V\right]+\frac{\Lambda_2}{S_p}\left[\iiint_{\mathbb{T}^3}\sum_i\left|\left(\nabla_{\boldsymbol{X}}\varphi_{(0)}\right)_i\right|^2\mathrm{d}V\right]\leq 0, \quad (2.7.31)$$

where $\nabla_{\boldsymbol{X}}$ represents taking the gradient with respect to the microscopic coordinates, and $\Lambda_1,\Lambda_2>0$ are the ellipticity constants defined in Appendix B. This convention extends to any additional variables, with subscripts indicating the variable of differentiation. Since both terms in (2.7.31) are non-negative, it follows they must be individually equal to zero. Thus we deduce

$$\nabla_{\boldsymbol{X}}\boldsymbol{u}_{(0)}+\left(\nabla_{\boldsymbol{X}}\boldsymbol{u}_{(0)}\right)^{\mathrm{Tr}}=\boldsymbol{0}\Rightarrow\ \boldsymbol{u}_{(0)}\text{ is a rigid body motion,} \quad (2.7.32)$$
$$\nabla_{\boldsymbol{X}}\varphi_{(0)}=\boldsymbol{0}\Rightarrow\varphi_{(0)}\text{ only depends on }t\text{ and }\boldsymbol{x}. \quad (2.7.33)$$

If we let

$$\boldsymbol{U}_{(0)}(t,\boldsymbol{x})=\iiint_{\mathbb{T}^3}\boldsymbol{u}_{(0)}(t,\boldsymbol{x},\boldsymbol{X})\,\mathrm{d}V, \quad (2.7.34)$$

we deduce that

$$\nabla_{\boldsymbol{X}}\left(\boldsymbol{u}_{(0)}-\boldsymbol{U}_{(0)}\right)+\left(\nabla_{\boldsymbol{X}}\left(\boldsymbol{u}_{(0)}-\boldsymbol{U}_{(0)}\right)\right)^{\mathrm{Tr}}=\boldsymbol{0}, \quad (2.7.35)$$

since $\boldsymbol{U}_{(0)}$ is independent of $\boldsymbol{X}$. From Korn's Inequality [43] we conclude that

$$\boldsymbol{u}_{(0)}(t,\boldsymbol{x},\boldsymbol{X})-\boldsymbol{U}_{(0)}(t,\boldsymbol{x})=\boldsymbol{0}\iff\boldsymbol{u}_{(0)}=\boldsymbol{U}_{(0)}(t,\boldsymbol{x})\text{ is only dependent on }t\text{ and }\boldsymbol{x}. \quad (2.7.36)$$

Equating $O(\varepsilon)$ coefficients in (2.7.13)-(2.7.16) and using the fact that $\boldsymbol{u}_{(0)}$ and $\varphi_{(0)}$ are independent of $\boldsymbol{X}$, we find that

$$\frac{\partial}{\partial X_i}\left(c^{kl}_{M,ij}\frac{\partial u_{M,(1)k}}{\partial X^l}\right)=0_j, \quad (2.7.37)$$
$$\frac{\partial}{\partial X_i}\left(-\epsilon^{Sk}_{M,i}\frac{\partial\varphi_{M,(1)}}{\partial X^k}\right)=0, \quad (2.7.38)$$

in the matrix phase, and

$$\frac{\partial}{\partial X_i}\left(c^{kl}_{I,ij}\frac{\partial u_{I,(1)k}}{\partial X^l}+e^k_{ij}\frac{\partial \varphi_{I,(1)}}{\partial X^k}\right)=0_j, \tag{2.7.39}$$

$$\frac{\partial}{\partial X_i}\left(S_p e^{kl}_i\frac{\partial u_{I,(1)k}}{\partial X^l}-\epsilon^{Sk}_{I,i}\frac{\partial \varphi_{I,(1)}}{\partial X^k}\right)=0, \tag{2.7.40}$$

in the inclusion phase. Equating $O(\varepsilon)$ coefficients in (2.7.17)-(2.7.20) yields the following continuity conditions

$$u_{M,(1)k}=u_{I,(1)k}, \tag{2.7.41}$$

$$\varphi_{M,(1)}=\varphi_{I,(1)}, \tag{2.7.42}$$

$$n^i\left[c^{kl}_{M,ij}\left(\frac{\partial u_{M,(1)k}}{\partial X^l}+\frac{\partial u_{(0)k}}{\partial x^l}\right)\right]=n^i\left[c^{kl}_{I,ij}\left(\frac{\partial u_{I,(1)k}}{\partial X^l}+\frac{\partial u_{(0)k}}{\partial x^l}\right)+e^k_{ij}\left(\frac{\partial \varphi_{I,(1)}}{\partial X^k}+\frac{\partial \varphi_{(0)}}{\partial x^k}\right)\right], \tag{2.7.43}$$

$$n^i\left[-\epsilon^{Sk}_{M,i}\left(\frac{\partial \varphi_{M,(1)}}{\partial X^k}+\frac{\partial \varphi_{(0)}}{\partial x^k}\right)\right]=n^i\left[S_p e^{kl}_i\left(\frac{\partial u_{I,(1)k}}{\partial X^l}+\frac{\partial u_{(0)k}}{\partial x^l}\right)-\epsilon^{Sk}_{I,i}\left(\frac{\partial \varphi_{I,(1)}}{\partial X^k}+\frac{\partial \varphi_{(0)}}{\partial x^k}\right)\right], \tag{2.7.44}$$

on the boundary between the two interfaces. Our aim is to derive an ansatz that reduces (2.7.37)-(2.7.44) to equations that only involve the microscale variable $\boldsymbol{X}$. This will enable us to solve the system defined by (2.7.37)-(2.7.44) numerically, irrespective of macroscale position $\boldsymbol{x}$. We note that $\boldsymbol{u}_{(1)}$ and $\varphi_{(1)}$ are the unknowns which we need to find. Since both equations are PDEs in the microscopic variable $\boldsymbol{X}$, both $\partial u_{(0)k}/\partial x^l$ and $\partial \varphi_{(0)}/\partial x^k$ may be treated as constants. Furthermore, due to the linearity of (2.7.37)-(2.7.40) and the linearity of the boundary conditions (2.7.41)-(2.7.44), we may solve separately for the particular solutions due to $\partial u_{(0)k}/\partial x^l$ and $\partial \varphi_{(0)}/\partial x^k$, and then add the results. Continuity conditions (2.7.43) and (2.7.44) rearrange to give

$$n^i\left[c^{kl}_{M,ij}\frac{\partial u_{M,(1)k}}{\partial X^l}-\left(c^{kl}_{I,ij}\frac{\partial u_{I,(1)k}}{\partial X^l}+e^k_{ij}\frac{\partial \varphi_{I,(1)}}{\partial X^k}\right)\right] = n^i\left[\left(c^{kl}_{I,ij}-c^{kl}_{M,ij}\right)\frac{\partial u_{(0)k}}{\partial x^l}+e^k_{ij}\frac{\partial \varphi_{(0)}}{\partial x^k}\right], \tag{2.7.45}$$

$$n^i \left[-\epsilon^{Sk}_{M,i} \frac{\partial \varphi_{M,(1)}}{\partial X^k} - \left(S_p e^{kl}_i \frac{\partial u_{I,(1)k}}{\partial X^l} - \epsilon^{Sk}_{I,i} \frac{\partial \varphi_{I,(1)}}{\partial X^k} \right) \right] = n^i \left[S_p e^{kl}_i \frac{\partial u_{(0)k}}{\partial x^l} + \left(\epsilon^{Sk}_{M,i} - \epsilon^{Sk}_{I,i} \right) \frac{\partial \varphi_{(0)}}{\partial x^k} \right]. \quad (2.7.46)$$

Firstly, we consider the case where the right hand sides (RHS) of (2.7.45) and (2.7.46) are purely *mechanically* driven, meaning we keep the terms with $\partial u_{(0)k}/\partial x^l$ and remove the terms with $\partial \varphi_{(0)}/\partial x^l$. Thus (2.7.45) and (2.7.46) yield

$$n^i \left[\left(c^{kl}_{M,ij} \frac{\partial u_{M,(1)k}}{\partial X^l} \right) - \left(c^{kl}_{I,ij} \frac{\partial u_{I,(1)k}}{\partial X^l} + e^k_{ij} \frac{\partial \varphi_{I,(1)}}{\partial X^k} \right) \right] = n^i \left(c^{kl}_{I,ij} - c^{kl}_{M,ij} \right) \frac{\partial u_{(0)k}}{\partial x^l}, \quad (2.7.47)$$

$$n^i \left[\left(-\epsilon^{Sk}_{M,i} \frac{\partial \varphi_{M,(1)}}{\partial X^k} \right) - \left(S_p e^{kl}_i \frac{\partial u_{I,(1)k}}{\partial X^l} - \epsilon^{Sk}_{I,i} \frac{\partial \varphi_{I,(1)}}{\partial X^k} \right) \right] = n^i S_p e^{kl}_i \frac{\partial u_{(0)k}}{\partial x^l}. \quad (2.7.48)$$

We pose the ansatzes

$$u_{(1)k}(t, \boldsymbol{x}, \boldsymbol{X}) = \frac{\partial u_{(0)a}}{\partial x^b}(t, \boldsymbol{x}) \Psi^{ab}_k(\boldsymbol{X}), \quad (2.7.49)$$

$$\varphi_{(1)}(t, \boldsymbol{x}, \boldsymbol{X}) = \frac{\partial u_{(0)a}}{\partial x^b}(t, \boldsymbol{x}) \psi^{ab}(\boldsymbol{X}). \quad (2.7.50)$$

After substituting (2.7.49) and (2.7.50) into (2.7.37)-(2.7.40) and continuity conditions (2.7.41), (2.7.42), (2.7.47) and (2.7.48), each term in each equation and continuity condition can be written as a product of the macroscopic derivative $\partial u_{(0)a}/\partial x^b$ and a function depending only on the microscopic variable $\boldsymbol{X}$. Since the macroscopic derivatives $\partial u_{(0)a}/\partial x^b$ are independent, they can independently be set to zero. We are therefore left with equations for Ψ^{ab}_k and ψ^{ab} that only involve the microscopic variable $\boldsymbol{X}$, namely

$$\frac{\partial}{\partial X_i} \left(c^{kl}_{M,ij} \frac{\partial \Psi^{ab}_{M,k}}{\partial X^l} \right) = 0_j, \quad (2.7.51)$$

$$\frac{\partial}{\partial X_i} \left(-\epsilon^{Sk}_{M,i} \frac{\partial \psi^{ab}_M}{\partial X^k} \right) = 0, \quad (2.7.52)$$

in the matrix phase, and

$$\frac{\partial}{\partial X_i}\left(c^{kl}_{I,ij}\frac{\partial \Psi^{ab}_{I,k}}{\partial X^l}+e^k_{ij}\frac{\partial \psi^{ab}_I}{\partial X^k}\right)=0_j, \tag{2.7.53}$$

$$\frac{\partial}{\partial X_i}\left(S_p e^{kl}_i\frac{\partial \Psi^{ab}_{I,k}}{\partial X^l}-\epsilon^{Sk}_{I,i}\frac{\partial \psi^{ab}_I}{\partial X^k}\right)=0, \tag{2.7.54}$$

in the inclusion phase, while satisfying the continuity conditions

$$\Psi^{ab}_{M,k}=\Psi^{ab}_{I,k}, \tag{2.7.55}$$

$$\psi^{ab}_M=\psi^{ab}_I, \tag{2.7.56}$$

$$n^i\left[\left(c^{kl}_{M,ij}\frac{\partial \Psi^{ab}_{M,k}}{\partial X^l}\right)-\left(c^{kl}_{I,ij}\frac{\partial \Psi^{ab}_{I,k}}{\partial X^l}+e^k_{ij}\frac{\partial \psi^{ab}_I}{\partial X^k}\right)\right]=n^i\left(c^{ab}_{I,ij}-c^{ab}_{M,ij}\right), \tag{2.7.57}$$

$$n^i\left[\left(-\epsilon^{Sk}_{M,i}\frac{\partial \psi^{ab}_M}{\partial X^k}\right)-\left(S_p e^{kl}_i\frac{\partial \Psi^{ab}_{I,k}}{\partial X^l}-\epsilon^{Sk}_{I,i}\frac{\partial \psi^{ab}_I}{\partial X^k}\right)\right]=n^i S_p e^{ab}_i, \tag{2.7.58}$$

which hold on the boundary $\partial\Gamma_I\cap\partial\Gamma_M$. Furthermore, Ψ^{ab}_k and ψ^{ab} satisfy periodic boundary conditions on the edges of the cell. For each $a,b\in\{1,2,3\}$, $\boldsymbol{\Psi}^{ab}$ and ψ^{ab} represent the response to a unit macroscopic strain applied in the ab-direction. We will apply a similar argument for when the RHS of (2.7.45) and (2.7.46) are purely *electrically* driven, meaning we keep the terms with $\partial\varphi_{(0)}/\partial x^k$ and remove the terms with $\partial u_{(0)k}/\partial x^l$. Thus (2.7.45) and (2.7.46) yield

$$n^i\left[\left(c^{kl}_{M,ij}\frac{\partial u_{M,(1)k}}{\partial X^l}\right)-\left(c^{kl}_{I,ij}\frac{\partial u_{I,(1)k}}{\partial X^l}+e^k_{ij}\frac{\partial \varphi_{I,(1)}}{\partial X^k}\right)\right]=n^i e^k_{ij}\frac{\partial \varphi_{(0)}}{\partial x^k}, \tag{2.7.59}$$

$$n^i\left[\left(-\epsilon^{Sk}_{M,i}\frac{\partial \varphi_{M,(1)}}{\partial X^k}\right)-\left(S_p e^{kl}_i\frac{\partial u_{I,(1)k}}{\partial X^l}-\epsilon^{Sk}_{I,i}\frac{\partial \varphi_{I,(1)}}{\partial X^k}\right)\right]=n^i\left(\epsilon^{Sk}_{M,i}-\epsilon^{Sk}_{I,i}\right)\frac{\partial \varphi_{(0)}}{\partial x^k}. \tag{2.7.60}$$

We make the ansatzes

$$u_{(1)k}(t,\,\boldsymbol{x},\,\boldsymbol{X})=\frac{\partial \varphi_{(0)}}{\partial x^f}(t,\,\boldsymbol{x})\Phi^f_k(\boldsymbol{X}), \tag{2.7.61}$$

$$\varphi_{(1)}(t,\,\boldsymbol{x},\,\boldsymbol{X})=\frac{\partial \varphi_{(0)}}{\partial x^f}(t,\,\boldsymbol{x})\phi^f(\boldsymbol{X}). \tag{2.7.62}$$

Substituting (2.7.61) and (2.7.62) into (2.7.37)-(2.7.40) and into continuity conditions (2.7.41), (2.7.42), (2.7.59) and (2.7.60), each term in each equation and continuity condition can be written as a product of the macroscopic derivative $\partial\varphi_{(0)}/\partial x^f$ and a function depending only on the microscopic variable $\boldsymbol{X}$. Once again, as the macroscopic derivatives $\partial\varphi_{(0)}/\partial x^f$ are independent, they can independently be set

to zero. We are left with equations for Φ_k^f and ϕ^f which only involve the microscopic variable $\boldsymbol{X}$, namely

$$\frac{\partial}{\partial X_i}\left(c_{M,ij}^{kl}\frac{\partial \Phi_{M,k}^f}{\partial X^l}\right) = 0_j, \tag{2.7.63}$$

$$\frac{\partial}{\partial X_i}\left(-\epsilon_{M,i}^{Sk}\frac{\partial \phi_M^f}{\partial X^k}\right) = 0, \tag{2.7.64}$$

in the matrix phase, and

$$\frac{\partial}{\partial X_i}\left(c_{I,ij}^{kl}\frac{\partial \Phi_{I,k}^f}{\partial X^l} + e_{ij}^k\frac{\partial \phi_I^f}{\partial X^k}\right) = 0_j, \tag{2.7.65}$$

$$\frac{\partial}{\partial X_i}\left(S_p e_i^{kl}\frac{\partial \Phi_{I,k}^f}{\partial X^l} - \epsilon_{I,i}^{Sk}\frac{\partial \phi_I^f}{\partial X^k}\right) = 0, \tag{2.7.66}$$

in the inclusion phase, while satisfying the following continuity conditions

$$\Phi_{M,k}^f = \Phi_{I,k}^f, \tag{2.7.67}$$

$$\phi_M^f = \phi_I^f, \tag{2.7.68}$$

$$n^i\left[\left(c_{M,ij}^{kl}\frac{\partial \Phi_{M,k}^f}{\partial X^l}\right) - \left(c_{I,ij}^{kl}\frac{\partial \Phi_{I,k}^f}{\partial X^l} + e_{ij}^k\frac{\partial \phi_I^f}{\partial X^k}\right)\right] = n^i e_{ij}^f, \tag{2.7.69}$$

$$n^i\left[\left(-\epsilon_{M,i}^{Sk}\frac{\partial \phi_M^f}{\partial X^k}\right) - \left(S_p e_i^{kl}\frac{\partial \Phi_{I,k}^f}{\partial X^l} - \epsilon_{I,i}^{Sk}\frac{\partial \phi_I^f}{\partial X^k}\right)\right] = n^i\left(\epsilon_{M,i}^{Sf} - \epsilon_{I,i}^{Sf}\right). \tag{2.7.70}$$

Furthermore Φ_k^f and ϕ^f satisfy periodic boundary conditions on the edges of the cell. For each $f \in \{1,2,3\}$, $\boldsymbol{\Phi}^f$ and ϕ^f represent the response to a unit electric field applied in the negative f-direction. Since (2.7.37)-(2.7.40) are linear, the general solutions for $\boldsymbol{u}_{(1)}$ and $\varphi_{(1)}$ are of the form

$$u_{(1)k}(t,\,\boldsymbol{x},\boldsymbol{X}) = \eta_{(1)k}(t,\;\boldsymbol{x}) + \frac{\partial u_{(0)a}}{\partial x^b}(t,\,\boldsymbol{x})\Psi_k^{ab}(\boldsymbol{X}) + \frac{\partial \varphi_{(0)}}{\partial x^f}(t,\,\boldsymbol{x})\Phi_k^f(\boldsymbol{X}), \tag{2.7.71}$$

$$\varphi_{(1)}(t,\,\boldsymbol{x},\boldsymbol{X}) = \Theta_{(1)}(t,\boldsymbol{x}) + \frac{\partial u_{(0)a}}{\partial x^b}(t,\,\boldsymbol{x})\psi^{ab}(\boldsymbol{X}) + \frac{\partial \varphi_{(0)}}{\partial x^f}(t,\,\boldsymbol{x})\phi^f(\boldsymbol{X}), \tag{2.7.72}$$

where $\boldsymbol{\eta}_{(1)}$ and $\Theta_{(1)}$ are arbitrary functions of t and $\boldsymbol{x}$. The problems defined by the systems (2.7.51)-(2.7.54) and (2.7.63)-(2.7.66), the respective continuity conditions (2.7.55)-(2.7.58) and (2.7.67)-(2.7.70), together with the periodic boundary conditions, are known as the cell problems. These play a crucial role in determining homogenised material parameters, namely the effective stiffness tensor $\boldsymbol{c}_{\text{eff}}$, the effective electromechanical tensor $\boldsymbol{e}_{\text{eff}}$ and the effective dielectric tensor $\boldsymbol{\epsilon}_{\text{eff}}$. The cell

problems may be solved numerically using the weak formulations given in Appendix C, implemented using the finite element library FEniCS and solved with a GMRES iterative solver.

2.7.2 Macroscale equations and effective coefficients

The $O(\varepsilon^2)$ versions of (2.7.13)-(2.7.16) are

$$\rho_M \frac{\partial^2 u_{M,(0)j}}{\partial t^2} = \frac{\partial}{\partial x_i}\left(c^{kl}_{M,ij}\left(\frac{\partial u_{M,(1)k}}{\partial X^l} + \frac{\partial u_{(0)k}}{\partial x^l}\right)\right) + \frac{\partial}{\partial X_i}\left(c^{kl}_{M,ij}\left(\frac{\partial u_{M,(2)k}}{\partial X^l} + \frac{\partial u_{M,(1)k}}{\partial x^l}\right)\right), \tag{2.7.73}$$

$$0 = \frac{\partial}{\partial x_i}\left(-\epsilon^{Sk}_{M,i}\left(\frac{\partial \varphi_{M,(1)}}{\partial X^k} + \frac{\partial \varphi_{(0)}}{\partial x^k}\right)\right) + \frac{\partial}{\partial X_i}\left(-\epsilon^{Sk}_{M,i}\left(\frac{\partial \varphi_{M,(2)}}{\partial X^k} + \frac{\partial \varphi_{M,(1)}}{\partial x^k}\right)\right), \tag{2.7.74}$$

in the matrix phase, and

$$\rho_I \frac{\partial^2 u_{I,(0)j}}{\partial t^2} = \frac{\partial}{\partial x_i}\left(c^{kl}_{I,ij}\left(\frac{\partial u_{I,(1)k}}{\partial X^l} + \frac{\partial u_{(0)k}}{\partial x^l}\right) + e^k_{ij}\left(\frac{\partial \varphi_{I,(1)}}{\partial X^k} + \frac{\partial \varphi_{(0)}}{\partial x^k}\right)\right) + \frac{\partial}{\partial X_i}\left(c^{kl}_{I,ij}\left(\frac{\partial u_{I,(2)k}}{\partial X^l} + \frac{\partial u_{I,(1)k}}{\partial x^l}\right) + e^k_{ij}\left(\frac{\partial \varphi_{I,(2)}}{\partial X^k} + \frac{\partial \varphi_{I,(1)}}{\partial x^k}\right)\right), \tag{2.7.75}$$

$$0 = \frac{\partial}{\partial x_i}\left(S_p e^{kl}_i\left(\frac{\partial u_{I,(1)k}}{\partial X^l} + \frac{\partial u_{(0)k}}{\partial x^l}\right) - \epsilon^{Sk}_{I,i}\left(\frac{\partial \varphi_{I,(1)}}{\partial X^k} + \frac{\partial \varphi_{(0)}}{\partial x^k}\right)\right) + \frac{\partial}{\partial X_i}\left(S_p e^{kl}_i\left(\frac{\partial u_{I,(2)k}}{\partial X^l} + \frac{\partial u_{I,(1)k}}{\partial x^l}\right) - \epsilon^{Sk}_{I,i}\left(\frac{\partial \varphi_{I,(2)}}{\partial X^k} + \frac{\partial \varphi_{I,(1)}}{\partial x^k}\right)\right), \tag{2.7.76}$$

in the inclusion phase.

The $O(\varepsilon^2)$ terms in (2.7.17)-(2.7.20) are

$$u_{M,(2)k} = u_{I,(2)k}, \tag{2.7.77}$$

$$\varphi_{M,(2)} = \varphi_{I,(2)}, \tag{2.7.78}$$

$$n^i\left(c^{kl}_{M,ij}\left(\frac{\partial u_{M,(1)k}}{\partial x^l} + \frac{\partial u_{M,(2)k}}{\partial X^l}\right)\right) = n^i\left(c^{kl}_{I,ij}\left(\frac{\partial u_{I,(1)k}}{\partial x^l} + \frac{\partial u_{I,(2)k}}{\partial X^l}\right) + e^k_{ij}\left(\frac{\partial \varphi_{I,(1)}}{\partial x^k} + \frac{\partial \varphi_{I,(2)}}{\partial X^k}\right)\right), \tag{2.7.79}$$

$$n^i \left(-\epsilon_{M,i}^{Sk} \left(\frac{\partial \varphi_{M,(1)}}{\partial x^k} + \frac{\partial \varphi_{M,(2)}}{\partial X^k} \right) \right)$$
$$= n^i \left(S_p e_i^{kl} \left(\frac{\partial u_{I,(1)k}}{\partial x^l} + \frac{\partial u_{I,(2)k}}{\partial X^l} \right) - \epsilon_{I,i}^{Sk} \left(\frac{\partial \varphi_{I,(1)}}{\partial x^k} + \frac{\partial \varphi_{I,(2)}}{\partial X^k} \right) \right), \quad (2.7.80)$$

along $\partial\Gamma_I$. We integrate (2.7.73) and (2.7.74) over Γ_M and (2.7.75) and (2.7.76) over Γ_I with respect to $\boldsymbol{X}$. Applying the Divergence Theorem, periodicity and the continuity conditions (2.7.77)-(2.7.80) and then substituting the ansatzes for $\boldsymbol{u}_{(1)}$ and $\varphi_{(1)}$ from (2.7.71) and (2.7.72) yields

$$\left(\iiint_{\Gamma_M} \rho_M \mathrm{d}V + \iiint_{\Gamma_I} \rho_I \mathrm{d}V \right) \frac{\partial^2 u_{(0)j}}{\partial t^2}$$
$$= \frac{\partial}{\partial x_i} \left(\iiint_{\Gamma_M} c_{M,ij}^{kl} \left(\frac{\partial u_{M,(1)k}}{\partial X^l} + \frac{\partial u_{(0)k}}{\partial x^l} \right) \mathrm{d}V \right)$$
$$+ \frac{\partial}{\partial x_i} \left(\iiint_{\Gamma_I} c_{I,ij}^{kl} \left(\frac{\partial u_{I,(1)k}}{\partial X^l} + \frac{\partial u_{(0)k}}{\partial x^l} \right) + e_{ij}^k \left(\frac{\partial \varphi_{I,(1)}}{\partial X^k} + \frac{\partial \varphi_{(0)}}{\partial x^k} \right) \mathrm{d}V \right), \quad (2.7.81)$$
$$0 = \frac{\partial}{\partial x_i} \left(\iiint_{\Gamma_M} -\epsilon_{M,i}^{Sk} \left(\frac{\partial \varphi_{M,(1)}}{\partial X^k} + \frac{\partial \varphi_{(0)}}{\partial x^k} \right) \mathrm{d}V \right)$$
$$+ \frac{\partial}{\partial x_i} \left(\iiint_{\Gamma_I} S_p e_i^{kl} \left(\frac{\partial u_{I,(1)k}}{\partial X^l} + \frac{\partial u_{(0)k}}{\partial x^l} \right) - \epsilon_{I,i}^{Sk} \left(\frac{\partial \varphi_{I,(1)}}{\partial X^k} + \frac{\partial \varphi_{(0)}}{\partial x^k} \right) \mathrm{d}V \right), \quad (2.7.82)$$

respectively. After changing dummy indices, (2.7.81) and (2.7.82) can be re-written

as follows

$$
\begin{aligned}
&\left(\iiint_{\Gamma_M} \rho_M \mathrm{d}V + \iiint_{\Gamma_I} \rho_I \mathrm{d}V\right) \frac{\partial^2 u_{(0)j}}{\partial t^2} \\
=\ & \frac{\partial^2 u_{(0)k}}{\partial x_i \partial x^l} \left(\iiint_{\Gamma_M} c^{k'l'}_{M,ij} \left(\frac{\partial \Psi^{kl}_{M.k'}}{\partial X^{l'}} + \delta^k_{k'} \delta^l_{l'} \right) \mathrm{d}V \right) \\
&+ \frac{\partial^2 u_{(0)k}}{\partial x_i \partial x^l} \left(\iiint_{\Gamma_I} c^{k'l'}_{I,ij} \left(\frac{\partial \Psi^{kl}_{I,k'}}{\partial X^{l'}} + \delta^k_{k'} \delta^l_{l'} \right) + e^{k'}_{ij} \frac{\partial \psi^{kl}_I}{\partial X^{k'}} \mathrm{d}V \right) \\
&+ \frac{\partial^2 \varphi_{(0)}}{\partial x_i \partial x^k} \left(\iiint_{\Gamma_M} c^{k'l'}_{M,ij} \frac{\partial \Phi^k_{M,k'}}{\partial X^{l'}} \mathrm{d}V \right) \\
&+ \frac{\partial^2 \varphi_{(0)}}{\partial x_i \partial x^k} \left(\iiint_{\Gamma_I} c^{k'l'}_{I,ij} \frac{\partial \Phi^k_{I,k'}}{\partial X^{l'}} + e^{k'}_{ij} \left(\frac{\partial \phi^k_I}{\partial X^{k'}} + \delta^k_{k'} \right) \mathrm{d}V \right), \qquad (2.7.83) \\
0 =\ & \frac{\partial^2 u_{(0)k}}{\partial x_i \partial x^l} \left(\iiint_{\Gamma_M} -\epsilon^{Sk'}_{M,i} \frac{\partial \psi^{kl}_M}{\partial X^{k'}} \mathrm{d}V \right) \\
&+ \frac{\partial^2 u_{(0)k}}{\partial x_i \partial x^l} \left(\iiint_{\Gamma_I} S_p e^{k'l'}_i \left(\frac{\partial \Psi^{kl}_{I,k'}}{\partial X^{l'}} + \delta^k_{k'} \delta^l_{l'} \right) - \epsilon^{Sk'}_{I,i} \frac{\partial \psi^{kl}_I}{\partial X^{k'}} \mathrm{d}V \right) \\
&+ \frac{\partial^2 \varphi_{(0)}}{\partial x_i \partial x^k} \left(\iiint_{\Gamma_M} -\epsilon^{Sk'}_{M,i} \left(\frac{\partial \phi^k_M}{\partial X^{k'}} + \delta^k_{k'} \right) \mathrm{d}V \right) \\
&+ \frac{\partial^2 \varphi_{(0)}}{\partial x_i \partial x^k} \left(\iiint_{\Gamma_I} S_p e^{k'l'}_i \frac{\partial \Phi^k_{I,k'}}{\partial X^{l'}} - \epsilon^{Sk'}_{I,i} \left(\frac{\partial \phi^k_I}{\partial X^{k'}} + \delta^k_{k'} \right) \mathrm{d}V \right), \qquad (2.7.84)
\end{aligned}
$$

respectively.

We define the effective stiffness tensor, the two effective electromechanical

tensors, the dielectric tensor and the effective mass density, respectively

$$
\begin{aligned}
c^{kl}_{\text{eff},ij} =& \iiint_{\Gamma_M} c^{k'l'}_{M,ij} \frac{\partial \Psi^{kl}_{M,k'}}{\partial X^{l'}} \mathrm{d}V \\
&+ \iiint_{\Gamma_I} c^{k'l'}_{I,ij} \frac{\partial \Psi^{kl}_{I,k'}}{\partial X^{l'}} + e^{k'}_{ij} \frac{\partial \psi^{kl}_{I}}{\partial X^{k'}} \mathrm{d}V + (1-\nu) c^{kl}_{M,ij} + \nu c^{kl}_{I,ij}, \qquad (2.7.85) \\
e^{k}_{\text{eff},ij} =& \iiint_{\Gamma_M} c^{k'l'}_{M,ij} \frac{\partial \Phi^{k}_{M,k'}}{\partial X^{l'}} \mathrm{d}V \\
&+ \iiint_{\Gamma_I} c^{k'l'}_{I,ij} \frac{\partial \Phi^{k}_{I,k'}}{\partial X^{l'}} + e^{k'}_{ij} \frac{\partial \phi^{k}_{I}}{\partial X^{k'}} \mathrm{d}V + \nu e^{k}_{ij}, \qquad (2.7.86) \\
h^{kl}_{i} =& \iiint_{\Gamma_M} -\frac{1}{S_p} \epsilon^{Sk'}_{M,i} \frac{\partial \psi^{kl}_{M}}{\partial X^{k'}} \mathrm{d}V \\
&+ \iiint_{\Gamma_I} e^{k'l'}_{i} \frac{\partial \Psi^{kl}_{I,k'}}{\partial X^{l'}} - \frac{1}{S_p} \epsilon^{Sk'}_{I,i} \frac{\partial \psi^{kl}_{I}}{\partial X^{k'}} \mathrm{d}V + \nu e^{kl}_{i} \qquad (2.7.87) \\
\epsilon^{Sk}_{\text{eff},i} =& \iiint_{\Gamma_M} \epsilon^{Sk'}_{M,i} \frac{\partial \phi^{k}_{M}}{\partial X^{k'}} \mathrm{d}V \\
&+ \iiint_{\Gamma_I} -S_p e^{k'l'}_{i} \frac{\partial \Phi^{k}_{I,k'}}{\partial X^{l'}} + \epsilon^{Sk'}_{I,i} \frac{\partial \phi^{k}_{I}}{\partial X^{k'}} \mathrm{d}V + (1-\nu) \epsilon^{Sk}_{M,i} + \nu \epsilon^{Sk}_{I,i}, \qquad (2.7.88) \\
\rho_{\text{eff}} =& \nu \rho_I + (1-\nu) \rho_M, \qquad (2.7.89)
\end{aligned}
$$

where ν is the volume fraction of the inclusion phase defined as

$$
\nu = \iiint_{\Gamma_I} \mathrm{d}V. \qquad (2.7.90)
$$

As shown in Appendix E, $h^{k}_{ij} = e^{k}_{\text{eff},ij}$, and thus we write (2.7.83) and (2.7.84), which are the equations for $\boldsymbol{u}_{(0)}$ and $\varphi_{(0)}$ that hold on the macroscale, as

$$
\rho_{\text{eff}} \frac{\partial^2 u_{(0)j}}{\partial t^2} = \frac{\partial}{\partial x_i} \left(c^{kl}_{\text{eff},ij} \frac{\partial u_{(0)k}}{\partial x^l} + e^{k}_{\text{eff},ij} \frac{\partial \varphi_{(0)}}{\partial x^k} \right), \qquad (2.7.91)
$$

$$
0 = \frac{\partial}{\partial x_i} \left(S_p \, e^{kl}_{\text{eff},i} \frac{\partial u_{(0)k}}{\partial x^l} - \epsilon^{Sk}_{\text{eff},i} \frac{\partial \varphi_{(0)}}{\partial x^k} \right). \qquad (2.7.92)
$$

We note that (2.7.91)-(2.7.92) now depend on the microscale through the effective material parameters $c^{kl}_{\text{eff},ij}$, $e^{k}_{\text{eff},ij}$ and $\epsilon^{Sk}_{\text{eff},i}$.

We have developed a robust framework for determining the effective material properties of bulk composites, which we will call the Asymptotic Homogenisation Model (AHM). In Chapter 3, we will calculate the effective coefficients using other methodologies in the literature and compare these results with the effective coefficient derived using our model. In Chapter 4, we will develop a simpler way to obtain approximations for the effective coefficient in cases where the volume fraction of the piezoelectric inclusions is small (that is, up to around $10 - 20\%$ of the composite

material). In Chapter 5, we will extend the framework to model bulk sensors, by incorporating wave theory. In Chapter 6, we will further extend the AHM by incorporating beam theory, to model thin-layer piezoelectric actuators, in order to account for a range of effects, including bending.

Chapter 3

Comparison of effective coefficients with those found using other methods, for 1-3 composites

3.1 Introduction

In this chapter, we will solve the mechanically and electrically driven cell problems derived in Chapter 2 for a 1-3 composite using FEM, and then use these solutions to determine the relevant effective coefficients. Since we are restricting our attention to 1-3 composites, a number of the effective coefficients are identically zero due to symmetry. In particular, assuming isotropy in the matrix phase and transverse isotropy about the Z-direction in the inclusion phase, the shear-normal coupling coefficients and off-diagonal dielectric coefficients vanish. As for the electromechanical tensor, only the tensor components comparable with this symmetry are retained. We will focus on a subset of coefficients derived from the ones defined in Chapter 2, namely κ_{eff}, μ_{eff}, $e_{\text{eff},13}$, $e_{\text{eff},33}$, $\epsilon^S_{\text{eff},33}$. As we will see shortly, these coefficients are related to the coefficients given in (2.7.85)-(2.7.88). We will then obtain results from three other methodologies, namely the Differential Effective Medium (DEM), the Method of Mixtures (MoM) and the Representative Volume Element (RVE) approaches. Finally, we will compare these results to those derived from our model using the same parameters.

We will assume isotropy in the matrix phase and transverse isotropy about the Z-direction in the inclusion phase (for definitions see Appendices D and F).

3.2 Coefficients derived using the Asymptotic Homogenisation Model

The effective bulk and shear moduli κ_{eff} and μ_{eff} are given by

$$\kappa_{\text{eff}} = \frac{1}{2}\left(c^{11}_{\text{eff},11} + c^{22}_{\text{eff},11}\right), \tag{3.2.1}$$

$$\mu_{\text{eff}} = \frac{1}{2}\left(c^{11}_{\text{eff},11} - c^{22}_{\text{eff},11}\right), \tag{3.2.2}$$

where $c^{11}_{\text{eff},11}$ and $c^{22}_{\text{eff},11}$ are computed using (2.7.85).

The transverse and longitudinal electromechanical coefficients $e_{\text{eff},13}$ and $e_{\text{eff},33}$ are given by

$$e_{\text{eff},13} = e^{3}_{\text{eff},11}, \tag{3.2.3}$$

$$e_{\text{eff},33} = e^{3}_{\text{eff},33}, \tag{3.2.4}$$

where $e^{3}_{\text{eff},11}$ and $e^{3}_{\text{eff},33}$ are computed using (2.7.86).

The transverse dielectric coefficient $\epsilon^{S3}_{\text{eff},3}$ is given by

$$\epsilon^{S}_{\text{eff},33} = \epsilon^{S3}_{\text{eff},3}, \tag{3.2.5}$$

where $\epsilon^{S3}_{\text{eff},3}$ is computed using (2.7.88).

3.3 Coefficients derived using the Differential Effective Medium approach

Using the DEM approach [4], the effective elastic parameters κ_{eff} and μ_{eff} are both functions of the volume fraction ν (defined in (2.7.90)) and are governed by

$$\frac{d\kappa_{\text{eff}}}{d\nu} = \left(\frac{1}{1-\nu}\right)(\kappa_I - \kappa_{\text{eff}})\,\frac{\kappa_{\text{eff}} + \mu_{\text{eff}}}{\kappa_I + \mu_{\text{eff}}}, \tag{3.3.1}$$

$$\frac{d\mu_{\text{eff}}}{d\nu} = \left(\frac{1}{1-\nu}\right)(\mu_I - \mu_{\text{eff}})\,\frac{2\mu_{\text{eff}}\left(\kappa_{\text{eff}} + \mu_{\text{eff}}\right)}{\left(\mu_I + \mu_{\text{eff}}\right)\kappa_{\text{eff}} + 2\mu_{\text{eff}}\mu_I}, \tag{3.3.2}$$

with initial conditions

$$\kappa_{\text{eff}}(0) = \kappa_M, \tag{3.3.3}$$

$$\mu_{\text{eff}}(0) = \mu_M. \tag{3.3.4}$$

The derivation of (3.3.1)-(3.3.2) in [4] involves using the low volume fraction approximations to κ_{eff} and μ_{eff} (see [34]), then iterating this procedure with infinitesimal

increments of the volume fraction at each step until the volume fraction of the inclusion equals 1.

We define the function, $p(\nu)$, that describes the mean transverse hydrostatic strain (see [4]) as

$$p(\nu) = \frac{\kappa_{\text{eff}}(\nu) - \kappa_M}{\nu\left(\kappa_I - \kappa_M\right)}. \tag{3.3.5}$$

From [4], we see the effective electromechanical coefficients e_{13} and e_{33} are given by

$$e_{\text{eff},13} = \nu p(\nu) e_{13}, \tag{3.3.6}$$

$$e_{\text{eff},33} = \nu\left(1 + \left(p(\nu) - 1\right)\frac{\left(\lambda_I - \lambda_M\right)e_{13}}{\left(\kappa_I - \kappa_M\right)e_{33}}\right)e_{33}. \tag{3.3.7}$$

The effective dielectric coefficient $\epsilon^S_{\text{eff},33}$ is given by

$$\epsilon^S_{\text{eff},33} = \epsilon^S_{M,33} + \nu\left(1 - \left(p(\nu) - 1\right)\frac{S_p\left(e_{13}\right)^2}{\left(\kappa_I - \kappa_M\right)\left(\epsilon^S_{I,33} - \epsilon^S_{M,33}\right)}\right)\left(\epsilon^S_{I,33} - \epsilon^S_{M,33}\right). \tag{3.3.8}$$

We note that in the limit as $\nu \to 1$: $p(\nu)$ tends to 1, therefore $e_{\text{eff},13}$, $e_{\text{eff},33}$ and $\epsilon^S_{\text{eff},33}$ tend to e_{13}, e_{33}, and $\epsilon^S_{I,33}$, respectively. This is expected as $\nu = 1$ corresponds to the material consisting entirely of the inclusion material. Hence, the effective properties reduce to those of the inclusion material. Having established the relevant formulae for the DEM method, we will now turn our attention to the formulae proposed by [53].

3.4 Coefficients derived using the Method of Mixtures approach

Using the MoM approach [53], the effective material properties are dependent on the material properties of the matrix and inclusion phases, as well as the volume fraction ν of the inclusion phase. The effective bulk modulus presented in [53] is given by

$$\kappa_{\text{eff}} = \frac{\kappa_M \kappa_I}{\nu\kappa_M + (1-\nu)\kappa_I}. \tag{3.4.1}$$

We will not be considering the effective shear modulus as a formula for this coefficient is not provided in [53].

The effective electromechanical coefficients, presented in [53] are

$$e_{\text{eff},13} = \frac{\nu e_{13}\kappa_M}{\nu\kappa_M + (1-\nu)\kappa_I}, \tag{3.4.2}$$

$$e_{\text{eff},33} = \nu\left[e_{33} - \frac{(1-\nu)e_{13}(\lambda_I - \lambda_M)}{\nu\kappa_M + (1-\nu)\kappa_I}\right], \tag{3.4.3}$$

Finally, the dielectric coefficient $\epsilon^S_{\text{eff},33}$ is given by

$$\epsilon^S_{\text{eff},33} = (1-\nu)\,\epsilon^S_{M,33} + \nu\left[\epsilon^S_{I,33} + S_p\frac{(1-\nu)\,(e_{13})^2}{\nu\kappa_M + (1-\nu)\kappa_I}\right]. \tag{3.4.4}$$

3.5 Coefficients derived using the Representative Volume Element approach

We use the RVE approach proposed in [44], which is similar to the AHM approach, but differs in several respects. In [44], Dirichlet rather than periodic boundary conditions are imposed on the external boundaries of the cell problem, and the governing PDEs are solved over domains containing multiple unit cells, whereas in our approach the problem is solved over a single unit cell only. In the limit of solving over infinitely many unit cells in the RVE domain, these results converge to those of the AHM approach, albeit at an increased computational cost.

Imposing Dirichlet boundary conditions on the external boundaries of the unit cell enables the average macroscopic strain and electric fields to be prescribed directly. The resulting averaged stress and dielectric displacement are then used to determine the effective coefficients arising in the stress-charge form of the piezoelectric constitutive equations, namely the effective stiffness, piezoelectric stress and permittivity tensors under constant strain conditions. Neumann conditions could be used within the RVE framework instead. However, these conditions prescribe traction and dielectric displacement quantities and are therefore associated more naturally with the strain-voltage form of the constitutive equations. Therefore, and to remain consistent with the formulation in [44], Dirichlet boundary conditions are used throughout this section.

We start with the stiffness parameters κ_{eff} and μ_{eff}. In order to find these two parameters, we need the cell functions $\hat{\boldsymbol{\Psi}}^{11}$ and $\hat{\psi}^{11}$.[1] Functions $\hat{\boldsymbol{\Psi}}^{11}$ and $\hat{\psi}^{11}$ satisfy (2.7.51)-(2.7.54) and continuity conditions (2.7.55)-(2.7.56). From [44], the jump conditions along the surface of the boundary $\partial\Gamma_M \cap \partial\Gamma_I$ which $\hat{\boldsymbol{\Psi}}^{11}$ and $\hat{\psi}^{11}$ both

[1] These two cell functions suffice as we only need to find the planar stiffness coefficients.

satisfy are given by

$$n^i\left[\left(c^{kl}_{M,ij}\frac{\partial\hat{\Psi}^{11}_{M,k}}{\partial X^l}\right)-\left(c^{kl}_{I,ij}\frac{\partial\hat{\Psi}^{11}_{I,k}}{\partial X^l}+e^k_{ij}\frac{\partial\hat{\psi}^{11}_I}{\partial X^k}\right)\right]=0_j, \tag{3.5.1}$$

$$n^i\left[\left(-\epsilon^{Sk}_{M,i}\frac{\partial\hat{\psi}^{11}_M}{\partial X^k}\right)-\left(S_p e^{kl}_i\frac{\partial\hat{\Psi}^{11}_{I,k}}{\partial X^l}-\epsilon^{Sk}_{I,i}\frac{\partial\hat{\psi}^{11}_I}{\partial X^k}\right)\right]=0. \tag{3.5.2}$$

Note that the right-hand sides of (3.5.1)-(3.5.2) are zero, because in this formulation, the forcing is now applied on the external boundary of the domain rather than the internal boundaries between neighbouring phases, which we saw in the AHM framework in Chapter 2. From [44], the cell functions $\hat{\mathbf{\Psi}}^{11}$ and $\hat{\psi}^{11}$ satisfy the following Dirichlet boundary conditions

$$\boldsymbol{n}\cdot\hat{\mathbf{\Psi}}^{11}=0 \text{ for } \partial[0,1]^3\setminus\{X=1\}, \tag{3.5.3}$$

$$\boldsymbol{n}\cdot\hat{\mathbf{\Psi}}^{11}=1 \text{ for } \{X=1\}, \tag{3.5.4}$$

$$\hat{\psi}^{11}=0 \text{ for } \partial[0,1]^3, \tag{3.5.5}$$

where $\partial[0,1]^3$ is the boundary of $[0,1]^3$.

Having found these cell functions, we find the effective stiffness coefficients $c^{11}_{\text{eff},11}$ and $c^{22}_{\text{eff},11}$. These are provided in [44], and read as

$$c^{11}_{\text{eff},11}=\iiint_{\Gamma_M}c^{kl}_{M,11}\frac{\partial\hat{\Psi}^{11}_{M,k}}{\partial X^l}\mathrm{d}V+\iiint_{\Gamma_I}c^{kl}_{I,11}\frac{\partial\hat{\Psi}^{11}_{I,k}}{\partial X^l}+e^k_{11}\frac{\partial\hat{\psi}^{11}_I}{\partial X^k}\mathrm{d}V, \tag{3.5.6}$$

$$c^{22}_{\text{eff},11}=c^{11}_{\text{eff},22}=\iiint_{\Gamma_M}c^{kl}_{M,22}\frac{\partial\hat{\Psi}^{11}_{M,k}}{\partial X^l}\mathrm{d}V+\iiint_{\Gamma_I}c^{kl}_{I,22}\frac{\partial\hat{\Psi}^{11}_{I,k}}{\partial X^l}+e^k_{22}\frac{\partial\hat{\psi}^{11}_I}{\partial X^k}\mathrm{d}V. \tag{3.5.7}$$

Note that these formulae are subtly different to the formulas provided in (2.7.85) primarily due to the difference in boundary conditions. The effective stiffness parameters are then determined using (3.2.1)-(3.2.2).

In order to find the electromechanical coefficients $e_{\text{eff},13}$ and $e_{\text{eff},33}$, we need to find the cell functions $\hat{\mathbf{\Phi}}^3$ and $\hat{\phi}^3$ which satisfy the PDEs (2.7.63)-(2.7.66), the continuity conditions (2.7.67)-(2.7.68) along the boundary $\partial\Gamma_M\cap\partial\Gamma_I$, and the jump conditions

$$n^i\left[\left(c^{kl}_{M,ij}\frac{\partial\hat{\Phi}^3_{M,k}}{\partial X^l}\right)-\left(c^{kl}_{I,ij}\frac{\partial\hat{\Phi}^3_{I,k}}{\partial X^l}+e^k_{ij}\frac{\partial\hat{\phi}^3_I}{\partial X^k}\right)\right]=0_j, \tag{3.5.8}$$

$$n^i\left[\left(-\epsilon^{Sk}_{M,i}\frac{\partial\hat{\phi}^3_M}{\partial X^k}\right)-\left(S_p e^{kl}_i\frac{\partial\hat{\Phi}^3_{I,k}}{\partial X^l}-\epsilon^{Sk}_{I,i}\frac{\partial\hat{\phi}^3_I}{\partial X^k}\right)\right]=0, \tag{3.5.9}$$

along $\partial\Gamma_M\cap\partial\Gamma_I$. From [44], the cell functions $\hat{\mathbf{\Phi}}^3$ and $\hat{\phi}^3$ satisfy the Dirichlet

boundary conditions

$$\boldsymbol{n} \cdot \hat{\boldsymbol{\Phi}}^3 = 0 \text{ for } \partial[0,1]^3, \tag{3.5.10}$$

$$\hat{\phi}^3 = 0 \text{ for } \partial[0,1]^3 \setminus \{Z = 1\}, \tag{3.5.11}$$

$$\hat{\phi}^3 = 1 \text{ for } \{Z = 1\}. \tag{3.5.12}$$

Having found these two cell functions, from [44] we find the effective electromechanical coefficients $e_{\text{eff},13}$ and $e_{\text{eff},33}$, namely

$$e_{\text{eff},13} = \iiint_{\Gamma_M} c^{kl}_{M,11} \frac{\partial \hat{\Phi}^3_{M,k}}{\partial X^l} \mathrm{d}V + \iiint_{\Gamma_I} c^{kl}_{I,11} \frac{\partial \hat{\Phi}^3_{I,k}}{\partial X^l} + e^k_{11} \frac{\partial \hat{\phi}^3_I}{\partial X^k} \mathrm{d}V, \tag{3.5.13}$$

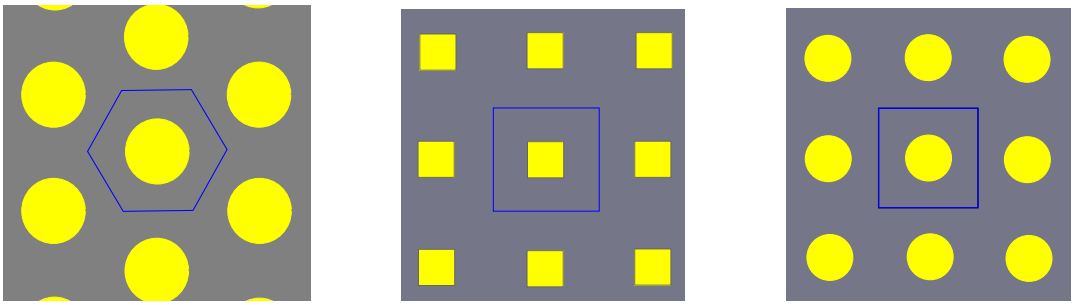
$$e_{\text{eff},33} = \iiint_{\Gamma_M} c^{kl}_{M,33} \frac{\partial \hat{\Phi}^3_{M,k}}{\partial X^l} \mathrm{d}V + \iiint_{\Gamma_I} c^{kl}_{I,33} \frac{\partial \hat{\Phi}^3_{I,k}}{\partial X^l} + e^k_{33} \frac{\partial \hat{\phi}^3_I}{\partial X^k} \mathrm{d}V. \tag{3.5.14}$$

From [44], the effective dielectric coefficient $\epsilon^S_{\text{eff},33}$ is

$$\epsilon^S_{\text{eff},33} = \iiint_{\Gamma_M} \epsilon^{Sk}_{M,3} \frac{\partial \hat{\phi}^3_M}{\partial X^k} \mathrm{d}V + \iiint_{\Gamma_I} -S_p e^{k'l'}_3 \frac{\partial \hat{\Phi}^3_{I,k'}}{\partial X^{l'}} + \epsilon^{Sk}_{I,3} \frac{\partial \hat{\phi}^3_I}{\partial X^k} \mathrm{d}V. \tag{3.5.15}$$

3.6 Comparison of the four approaches

We compare the behaviour of the effective material properties found using the four approaches, where (when necessary) we solve the underpinning cell problems using the weak formulations provided in (C.0.15) and (C.0.16) established in Appendix C.



(a) Cylindrical pillars in a hexagonal lattice.

(b) Square pillars in a square lattice.

(c) Cylindrical pillars in a square lattice.

Figure 3.1: Schematic of geometries to be used in our comparison.

We consider the three geometries in Figure 3.1[2], comparing the effective coefficients for all four methods for the square lattice cases, and excluding the RVE

[2]The geometry in Figure 3.1a was used in [4], whereas the geometry in Figure 3.1b was used in [53].

method for the hexagonal lattice. We note that the DEM and the MoM formulae depend on the volume fraction of the inclusion material and are not affected by the changes to the microscale geometry.

In order to compute the effective coefficients for cylindrical pillars in a hexagonal lattice using the AHM, we must refine the approach established in Chapter 2 by assuming that the terms in the asymptotic expansions (2.7.2) and (2.7.3) are periodic in the directions $\boldsymbol{e}_1 = (\frac{\sqrt{3}}{2}, \frac{1}{2}, 0)^{\mathrm{Tr}}$, $\boldsymbol{e}_2 = (\frac{\sqrt{3}}{2}, -\frac{1}{2}, 0)^{\mathrm{Tr}}$ and $\boldsymbol{e}_3 = (0, 0, 1)^{\mathrm{Tr}}$. Since

$$\boldsymbol{e}_1 + \boldsymbol{e}_2 = (\sqrt{3}, 0, 0)^{\mathrm{Tr}}, \tag{3.6.1}$$

$$\boldsymbol{e}_1 - \boldsymbol{e}_2 = (0, 1, 0)^{\mathrm{Tr}}, \tag{3.6.2}$$

it follows that the functions in the expansions are $\sqrt{3}$-periodic in X and 1-periodic in both Y and Z. This means that we may solve the cell equations on the cuboid $\left[0, \sqrt{3}\right] \times [0, 1] \times [0, 1]$. The way the inclusions are arranged in this new set-up are shown in Figure 3.2.

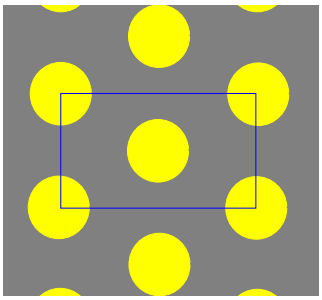
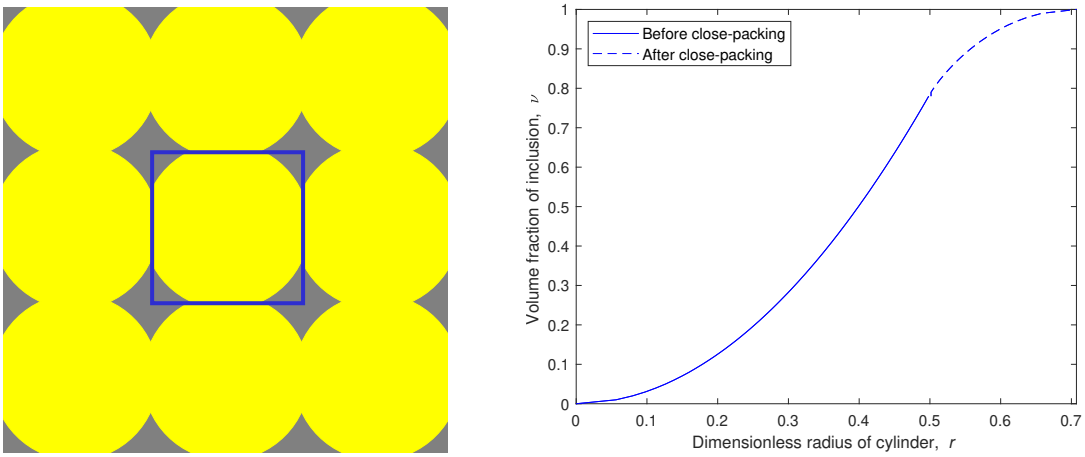


Figure 3.2: Schematic showing the cross-section of the cell with cylindrical pillars in a hexagonal lattice, for which we use AHM to homogenise the material.

We use the integration formulae given in (2.7.85)-(2.7.88) but, since the volume of this new cell is $\sqrt{3}$, we multiply the integral expressions by a factor of $\frac{1}{\sqrt{3}}$.

We note that when the dimensionless radius of the cylindrical pillars is 0.5 the inclusions touch, a phenomenon called close-packing. We note that when the dimensionless radius of the cylindrical pillars is 0.5, the inclusions touch, a phenomenon called close-packing. Above the close-packing volume fraction, the cylindrical inclusions extend beyond the boundaries of the unit cell and therefore appear truncated when viewed within a single cell, as illustrated in Figure 3.3a for the case of cylindrical pillars in a square lattice. As shown in Figure 3.3b, before close-packing is reached (namely when $r < 0.5$), the volume fraction is equal to the area of the circle, πr^2. After the cylinders touch ($r > 0.5$), part of the circle lies outside the unit cell, and therefore the volume fraction increases more slowly with radius than before.



(a) Schematic of close-packing for cylindrical pillars in a square lattice.

(b) Graph showing how volume fraction changes with radius of the cylinder.

Figure 3.3: Schematic for close-packing (left) and graph of volume fraction against inclusion radius (right).

In Figures 3.4-3.8, we present the effective coefficients both before (solid or dot-dashed lines) and after (dashed lines) the close-packing. For ease of comparison between the methods, and for exposition to our industrial sponsors, the results are presented using dimensional rather than dimensionless coefficients. In each example, we use Stycast as the matrix material and PZTA5 as the inclusion material; the material parameters of both phases are given in Table 2.1.

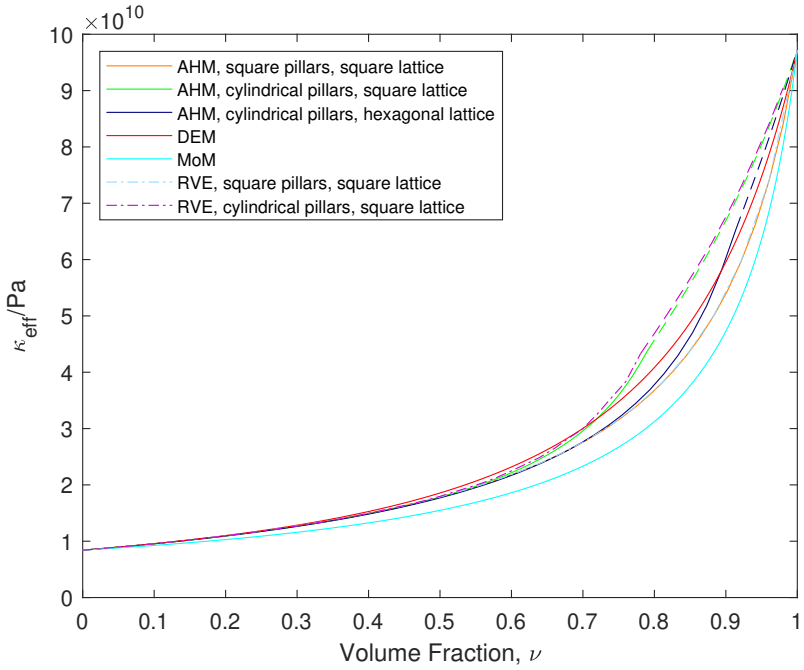


Figure 3.4: Graph showing how κ_{eff} (the bulk modulus), depends on ν. The results from the AHM, DEM, MoM, RVE approaches are computed using equations (2.7.85) and (3.2.1), equations (3.3.1)-(3.3.4), equation (3.4.1), and equations (3.5.6)-(3.5.7) together with equation (3.2.1), respectively. The RVE results for square pillars in a square lattice (shown in medium blue) overlap with the AHM results for square pillars in a square lattice (shown in orange) throughout the plotted range.

In Figure 3.4, we show how κ_{eff} varies with ν. We see that all methods agree for small volume fractions, (i.e., $\nu \leq 0.1$), and have roughly the same shape. In comparison to AHM, the least accurate method for moderate volume fractions is the MoM approach, followed by the DEM approach. The RVE formula has close agreement with the AHM formula for all volume fractions for both square lattice geometries, although we see closer agreement where the pillars are square rather than cylindrical.

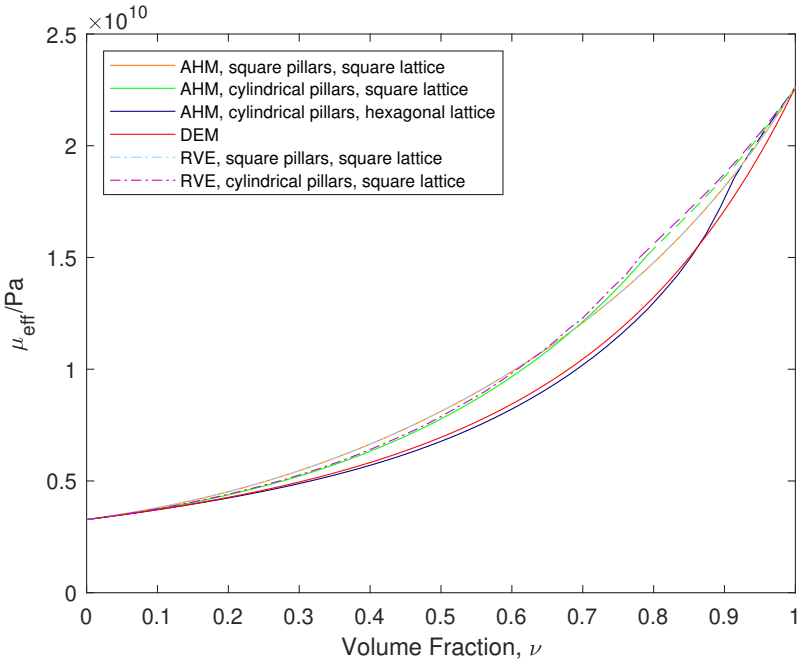


Figure 3.5: Graph showing how μ_{eff} (the shear modulus), depends on ν. The results from the AHM, DEM, RVE approaches are computed using equations (2.7.85) and (3.2.2), equations (3.3.1)-(3.3.4), and equations (3.5.6)-(3.5.7) together with equation (3.2.2), respectively. Results for the MoM solution are not shown, due to the fact that [53] does not contain a formula for μ_{eff}. The RVE results for square pillars in a square lattice (shown in medium blue) overlaps with the AHM results for square pillars in a square lattice (shown in orange) throughout the plotted range.

In Figure 3.5, we show how μ_{eff} varies with ν. The influence of lattice structure is more pronounced for the effective shear modulus than for the effective bulk modulus (Figure 3.4). The geometries with a square lattice (orange, green and magenta curves) give results that are close to one another, as is the case for geometries with a hexagonal lattice structure (navy blue and red curves). This indicates that the shape of the pillars only has a small effect on the effective shear modulus, whereas the lattice arrangement plays a more significant role. As expected from [4], we see that the DEM formulae agree very well with the AHM formulae for cylindrical pillars in a hexagonal lattice. As with κ_{eff}, the RVE method has close agreement with the AHM formulae for all volume fractions for the case of square pillars in a square lattice. However, there is less strong agreement where the pillars are cylindrical.

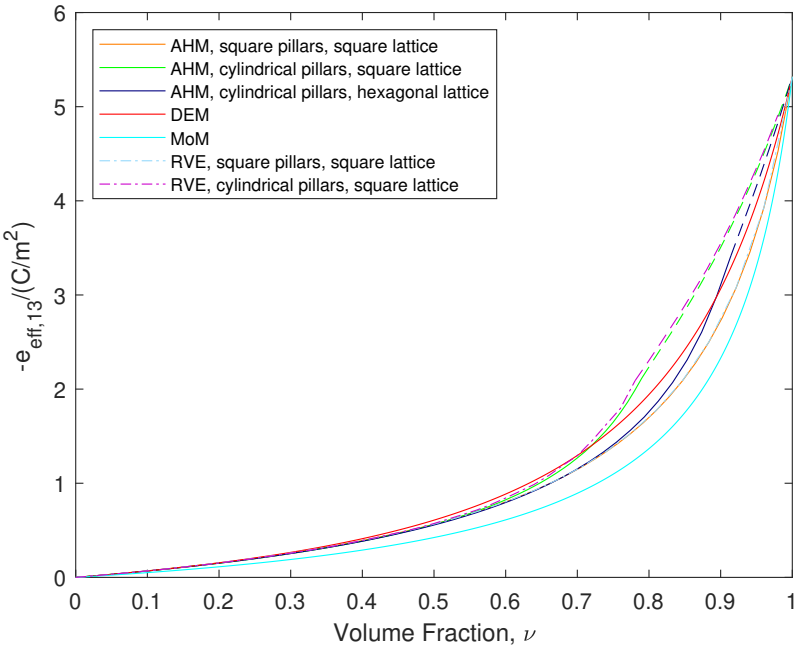


Figure 3.6: Graph showing how $-e_{\text{eff},13}$ (the electromechanical stress coefficient), depends on ν. The results from the AHM, DEM, MoM, RVE approaches are computed using equations (2.7.86) and (3.2.3), equations (3.3.5) and (3.3.6), equation (3.4.2), and equation (3.5.13), respectively. The RVE results for square pillars in a square lattice (shown in medium blue) overlaps with the AHM results for square pillars in a square lattice (shown in orange) throughout the plotted range.

In Figure 3.6 we show how $e_{\text{eff},13}$ varies with ν. We see that the MoM formula (shown in cyan) underestimates the electromechanical stress coefficient. We note that, as for κ_{eff}, both the lattice structure and the pillar shape noticeably impact the effective coefficients. Curiously, the curve corresponding to the AHM predictions for a hexagonal lattice with cylindrical pillars (the navy blue curve) matches up better with the curve for square lattice with square pillars (the medium blue curve) for the RVE formula than with the curve for the DEM formula (the red curve). Both curves found using the RVE method (i.e., the medium blue and magenta curves) match up very well with the corresponding formulae using the AHM (i.e. orange and green respectively).

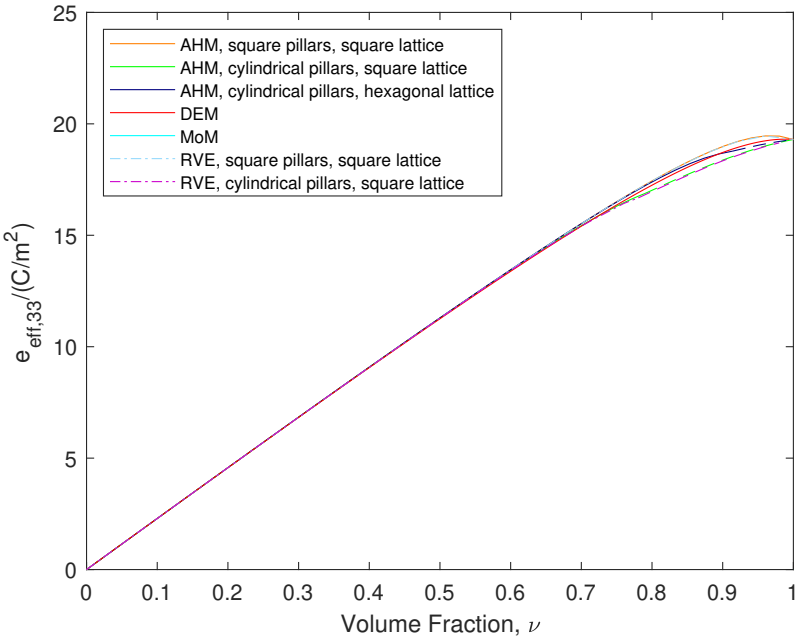


Figure 3.7: Graph showing how $e_{\text{eff},33}$ (the thickness-mode electromechanical coefficient), depends on ν. The results from the AHM, DEM, MoM, RVE approaches are computed using equations (2.7.86) and (3.2.4), equations (3.3.5) and (3.3.7), equation (3.4.3), and equation (3.5.14), respectively. The RVE results for square pillars in a square lattice (shown in medium blue) overlaps with the AHM results for square pillars in a square lattice (shown in orange) throughout the plotted range.

In Figure 3.7, we show how $e_{\text{eff},33}$ varies with ν. We see that the results of all four approaches agree very closely until the close-packing limits are exceeded. As shown, $e_{\text{eff},33}$ is not affected by the lattice structure or the shape of the pillars. In this case, only the volume fraction of the pillars affects the effective coefficient.

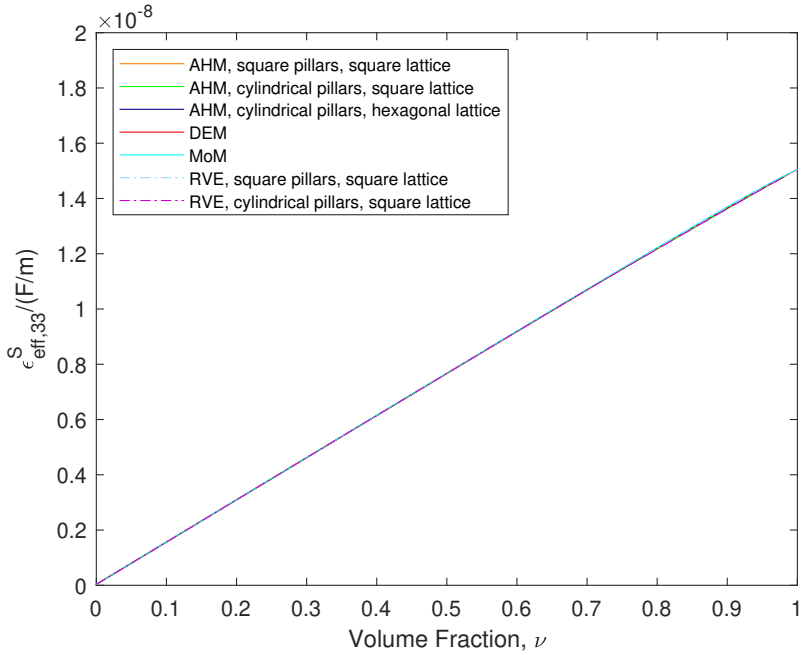


Figure 3.8: Graph showing how $\epsilon^S_{\text{eff},33}$ (the thickness-mode dielectric coefficient) depends on ν. The results from the AHM, DEM, MoM, RVE approaches are computed using equations (2.7.88) and (3.2.5), equations (3.3.5) and (3.3.8), equation (3.4.4), and equation (3.5.15), respectively. As there is excellent agreement for all curves, not all curves are visible.

In Figure 3.8, we show how $\epsilon^S_{\text{eff},33}$ varies with ν. We see that for all four approaches, there is excellent agreement for all volume fractions, even beyond close-packing limits. We conclude $\epsilon^S_{\text{eff},33}$ does not vary with inclusion shape or lattice arrangements.

The results of this chapter show that the agreement of DEM and MoM predictions with AHM predictions decreases as the volume fraction of the inclusions increases. The MoM approach shows the greatest deviation from the AHM predictions as the volume fraction increases, and although it predicts the thickness-mode coefficients well, it shows less agreement for the planar-mode coefficients. This is followed by the DEM approach which shows strong agreement for both planar- and thickness-mode coefficients at low volume fractions, but exhibits increasing deviation from the AHM predictions as the volume fraction increases. In contrast, the RVE method shows close agreement with our model for all coefficients and geometries up to close-packing.

Chapter 4

The Limit of Small Volume Fraction of Inclusions

4.1 Introduction

In Chapter 2, we posed and homogenised a model for a composite material with a periodic lattice, providing the framework for finding the effective material coefficients, namely the stiffness, electromechanical and dielectric constants. We demonstrated that, unlike other averaging methods, this approach is valid for a wide range of shape, size and orientation of inclusions, and lattice structures. We also showed that we can use FEM to numerically solve the system of PDEs for the cell functions and then integrate the solutions to give the effective coefficients. We compared the effective parameters derived under the AHM with those observed from other methodologies, namely the MoM [53], the DEM [4] and the RVE [44] methods for composites with the same individual-phase material parameters. We concluded that the RVE method had the best overall agreement with the AHM.

In this chapter, we will find approximations for the effective coefficients when the volume fraction of the inclusion to the composite, ν, is small (up to around 10%-20%). We will consider the case where the inclusions are cylindrical pillars with a very small radius, arranged in a square lattice which is aligned and poled in the Z-direction, and derive approximations for solutions to the cell functions.

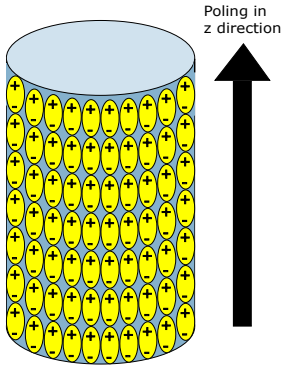


Figure 4.1: Piezoelectric material poled in Z-direction.

Once we find the approximations to the cell functions, we will use them to find the approximations of the effective coefficients. The low volume fraction technique gives us closed-form formulae for the effective coefficients, which are much easier to implement than numerically solving the cell problems and then performing the necessary integrals to determine the effective coefficients.

We first derive approximations to the cell functions in the limit of small r (the dimensionless radius of the cylinders) by assuming there is an expansion that is valid near the origin (i.e., in the vicinity of the cylinder, called the inner expansion) and also an expansion that is valid away from the origin (called the outer expansion). We then find the leading-order term of the inner expansion by solving the cell functions in the inner region. This ensures that the solution satisfies the appropriate continuity and jump conditions. We then re-write this solution in terms of outer variables to derive the matching condition for the leading-order term(s) in the outer expansion. Subsequently we solve the first term(s) in the outer expansion, re-write this solution in terms of the inner variables and match the two solutions together using the Van Dyke Matching rule [7]. We continue in this way until we have found a satisfactory number of terms for both the inner and outer expansions. Once we have derived the solutions, we then substitute them into the integral formulae for the effective coefficients, (2.7.85)-(2.7.88), to deduce an expansion for each coefficient in the limit $\nu \to 0$.

As we recall, the mechanical and electrical cell problems are essentially time-independent linearised piezoelectric equations with continuity and jump conditions imposed on the boundary of the interface between the two phases. We will solve one mechanical cell problem for each component of the stress tensor, and one electrical problem for each component of the electric field.

In this section, we will be exploring how to find solutions to the mechanical cell problems for a 1-3 composite where the matrix and inclusion phases are both transversely

isotropic. The domain Γ is the unit cell centred at $(0,0,0)$ (i.e., $\Gamma = (-0.5, 0.5)^3$), the inclusion region is the set $\Gamma_I = \{(X,Y,Z) \in \Gamma : X^2 + Y^2 < r^2\}$ where $r \ll 1$ and the inclusion material is poled in the Z-direction. The matrix region is the set $\Gamma_M = \Gamma / \Gamma_I$.

4.2 Mechanical cell problems

In this section, we will be deriving approximate solutions to the mechanically driven cell problems defined by the system (F.2.1)-(F.2.12) in §F.2.

4.2.1 Simplifying the equations

In addition to assuming the conditions in (F.1.1)-(F.1.5), we will also assume that the material is fully isotropic in the matrix phase and transversely isotropic about the Z-direction in the inclusion phase. In both phases, the coefficients satisfy the following properties,

i.
$$c^{\gamma\iota}_{\alpha\beta} = \lambda \delta_{\alpha\beta}\delta^{\gamma\iota} + \mu\left(\delta^{\gamma}_{\alpha}\delta^{\iota}_{\beta} + \delta^{\iota}_{\alpha}\delta^{\gamma}_{\beta}\right), \tag{4.2.1}$$

ii.
$$c^{\beta 3}_{\alpha 3} = c_{44}\delta^{\beta}_{\alpha}, \tag{4.2.2}$$

iii.
$$c^{33}_{\alpha\beta} = c^{\alpha\beta}_{33} = c_{13}\delta_{\alpha\beta}, \tag{4.2.3}$$

iv.
$$e^{3}_{\alpha\beta} = e_{13}\delta_{\alpha\beta}, \tag{4.2.4}$$

v.
$$e^{\beta}_{\alpha 3} = e_{51}\delta^{\beta}_{\alpha}, \tag{4.2.5}$$

vi.
$$\epsilon^{S\beta}_{\alpha} = \epsilon^{S}_{11}\delta^{\beta}_{\alpha}. \tag{4.2.6}$$

where $\alpha, \beta, \gamma, \iota \in \{1,2\}$. Throughout the rest of this thesis, we will use the convention that Greek indices and summation of Greek indices refer to planar directions only. In the rest of this chapter, we will let $|\boldsymbol{X}| = |(X,Y,0)|$ since we are dealing with a 2D problem. We define the parameters

$$\kappa_I = \lambda_I + \mu_I, \tag{4.2.7}$$
$$\kappa_M = \lambda_M + \mu_M, \tag{4.2.8}$$

to be the bulk moduli for the inclusion phase and matrix phase respectively. Since our system is transversely isotropic, we may use the relationships in (4.2.1)-(4.2.6) to re-write (F.2.1)-(F.2.6) as

$$\kappa_M \frac{\partial}{\partial X^\alpha}\left(\nabla_{\boldsymbol{X}} \cdot \boldsymbol{\Psi}_M^{ab}\right) + \mu_M \nabla_{\boldsymbol{X}}^2 \Psi_{M,\alpha}^{ab} = 0_\alpha \text{ when } |\boldsymbol{X}| > r, \tag{4.2.9}$$

$$\kappa_I \frac{\partial}{\partial X^\alpha}\left(\nabla_{\boldsymbol{X}} \cdot \boldsymbol{\Psi}_I^{ab}\right) + \mu_I \nabla_{\boldsymbol{X}}^2 \Psi_{I,\alpha}^{ab} = 0_\alpha \text{ when } |\boldsymbol{X}| < r, \tag{4.2.10}$$

$$\nabla_{\boldsymbol{X}}^2 \Psi_{M,3}^{ab} = 0 \text{ when } |\boldsymbol{X}| > r, \tag{4.2.11}$$

$$\nabla_{\boldsymbol{X}}^2 \Psi_{I,3}^{ab} = 0 \text{ when } |\boldsymbol{X}| < r, \tag{4.2.12}$$

$$\nabla_{\boldsymbol{X}}^2 \psi_M^{ab} = 0 \text{ when } |\boldsymbol{X}| > r, \tag{4.2.13}$$

$$\nabla_{\boldsymbol{X}}^2 \psi_I^{ab} = 0 \text{ when } |\boldsymbol{X}| < r, \tag{4.2.14}$$

while the continuity conditions (F.2.7)-(F.2.12) can be re-written as

$$\Psi_{M,\alpha}^{ab} = \Psi_{I,\alpha}^{ab}, \tag{4.2.15}$$

$$\Psi_{M,3}^{ab} = \Psi_{I,3}^{ab}, \tag{4.2.16}$$

$$\psi_M^{ab} = \psi_I^{ab}, \tag{4.2.17}$$

$$\begin{aligned}\left[\lambda_M \nabla_{\boldsymbol{X}} \cdot \boldsymbol{\Psi}_M^{ab} n_\alpha + \mu_M \left(\boldsymbol{n} \cdot \nabla_{\boldsymbol{X}} \boldsymbol{\Psi}_{M,\alpha}^{ab} + n^\beta \frac{\partial \Psi_{M,\beta}^{ab}}{\partial X^\alpha}\right)\right] \\ - \left[\lambda_I \nabla_{\boldsymbol{X}} \cdot \boldsymbol{\Psi}_I^{ab} n_\alpha + \mu_I \left(\boldsymbol{n} \cdot \nabla_{\boldsymbol{X}} \boldsymbol{\Psi}_{I,\alpha}^{ab} + n^\beta \frac{\partial \Psi_{I,\beta}^{ab}}{\partial X^\alpha}\right)\right] \\ = (\lambda_I - \lambda_M)\delta^{ab} n_\alpha + (\mu_I - \mu_M)\left(\delta_\alpha^b n^a + \delta_\alpha^a n^b\right),\end{aligned} \tag{4.2.18}$$

$$\boldsymbol{n} \cdot \left[c_{M,44} \nabla_{\boldsymbol{X}} \Psi_{M,3}^{ab} - c_{I,44} \nabla_{\boldsymbol{X}} \Psi_{I,3}^{ab} - e_{51} \nabla_{\boldsymbol{X}} \psi_I^{ab}\right] = n^\alpha \left(c_{I,\alpha 3}^{ab} - c_{M,\alpha 3}^{ab}\right), \tag{4.2.19}$$

$$\boldsymbol{n} \cdot \left[\epsilon_{I,11}^S \nabla_{\boldsymbol{X}} \psi_I^{ab} - \epsilon_{M,11}^S \nabla_{\boldsymbol{X}} \psi_M^{ab} - S_p e_{51} \nabla_{\boldsymbol{X}} \Psi_{I,3}^{ab}\right] = S_p n^\alpha e_\alpha^{ab}, \tag{4.2.20}$$

whenever $|\boldsymbol{X}| = r$.

4.2.2 Rescaling the PDEs to the inner region

We now consider the limit $r \to 0$. We rescale

$$\boldsymbol{X} = (X, Y) = r(\xi, \eta) = r(\xi_1, \xi_2) = r\boldsymbol{\xi}, \tag{4.2.21}$$

so that the inclusion has unit radius in the scaled coordinate system. Note that, for convenience, we will be using (ξ, η) and (ξ_1, ξ_2) interchangeably.

The radial coordinates $\rho = |(\xi, \eta)|$ and $R = |(X, Y)|$ are related through

$$R = r\rho. \tag{4.2.22}$$

The displacement function $\mathbf{\Psi}^{ab}$ satisfies

$$\kappa_M \frac{\partial}{\partial \xi^\alpha} \left(\nabla_{\boldsymbol{\xi}} \cdot \mathbf{\Psi}^{ab}_{M,(in)} \right) + \mu_M \nabla^2_{\boldsymbol{\xi}} \Psi^{ab}_{M,(in)\alpha} = 0_\alpha \text{ when } \rho > 1, \tag{4.2.23}$$

$$\kappa_I \frac{\partial}{\partial \xi^\alpha} \left(\nabla_{\boldsymbol{\xi}} \cdot \mathbf{\Psi}^{ab}_{I,(in)} \right) + \mu_I \nabla^2_{\boldsymbol{\xi}} \Psi^{ab}_{I,(in)\alpha} = 0_\alpha \text{ when } \rho < 1, \tag{4.2.24}$$

along with the continuity conditions

$$\Psi^{ab}_{M,(in)\alpha} = \Psi^{ab}_{I,(in)\alpha}, \tag{4.2.25}$$

$$\begin{aligned} &\left[\lambda_M \nabla_{\boldsymbol{\xi}} \cdot \mathbf{\Psi}^{ab}_{M,(in)} n_\alpha + \mu_M \left(\boldsymbol{n} \cdot \nabla_{\boldsymbol{\xi}} \mathbf{\Psi}^{ab}_{M,(in)\alpha} + n^\beta \frac{\partial \Psi^{ab}_{M,(in)\beta}}{\partial \xi^\alpha} \right) \right] \\ &\quad - \left[\lambda_I \nabla_{\boldsymbol{\xi}} \cdot \mathbf{\Psi}^{ab}_{I,(in)} n_\alpha + \mu_I \left(\boldsymbol{n} \cdot \nabla_{\boldsymbol{\xi}} \mathbf{\Psi}^{ab}_{I,(in)\alpha} + n^\beta \frac{\partial \Psi^{ab}_{I,(in)\beta}}{\partial \xi^\alpha} \right) \right] \\ &\quad = r \left[(\lambda_I - \lambda_M) \delta^{ab} n_\alpha + (\mu_I - \mu_M) \left(\delta^b_\alpha n^a + \delta^a_\alpha n^b \right) \right], \end{aligned} \tag{4.2.26}$$

on the boundary ∂I where $\rho = 1$ and I denotes the inclusion region.

The scalar functions $\Psi^{ab}_{(in)3}$ and $\psi^{ab}_{(in)}$ satisfy the equations

$$\nabla^2_{\boldsymbol{\xi}} \Psi^{ab}_{M,(in)3} = 0 \text{ when } \rho > 1, \tag{4.2.27}$$

$$\nabla^2_{\boldsymbol{\xi}} \Psi^{ab}_{I,(in)3} = 0 \text{ when } \rho < 1, \tag{4.2.28}$$

$$\nabla^2_{\boldsymbol{\xi}} \psi^{ab}_{M,(in)} = 0 \text{ when } \rho > 1, \tag{4.2.29}$$

$$\nabla^2_{\boldsymbol{\xi}} \psi^{ab}_{I,(in)} = 0 \text{ when } \rho < 1, \tag{4.2.30}$$

along with continuity conditions

$$\Psi^{ab}_{M,3} = \Psi^{ab}_{I,3}, \tag{4.2.31}$$

$$\psi^{ab}_M = \psi^{ab}_I, \tag{4.2.32}$$

$$\boldsymbol{n} \cdot \left[\mu_M \nabla_{\boldsymbol{\xi}} \Psi^{ab}_{M,(in)3} - \mu_I \nabla_{\boldsymbol{\xi}} \Psi^{ab}_{I,(in)3} - e_{51} \nabla_{\boldsymbol{\xi}} \psi^{ab}_{I,(in)} \right] = r(\mu_I - \mu_M) \left(\delta^b_3 n^a + \delta^a_3 n^b \right), \tag{4.2.33}$$

$$\boldsymbol{n} \cdot \left[\epsilon^S_{I,11} \nabla_{\boldsymbol{\xi}} \psi^{ab}_{I,(in)} - \epsilon^S_{M,11} \nabla_{\boldsymbol{\xi}} \psi^{ab}_{M,(in)} - S_p e_{51} \nabla_{\boldsymbol{\xi}} \Psi^{ab}_{I,(in)3} \right] = r n^\alpha S_p e^{ab}_\alpha. \tag{4.2.34}$$

The domain of the inclusion is the unit circle, while the domain of the matrix phase is the remainder of $\mathbb{R}^2$, as illustrated in Figure 4.2.

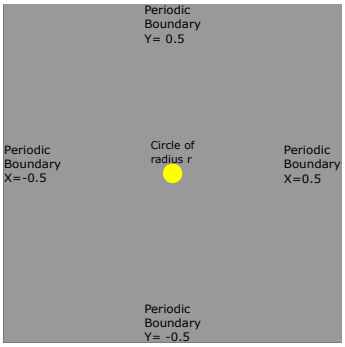


Figure 4.2: Unit cell with inclusion of radius $0 < r \ll 1$ with respect to microscale variable $\boldsymbol{X}$.

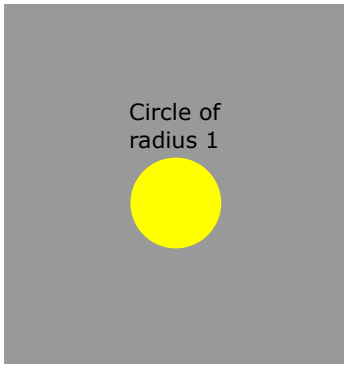


Figure 4.3: The inclusion now has radius 1 with respect to the new scaling $\boldsymbol{\xi} = \boldsymbol{X}/r$.

4.2.3 Solutions to cell problems

For each $a, b \in \{1, 2, 3\}$, there is a corresponding cell problem, where each ordered pair (a, b) corresponds to a straining direction from the strain tensor. Since three of the problems are duplicates of other problems, this reduces the number of cell problems we must solve to six. Equation (4.2.35) shows the strain tensor $\boldsymbol{S}$, which is the symmetric part of the gradient of the displacement

$$\boldsymbol{S} = \begin{pmatrix} S_{11} & S_{12} & S_{13} \\ S_{12} & S_{22} & S_{23} \\ S_{13} & S_{23} & S_{33} \end{pmatrix}, \tag{4.2.35}$$

where each colour represents a different cell problem. Note that in the limit as $r \to 0$, the solutions to the outer problems tend to zero as the outer problem does not see any inclusion and hence the solution is trivial. We thus deduce that

$$\boldsymbol{\Psi}^{ab}_{(out)} = o(1), \qquad \psi^{ab}_{(out)} = o(1). \tag{4.2.36}$$

4.2.3.1 The 11-problem

From (F.4.1), we see that

$$\Psi^{11}_3 = 0, \tag{4.2.37}$$

$$\psi^{11} = 0. \tag{4.2.38}$$

This means we only need to solve (4.2.9)-(4.2.10), subject to continuity conditions (4.2.15) and (4.2.18).

4.2.3.1.1 The leading-order inner problem

Based on the jump condition (4.2.26), we expand the inner problem as

$$\Psi^{11}_{(in)\alpha} \sim r\Psi^{11}_{(in)(0)\alpha}. \tag{4.2.39}$$

Then $\boldsymbol{\Psi}^{11}_{(in)(0)}$ satisfies (4.2.23) in the matrix phase ($\rho > 1$), (4.2.24) in the inclusion phase ($\rho < 1$), the continuity condition (4.2.25) and the jump condition

$$\begin{aligned}
&\left[\lambda_M \nabla_{\boldsymbol{\xi}} \cdot \boldsymbol{\Psi}^{11}_{M,(in)(0)} n_\alpha + \mu_M \left(\boldsymbol{n} \cdot \nabla_{\boldsymbol{\xi}} \Psi^{11}_{M,(in)(0)\alpha} + n^\beta \frac{\partial \Psi^{11}_{M,(in)(0)\beta}}{\partial \xi^\alpha}\right)\right] \\
&\qquad - \left[\lambda_I \nabla_{\boldsymbol{\xi}} \cdot \boldsymbol{\Psi}^{11}_{I,(in)(0)} n_\alpha + \mu_I \left(\boldsymbol{n} \cdot \nabla_{\boldsymbol{\xi}} \Psi^{11}_{I,(in)(0)\alpha} + n^\beta \frac{\partial \Psi^{11}_{I,(in)(0)\beta}}{\partial \xi^\alpha}\right)\right] \\
&= (\kappa_I - \kappa_M)\left(\cos(\theta)\delta^1_\alpha + \sin(\theta)\delta^2_\alpha\right) + (\mu_I - \mu_M)\left(\cos(\theta)\delta^1_\alpha - \sin(\theta)\delta^2_\alpha\right),
\end{aligned} \tag{4.2.40}$$

with $\Psi^{11}_{M,(in)(0)\alpha} = o(\rho)$ as $\rho \to \infty$ to match with the outer solution and θ denoting the azimuthal angle. As we shall see shortly, in order to impose periodicity to the solutions to the outer problems, we will need to take lattice sums of translated copies of the inner solution. We must therefore impose that the leading-order term in the inner expansion tends to zero as $\rho \to \infty$.

Our approach is to use basis functions which satisfy certain jump conditions, to find the solutions that satisfy the jump conditions in (4.2.40).
We define the vector fields $\boldsymbol{K}_I$ and $\boldsymbol{K}_M$ by

$$K_{M,1}(\xi,\eta) = -\frac{1}{2(\kappa_I + \mu_M)}\frac{\xi}{\xi^2+\eta^2}, \qquad K_{M,2}(\xi,\eta) = -\frac{1}{2(\kappa_I + \mu_M)}\frac{\eta}{\xi^2+\eta^2}, \tag{4.2.41}$$

for $\rho > 1$,

$$K_{I,1}(\xi,\eta) = -\frac{1}{2(\kappa_I + \mu_M)}\xi, \qquad K_{I,2}(\xi,\eta) = -\frac{1}{2(\kappa_I + \mu_M)}\eta, \tag{4.2.42}$$

for $\rho < 1$.
We define the vector fields $\boldsymbol{\Lambda}_I$ and $\boldsymbol{\Lambda}_M$ by

$$\Lambda_{M,1}(\xi,\eta) = \frac{\mu_M}{\kappa_M\mu_M + \mu_I\kappa_M + 2\mu_M\mu_I}\left(-\frac{\xi}{\xi^2+\eta^2}\right) + \frac{\kappa_M}{\kappa_M\mu_M + \mu_I\kappa_M + 2\mu_M\mu_I}\left(\frac{\xi(\eta^2-\xi^2)}{(\xi^2+\eta^2)^2} + \frac{1}{2}\frac{\xi(\xi^2-3\eta^2)}{(\xi^2+\eta^2)^3}\right), \quad (4.2.43)$$

$$\Lambda_{M,2}(\xi,\eta) = \frac{\mu_M}{\kappa_M\mu_M + \mu_I\kappa_M + 2\mu_M\mu_I}\left(\frac{\eta}{\xi^2+\eta^2}\right) + \frac{\kappa_M}{\kappa_M\mu_M + \mu_I\kappa_M + 2\mu_M\mu_I}\left(\frac{\eta(\eta^2-\xi^2)}{(\xi^2+\eta^2)^2} + \frac{1}{2}\frac{\eta(3\xi^2-\eta^2)}{(\xi^2+\eta^2)^3}\right), \quad (4.2.44)$$

$$\Lambda_{I,1}(\xi,\eta) = -\frac{1}{2}\frac{\kappa_M + 2\mu_M}{\kappa_M\mu_M + \mu_I\kappa_M + 2\mu_M\mu_I}\xi, \quad (4.2.45)$$

$$\Lambda_{I,2}(\xi,\eta) = \frac{1}{2}\frac{\kappa_M + 2\mu_M}{\kappa_M\mu_M + \mu_I\kappa_M + 2\mu_M\mu_I}\eta. \quad (4.2.46)$$

The vector fields $\boldsymbol{K}$ and $\boldsymbol{\Lambda}$ satisfy (4.2.9)-(4.2.10) and the continuity condition (4.2.25) on the boundary $S^1 = \{(\xi,\eta) : \xi^2+\eta^2 = 1\}$. The jump conditions that $\boldsymbol{K}$ and $\boldsymbol{\Lambda}$ satisfy on the boundary are given by

$$\begin{aligned}
& n^\beta\left[c^{\gamma\iota}_{M,\alpha\beta}\frac{\partial K_{M,\gamma}}{\partial\xi^\iota} - c^{\gamma\iota}_{I,\alpha\beta}\frac{\partial K_{I,\gamma}}{\partial\xi^\iota}\right] \\
&= \left[\lambda_M\nabla_{\boldsymbol{\xi}}\cdot(\boldsymbol{K}_M)\,n_\alpha + \mu_M\left(\boldsymbol{n}\cdot\nabla_{\boldsymbol{\xi}}K_{M,\alpha} + n^\beta\frac{\partial K_{M,\beta}}{\partial\xi^\alpha}\right)\right] \\
&\quad - \left[\lambda_I\nabla_{\boldsymbol{\xi}}\cdot(\boldsymbol{K}_I)\,n_\alpha + \mu_I\left(\boldsymbol{n}\cdot\nabla_{\boldsymbol{\xi}}K_{I,\alpha} + n^\beta\frac{\partial K_{I,\beta}}{\partial\xi^\alpha}\right)\right] \\
&= \cos(\theta)\delta^1_\alpha + \sin(\theta)\delta^2_\alpha, \quad (4.2.47)\\
& n^\beta\left[c^{\gamma\iota}_{M,\alpha\beta}\frac{\partial \Lambda_{M,\gamma}}{\partial\xi^\iota} - c^{\gamma\iota}_{I,\alpha\beta}\frac{\partial \Lambda_{I,\gamma}}{\partial\xi^\iota}\right] \\
&= \left[\lambda_M\nabla_{\boldsymbol{\xi}}\cdot(\boldsymbol{\Lambda}_M)\,n_\alpha + \mu_M\left(\boldsymbol{n}\cdot\nabla_{\boldsymbol{\xi}}\Lambda_{M,\alpha} + n^\beta\frac{\partial \Lambda_{M,\beta}}{\partial\xi^\alpha}\right)\right] \\
&\quad - \left[\lambda_I\nabla_{\boldsymbol{\xi}}\cdot(\boldsymbol{\Lambda}_I)\,n_\alpha + \mu_I\left(\boldsymbol{n}\cdot\nabla_{\boldsymbol{\xi}}\Lambda_{I,\alpha} + n^\beta\frac{\partial \Lambda_{I,\beta}}{\partial\xi^\alpha}\right)\right] \\
&= \cos(\theta)\delta^1_\alpha - \sin(\theta)\delta^2_\alpha. \quad (4.2.48)
\end{aligned}$$

By inspection, $|\boldsymbol{K}_M|, |\boldsymbol{\Lambda}_M| = o(\rho)$ as $\rho\to\infty$. These two functions will be used to help find inner solutions which are continuous on the boundary S^1. The solutions to the inner problems will be linear combinations of the solutions $\boldsymbol{K}$ and $\boldsymbol{\Lambda}$.

Using (4.2.40), we deduce that

$$\begin{aligned}\Psi^{11}_{M,(in)(0)\alpha} &= (\kappa_I - \kappa_M)K_{M,\alpha} + (\mu_I - \mu_M)\Lambda_{M,\alpha},\\ \Psi^{11}_{I,(in)(0)\alpha} &= (\kappa_I - \kappa_M)K_{I,\alpha} + (\mu_I - \mu_M)\Lambda_{I,\alpha}.\end{aligned} \tag{4.2.49}$$

4.2.3.1.2 Outer limit of the leading-order inner solution

Using (4.2.39), (4.2.49) and the formulae for $\boldsymbol{K}$ and $\boldsymbol{\Lambda}$ found in (4.2.41)-(4.2.46), we deduce

$$\begin{aligned}(1.t.i)\Psi^{11}_{M,1} =& - r\left(\frac{(\kappa_I - \kappa_M)}{2\,(\kappa_I + \mu_M)}\right)\left(\frac{\xi}{\xi^2+\eta^2}\right)\\ &- r\frac{(\mu_I - \mu_M)\mu_M}{\kappa_M\mu_M + \mu_I\kappa_M + 2\mu_M\mu_I}\left(\frac{\xi}{\xi^2+\eta^2}\right)\\ &+ r\frac{(\mu_I - \mu_M)\kappa_M}{\kappa_M\mu_M + \mu_I\kappa_M + 2\mu_M\mu_I}\left(\frac{\xi(\eta^2-\xi^2)}{(\xi^2+\eta^2)^2} + \frac{1}{2}\frac{\xi(\xi^2-3\eta^2)}{(\xi^2+\eta^2)^3}\right),\end{aligned} \tag{4.2.50}$$

$$\begin{aligned}(1.t.i)\Psi^{11}_{M,2} =& - r\left(\frac{(\kappa_I - \kappa_M)}{2\,(\kappa_I + \mu_M)}\right)\left(\frac{\eta}{\xi^2+\eta^2}\right)\\ &+ r\frac{(\mu_I - \mu_M)\mu_M}{\kappa_M\mu_M + \mu_I\kappa_M + 2\mu_M\mu_I}\left(\frac{\eta}{\xi^2+\eta^2}\right)\\ &+ r\frac{(\mu_I - \mu_M)\kappa_M}{\kappa_M\mu_M + \mu_I\kappa_M + 2\mu_M\mu_I}\left(\frac{\eta(\eta^2-\xi^2)}{(\xi^2+\eta^2)^2} + \frac{1}{2}\frac{\eta(3\xi^2-\eta^2)}{(\xi^2+\eta^2)^3}\right).\end{aligned} \tag{4.2.51}$$

If we write (4.2.50)-(4.2.51) in terms of outer variables and then expand them, we find

$$\begin{aligned}(1.t.o)(1.t.i)\Psi^{11}_{M,1} =& - r^2\left(\frac{(\kappa_I - \kappa_M)}{2\,(\kappa_I + \mu_M)}\right)\left(\frac{X}{X^2+Y^2}\right)\\ &- r^2\frac{(\mu_I - \mu_M)\mu_M}{\kappa_M\mu_M + \mu_I\kappa_M + 2\mu_M\mu_I}\left(\frac{X}{X^2+Y^2}\right)\\ &+ r^2\frac{(\mu_I - \mu_M)\kappa_M}{\kappa_M\mu_M + \mu_I\kappa_M + 2\mu_M\mu_I}\left(\frac{X(Y^2-X^2)}{(X^2+Y^2)^2}\right),\end{aligned} \tag{4.2.52}$$

$$\begin{aligned}(1.t.o)(1.t.i)\Psi^{11}_{M,2} =& - r^2\left(\frac{(\kappa_I - \kappa_M)}{2\,(\kappa_I + \mu_M)}\right)\left(\frac{Y}{X^2+Y^2}\right)\\ &+ r^2\frac{(\mu_I - \mu_M)\mu_M}{\kappa_M\mu_M + \mu_I\kappa_M + 2\mu_M\mu_I}\left(\frac{Y}{X^2+Y^2}\right)\\ &+ r^2\frac{(\mu_I - \mu_M)\kappa_M}{\kappa_M\mu_M + \mu_I\kappa_M + 2\mu_M\mu_I}\left(\frac{Y(Y^2-X^2)}{(X^2+Y^2)^2}\right).\end{aligned} \tag{4.2.53}$$

Thus we then find that the outer expansion for $\mathbf{\Psi}^{11}$ takes the form

$$\Psi^{11}_{(out)\alpha} = r^2 \Psi^{11}_{(out)(0)\alpha} + \cdots , \tag{4.2.54}$$

where $\Psi^{11}_{(out)(0)\alpha}$ satisfies the matching condition

$$\begin{aligned}
\Psi^{11}_{(out)(0)1} \sim & - \left(\frac{(\kappa_I - \kappa_M)}{2\,(\kappa_I + \mu_M)} \right) \left(\frac{X}{X^2 + Y^2} \right) \\
& - \frac{(\mu_I - \mu_M)\mu_M}{\kappa_M \mu_M + \mu_I \kappa_M + 2\mu_M \mu_I} \left(\frac{X}{X^2 + Y^2} \right) \\
& + \frac{(\mu_I - \mu_M)\kappa_M}{\kappa_M \mu_M + \mu_I \kappa_M + 2\mu_M \mu_I} \left(\frac{X(Y^2 - X^2)}{(X^2 + Y^2)^2} \right), \qquad (4.2.55) \\
\Psi^{11}_{(out)(0)2} \sim & - \left(\frac{(\kappa_I - \kappa_M)}{2\,(\kappa_I + \mu_M)} \right) \left(\frac{Y}{X^2 + Y^2} \right) \\
& + \frac{(\mu_I - \mu_M)\mu_M}{\kappa_M \mu_M + \mu_I \kappa_M + 2\mu_M \mu_I} \left(\frac{Y}{X^2 + Y^2} \right) \\
& + \frac{(\mu_I - \mu_M)\kappa_M}{\kappa_M \mu_M + \mu_I \kappa_M + 2\mu_M \mu_I} \left(\frac{Y(Y^2 - X^2)}{(X^2 + Y^2)^2} \right), \qquad (4.2.56)
\end{aligned}$$

as $R \to 0$.

4.2.3.1.3 First order outer solution

The matching conditions (4.2.55)-(4.2.56) give us enough information to uniquely find the solution for $\Psi^{11}_{(out)(0)\alpha}$. The functions in (4.2.55)-(4.2.56) satisfy the outer equations but are not periodic. To make $\Psi^{11}_{(out)(0)1}$ and $\Psi^{11}_{(out)(0)2}$ periodic we take a lattice sum of these functions by adding translated copies of these solutions by integer shifts in the $X-$ and $Y-$directions. This construction is standard for forming periodic solutions (see Helsing [33]). This process yields

$$
\begin{aligned}
&(1.t.o)\Psi_1^{11} \\
&\quad = -r^2\left(\frac{(\kappa_I-\kappa_M)}{2\left(\kappa_I+\mu_M\right)}+\frac{(\mu_I-\mu_M)\mu_M}{\kappa_M\mu_M+\kappa_M\mu_I+2\mu_M\mu_I}\right)\left(\sum_{l=-\infty}^{\infty}\sum_{k=-\infty}^{\infty}\frac{X-k}{(X-k)^2+(Y-l)^2}\right) \\
&\qquad + r^2\frac{(\mu_I-\mu_M)\kappa_M}{\kappa_M\mu_M+\mu_I\kappa_M+2\mu_M\mu_I}\left(\sum_{l=-\infty}^{\infty}\sum_{k=-\infty}^{\infty}\frac{(X-k)((Y-l)^2-(X-k)^2)}{((X-k)^2+(Y-l)^2)^2}\right),
\end{aligned}
\tag{4.2.57}
$$

$$
\begin{aligned}
&(1.t.o)\Psi_2^{11} \\
&\quad = -r^2\left(\frac{(\kappa_I-\kappa_M)}{2\left(\kappa_I+\mu_M\right)}-\frac{(\mu_I-\mu_M)\mu_M}{\kappa_M\mu_M+\kappa_M\mu_I+2\mu_M\mu_I}\right)\left(\sum_{k=-\infty}^{\infty}\sum_{l=-\infty}^{\infty}\frac{Y-l}{(X-k)^2+(Y-l)^2}\right) \\
&\qquad + r^2\frac{(\mu_I-\mu_M)\kappa_M}{\kappa_M\mu_M+\mu_I\kappa_M+2\mu_M\mu_I}\left(\sum_{k=-\infty}^{\infty}\sum_{l=-\infty}^{\infty}\frac{(Y-l)((Y-l)^2-(X-k)^2)}{((X-k)^2+(Y-l)^2)^2}\right).
\end{aligned}
\tag{4.2.58}
$$

The expressions in (4.2.57) and (4.2.58) are only conditionally convergent, so care must be taken in specifying the order of summation. The order of summations in (4.2.57) and (4.2.58) are chosen to ensure that the resulting functions are 1-periodic in both X and Y. Alternative orderings may lead to different values. However, by using lattice sums, it can be shown that such differences are at most linear in X and Y. These differences correspond to homogeneous solutions of the outer problem, therefore do not affect the validity of the solution. The same consideration applies to all lattice sums used in this chapter, where the ordering of the summations are consistently chosen to enforce periodicity. Since all the functions being summed decay at $\mathcal{O}\left(\frac{1}{R}\right)$, and ambiguity arising from conditional convergence only contribute through linear terms, it follows that alternative orderings do not affect the validity of the solution.

4.2.3.1.4 Inner limit of the first order outer solution

If we Taylor expand (4.2.57)-(4.2.58) around $(X, Y) = (0, 0)$ using the expansions found in (H.0.5)-(H.0.6) and (H.0.11)-(H.0.12), we deduce that

$$\begin{aligned}(2.t.i)(1.t.o)\Psi_1^{11} =& r\left(\frac{(\kappa_M-\kappa_I)}{2\left(\kappa_I+\mu_M\right)}+\frac{(\mu_M-\mu_I)\mu_M}{\kappa_M\mu_M+\kappa_M\mu_I+2\mu_M\mu_I}\right)\left(\frac{\xi}{\xi^2+\eta^2}\right)\\ &+r\frac{(\mu_I-\mu_M)\kappa_M}{\kappa_M\mu_M+\mu_I\kappa_M+2\mu_M\mu_I}\left(\frac{\xi(\eta^2-\xi^2)}{(\xi^2+\eta^2)^2}\right)\\ &+r\frac{(\mu_I-\mu_M)}{2}\frac{\kappa_M}{\kappa_M\mu_M+\mu_I\kappa_M+2\mu_M\mu_I}\left(\frac{\xi(\xi^2-3\eta^2)}{(\xi^2+\eta^2)^3}\right)+r^3A\xi,\end{aligned} \tag{4.2.59}$$

$$\begin{aligned}(2.t.i)(1.t.o)\Psi_2^{11} =& r\left(\frac{(\kappa_M-\kappa_I)}{2\left(\kappa_I+\mu_M\right)}+\frac{(\mu_I-\mu_M)\mu_M}{\kappa_M\mu_M+\kappa_M\mu_I+2\mu_M\mu_I}\right)\left(\frac{\eta}{\xi^2+\eta^2}\right)\\ &+r\frac{(\mu_I-\mu_M)\kappa_M}{\kappa_M\mu_M+\mu_I\kappa_M+2\mu_M\mu_I}\left(\frac{\eta(\eta^2-\xi^2)}{(\xi^2+\eta^2)^2}\right)\\ &+r\frac{(\mu_I-\mu_M)}{2}\frac{\kappa_M}{\kappa_M\mu_M+\mu_I\kappa_M+2\mu_M\mu_I}\left(\frac{\eta(3\xi^2-\eta^2)}{(\xi^2+\eta^2)^3}\right)+r^3B\eta,\end{aligned} \tag{4.2.60}$$

where

$$A=\pi\left(\frac{(\kappa_I-\kappa_M)}{2(\kappa_I+\mu_M)}+\frac{(\mu_I-\mu_M)}{\kappa_M\mu_M+\kappa_M\mu_I+2\mu_M\mu_I}\left(\mu_M+\kappa_M\gamma\right)\right), \tag{4.2.61}$$

$$B=\pi\left(\frac{(\kappa_I-\kappa_M)}{2(\kappa_I+\mu_M)}-\frac{(\mu_I-\mu_M)}{\kappa_M\mu_M+\kappa_M\mu_I+2\mu_M\mu_I}\left(\mu_M+\kappa_M\gamma\right)\right), \tag{4.2.62}$$

and for convenience, we define

$$\gamma=1+4\sum_{l=1}^{\infty}\pi^2 l\coth(\pi l)\operatorname{csch}^2(\pi l), \tag{4.2.63}$$

which arises from the evaluation of the corresponding lattice sums.

4.2.3.1.5 Second order inner solution

We see that the inner expansion in the inner region should proceed as

$$\Psi_{(in)\alpha}^{11}\sim r\Psi_{(in)(0)\alpha}^{11}+r^3\Psi_{(in)(1)\alpha}^{11}, \tag{4.2.64}$$

where $\Psi_{(in)(1)\alpha}^{11}$ has the matching condition

$$\Psi_{(in)(1)\alpha}^{11}\sim A\xi,\qquad \Psi_{(in)(1)\alpha}^{11}\sim B\eta, \tag{4.2.65}$$

as $\rho\to\infty$.

The cell function $\boldsymbol{\Psi}^{11}_{(in)(1)}$ satisfies (4.2.23) in the matrix phase ($\rho > 1$), (4.2.24) in the inclusion phase ($\rho < 1$), the continuity condition (4.2.25) and the jump condition

$$\left[\lambda_M \nabla_{\boldsymbol{\xi}} \cdot \boldsymbol{\Psi}^{11}_{M,(in)(1)} n_\alpha + \mu_M \left(\boldsymbol{n} \cdot \nabla_{\boldsymbol{\xi}} \Psi^{11}_{M,(in)(1)\alpha} + n^\beta \frac{\partial \Psi^{11}_{M,(in)(0)\beta}}{\partial \xi^\alpha}\right)\right]$$
$$- \left[\lambda_I \nabla_{\boldsymbol{\xi}} \cdot \boldsymbol{\Psi}^{11}_{I,(in)(1)} n_\alpha + \mu_I \left(\boldsymbol{n} \cdot \nabla_{\boldsymbol{\xi}} \Psi^{11}_{I,(in)(1)\alpha} + n^\beta \frac{\partial \Psi_{I,(in)(0)\beta}}{\partial \xi^\alpha}\right)\right] = 0. \tag{4.2.66}$$

The solution for $\boldsymbol{\Psi}^{11}_{M,(in)(1)}$ and $\boldsymbol{\Psi}^{11}_{I,(in)(1)}$ that satisfies the jump condition (4.2.66) and the matching condition (4.2.65) is

$$\Psi^{11}_{M,(in)(1)1} = A\xi + (\kappa_I - \kappa_M)(A+B)K_{M,1} + (\mu_I - \mu_M)(A-B)\Lambda_{M1}, \tag{4.2.67}$$
$$\Psi^{11}_{M,(in)(1)2} = B\eta + (\kappa_I - \kappa_M)(A+B)K_{M,2} + (\mu_I - \mu_M)(A-B)\Lambda_{M2}, \tag{4.2.68}$$
$$\Psi^{11}_{I,(in)(1)1} = A\xi + (\kappa_I - \kappa_M)(A+B)K_{I,1} + (\mu_I - \mu_M)(A-B)\Lambda_{I1}, \tag{4.2.69}$$
$$\Psi^{11}_{I,(in)(1)2} = B\eta + (\kappa_I - \kappa_M)(A+B)K_{I,2} + (\mu_I - \mu_M)(A-B)\Lambda_{I2}, \tag{4.2.70}$$

where we recall that $\boldsymbol{K}$, $\boldsymbol{\Lambda}$ are given in (4.2.41)-(4.2.46).

We find that in order to evaluate the effective coefficients we need the inner solution evaluated on the surface of the inclusion, which is

$$(2.t.i)\Psi^{11}_{I,(in)1} = r\left(\frac{(\kappa_M - \kappa_I)}{2(\kappa_I + \mu_M)} - \frac{(\mu_I - \mu_M)}{2}\frac{\kappa_M + 2\mu_M}{\kappa_M\mu_M + \mu_I\kappa_M + 2\mu_M\mu_I}\right)\xi$$
$$+ r^3\left(A - \frac{(\kappa_I - \kappa_M)(A+B)}{2(\kappa_I + \mu_M)} - \frac{(\mu_I - \mu_M)(A-B)}{2}\frac{\kappa_M + 2\mu_M}{\kappa_M\mu_M + \mu_I\kappa_M + 2\mu_M\mu_I}\right)\xi, \tag{4.2.71}$$

$$(2.t.i)\Psi^{11}_{I,(in)2} = r\left(\frac{(\kappa_M - \kappa_I)}{2(\kappa_I + \mu_M)} + \frac{(\mu_I - \mu_M)}{2}\frac{\kappa_M + 2\mu_M}{\kappa_M\mu_M + \mu_I\kappa_M + 2\mu_M\mu_I}\right)\eta$$
$$+ r^3\left(B - \frac{(\kappa_I - \kappa_M)(A+B)}{2(\kappa_I + \mu_M)} + \frac{(\mu_I - \mu_M)(A-B)}{2}\frac{\kappa_M + 2\mu_M}{\kappa_M\mu_M + \mu_I\kappa_M + 2\mu_M\mu_I}\right)\eta. \tag{4.2.72}$$

Using (4.2.61)-(4.2.63), we see that (4.2.71)-(4.2.72) can be re-written as

$$\Psi^{11}_{I,(in)1} = r\left(\frac{(\kappa_M-\kappa_I)}{2\left(\kappa_I+\mu_M\right)}-\frac{(\mu_I-\mu_M)}{2}\frac{\kappa_M+2\mu_M}{\kappa_M\mu_M+\mu_I\kappa_M+2\mu_M\mu_I}\right)\xi + r^3\left(\frac{(\kappa_I-\kappa_M)(\kappa_M+\mu_M)}{2(\kappa_I+\mu_M)^2}\right)\pi\xi + r^3\left(\frac{2\mu_M(\kappa_M+\mu_M)(\mu_I-\mu_M)\left(\mu_M+\kappa_M\left(1+4\sum_{l=1}^{\infty}\pi^2 l\coth(\pi l)\operatorname{csch}^2(\pi l)\right)\right)}{(\kappa_M(\mu_I+\mu_M)+2\mu_I\mu_M)^2}\right)\pi\xi, \tag{4.2.73}$$

$$\Psi^{11}_{I,(in)2} = r\left(\frac{(\kappa_M-\kappa_I)}{2\left(\kappa_I+\mu_M\right)}+\frac{(\mu_I-\mu_M)}{2}\frac{\kappa_M+2\mu_M}{\kappa_M\mu_M+\mu_I\kappa_M+2\mu_M\mu_I}\right)\eta + r^3\left(\frac{(\kappa_I-\kappa_M)(\kappa_M+\mu_M)}{2(\kappa_I+\mu_M)^2}\right)\pi\eta - r^3\left(\frac{2\mu_M(\kappa_M+\mu_M)(\mu_I-\mu_M)\left(\mu_M+\kappa_M\left(1+4\sum_{l=1}^{\infty}\pi^2 l\coth(\pi l)\operatorname{csch}^2(\pi l)\right)\right)}{(\kappa_M(\mu_I+\mu_M)+2\mu_I\mu_M)^2}\right)\pi\eta. \tag{4.2.74}$$

We now have the first two terms in the inner expansion of $\mathbf{\Psi}^{11}$, which we will be able to use to approximate the $11-$coefficients of each of the stiffness and electromechanical tensors.

4.2.3.2 The 22-problem

From (F.4.1), we see that

$$\Psi^{22}_3 = 0, \tag{4.2.75}$$

$$\psi^{22} = 0. \tag{4.2.76}$$

This means we only need to solve (4.2.9)-(4.2.10), subject to continuity conditions (4.2.15) and (4.2.18).

The cell function $\mathbf{\Psi}^{22}_{(in)(0)}$ satisfies (4.2.23) in the matrix phase ($\rho > 1$), (4.2.24) in the inclusion phase ($\rho < 1$), the continuity condition (4.2.25) and the jump condition

$$\left[\lambda_M \nabla_{\boldsymbol{\xi}} \cdot \boldsymbol{\Psi}^{22}_{M,(in)(0)} n_\alpha + \mu_M \left(\boldsymbol{n} \cdot \nabla_{\boldsymbol{\xi}} \Psi^{22}_{M,(in)(0)\alpha} + n^\beta \frac{\partial \Psi^{22}_{M,(in)(0)\beta}}{\partial \xi^\alpha} \right) \right]$$
$$- \left[\lambda_I \nabla_{\boldsymbol{\xi}} \cdot \boldsymbol{\Psi}^{22}_{I,(in)(0)} n_\alpha + \mu_I \left(\boldsymbol{n} \cdot \nabla_{\boldsymbol{\xi}} \Psi^{22}_{I,(in)(0)\alpha} + n^\beta \frac{\partial \Psi^{22}_{I,(in)(0)\beta}}{\partial \xi^\alpha} \right) \right]$$
$$= (\kappa_I - \kappa_M) \left(\cos(\theta)\delta^1_\alpha + \sin(\theta)\delta^2_\alpha \right) - (\mu_I - \mu_M) \left(\cos(\theta)\delta^1_\alpha - \sin(\theta)\delta^2_\alpha \right). \quad (4.2.77)$$

Since the 22-problem is similar to the 11-problem, except with the X- and Y-directions flipped, we can use the 11-solution from (4.2.73) and (4.2.74) to deduce the solution to the 22-problem on the boundary ∂I. This is given by

$$\Psi^{22}_{I,(in)1} = r \left(\frac{(\kappa_M - \kappa_I)}{2\,(\kappa_I + \mu_M)} + \frac{(\mu_I - \mu_M)}{2} \frac{\kappa_M + 2\mu_M}{\kappa_M \mu_M + \mu_I \kappa_M + 2\mu_M \mu_I} \right) \xi$$
$$+ r^3 \left(\frac{(\kappa_I - \kappa_M)(\kappa_M + \mu_M)}{2(\kappa_I + \mu_M)^2} \right) \pi \xi$$
$$- r^3 \left(\frac{2\mu_M(\kappa_M + \mu_M)(\mu_I - \mu_M) \left(\mu_M + \kappa_M \left(1 + 4 \sum_{l=1}^{\infty} \pi^2 l \coth(\pi l)\, \mathrm{csch}^2(\pi l) \right) \right)}{(\kappa_M(\mu_I + \mu_M) + 2\mu_I \mu_M)^2} \right) \pi \xi, \quad (4.2.78)$$

$$\Psi^{22}_{I,(in)2} = r \left(\frac{(\kappa_M - \kappa_I)}{2\,(\kappa_I + \mu_M)} - \frac{(\mu_I - \mu_M)}{2} \frac{\kappa_M + 2\mu_M}{\kappa_M \mu_M + \mu_I \kappa_M + 2\mu_M \mu_I} \right) \eta$$
$$+ r^3 \left(\frac{(\kappa_I - \kappa_M)(\kappa_M + \mu_M)}{2(\kappa_I + \mu_M)^2} \right) \pi \eta$$
$$+ r^3 \left(\frac{2\mu_M(\kappa_M + \mu_M)(\mu_I - \mu_M) \left(\mu_M + \kappa_M \left(1 + 4 \sum_{l=1}^{\infty} \pi^2 l \coth(\pi l)\, \mathrm{csch}^2(\pi l) \right) \right)}{(\kappa_M(\mu_I + \mu_M) + 2\mu_I \mu_M)^2} \right) \pi \eta. \quad (4.2.79)$$

We now have the first two terms in the inner expansion of $\boldsymbol{\Psi}^{22}$, which we will be able to use to approximate the 22-coefficients of each of the stiffness and electromechanical tensors.

4.2.3.3 The 33-problem

From (F.4.2), we see that

$$\Psi_3^{33} = 0, \tag{4.2.80}$$

$$\psi^{33} = 0. \tag{4.2.81}$$

This means we only need to solve (4.2.9)-(4.2.10), subject to continuity conditions (4.2.15) and (4.2.18).

4.2.3.3.1 The leading-order inner problem

Based on the jump conditions (4.2.26), we expand the problem as

$$\Psi^{33}_{(in)\alpha} \sim r\Psi^{33}_{(in)(0)\alpha}, \qquad \psi^{33}_{(in)} \sim r\psi^{33}_{(in)(0)}. \tag{4.2.82}$$

The cell function $\mathbf{\Psi}^3_{(in)(0)}$ satisfies (4.2.23) in the matrix phase ($\rho > 1$), (4.2.24) in the inclusion phase ($\rho < 1$), the continuity condition (4.2.25) and the jump condition

$$\begin{aligned}\left[\lambda_M \nabla_{\boldsymbol{\xi}} \cdot \mathbf{\Psi}^{33}_{M,(in)(0)} n_\alpha + \mu_M \left(\boldsymbol{n} \cdot \nabla_{\boldsymbol{\xi}} \Psi^{33}_{M,(in)(0)\alpha} + n^\beta \frac{\partial \Psi^{33}_{M,(in)(0)\beta}}{\partial \xi^\alpha}\right)\right] \\ - \left[\lambda_I \nabla_{\boldsymbol{\xi}} \cdot \mathbf{\Psi}^{33}_{I,(in)(0)} n_\alpha + \mu_I \left(\boldsymbol{n} \cdot \nabla_{\boldsymbol{\xi}} \Psi^{33}_{I,(in)(0)\alpha} + n^\beta \frac{\partial \Psi^{33}_{I,(in)(0)\beta}}{\partial \xi^\alpha}\right)\right] \\ = (\lambda_I - \lambda_M)\left(\cos(\theta)\delta^1_\alpha + \sin(\theta)\delta^2_\alpha\right).\end{aligned} \tag{4.2.83}$$

The solution is

$$\Psi^{33}_{M,(in)(0)\alpha} = (\lambda_I - \lambda_M) K_{M,\alpha}, \qquad \Psi^{33}_{I,(in)(0)\alpha} = (\lambda_I - \lambda_M) K_{I,\alpha}, \tag{4.2.84}$$

that is,

$$r\Psi^{33}_{M,(in)(0)1} = -r\frac{(\lambda_I - \lambda_M)}{2(\kappa_I + \mu_M)}\left(\frac{\xi}{\xi^2 + \eta^2}\right), \tag{4.2.85}$$

$$r\Psi^{33}_{M,(in)(0)2} = -r\frac{(\lambda_I - \lambda_M)}{2(\kappa_I + \mu_M)}\left(\frac{\eta}{\xi^2 + \eta^2}\right). \tag{4.2.86}$$

4.2.3.3.2 Outer limit of leading-order inner solution

Writing (4.2.85)-(4.2.86) in terms of outer variables, we find

$$(1.t.o)(1.t.i)\Psi^{33}_{M,1} = -r^2\frac{(\lambda_I-\lambda_M)}{2\left(\kappa_I+\mu_M\right)}\left(\frac{X}{X^2+Y^2}\right), \tag{4.2.87}$$

$$(1.t.o)(1.t.i)\Psi^{33}_{M,2} = -r^2\frac{(\lambda_I-\lambda_M)}{2\left(\kappa_I+\mu_M\right)}\left(\frac{Y}{X^2+Y^2}\right). \tag{4.2.88}$$

4.2.3.3.3 Leading-order outer solution

From (4.2.87) and (4.2.88), we see that the one-term outer solution for $\mathbf{\Psi}^{33}$ takes the form

$$\Psi^{33}_{(out)\alpha} \sim r^2\Psi^{33}_{(out)(0)\alpha}, \tag{4.2.89}$$

where $\Psi^{33}_{(out)(0)\alpha}$ satisfies the matching condition

$$\Psi^{33}_{M,(out)(0)1}\sim -\frac{(\lambda_I-\lambda_M)}{2\left(\kappa_I+\mu_M\right)}\left(\frac{X}{X^2+Y^2}\right), \tag{4.2.90}$$

$$\Psi^{33}_{M,(out)(0)2}\sim -\frac{(\lambda_I-\lambda_M)}{2\left(\kappa_I+\mu_M\right)}\left(\frac{Y}{X^2+Y^2}\right), \tag{4.2.91}$$

as $R\to 0$. In addition $\Psi^{33}_{(out)(0)\alpha}$ must also satisfy (4.2.9) along with periodic boundary conditions on the boundary $\partial\Gamma$. We find

$$\Psi^{33}_{(out)(0)1} = -r^2\frac{(\lambda_I-\lambda_M)}{2\left(\kappa_I+\mu_M\right)}\sum_{l=-\infty}^{\infty}\sum_{k=-\infty}^{\infty}\frac{X-k}{(X-k)^2+(Y-l)^2}, \tag{4.2.92}$$

$$\Psi^{33}_{(out)(0)2} = -r^2\frac{(\lambda_I-\lambda_M)}{2\left(\kappa_I+\mu_M\right)}\sum_{k=-\infty}^{\infty}\sum_{l=-\infty}^{\infty}\frac{Y-l}{(X-k)^2+(Y-l)^2}. \tag{4.2.93}$$

4.2.3.3.4 Inner limit of first order outer solution

If we Taylor expand this expression around $(X,Y)=(0,0)$ using the expansions found in (H.0.5)-(H.0.6) and then re-write in terms of inner variables, we deduce that

$$(2.t.i)(1.t.o)\Psi^{33}_{M,1} = -r\frac{(\lambda_I-\lambda_M)}{2\left(\kappa_I+\mu_M\right)}\left(\frac{\xi}{\xi^2+\eta^2}\right)+r^3\pi\frac{(\lambda_I-\lambda_M)}{2\left(\kappa_I+\mu_M\right)}\xi, \tag{4.2.94}$$

$$(2.t.i)(1.t.o)\Psi^{33}_{M,2} = -r\frac{(\lambda_I-\lambda_M)}{2\left(\kappa_I+\mu_M\right)}\left(\frac{\eta}{\xi^2+\eta^2}\right)+r^3\pi\frac{(\lambda_I-\lambda_M)}{2\left(\kappa_I+\mu_M\right)}\eta. \tag{4.2.95}$$

4.2.3.3.5 Second order inner solution

From (4.2.94)-(4.2.95) we deduce the inner expansion of $\Psi^{33}_{(in)\alpha}$ (up to two terms) takes the form

$$\Psi^{33}_{(in)\alpha} \sim r\Psi^{33}_{(in)(0)\alpha} + r^3\Psi^{33}_{(in)(1)\alpha}, \tag{4.2.96}$$

where $\mathbf{\Psi}^{33}_{(in)(1)}$ satisfies the matching condition

$$\Psi^{33}_{(in)(1)1} \sim \pi\frac{(\lambda_I - \lambda_M)}{2\left(\kappa_I + \mu_M\right)}\xi, \tag{4.2.97}$$

$$\Psi^{33}_{(in)(1)2} \sim \pi\frac{(\lambda_I - \lambda_M)}{2\left(\kappa_I + \mu_M\right)}\eta, \tag{4.2.98}$$

as $\rho \to \infty$. The cell function $\mathbf{\Psi}^{33}_{(in)(1)}$ satisfies (4.2.23) in the matrix phase ($\rho > 1$), (4.2.24) in the inclusion phase ($\rho < 1$), the continuity condition (4.2.25) and the jump condition

$$\left[\lambda_M \nabla_{\boldsymbol{\xi}} \cdot \mathbf{\Psi}^{33}_{M,(in)(1)} n_\alpha + \mu_M \left(\boldsymbol{n} \cdot \nabla_{\boldsymbol{\xi}} \Psi^{33}_{M,(in)(1)\alpha} + n^\beta \frac{\partial \Psi^{33}_{M,(in)(1)\beta}}{\partial \xi^\alpha}\right)\right]$$
$$- \left[\lambda_I \nabla_{\boldsymbol{\xi}} \cdot \mathbf{\Psi}^{33}_{I,(in)(1)} n_\alpha + \mu_I \left(\boldsymbol{n} \cdot \nabla_{\boldsymbol{\xi}} \Psi^{33}_{I,(in)(1)\alpha} + n^\beta \frac{\partial \Psi^{33}_{I,(in)(1)\beta}}{\partial \xi^\alpha}\right)\right] = 0_\alpha. \tag{4.2.99}$$

The solution is

$$\Psi^{33}_{M,(in)(1)1} = \frac{(\lambda_I - \lambda_M)}{2\left(\kappa_I + \mu_M\right)}\pi\xi - \left(\frac{(\lambda_I - \lambda_M)(\kappa_I - \kappa_M)}{2\left(\kappa_I + \mu_M\right)^2}\right)\pi\left(\frac{\xi}{\xi^2 + \eta^2}\right), \tag{4.2.100}$$

$$\Psi^{33}_{M,(in)(1)2} = \frac{(\lambda_I - \lambda_M)}{2\left(\kappa_I + \mu_M\right)}\pi\eta - \left(\frac{(\lambda_I - \lambda_M)(\kappa_I - \kappa_M)}{2\left(\kappa_I + \mu_M\right)^2}\right)\pi\left(\frac{\eta}{\xi^2 + \eta^2}\right), \tag{4.2.101}$$

$$\Psi^{33}_{I,(in)(1)1} = \left(\frac{(\lambda_I - \lambda_M)}{2\left(\kappa_I + \mu_M\right)}\right)\left(\frac{\kappa_M + \mu_M}{\kappa_I + \mu_M}\right)\pi\xi, \tag{4.2.102}$$

$$\Psi^{33}_{I,(in)(1)2} = \left(\frac{(\lambda_I - \lambda_M)}{2\left(\kappa_I + \mu_M\right)}\right)\left(\frac{\kappa_M + \mu_M}{\kappa_I + \mu_M}\right)\pi\eta. \tag{4.2.103}$$

We find that in order to evaluate the effective coefficients we need the inner solution evaluated on the surface of the inclusion, which is

$$\Psi^{33}_{(in)1} = -r\left(\frac{(\lambda_I - \lambda_M)}{2\left(\kappa_I + \mu_M\right)}\right)\xi + r^3\left(\frac{(\lambda_I - \lambda_M)}{2\left(\kappa_I + \mu_M\right)}\right)\left(\frac{\kappa_M + \mu_M}{\kappa_I + \mu_M}\right)\pi\xi, \tag{4.2.104}$$

$$\Psi^{33}_{(in)2} = -r\left(\frac{(\lambda_I - \lambda_M)}{2\left(\kappa_I + \mu_M\right)}\right)\eta + r^3\left(\frac{(\lambda_I - \lambda_M)}{2\left(\kappa_I + \mu_M\right)}\right)\left(\frac{\kappa_M + \mu_M}{\kappa_I + \mu_M}\right)\pi\eta. \tag{4.2.105}$$

We now have the first two terms in the inner expansion of $\mathbf{\Psi}^{33}$, which we will be able to use to approximate the 33−coefficients of each of the stiffness and electromechanical tensors.

4.2.3.4 The 23-problem

From (F.4.3), we see that

$$\Psi_{\alpha}^{23} = 0_{\alpha}. \tag{4.2.106}$$

This means we only need to solve (4.2.11)-(4.2.14), subject to continuity conditions (4.2.16)-(4.2.17) and (4.2.19)-(4.2.20).

4.2.3.4.1 The leading-order inner problem

Based on the jump conditions (4.2.34)-(4.2.33), we expand the inner problem as

$$\Psi_{(in)3}^{23} \sim r\Psi_{(in)(0)3}^{23}, \qquad \psi_{(in)}^{23} \sim r\psi_{(in)(0)}^{23}. \tag{4.2.107}$$

The cell functions $\Psi_{M,(in)(0)3}^{23}$, $\Psi_{I,(in)(0)3}^{23}$, $\psi_{M,(in)(0)}^{23}$ and $\psi_{I,(in)(0)}^{23}$ satisfy (4.2.27)-(4.2.30), along with the continuity conditions (4.2.31)-(4.2.32) and the jump conditions[1]

$$\boldsymbol{n} \cdot \left[\mu_M \nabla_{\boldsymbol{\xi}} \Psi_{M,(in)(0)3}^{23} - \mu_I \nabla_{\boldsymbol{\xi}} \Psi_{I,(in)(0)3}^{23} - e_{51} \nabla_{\boldsymbol{\xi}} \psi_{I,(in)(0)}^{23}\right] = n^2(\mu_I - \mu_M), \tag{4.2.108}$$

$$\boldsymbol{n} \cdot \left[\epsilon_{I,11}^{S} \nabla_{\boldsymbol{\xi}} \psi_{I,(in)(0)}^{23} - \epsilon_{M,11}^{S} \nabla_{\boldsymbol{\xi}} \psi_{M,(in)(0)}^{23} - S_p e_{51} \nabla_{\boldsymbol{\xi}} \Psi_{I,(in)(0)3}^{23}\right] = n^2 S_p e_{51}. \tag{4.2.109}$$

The solution is

$$\begin{aligned}
\Psi_{M,(in)(0)3}^{23} &= -\left(\frac{(\mu_I - \mu_M)\left(\epsilon_{I,11}^{S} + \epsilon_{M,11}^{S}\right) + S_p\left(e_{51}\right)^2}{(\mu_I + \mu_M)\left(\epsilon_{I,11}^{S} + \epsilon_{M,11}^{S}\right) + S_p\left(e_{51}\right)^2}\right) \frac{\eta}{\xi^2 + \eta^2}, \\
\Psi_{I,(in)(0)3}^{23} &= -\left(\frac{(\mu_I - \mu_M)\left(\epsilon_{I,11}^{S} + \epsilon_{M,11}^{S}\right) + S_p\left(e_{51}\right)^2}{(\mu_I + \mu_M)\left(\epsilon_{I,11}^{S} + \epsilon_{M,11}^{S}\right) + S_p\left(e_{51}\right)^2}\right) \eta,
\end{aligned} \tag{4.2.110}$$

$$\begin{aligned}
\psi_{M,(in)(0)}^{23} &= \left(\frac{2\mu_M S_p e_{51}}{(\mu_I + \mu_M)\left(\epsilon_{I,11}^{S} + \epsilon_{M,11}^{S}\right) + S_p\left(e_{51}\right)^2}\right) \frac{\eta}{\xi^2 + \eta^2}, \\
\psi_{I,(in)(0)}^{23} &= \left(\frac{2\mu_M S_p e_{51}}{(\mu_I + \mu_M)\left(\epsilon_{I,11}^{S} + \epsilon_{M,11}^{S}\right) + S_p\left(e_{51}\right)^2}\right) \eta.
\end{aligned} \tag{4.2.111}$$

[1]Note that n^2 represents the Y component of the unit normal vector $\boldsymbol{n}$.

4.2.3.4.2 Outer limit of the leading-order inner solution

Writing (4.2.110)-(4.2.111) in terms of outer variables, we deduce that the outer limit of the leading-order inner is

$$(1.t.o)(1.t.i)\Psi^{23}_{M,3} = -r^2\left(\frac{(\mu_I-\mu_M)\left(\epsilon^S_{I,11}+\epsilon^S_{M,11}\right)+S_p\left(e_{51}\right)^2}{(\mu_I+\mu_M)\left(\epsilon^S_{I,11}+\epsilon^S_{M,11}\right)+S_p\left(e_{51}\right)^2}\right)\frac{Y}{X^2+Y^2}, \quad (4.2.112)$$

$$(1.t.o)(1.t.i)\Psi^{23}_{M,3} = r^2\left(\frac{2\mu_M S_p e_{51}}{(\mu_I+\mu_M)\left(\epsilon^S_{I,11}+\epsilon^S_{M,11}\right)+S_p\left(e_{51}\right)^2}\right)\frac{Y}{X^2+Y^2}. \quad (4.2.113)$$

4.2.3.4.3 First leading-order outer solution

The outer expansions for $\Psi^{23}_{(out),3}$ and $\psi^{23}_{(out)}$ take the form

$$\Psi^{23}_{(out),3} \sim r^2\Psi^{23}_{(out)(0)3}, \qquad \psi^{23}_{(out)} \sim r^2\psi^{23}_{(out)(0)}, \quad (4.2.114)$$

where $\Psi^{23}_{(in)(0)3}$ and $\psi^{23}_{(in)(0)}$ have the matching conditions

$$\Psi^{23}_{(out)(0)3} \sim -\left(\frac{(\mu_I-\mu_M)\left(\epsilon^S_{I,11}+\epsilon^S_{M,11}\right)+S_p\left(e_{51}\right)^2}{(\mu_I+\mu_M)\left(\epsilon^S_{I,11}+\epsilon^S_{M,11}\right)+S_p\left(e_{51}\right)^2}\right)\frac{Y}{X^2+Y^2}, \quad (4.2.115)$$

$$\psi^{23}_{(out)(0)} \sim \left(\frac{2\mu_M S_p e_{51}}{(\mu_I+\mu_M)\left(\epsilon^S_{I,11}+\epsilon^S_{M,11}\right)+S_p\left(e_{51}\right)^2}\right)\frac{Y}{X^2+Y^2}, \quad (4.2.116)$$

as $R \to 0$. The functions $\Psi^{23}_{(out)(0)3}$ and $\psi^{23}_{(out)(0)}$ satisfy (4.2.11) and (4.2.13) along with being periodic on the boundary $\partial\Gamma$.

As before, we may write the solution from $\Psi^{23}_{(out)(0)3}$ and $\psi^{23}_{(out)(0)}$ in terms of the lattice sums as

$$\begin{aligned}\Psi^{23}_{(out)(0)3} = &-\left(\frac{(\mu_I-\mu_M)\left(\epsilon^S_{I,11}+\epsilon^S_{M,11}\right)+S_p\left(e_{51}\right)^2}{(\mu_I+\mu_M)\left(\epsilon^S_{I,11}+\epsilon^S_{M,11}\right)+S_p\left(e_{51}\right)^2}\right)\\ &\times\sum_{k=-\infty}^{\infty}\sum_{l=-\infty}^{\infty}\frac{Y-l}{(X-k)^2+(Y-l)^2}, \quad (4.2.117)\\ \psi^{23}_{(out)(0)} = &\left(\frac{2\mu_M S_p e_{51}}{(\mu_I+\mu_M)\left(\epsilon^S_{I,11}+\epsilon^S_{M,11}\right)+S_p\left(e_{51}\right)^2}\right)\\ &\times\sum_{k=-\infty}^{\infty}\sum_{l=-\infty}^{\infty}\frac{Y-l}{(X-k)^2+(Y-l)^2}. \quad (4.2.118)\end{aligned}$$

4.2.3.4.4 Inner limit of first leading-order outer solution

If we Taylor expand (4.2.117)-(4.2.118) using the expansions found in (H.0.5)-(H.0.6) and re-write in terms of inner variables, we deduce that

$$\begin{aligned}(2.t.i)(1.t.o)\Psi^{23}_{M,3} =& -r\left(\frac{(\mu_I-\mu_M)\left(\epsilon^S_{I,11}+\epsilon^S_{M,11}\right)+S_p\left(e_{51}\right)^2}{(\mu_I+\mu_M)\left(\epsilon^S_{I,11}+\epsilon^S_{M,11}\right)+S_p\left(e_{51}\right)^2}\right)\frac{\eta}{\xi^2+\eta^2}\\ &+r^3\left(\frac{(\mu_I-\mu_M)\left(\epsilon^S_{I,11}+\epsilon^S_{M,11}\right)+S_p\left(e_{51}\right)^2}{(\mu_I+\mu_M)\left(\epsilon^S_{I,11}+\epsilon^S_{M,11}\right)+S_p\left(e_{51}\right)^2}\right)\pi\eta, \qquad (4.2.119)\\ (2.t.i)(1.t.o)\psi^{23}_{M,(0)} =& \quad r\left(\frac{2\mu_M S_p e_{51}}{(\mu_I+\mu_M)\left(\epsilon^S_{I,11}+\epsilon^S_{M,11}\right)+S_p\left(e_{51}\right)^2}\right)\frac{\eta}{\xi^2+\eta^2}\\ &-r^3\left(\frac{2\mu_M S_p e_{51}}{(\mu_I+\mu_M)\left(\epsilon^S_{I,11}+\epsilon^S_{M,11}\right)+S_p\left(e_{51}\right)^2}\right)\pi\eta. \qquad (4.2.120)\end{aligned}$$

4.2.3.4.5 Second order inner solution

From (4.2.119)-(4.2.120), we deduce that the inner expansions $\Psi^{23}_{(in)3}$ and $\psi^{23}_{(in)}$ proceed as

$$\begin{aligned}\Psi^{23}_{(in)3} &\sim r\Psi^{23}_{(in)(0)3}+r^3\Psi^{23}_{(in)(1)3},\\ \psi^{23}_{(in)} &\sim r\psi^{23}_{(in)(0)}+r^3\psi^{23}_{(in)(1)},\end{aligned} \qquad (4.2.121)$$

where $\Psi^{23}_{(in)(1)3}$ and $\psi^{23}_{(in)(1)}$ have the matching conditions

$$\Psi^{23}_{(in)(1)3} \sim \left(\frac{(\mu_I-\mu_M)\left(\epsilon^S_{I,11}+\epsilon^S_{M,11}\right)+S_p\left(e_{51}\right)^2}{(\mu_I+\mu_M)\left(\epsilon^S_{I,11}+\epsilon^S_{M,11}\right)+S_p\left(e_{51}\right)^2}\right)\pi\eta, \qquad (4.2.122)$$

$$\psi^{23}_{(in)(1)} \sim -\left(\frac{2\mu_M S_p e_{51}}{(\mu_I+\mu_M)\left(\epsilon^S_{I,11}+\epsilon^S_{M,11}\right)+S_p\left(e_{51}\right)^2}\right)\pi\eta, \qquad (4.2.123)$$

as $\rho\to\infty$. The functions $\Psi^{23}_{(in)(1)3}$ and $\psi^{23}_{(in)(1)}$ satisfy (4.2.27)-(4.2.30) along with continuity conditions (4.2.31)-(4.2.32), the matching conditions (4.2.122)-(4.2.123) and the jump conditions

$$\boldsymbol{n}\cdot\left[\mu_M\nabla_{\boldsymbol{\xi}}\Psi^{23}_{M,(in)(1)3}-\mu_I\nabla_{\boldsymbol{\xi}}\Psi^{23}_{I,(in)(1)3}-e_{51}\nabla_{\boldsymbol{\xi}}\psi^{23}_{I,(in)(1)}\right]=0, \qquad (4.2.124)$$

$$\boldsymbol{n}\cdot\left[\epsilon^S_{I,11}\nabla_{\boldsymbol{\xi}}\psi^{23}_{I,(in)(1)}-\epsilon^S_{M,11}\nabla_{\boldsymbol{\xi}}\psi^{23}_{M,(in)(1)}-S_p e_{51}\nabla_{\boldsymbol{\xi}}\Psi^{23}_{I,(in)(1)3}\right]=0. \qquad (4.2.125)$$

The solution is

$$\psi^{23}_{M,(in)(1)3} = \left(\frac{(\mu_I - \mu_M)\left(\epsilon^S_{I,11} + \epsilon^S_{M,11}\right) + S_p\left(e_{51}\right)^2}{(\mu_I + \mu_M)\left(\epsilon^S_{I,11} + \epsilon^S_{M,11}\right) + S_p\left(e_{51}\right)^2} \right) \pi\eta$$
$$+ \left(\frac{4\left(e_{51}\right)^2 \epsilon^S_{M,11}\mu_M S_p}{\left((\epsilon^S_{I,11} + \epsilon^S_{M,11})(\mu_I + \mu_M) + S_p\left(e_{51}\right)^2\right)^3} \right) \pi \frac{\eta}{\xi^2 + \eta^2}$$
$$- \left(\frac{\left(\left(e_{51}\right)^2 S_p + (\epsilon^S_{I,11} + \epsilon^S_{M,11})(\mu_I - \mu_M)\right)^2}{\left((\epsilon^S_{I,11} + \epsilon^S_{M,11})(\mu_I + \mu_M) + S_p\left(e_{51}\right)^2\right)^2} \right) \pi \frac{\eta}{\xi^2 + \eta^2}, \tag{4.2.126}$$

$$\psi^{23}_{I,(in)(1)3} = \left(\frac{2\mu_M\left(\left(e_{51}\right)^2 S_p(\epsilon^S_{I,11} + 3\epsilon^S_{M,11}) + (\epsilon^S_{I,11} + \epsilon^S_{M,11})^2(\mu_I - \mu_M)\right)}{\left(\left(e_{51}\right)^2 S_p + (\epsilon^S_{I,11} + \epsilon^S_{M,11})(\mu_I + \mu_M)\right)^2} \right) \pi\eta, \tag{4.2.127}$$

$$\psi^{23}_{M,(in)(1)} = -\left(\frac{2\mu_M S_p e_{51}}{(\mu_I + \mu_M)\left(\epsilon^S_{I,11} + \epsilon^S_{M,11}\right) + S_p\left(e_{51}\right)^2} \right) \pi\eta$$
$$+ 2e_{51}\mu_M S_p \left(\frac{{e_{51}}^2 S_p + (\epsilon^S_{I,11} + \epsilon^S_{M,11})(\mu_I - \mu_M)}{\left({e_{51}}^2 S_p + (\epsilon^S_{I,11} + \epsilon^S_{M,11})(\mu_I + \mu_M)\right)^2} \right) \pi \frac{\eta}{\xi^2 + \eta^2}$$
$$+ 2e_{51}\mu_M S_p \left(\frac{{e_{51}}^2 S_p + (\epsilon_{I,11} - \epsilon_{M,11})(\mu_I + \mu_M)}{\left({e_{51}}^2 S_p + (\epsilon^S_{I,11} + \epsilon^S_{M,11})(\mu_I + \mu_M)\right)^3} \right) \pi \frac{\eta}{\xi^2 + \eta^2}, \tag{4.2.128}$$

$$\psi^{23}_{I,(in)(1)} = \left(\frac{2e_{51}\mu_M S_p\left(\left(e_{51}\right)^2 S_p + \epsilon^S_{I,11}(\mu_I - \mu_M) - \epsilon^S_{M,11}(\mu_I + 3\mu_M)\right)}{\left({e_{51}}^2 S_p + (\epsilon^S_{I,11} + \epsilon^S_{M,11})(\mu_I + \mu_M)\right)^2} \right) \pi\eta. \tag{4.2.129}$$

We find that in order to evaluate the effective coefficients, we need the inner solution evaluated on the surface of the inclusion, which is

$$\Psi^{23}_{(in)3} \sim -r \left(\frac{(\mu_I - \mu_M)\left(\epsilon^S_{I,11} + \epsilon^S_{M,11}\right) + S_p\left(e_{51}\right)^2}{(\mu_I + \mu_M)\left(\epsilon^S_{I,11} + \epsilon^S_{M,11}\right) + S_p\left(e_{51}\right)^2} \right) \eta$$
$$+ r^3 \left(\frac{2\mu_M\left(\left(e_{51}\right)^2 S_p(\epsilon^S_{I,11} + 3\epsilon^S_{M,11}) + (\epsilon^S_{I,11} + \epsilon^S_{M,11})^2(\mu_I - \mu_M)\right)}{\left(\left(e_{51}\right)^2 S_p + (\epsilon^S_{I,11} + \epsilon^S_{M,11})(\mu_I + \mu_M)\right)^2} \right) \pi\eta, \tag{4.2.130}$$

$$\psi^{23}_{(in)} \sim r\left(\frac{2\mu_M S_p e_{51}}{(\mu_I+\mu_M)\left(\epsilon^S_{I,11}+\epsilon^S_{M,11}\right)+S_p\left(e_{51}\right)^2}\right)\eta$$
$$+ r^3\left(\frac{2e_{51}\mu_M S_p\left(\left(e_{51}\right)^2 S_p+\epsilon^S_{I,11}(\mu_I-\mu_M)-\epsilon^S_{M,11}(\mu_I+3\mu_M)\right)}{\left({e_{51}}^2 S_p+(\epsilon^S_{I,11}+\epsilon^S_{M,11})(\mu_I+\mu_M)\right)^2}\right)\pi\eta. \quad (4.2.131)$$

We now have the first two terms in the inner expansion of Ψ^{23}_3 and ψ^{23}, which we will be able to use to approximate the 23−coefficients of each of the stiffness and electromechanical tensors.

4.2.3.5 The 13-problem

From (F.4.3), we see that

$$\Psi^{13}_\alpha = 0_\alpha. \quad (4.2.132)$$

This means we only need to solve (4.2.11)-(4.2.14), subject to continuity conditions (4.2.19)-(4.2.20). We can evaluate $\mathbf{\Psi}^{13}$ and ψ^{13} by symmetry using $\mathbf{\Psi}^{23}$ and ψ^{23} with the X- and Y- directions flipped.

We find that the inner solution evaluated on the surface of the inclusion is

$$\Psi^{13}_{(in)3} \sim -r\left(\frac{(\mu_I-\mu_M)\left(\epsilon^S_{I,11}+\epsilon^S_{M,11}\right)+S_p\left(e_{51}\right)^2}{(\mu_I+\mu_M)\left(\epsilon^S_{I,11}+\epsilon^S_{M,11}\right)+S_p\left(e_{51}\right)^2}\right)\xi$$
$$+ r^3\left(\frac{2\mu_M\left(\left(e_{51}\right)^2 S_p(\epsilon^S_{I,11}+3\epsilon^S_{M,11})+(\epsilon^S_{I,11}+\epsilon^S_{M,11})^2(\mu_I-\mu_M)\right)}{\left(\left(e_{51}\right)^2 S_p+(\epsilon^S_{I,11}+\epsilon^S_{M,11})(\mu_I+\mu_M)\right)^2}\right)\pi\xi, \quad (4.2.133)$$

$$\psi^{13}_{(in)} \sim r\left(\frac{2\mu_M S_p e_{51}}{(\mu_I+\mu_M)\left(\epsilon^S_{I,11}+\epsilon^S_{M,11}\right)+S_p\left(e_{51}\right)^2}\right)\xi$$
$$+ r^3\left(\frac{2e_{51}\mu_M S_p\left(\left(e_{51}\right)^2 S_p+\epsilon^S_{I,11}(\mu_I-\mu_M)-\epsilon^S_{M,11}(\mu_I+3\mu_M)\right)}{\left(\left(e_{51}\right)^2 S_p+(\epsilon^S_{I,11}+\epsilon^S_{M,11})(\mu_I+\mu_M)\right)^2}\right)\pi\xi. \quad (4.2.134)$$

We now have the first two terms in the inner expansion of Ψ^{13}_3 and ψ^{13}, which we will be able to use to approximate the 13−coefficients of each of the stiffness and electromechanical tensors.

4.2.3.6 The 12-problem

From (F.4.1), we see that

$$\Psi_3^{12} = 0, \tag{4.2.135}$$

$$\psi^{12} = 0. \tag{4.2.136}$$

This means we only need to solve (4.2.9)-(4.2.10), subject to continuity conditions (4.2.15) and (4.2.18).

4.2.3.6.1 The leading-order inner problem

Based on the jump conditions (4.2.26), we expand the problem as

$$\Psi_{(in)\alpha}^{12} \sim r\Psi_{(in)(0)\alpha}^{12}. \tag{4.2.137}$$

The cell function $\boldsymbol{\Psi}_{(in)(0)}^{12}$ satisfies (4.2.23) in the matrix phase ($\rho > 1$), (4.2.24) in the inclusion phase ($\rho < 1$), the continuity condition (4.2.25) and the jump condition

$$\begin{aligned}
&\left[\lambda_M \nabla_{\boldsymbol{\xi}} \cdot \boldsymbol{\Psi}_{M,(in)(0)}^{12} n_\alpha + \mu_M \left(\boldsymbol{n} \cdot \nabla_{\boldsymbol{\xi}} \Psi_{M,(in)(0)\alpha}^{12} + n^\beta \frac{\partial \Psi_{M,(in)(0)\beta}^{12}}{\partial \xi^\alpha}\right)\right] \\
&- \left[\lambda_I \nabla_{\boldsymbol{\xi}} \cdot \boldsymbol{\Psi}_{I,(in)(0)}^{12} n_\alpha + \mu_I \left(\boldsymbol{n} \cdot \nabla_{\boldsymbol{\xi}} \Psi_{I,(in)(0)\alpha}^{12} + n^\beta \frac{\partial \Psi_{I,(in)(0)\beta}^{12}}{\partial \xi^\alpha}\right)\right] \\
&= (\mu_I - \mu_M)\left(n^2 \delta_\alpha^1 + n^1 \delta_\alpha^2\right) \\
&= (\mu_I - \mu_M)\left(\left(\frac{n^1 + n^2}{\sqrt{2}}\right)\left(\frac{\delta_\alpha^1 + \delta_\alpha^2}{\sqrt{2}}\right) - \left(\frac{-n^1 + n^2}{\sqrt{2}}\right)\left(\frac{-\delta_\alpha^1 + \delta_\alpha^2}{\sqrt{2}}\right)\right).
\end{aligned} \tag{4.2.138}$$

If we define the matrix

$$P = \frac{1}{\sqrt{2}} \begin{pmatrix} 1 & -1 \\ 1 & 1 \end{pmatrix}, \tag{4.2.139}$$

then the solution to (4.2.9)-(4.2.10) along with continuity conditions (4.2.15) and (4.2.18) is given by

$$\begin{aligned}
\Psi_{M,(in)(0)\alpha}^{12} &= (\mu_I - \mu_M) P_\alpha^\beta \Lambda_{M\beta}\left(P^{-1}\boldsymbol{\xi}\right), \\
\Psi_{I,(in)(0)\alpha}^{12} &= (\mu_I - \mu_M) P_\alpha^\beta \Lambda_{I\beta}\left(P^{-1}\boldsymbol{\xi}\right),
\end{aligned} \tag{4.2.140}$$

yielding

$$\begin{aligned}\Psi^{12}_{M,(in)(0)1} =& -2(\mu_I-\mu_M)\frac{\mu_M}{\kappa_M\mu_M+\mu_I\kappa_M+2\mu_M\mu_I}\left(\frac{\eta}{\xi^2+\eta^2}\right)\\ &-2(\mu_I-\mu_M)\frac{\kappa_M}{\kappa_M\mu_M+\mu_I\kappa_M+2\mu_M\mu_I}\left(\frac{\xi^2\eta}{(\xi^2+\eta^2)^2}\right)\\ &+\frac{(\mu_I-\mu_M)}{2}\frac{\kappa_M}{\kappa_M\mu_M+\mu_I\kappa_M+2\mu_M\mu_I}\left(-\tfrac{\eta}{(\xi^2+\eta^2)^2}+4\tfrac{\xi^2\eta}{(\xi^2+\eta^2)^3}\right),\end{aligned} \tag{4.2.141}$$

$$\begin{aligned}\Psi^{12}_{M,(in)(0)2} =& -2(\mu_I-\mu_M)\frac{\mu_M}{\kappa_M\mu_M+\mu_I\kappa_M+2\mu_M\mu_I}\left(\frac{\xi}{\xi^2+\eta^2}\right)\\ &-2(\mu_I-\mu_M)\frac{\kappa_M}{\kappa_M\mu_M+\mu_I\kappa_M+2\mu_M\mu_I}\left(\frac{\xi\eta^2}{(\xi^2+\eta^2)^2}\right)\\ &+\frac{(\mu_I-\mu_M)}{2}\frac{\kappa_M}{\kappa_M\mu_M+\mu_I\kappa_M+2\mu_M\mu_I}\left(-\tfrac{\xi}{(\xi^2+\eta^2)^2}+4\tfrac{\xi\eta^2}{(\xi^2+\eta^2)^3}\right).\end{aligned} \tag{4.2.142}$$

4.2.3.6.2 Outer limit of the leading-order inner solution

If we re-write (4.2.141)-(4.2.142) in terms of outer variables, we deduce that

$$\begin{aligned}(1.t.o)(1.t.i)\Psi^{12}_{M,1} =& -2(\mu_I-\mu_M)r^2\frac{\mu_M}{\kappa_M\mu_M+\mu_I\kappa_M+2\mu_M\mu_I}\left(\frac{Y}{X^2+Y^2}\right)\\ &-2(\mu_I-\mu_M)r^2\frac{\kappa_M}{\kappa_M\mu_M+\mu_I\kappa_M+2\mu_M\mu_I}\left(\frac{X^2Y}{(X^2+Y^2)^2}\right),\end{aligned} \tag{4.2.143}$$

$$\begin{aligned}(1.t.o)(1.t.i)\Psi^{12}_{M,2} =& -2(\mu_I-\mu_M)r^2\frac{\mu_M}{\kappa_M\mu_M+\mu_I\kappa_M+2\mu_M\mu_I}\left(\frac{X}{X^2+Y^2}\right)\\ &-2(\mu_I-\mu_M)r^2\frac{\kappa_M}{\kappa_M\mu_M+\mu_I\kappa_M+2\mu_M\mu_I}\left(\frac{XY^2}{(X^2+Y^2)^2}\right).\end{aligned} \tag{4.2.144}$$

4.2.3.6.3 First-leading-order outer solution

From (4.2.143)-(4.2.144), we see that the outer expansion proceeds as

$$\Psi^{12}_{(out)\alpha} \sim r^2\Psi^{12}_{(out)(0)\alpha}, \tag{4.2.145}$$

where $\Psi^{12}_{(out)(0)\alpha}$ has the matching condition

$$\begin{aligned}\Psi^{12}_{(out)(0)1} \sim & -2(\mu_I-\mu_M)\frac{\mu_M}{\kappa_M\mu_M+\mu_I\kappa_M+2\mu_M\mu_I}\left(\frac{Y}{X^2+Y^2}\right)\\ & -2(\mu_I-\mu_M)\frac{\kappa_M}{\kappa_M\mu_M+\mu_I\kappa_M+2\mu_M\mu_I}\left(\frac{X^2Y}{(X^2+Y^2)^2}\right), \qquad (4.2.146)\\ \Psi^{12}_{(out)(0)2} \sim & -2(\mu_I-\mu_M)\frac{\mu_M}{\kappa_M\mu_M+\mu_I\kappa_M+2\mu_M\mu_I}\left(\frac{X}{X^2+Y^2}\right)\\ & -2(\mu_I-\mu_M)\frac{\kappa_M}{\kappa_M\mu_M+\mu_I\kappa_M+2\mu_M\mu_I}\left(\frac{XY^2}{(X^2+Y^2)^2}\right), \qquad (4.2.147)\end{aligned}$$

as $R\to 0$. The cell function $\Psi^{12}_{(out)(0)\alpha}$ must also satisfy the equation (4.2.9) with periodic boundary conditions on the boundary $\partial\Gamma$. We find that

$$\begin{aligned}\Psi^{12}_{(out)(0)1} = & -2(\mu_I-\mu_M)\frac{\mu_M}{\kappa_M\mu_M+\mu_I\kappa_M+2\mu_M\mu_I}\sum_{l=-\infty}^{\infty}\sum_{k=-\infty}^{\infty}\frac{(Y-l)}{(X-k)^2+(Y-l)^2}\\ & -2(\mu_I-\mu_M)\frac{\kappa_M}{\kappa_M\mu_M+\mu_I\kappa_M+2\mu_M\mu_I}\sum_{l=-\infty}^{\infty}\sum_{k=-\infty}^{\infty}\frac{(X-k)^2(Y-l)}{((X-k)^2+(Y-l)^2)^2}, \qquad (4.2.148)\\ \Psi^{12}_{(out)(0)2} = & -2(\mu_I-\mu_M)\frac{\mu_M}{\kappa_M\mu_M+\mu_I\kappa_M+2\mu_M\mu_I}\sum_{k=-\infty}^{\infty}\sum_{l=-\infty}^{\infty}\frac{(X-k)}{(X-k)^2+(Y-l)^2}\\ & -2(\mu_I-\mu_M)\frac{\kappa_M}{\kappa_M\mu_M+\mu_I\kappa_M+2\mu_M\mu_I}\sum_{k=-\infty}^{\infty}\sum_{l=-\infty}^{\infty}\frac{(X-k)(Y-l)^2}{((X-k)^2+(Y-l)^2)^2}. \qquad (4.2.149)\end{aligned}$$

4.2.3.6.4 Inner limit of the two-term outer expansion

If we Taylor expand (4.2.148)-(4.2.149) this expression around $(X,Y)=(0,0)$ using the expansions found in (H.0.11)-(H.0.12), and re-write in terms of outer variables, we deduce

$$
\begin{aligned}
(2.t.i)(1.t.o)\Psi^{12}_{M,1} =& -2(\mu_I-\mu_M)r\frac{\mu_M}{\kappa_M\mu_M+\mu_I\kappa_M+2\mu_M\mu_I}\left(\frac{\eta}{\xi^2+\eta^2}\right)\\
&-2(\mu_I-\mu_M)r\frac{\kappa_M}{\kappa_M\mu_M+\mu_I\kappa_M+2\mu_M\mu_I}\left(\frac{\xi^2\eta}{(\xi^2+\eta^2)^2}\right)\\
&+\frac{(\mu_I-\mu_M)}{2}r\frac{\kappa_M}{\kappa_M\mu_M+\mu_I\kappa_M+2\mu_M\mu_I}\left(-\frac{\eta}{(\xi^2+\eta^2)^2}+\frac{4\xi^2\eta}{(\xi^2+\eta^2)^3}\right)\\
&-\frac{2(\mu_I-\mu_M)}{\kappa_M\mu_M+\mu_I\kappa_M+2\mu_M\mu_I}\pi r^3\eta\\
&\times\left(\mu_M+\kappa_M\left(1+2\sum_{l=1}^{\infty}\pi^2 l\coth(\pi l)\,\mathrm{csch}^2(\pi l)\right)\right), \qquad (4.2.150)\\
(2.t.i)(1.t.o)\Psi^{12}_{M,2} =& -2(\mu_I-\mu_M)r\frac{\mu_M}{\kappa_M\mu_M+\mu_I\kappa_M+2\mu_M\mu_I}\left(\frac{\xi}{\xi^2+\eta^2}\right)\\
&-2(\mu_I-\mu_M)r\frac{\kappa_M}{\kappa_M\mu_M+\mu_I\kappa_M+2\mu_M\mu_I}\left(\frac{\xi\eta^2}{(\xi^2+\eta^2)^2}\right)\\
&+\frac{(\mu_I-\mu_M)}{2}r\frac{\kappa_M}{\kappa_M\mu_M+\mu_I\kappa_M+2\mu_M\mu_I}\left(-\frac{\xi}{(\xi^2+\eta^2)^2}+\frac{4\xi\eta^2}{(\xi^2+\eta^2)^3}\right)\\
&-\frac{2(\mu_I-\mu_M)}{\kappa_M\mu_M+\mu_I\kappa_M+2\mu_M\mu_I}\pi r^3\xi\\
&\times\left(\mu_M+\kappa_M\left(1+2\sum_{l=1}^{\infty}\pi^2 l\coth(\pi l)\,\mathrm{csch}^2(\pi l)\right)\right). \qquad (4.2.151)
\end{aligned}
$$

4.2.3.6.5 Second order inner solution

From (4.2.150)-(4.2.151), we deduce that the inner expansion of $\mathbf{\Psi}^{12}_{(in)}$ is of the form

$$
\Psi^{12}_{(in)\alpha}\sim r\Psi^{12}_{(in)(0)\alpha}+r^3\Psi^{12}_{(in)(1)\alpha}, \qquad (4.2.152)
$$

where $\Psi^{12}_{(in)(1)\alpha}$ has the matching condition

$$
\begin{aligned}
\Psi^{12}_{(in)(1)1}\sim& -\frac{2(\mu_I-\mu_M)}{\kappa_M\mu_M+\mu_I\kappa_M+2\mu_M\mu_I}\pi\\
&\times\left(\mu_M+\kappa_M\left(1+2\sum_{l=1}^{\infty}\pi^2 l\coth(\pi l)\,\mathrm{csch}^2(\pi l)\right)\right)\eta, \qquad (4.2.153)
\end{aligned}
$$

$$
\begin{aligned}
\Psi^{12}_{(in)(1)2}\sim& -\frac{2(\mu_I-\mu_M)}{\kappa_M\mu_M+\mu_I\kappa_M+2\mu_M\mu_I}\pi\\
&\times\left(\mu_M+\kappa_M\left(1+2\sum_{l=1}^{\infty}\pi^2 l\coth(\pi l)\,\mathrm{csch}^2(\pi l)\right)\right)\xi, \qquad (4.2.154)
\end{aligned}
$$

as $\rho \to \infty$. The cell function $\boldsymbol{\Psi}^{12}_{(in)(1)}$ satisfies (4.2.23) in the matrix phase ($\rho > 1$), (4.2.24) in the inclusion phase ($\rho < 1$), the continuity condition (4.2.25) and the jump condition

$$\left[\lambda_M \nabla_{\boldsymbol{\xi}} \cdot \boldsymbol{\Psi}^{12}_{M,(in)(0)} n_\alpha + \mu_M \left(\boldsymbol{n} \cdot \nabla_{\boldsymbol{\xi}} \Psi^{12}_{M,(in)(0)\alpha} + n^\beta \frac{\partial \Psi^{12}_{M,(in)(0)\beta}}{\partial \xi^\alpha}\right)\right] - \left[\lambda_I \nabla_{\boldsymbol{\xi}} \cdot \boldsymbol{\Psi}^{12}_{I,(in)(0)} n_\alpha + \mu_I \left(\boldsymbol{n} \cdot \nabla_{\boldsymbol{\xi}} \Psi^{12}_{I,(in)(0)\alpha} + n^\beta \frac{\partial \Psi^{12}_{I,(in)(0)\beta}}{\partial \xi^\alpha}\right)\right] = 0. \quad (4.2.155)$$

Solving the boundary value problem defined by (4.2.23)-(4.2.24), together with the matching conditions (4.2.153)-(4.2.154), yields

$$\Psi^{12}_{I,(in)(1)1} = -\pi \left(\frac{4\mu_M(\mu_I - \mu_M)(\kappa_M + \mu_M)}{(\kappa_M\mu_M + \mu_I\kappa_M + 2\mu_M\mu_I)^2}\right) \times \left(\mu_M + \kappa_M \left(1 + 2\sum_{l=1}^{\infty} \pi^2 l \coth(\pi l)\,\mathrm{csch}^2(\pi l)\right)\right)\eta, \quad (4.2.156)$$

$$\Psi^{12}_{I,(in)(1)2} = -\pi \left(\frac{4\mu_M(\mu_I - \mu_M)(\kappa_M + \mu_M)}{(\kappa_M\mu_M + \mu_I\kappa_M + 2\mu_M\mu_I)^2}\right) \times \left(\mu_M + \kappa_M \left(1 + 2\sum_{l=1}^{\infty} \pi^2 l \coth(\pi l)\,\mathrm{csch}^2(\pi l)\right)\right)\xi. \quad (4.2.157)$$

We find that in order to evaluate the effective coefficients we need the inner solution evaluated on the surface of the inclusion, which is

$$\Psi^{12}_{(in)1} \sim -r\frac{(\mu_I - \mu_M)}{2}\frac{\kappa_M + 2\mu_M}{\kappa_M\mu_M + \mu_I\kappa_M + 2\mu_M\mu_I}\eta - r^3\left(\frac{4\mu_M(\mu_I - \mu_M)(\kappa_M + \mu_M)}{(\kappa_M\mu_M + \mu_I\kappa_M + 2\mu_M\mu_I)^2}\right)\pi \times \left(\mu_M + \kappa_M \left(1 + 2\sum_{l=1}^{\infty} \pi^2 l \coth(\pi l)\,\mathrm{csch}^2(\pi l)\right)\right)\eta, \quad (4.2.158)$$

$$\Psi^{12}_{(in)2} \sim -r\frac{(\mu_I - \mu_M)}{2}\frac{\kappa_M + 2\mu_M}{\kappa_M\mu_M + \mu_I\kappa_M + 2\mu_M\mu_I}\xi - r^3\left(\frac{4\mu_M(\mu_I - \mu_M)(\kappa_M + \mu_M)}{(\kappa_M\mu_M + \mu_I\kappa_M + 2\mu_M\mu_I)^2}\right)\pi \times \left(\mu_M + \kappa_M \left(1 + 2\sum_{l=1}^{\infty} \pi^2 l \coth(\pi l)\,\mathrm{csch}^2(\pi l)\right)\right)\xi. \quad (4.2.159)$$

We now have the first two terms in the inner expansion of $\boldsymbol{\Psi}^{12}$, which we will be able to use to approximate the 12−coefficients of each of the stiffness and electromechanical tensors.

4.3 Electrical cell problems

In this section, we will be deriving approximate solutions to the electrically driven cell problems defined by the system (F.3.1)-(F.3.12).

4.3.1 Simplifying the equations

Applying the same process we used in subsection §4.2.1, we see that, for transversely isotropic materials, (F.3.1)-(F.3.6) simplify to

$$\kappa_M \frac{\partial}{\partial X^\alpha}\left(\nabla_{\boldsymbol{X}} \cdot \boldsymbol{\Phi}_M^f\right) + \mu_M \nabla_{\boldsymbol{X}}^2 \Phi_{M,\alpha}^f = 0 \text{ when } |\boldsymbol{X}| > r, \tag{4.3.1}$$

$$\kappa_I \frac{\partial}{\partial X^\alpha}\left(\nabla_{\boldsymbol{X}} \cdot \boldsymbol{\Phi}_I^f\right) + \mu_I \nabla_{\boldsymbol{X}}^2 \Phi_{I,\alpha}^f = 0 \text{ when } |\boldsymbol{X}| < r, \tag{4.3.2}$$

$$\nabla_{\boldsymbol{X}}^2 \Phi_{M,3}^f = 0 \text{ when } |\boldsymbol{X}| > r, \tag{4.3.3}$$

$$\nabla_{\boldsymbol{X}}^2 \Phi_{I,3}^f = 0 \text{ when } |\boldsymbol{X}| < r, \tag{4.3.4}$$

$$\nabla_{\boldsymbol{X}}^2 \phi_M^f = 0 \text{ when } |\boldsymbol{X}| > r, \tag{4.3.5}$$

$$\nabla_{\boldsymbol{X}}^2 \phi_I^f = 0 \text{ when } |\boldsymbol{X}| < r, \tag{4.3.6}$$

while (F.3.7)-(F.3.12) can be re-written as

$$\Phi_{M,\alpha}^f = \Phi_{I,\alpha}^f, \tag{4.3.7}$$

$$\Phi_{M,3}^f = \Phi_{I,3}^f, \tag{4.3.8}$$

$$\phi_M^f = \phi_I^f, \tag{4.3.9}$$

$$\left[\lambda_M \nabla_{\boldsymbol{X}} \cdot \boldsymbol{\Phi}_M^f n_\alpha + \mu_M \left(\boldsymbol{n} \cdot \nabla_{\boldsymbol{X}} \Phi_{M,\alpha}^f + n_\beta \frac{\partial \Phi_{M,\beta}^f}{\partial X^\alpha}\right)\right] - \left[\lambda_I \nabla_{\boldsymbol{X}} \cdot \boldsymbol{\Phi}_I^f n_\alpha + \mu_I \left(\boldsymbol{n} \cdot \nabla_{\boldsymbol{X}} \Phi_{I,\alpha}^f + n_\beta \frac{\partial \Phi_{I,\beta}^f}{\partial X^\alpha}\right)\right] = n^\beta e_{\alpha\beta}^f, \tag{4.3.10}$$

$$\boldsymbol{n} \cdot \left[c_{M,44} \nabla_{\boldsymbol{X}} \Phi_{M,3}^f - c_{I,44} \nabla_{\boldsymbol{X}} \Phi_{I,3}^f - e_{51} \nabla_{\boldsymbol{X}} \phi_I^f\right] = n^\alpha e_{\alpha 3}^f, \tag{4.3.11}$$

$$\boldsymbol{n} \cdot \left[\epsilon_{I,11}^S \nabla_{\boldsymbol{X}} \phi_I^f - \epsilon_{M,11}^S \nabla_{\boldsymbol{X}} \phi_M^f - S_p e_{51} \nabla_{\boldsymbol{X}} \Phi_{I,3}^f\right] = n^f \left[\epsilon_{M,11}^S - \epsilon_{I,11}^S\right], \tag{4.3.12}$$

on $|\boldsymbol{X}| = r$, where $f \in 1, 2, 3$.

4.3.2 Rescaling the PDEs in the inner region

We now consider the limit $r \to 0$. We rescale

$$\boldsymbol{X} = (X, Y) = r(\xi, \eta) = r\boldsymbol{\xi}, \tag{4.3.13}$$

so that the inclusion has unit radius in the scaled coordinate system. The radial coordinates $\rho = |(\xi, \eta)|$ and $R = |(X, Y)|$ are related through

$$R = r\rho. \tag{4.3.14}$$

The displacement function $\boldsymbol{\Phi}^f$ satisfies

$$\kappa_M \frac{\partial}{\partial \xi^\alpha} \left(\nabla_{\boldsymbol{\xi}} \cdot \boldsymbol{\Phi}^f_{M,(in)} \right) + \mu_M \nabla^2_{\boldsymbol{\xi}} \Phi^f_{M,(in)\alpha} = 0 \text{ when } \rho > 1, \tag{4.3.15}$$

$$\kappa_I \frac{\partial}{\partial \xi^\alpha} \left(\nabla_{\boldsymbol{\xi}} \cdot \boldsymbol{\Phi}^f_{I,(in)} \right) + \mu_I \nabla^2_{\boldsymbol{\xi}} \Phi^f_{I,(in)\alpha} = 0 \text{ when } \rho < 1, \tag{4.3.16}$$

along with the continuity conditions

$$\Phi^f_{M,\alpha} = \Phi^f_{I,\alpha}, \tag{4.3.17}$$

$$\begin{aligned} &\left[\lambda_M \nabla_{\boldsymbol{\xi}} \cdot \boldsymbol{\Phi}^f_{M,(in)} n_\alpha + \mu_M \left(\boldsymbol{n} \cdot \nabla_{\boldsymbol{\xi}} \Phi^f_{M,(in)\alpha} + n^\beta \frac{\partial \Phi^f_{M,(in)(0)\beta}}{\partial \xi^\alpha} \right) \right] \\ &- \left[\lambda_I \nabla_{\boldsymbol{\xi}} \cdot \boldsymbol{\Phi}^f_{I,(in)} n_\alpha + \mu_I \left(\boldsymbol{n} \cdot \nabla_{\boldsymbol{\xi}} \Phi^f_{I,(in)\alpha} + n^\beta \frac{\partial \Phi^f_{I,(in)(0)\beta}}{\partial \xi^\alpha} \right) \right] = r n^\beta e^f_{\alpha\beta}, \end{aligned} \tag{4.3.18}$$

on the boundary ∂I (where $\rho = 1$). The right hand side of (4.3.18) will depend on f.

The scalar functions $\Phi^f_{(in)(0)3}$ and $\phi^f_{(in)(0)}$ satisfy the equations

$$\nabla^2_{\boldsymbol{\xi}} \Phi^f_{M,(in)3} = 0 \qquad \text{when } \rho > 1, \tag{4.3.19}$$

$$\nabla^2_{\boldsymbol{\xi}} \Phi^f_{I,(in)3} = 0 \qquad \text{when } \rho < 1, \tag{4.3.20}$$

$$\nabla^2_{\boldsymbol{\xi}} \phi^f_{M,(in)} = 0 \qquad \text{when } \rho > 1, \tag{4.3.21}$$

$$\nabla^2_{\boldsymbol{\xi}} \phi^f_{I,(in)} = 0 \qquad \text{when } \rho < 1, \tag{4.3.22}$$

along with continuity conditions

$$\Phi^f_{M,3} = \Phi^f_{I,3}, \tag{4.3.23}$$

$$\phi^f_M = \phi^f_I, \tag{4.3.24}$$

$$\boldsymbol{n}\cdot\left[\mu_M\nabla_{\boldsymbol{\xi}}\Phi^f_{M,(in)(0)3}-\mu_I\nabla_{\boldsymbol{\xi}}\Phi^f_{I,(in)(0)3}-e_{51}\nabla_{\boldsymbol{\xi}}\phi^f_{I,(in)(0)}\right]=rn^\alpha e^f_{\alpha 3}, \tag{4.3.25}$$

$$\boldsymbol{n}\cdot\left[\epsilon^S_{I,11}\nabla_{\boldsymbol{\xi}}\phi^f_{I,(in)(0)}-\epsilon^S_{M,11}\nabla_{\boldsymbol{\xi}}\phi^f_{M,(in)(0)}-S_pe_{51}\nabla_{\boldsymbol{\xi}}\Phi^f_{I,(in)(0)3}\right]=rn^f\left(\epsilon^S_{M,11}-\epsilon^S_{I,11}\right). \tag{4.3.26}$$

4.3.3 Solutions to cell problems

For each $f\in\{1,2,3\}$, there is a corresponding cell problem (where each number f corresponds to a forcing direction in 3D space). Since there are three spatial directions, there are three electrical problems. Equation (4.3.27) shows the electric field E, which is the negative gradient of the displacement

$$\boldsymbol{E}=\begin{pmatrix}E_1\\E_2\\E_3\end{pmatrix}, \tag{4.3.27}$$

where each colour in (4.3.27) corresponds to a different cell problem. Note that in the limit as $r\to 0$, the solutions to the outer problems tend to zero as the outer problem does not see any inclusion and hence the solution is trivial. We thus deduce that

$$\boldsymbol{\Phi}^f_{(out)}=o(1),\qquad \phi^f_{(out)}=o(1). \tag{4.3.28}$$

4.3.3.1 The 1-problem

From (F.4.4), we see that

$$\Phi^1_\beta=0_\beta. \tag{4.3.29}$$

This means we only need to solve (4.2.11)-(4.2.14), subject to continuity conditions (4.2.16)-(4.2.17) and (4.2.19)-(4.2.20).

4.3.3.1.1 The leading-order inner problem

Based on the jump conditions (4.2.34)-(4.2.33), we expand the problem as

$$\Phi^1_{(in)3}\sim r\Phi^1_{(in)(0)3},\qquad \phi^1_{(in)}\sim r\phi^1_{(in)(0)}. \tag{4.3.30}$$

The functions $\Phi^1_{(in)(0)3}$ and $\phi^1_{(in)(0)}$ satisfy (4.2.11) and (4.2.13) when $\rho>1$, (4.2.12) and (4.2.14) when $\rho<1$ along with the continuity conditions (4.2.16)-

(4.2.17) as well as the jump conditions

$$\boldsymbol{n}\cdot\left[\mu_M\nabla_{\boldsymbol{\xi}}\Phi^1_{M,(in)(0)3}-\mu_I\nabla_{\boldsymbol{\xi}}\Phi^1_{I,(in)(0)3}-e_{51}\nabla_{\boldsymbol{\xi}}\phi^1_{I,(in)(0)}\right]=n^1e_{51}, \tag{4.3.31}$$

$$\boldsymbol{n}\cdot\left[\epsilon^S_{I,11}\nabla_{\boldsymbol{\xi}}\phi^1_{I,(in)(0)}-\epsilon^S_{M,11}\nabla_{\boldsymbol{\xi}}\phi^1_{M,(in)(0)}-S_pe_{51}\nabla_{\boldsymbol{\xi}}\Phi^1_{I,(in)(0)3}\right]=n^1\left(\epsilon^S_{M,11}-\epsilon^S_{I,11}\right). \tag{4.3.32}$$

We find that

$$\Phi^1_{M,(in)(0)3}=-\left(\frac{2e_{51}\epsilon^S_{M,11}}{\left(\epsilon^S_{I,11}+\epsilon^S_{M,11}\right)(\mu_I+\mu_M)+S_p\left(e_{51}\right)^2}\right)\frac{\xi}{\xi^2+\eta^2}, \tag{4.3.33}$$

$$\Phi^1_{I,(in)(0)3}=-\left(\frac{2e_{51}\epsilon^S_{M,11}}{\left(\epsilon^S_{I,11}+\epsilon^S_{M,11}\right)(\mu_I+\mu_M)+S_p\left(e_{51}\right)^2}\right)\xi, \tag{4.3.34}$$

$$\phi^1_{M,(in)(0)}=-\left(\frac{\left(\epsilon^S_{I,11}-\epsilon^S_{M,11}\right)(\mu_I+\mu_M)+S_p\left(e_{51}\right)^2}{\left(\epsilon^S_{I,11}+\epsilon^S_{M,11}\right)(\mu_I+\mu_M)+S_p\left(e_{51}\right)^2}\right)\frac{\xi}{\xi^2+\eta^2}, \tag{4.3.35}$$

$$\phi^1_{I,(in)(0)}=-\left(\frac{\left(\epsilon^S_{I,11}-\epsilon^S_{M,11}\right)(\mu_I+\mu_M)+S_p\left(e_{51}\right)^2}{\left(\epsilon^S_{I,11}+\epsilon^S_{M,11}\right)(\mu_I+\mu_M)+S_p\left(e_{51}\right)^2}\right)\xi. \tag{4.3.36}$$

4.3.3.1.2 Outer limit of the leading-order inner solution

If we multiply (4.3.33) and (4.3.35) by r and then rewrite these expressions in terms of outer variables, we deduce

$$(1.t.o)(1.t.i)\Phi^1_{M,3}=-r^2\left(\frac{2e_{51}\epsilon^S_{M,11}}{\left(\epsilon^S_{I,11}+\epsilon^S_{M,11}\right)(\mu_I+\mu_M)+S_p\left(e_{51}\right)^2}\right)\frac{X}{X^2+Y^2}, \tag{4.3.37}$$

$$(1.t.o)(1.t.i)\phi^1_M=-r^2\left(\frac{\left(\epsilon^S_{I,11}-\epsilon^S_{M,11}\right)(\mu_I+\mu_M)+S_p\left(e_{51}\right)^2}{\left(\epsilon^S_{I,11}+\epsilon^S_{M,11}\right)(\mu_I+\mu_M)+S_p\left(e_{51}\right)^2}\right)\frac{X}{X^2+Y^2}. \tag{4.3.38}$$

4.3.3.1.3 First leading-order outer solution

From (4.3.37)-(4.3.38), we see that the one-term outer expansions for both $\Phi^1_{M,3}$ and ϕ^1_M takes the form

$$\Phi^1_{(out)3}\sim r^2\Phi^1_{(0)(out)3}, \tag{4.3.39}$$

$$\phi^1_{(out)}\sim r^2\phi^1_{(0)(out)}, \tag{4.3.40}$$

where the functions $\Phi^1_{(out)3}$ and $\phi^1_{(out)}$ have the matching conditions

$$\Phi^1_{(0)(out)3} \sim -\left(\frac{2e_{51}\epsilon^S_{M,11}}{\left(\epsilon^S_{I,11}+\epsilon^S_{M,11}\right)(\mu_I+\mu_M)+S_p\left(e_{51}\right)^2}\right)\frac{X}{X^2+Y^2}, \tag{4.3.41}$$

$$\phi^1_{(0)(out)} \sim -\left(\frac{\left(\epsilon^S_{I,11}-\epsilon^S_{M,11}\right)(\mu_I+\mu_M)+S_p\left(e_{51}\right)^2}{\left(\epsilon^S_{I,11}+\epsilon^S_{M,11}\right)(\mu_I+\mu_M)+S_p\left(e_{51}\right)^2}\right)\frac{X}{X^2+Y^2}, \tag{4.3.42}$$

as $R \to 0$. The functions $\Phi^1_{(0)(out)3}$ and $\phi^1_{(0)(out)}$ must also satisfy (4.3.3) and (4.3.5).

We find that

$$\Phi^1_{(0)(out)3} \sim -\left(\frac{2e_{51}\epsilon^S_{M,11}}{\left(\epsilon^S_{I,11}+\epsilon^S_{M,11}\right)(\mu_I+\mu_M)+S_p\left(e_{51}\right)^2}\right)\sum_{l=-\infty}^{\infty}\sum_{k=-\infty}^{\infty}\frac{X-k}{(X-k)^2+(Y-l)^2}, \tag{4.3.43}$$

$$\phi^1_{(0)(out)} \sim -\left(\frac{\left(\epsilon^S_{I,11}-\epsilon^S_{M,11}\right)(\mu_I+\mu_M)+S_p\left(e_{51}\right)^2}{\left(\epsilon^S_{I,11}+\epsilon^S_{M,11}\right)(\mu_I+\mu_M)+S_p\left(e_{51}\right)^2}\right)\sum_{l=-\infty}^{\infty}\sum_{k=-\infty}^{\infty}\frac{X-k}{(X-k)^2+(Y-l)^2}. \tag{4.3.44}$$

4.3.3.1.4 Inner limit of the first leading-order outer solution

If we Taylor expand (4.3.43)-(4.3.44) about $(X,Y)=(0,0)$ using the expansions found in (H.0.5) and then re-write in terms of inner variables, we deduce that

$$\begin{aligned}(2.t.i)(1.t.o)\Phi^1_{M,3} =& -r\left(\frac{2e_{51}\epsilon^S_{M,11}}{\left(\epsilon^S_{I,11}+\epsilon^S_{M,11}\right)(\mu_I+\mu_M)+S_p\left(e_{51}\right)^2}\right)\frac{\xi}{\xi^2+\eta^2}\\ &+r^3\left(\frac{2e_{51}\epsilon^S_{M,11}}{\left(\epsilon^S_{I,11}+\epsilon^S_{M,11}\right)(\mu_I+\mu_M)+S_p\left(e_{51}\right)^2}\right)\pi\xi,\end{aligned} \tag{4.3.45}$$

$$\begin{aligned}(2.t.i)(1.t.o)\phi^1_M =& -r\left(\frac{\left(\epsilon^S_{I,11}-\epsilon^S_{M,11}\right)(\mu_I+\mu_M)+S_p\left(e_{51}\right)^2}{\left(\epsilon^S_{I,11}+\epsilon^S_{M,11}\right)(\mu_I+\mu_M)+S_p\left(e_{51}\right)^2}\right)\frac{\xi}{\xi^2+\eta^2}\\ &+r^3\left(\frac{\left(\epsilon^S_{I,11}-\epsilon^S_{M,11}\right)(\mu_I+\mu_M)+S_p\left(e_{51}\right)^2}{\left(\epsilon^S_{I,11}+\epsilon^S_{M,11}\right)(\mu_I+\mu_M)+S_p\left(e_{51}\right)^2}\right)\pi\xi.\end{aligned} \tag{4.3.46}$$

4.3.3.1.5 Second order inner solution

This process tells us the inner expansions proceed as

$$\Phi^1_{(in)3} \sim r\Phi^1_{(in)(0)3}+r^3\Phi^1_{(in)(1)3}, \tag{4.3.47}$$

$$\phi^1_{(out)} \sim r\phi^1_{(0)(in)}+r^3\phi^1_{(1)(in)}, \tag{4.3.48}$$

where the functions $\mathbf{\Phi}^1_{(1)(in)3}$ and $\phi^1_{(1)(in)}$ have the matching conditions

$$\Phi^1_{(1)(in)3} \sim \left(\frac{2e_{51}\epsilon^S_{M,11}}{\left(\epsilon^S_{I,11}+\epsilon^S_{M,11}\right)(\mu_I+\mu_M)+S_p\left(e_{51}\right)^2} \right) \pi\xi, \tag{4.3.49}$$

$$\phi^1_{(1)(in)} \sim \left(\frac{\left(\epsilon^S_{I,11}-\epsilon^S_{M,11}\right)(\mu_I+\mu_M)+S_p\left(e_{51}\right)^2}{\left(\epsilon^S_{I,11}+\epsilon^S_{M,11}\right)(\mu_I+\mu_M)+S_p\left(e_{51}\right)^2} \right) \pi\xi, \tag{4.3.50}$$

as $\rho \to \infty$. The functions $\Phi^1_{(1)(in)3}$ and $\phi^1_{(1)(in)}$ satisfy (4.2.11) and (4.2.13) when $\rho > 1$, (4.2.12) and (4.2.14) when $\rho < 1$, along with the continuity conditions (4.2.16)-(4.2.17) as well as the jump conditions

$$\boldsymbol{n} \cdot \left[\mu_M \nabla_{\boldsymbol{\xi}} \Phi^1_{M,(in)(1),3} - \mu_I \nabla_{\boldsymbol{\xi}} \Phi^1_{I,(in)(1),3} - e_{51} \nabla_{\boldsymbol{\xi}} \phi^1_{I,(in)(1)} \right] = 0, \tag{4.3.51}$$

$$\boldsymbol{n} \cdot \left[\epsilon^S_{I,11} \nabla_{\boldsymbol{\xi}} \phi^1_{I,(in)(1)} - \epsilon^S_{M,11} \nabla_{\boldsymbol{\xi}} \phi^1_{M,(in)(1)} - S_p e_{51} \nabla_{\boldsymbol{\xi}} \Phi^1_{I,(in)(1),3} \right] = 0. \tag{4.3.52}$$

We find that

$$\Phi^1_{I,(in)3} = \frac{2e_{51}\epsilon^S_{M,11}\left(\left(e_{51}\right)^2 S_p + \epsilon^S_{I,11}(\mu_I-\mu_M) - \epsilon^S_{M,11}(\mu_I+3\mu_M)\right)}{\left(\left(e_{51}\right)^2 S_p + \epsilon^S_{I,11}(\mu_I+\mu_M) + \epsilon^S_{M,11}(\mu_I+\mu_M)\right)^2}\pi\xi, \tag{4.3.53}$$

$$\phi^1_{I,(in)} = -\frac{2\epsilon^S_{M,11}\left(\left(e_{51}\right)^2 S_p(\mu_I+3\mu_M) + \epsilon^S_{I,11}(\mu_I+\mu_M)^2 - \epsilon^S_{M,11}(\mu_I+\mu_M)^2\right)}{\left(\left(e_{51}\right)^2 S_p + \epsilon^S_{I,11}(\mu_I+\mu_M) + \epsilon^S_{M,11}(\mu_I+\mu_M)\right)^2}\pi\xi, \tag{4.3.54}$$

on the boundary ∂I.

We now have the first two terms in the inner expansion of Φ^1_3 and ϕ^1, which we will be able to use to approximate the 1-coefficients of the dielectric tensor.

4.3.3.2 The 2-problem

From (F.4.4), we see that

$$\Phi^2_\beta = 0_\beta. \tag{4.3.55}$$

This means we only need to solve (4.2.11)-(4.2.14), subject to continuity conditions (4.2.16)-(4.2.17) and (4.2.19)-(4.2.20). We will now solve the cell problem corresponding to the Y-direction. Since the problem has rotational symmetry, the solution to the Y-problem is given by the solution in §4.3.3.1, with X replaced with Y (and vice versa) and ξ replaced with η (and vice versa). The solutions to the 2-problem

evaluated on the boundary of the inclusion are given by

$$\Phi^2_{I,(in)3} \sim -r\left(\frac{2e_{51}\epsilon^S_{M,11}}{\left(\epsilon^S_{I,11}+\epsilon^S_{M,11}\right)(\mu_I+\mu_M)+S_p\left(e_{51}\right)^2}\right)\eta + r^3\frac{2e_{51}\epsilon^S_{M,11}\left(\left(e_{51}\right)^2(-S_p)+\epsilon^S_{I,11}(\mu_M-\mu_I)+\epsilon^S_{M,11}(\mu_I+3\mu_M)\right)}{\left(\left(e_{51}\right)^2 S_p+(\epsilon^S_{I,11}+\epsilon^S_{M,11})(\mu_I+\mu_M)\right)^2}\pi\eta, \tag{4.3.56}$$

$$\phi^2_{I,(in)} \sim -r\left(\frac{\left(\epsilon^S_{I,11}-\epsilon^S_{M,11}\right)(\mu_I+\mu_M)+S_p\left(e_{51}\right)^2}{\left(\epsilon^S_{I,11}+\epsilon^S_{M,11}\right)(\mu_I+\mu_M)+S_p\left(e_{51}\right)^2}\right)\eta - r^3\frac{2\epsilon^S_{M,11}\left(\left(e_{51}\right)^2 S_p(\mu_I+3\mu_M)+\epsilon^S_{I,11}(\mu_I+\mu_M)^2-\epsilon^S_{M,11}(\mu_I+\mu_M)^2\right)}{\left(\left(e_{51}\right)^2 S_p+\epsilon^S_{I,11}(\mu_I+\mu_M)+\epsilon^S_{M,11}(\mu_I+\mu_M)\right)^2}\pi\eta. \tag{4.3.57}$$

We now have the first two terms in the inner expansion of Φ^2_3 and ϕ^2, which we will be able to use to approximate the 2-coefficients of the dielectric tensor.

4.3.3.3 The 3-problem

From (F.4.5), we see that

$$\Phi^3_3 = \phi^3 = 0. \tag{4.3.58}$$

This means we only need to solve (4.3.3)-(4.3.6), subject to continuity conditions (4.3.7) and (4.3.10). We will now solve the cell problem corresponding to the Z-direction. The cell function $\mathbf{\Phi}^3_{(in)(0)}$ satisfies (4.3.1) when $\rho > 1$ (4.3.2) when $\rho < 1$, along with the continuity condition (4.3.7), and the jump conditions

$$\left[\lambda_M \nabla_{\boldsymbol{\xi}}\cdot\mathbf{\Phi}^3_{M,(in)(0)}n_\alpha+\mu_M\left(\boldsymbol{n}\cdot\nabla_{\boldsymbol{\xi}}\Phi^3_{M,(in)(0)\alpha}+n^\beta\frac{\partial\Phi^3_{M,(in)(0)\beta}}{\partial\xi^\alpha}\right)\right] - \left[\lambda_I\nabla_{\boldsymbol{\xi}}\cdot\mathbf{\Phi}^3_{I,(in)(0)}n_\alpha+\mu_I\left(\boldsymbol{n}\cdot\nabla_{\boldsymbol{\xi}}\Phi^3_{I,(in)(0)\alpha}+n^\beta\frac{\partial\Phi^3_{I,(in)(0)\beta}}{\partial\xi^\alpha}\right)\right] = e_{13}\left(\cos(\theta)\delta^1_\alpha+\sin(\theta)\delta^2_\alpha\right). \tag{4.3.59}$$

The RHS of (4.3.59) is directly proportional to the RHS of (4.2.83). Thus from (4.2.104) and (4.2.105), we deduce that the two-term asymptotic expansion for $\Phi^3_{(in)\alpha}$, evaluated on the boundary of the inclusion, is given by

$$\Phi^3_{(in)1} = -r\left(\frac{e_{13}}{2\left(\kappa_I+\mu_M\right)}\right)\xi \ + r^3\left(\frac{e_{13}}{2\left(\kappa_I+\mu_M\right)}\right)\left(\frac{\kappa_M+\mu_M}{\kappa_I+\mu_M}\right)\pi\xi, \tag{4.3.60}$$

$$\Phi^3_{(in)2} = -r\left(\frac{e_{13}}{2\left(\kappa_I+\mu_M\right)}\right)\eta \ + r^3\left(\frac{e_{13}}{2\left(\kappa_I+\mu_M\right)}\right)\left(\frac{\kappa_M+\mu_M}{\kappa_I+\mu_M}\right)\pi\eta. \tag{4.3.61}$$

We now have the first two terms in the inner expansion of $\mathbf{\Phi}^3$, which we will be able to use to approximate the 3-coefficients of the dielectric tensor.

4.4 Formulae for effective coefficients

4.4.1 Establishing the integral formulae

Using the Divergence Theorem, (2.7.85)-(2.7.88) yield

$$c^{kl}_{\text{eff},ij} = c^{kl}_{M,ij} + \nu\left(c^{kl}_{I,ij} - c^{kl}_{M,ij}\right) + \iint_{\partial\Gamma_I} n_{l'}\left[\left(c^{k'l'}_{I,ij} - c^{k'l'}_{M,ij}\right)\Psi^{kl}_{k'} + e^{l'}_{ij}\psi^{kl}\right]\mathrm{d}S, \tag{4.4.1}$$

$$e^{k}_{\text{eff},ij} = \nu e^{k}_{ij} + \iint_{\partial\Gamma_I} n_{l'}\left[\left(c^{k'l'}_{I,ij} - c^{k'l'}_{M,ij}\right)\Phi^{k}_{k'} + e^{l'}_{ij}\phi^{k}\right]\mathrm{d}S, \tag{4.4.2}$$

$$\epsilon^{Sk}_{\text{eff},i} = \epsilon^{Sk}_{M,i} + \nu\left(\epsilon^{Sk}_{I,i} - \epsilon^{Sk}_{M,i}\right) + \iint_{\partial\Gamma_I} n_{l'}\left[-S_p e^{k'l'}_{i}\Phi^{k}_{k'} + \left(\epsilon^{Sl'}_{I,i} - \epsilon^{Sl'}_{M,i}\right)\phi^{k}\right]\mathrm{d}S, \tag{4.4.3}$$

where $\boldsymbol{n}$ is the unit normal to ∂I pointing out of I, n_l is the component of $\boldsymbol{n}$ in the l-direction and dS is the surface area measure with respect to the scaling (X, Y, Z). To integrate the integrals in (4.4.1)-(4.4.3), we introduce the parametrisation of a cylinder of radius r

$$\begin{pmatrix} X \\ Y \\ Z \end{pmatrix} = \begin{pmatrix} r\cos(\theta) \\ r\sin(\theta) \\ Z \end{pmatrix}. \tag{4.4.4}$$

Using (4.4.4), we see that

$$dS = r d\theta dZ. \tag{4.4.5}$$

Using (4.4.5) and the fact that the solutions to both the mechanical and electrical cell problems are independent of the Z-coordinate, (4.4.1)-(4.4.3) simplify to

$$c^{kl}_{\text{eff},ij} = c^{kl}_{M,ij} + \nu\left(c^{kl}_{I,ij} - c^{kl}_{M,ij}\right) \ + r\int_0^{2\pi} n_{l'}\left[\left(c^{k'l'}_{I,ij} - c^{k'l'}_{M,ij}\right)\Psi^{kl}_{k'} + e^{l'}_{ij}\psi^{kl}\right]\mathrm{d}\theta, \tag{4.4.6}$$

$$e^{k}_{\text{eff},ij} = \nu e^{k}_{ij} + r\int_0^{2\pi} n_{l'}\left[\left(c^{k'l'}_{I,ij} - c^{k'l'}_{M,ij}\right)\Phi^{k}_{k'} + e^{l'}_{ij}\phi^{k}\right]\mathrm{d}\theta, \tag{4.4.7}$$

$$\epsilon^{Sk}_{\text{eff},i} = \epsilon^{Sk}_{M,i} + \nu\left(\epsilon^{Sk}_{I,i} - \epsilon^{Sk}_{M,i}\right) + r\int_0^{2\pi} n_{l'}\left[-S_p e^{k'l'}_{i}\Phi^{k}_{k'} + \left(\epsilon^{Sl'}_{I,i} - \epsilon^{Sl'}_{M,i}\right)\phi^{k}\right]\mathrm{d}\theta. \tag{4.4.8}$$

Using the inner expansions given in §4.2.3 and §4.3.3, we see that (4.4.6)-(4.4.8) can

be re-written as

$$c^{kl}_{\text{eff},ij} = c^{kl}_{M,ij} + \nu\Big(c^{kl}_{I,ij} - c^{kl}_{M,ij}\Big) + r^2\int_0^{2\pi} n_{l'}\left[\Big(c^{k'l'}_{I,ij} - c^{k'l'}_{M,ij}\Big)\Psi^{kl}_{(0)k'} + e^{l'}_{ij}\psi^{kl}_{(0)}\right]\mathrm{d}\theta$$
$$+ r^4\int_0^{2\pi} n_{l'}\left[\Big(c^{k'l'}_{I,ij} - c^{k'l'}_{M,ij}\Big)\Psi^{kl}_{(1)k'} + e^{l'}_{ij}\psi^{kl}_{(1)}\right]\mathrm{d}\theta, \tag{4.4.9}$$

$$e^{k}_{\text{eff},ij} = \nu e^{k}_{ij} + r^2\int_0^{2\pi} n_{l'}\left[\Big(c^{k'l'}_{I,ij} - c^{k'l'}_{M,ij}\Big)\Phi^{k}_{(0)k'} + e^{l'}_{ij}\phi^{k}_{(0)}\right]\mathrm{d}\theta$$
$$+ r^4\int_0^{2\pi} n_{l'}\left[\Big(c^{k'l'}_{I,ij} - c^{k'l'}_{M,ij}\Big)\Phi^{k}_{(1)k'} + e^{l'}_{ij}\phi^{k}_{(1)}\right]\mathrm{d}\theta, \tag{4.4.10}$$

$$\epsilon^{Sk}_{\text{eff},i} = \epsilon^{Sk}_{M,i} + \nu\Big(\epsilon^{Sk}_{I,i} - \epsilon^{Sk}_{M,i}\Big) + r^2\int_0^{2\pi} n_{l'}\left[-S_p e^{k'l'}_{i}\Phi^{k}_{(0)k'} + \Big(\epsilon^{Sl'}_{I,i} - \epsilon^{Sl'}_{M,i}\Big)\phi^{k}_{(0)}\right]\mathrm{d}\theta$$
$$+ r^4\int_0^{2\pi} n_{l'}\left[-S_p e^{k'l'}_{i}\Phi^{k}_{(1)k'} + \Big(\epsilon^{Sl'}_{I,i} - \epsilon^{Sl'}_{M,i}\Big)\phi^{k}_{(1)}\right]\mathrm{d}\theta. \tag{4.4.11}$$

Using the fact that $\nu = \pi r^2$ (i.e., the volume of a cylinder of radius r and height 1), (4.4.9)-(4.4.11) can be re-written as

$$c^{kl}_{\text{eff},ij} = c^{kl}_{M,ij} + \nu\Big(c^{kl}_{I,ij} - c^{kl}_{M,ij}\Big) + \frac{\nu}{\pi}\int_0^{2\pi} n_{l'}\left[\Big(c^{k'l'}_{I,ij} - c^{k'l'}_{M,ij}\Big)\Psi^{kl}_{(0)k'} + e^{l'}_{ij}\psi^{kl}_{(0)}\right]\mathrm{d}\theta$$
$$+ \left(\frac{\nu}{\pi}\right)^2\int_0^{2\pi} n_{l'}\left[\Big(c^{k'l'}_{I,ij} - c^{k'l'}_{M,ij}\Big)\Psi^{kl}_{(1)k'} + e^{l'}_{ij}\psi^{kl}_{(1)}\right]\mathrm{d}\theta, \tag{4.4.12}$$

$$e^{k}_{\text{eff},ij} = \nu e^{k}_{ij} + \frac{\nu}{\pi}\int_0^{2\pi} n_{l'}\left[\Big(c^{k'l'}_{I,ij} - c^{k'l'}_{M,ij}\Big)\Phi^{k}_{(0)k'} + e^{l'}_{ij}\phi^{k}_{(0)}\right]\mathrm{d}\theta$$
$$+ \left(\frac{\nu}{\pi}\right)^2\int_0^{2\pi} n_{l'}\left[\Big(c^{k'l'}_{I,ij} - c^{k'l'}_{M,ij}\Big)\Phi^{k}_{(1)k'} + e^{l'}_{ij}\phi^{k}_{(1)}\right]\mathrm{d}\theta, \tag{4.4.13}$$

$$\epsilon^{Sk}_{\text{eff},i} = \epsilon^{Sk}_{M,i} + \nu\Big(\epsilon^{Sk}_{I,i} - \epsilon^{Sk}_{M,i}\Big) + \frac{\nu}{\pi}\int_0^{2\pi} n_{l'}\left[-S_p e^{k'l'}_{i}\Phi^{k}_{(0)k'} + \Big(\epsilon^{Sl'}_{I,i} - \epsilon^{Sl'}_{M,i}\Big)\phi^{k}_{(0)}\right]\mathrm{d}\theta$$
$$+ \left(\frac{\nu}{\pi}\right)^2\int_0^{2\pi} n_{l'}\left[-S_p e^{k'l'}_{i}\Phi^{k}_{(1)k'} + \Big(\epsilon^{Sl'}_{I,i} - \epsilon^{Sl'}_{M,i}\Big)\phi^{k}_{(1)}\right]\mathrm{d}\theta. \tag{4.4.14}$$

4.4.2 Low volume fraction formulae

4.4.2.1 Effective stiffness tensor coefficients

We will make use of (4.4.12) along with the solutions to the cell problem found in subsections §4.2.3.1-§4.2.3.6 to determine the effective stiffness tensor coefficients. From Appendix E, we see that c_{eff} satisfies the symmetries

$$c^{kl}_{\text{eff},ij} = c^{lk}_{\text{eff},ij} = c^{kl}_{\text{eff},ji} = c^{ij}_{\text{eff},kl}, \tag{4.4.15}$$

for all $i, j, k, l \in \{1, 2, 3\}$. Thus the stiffness tensor components are given by

$$\begin{aligned} c^{11}_{\text{eff},11} = c^{22}_{\text{eff},22} &= (\lambda_M + 2\mu_M) \\ &+ \nu \left((\kappa_I - \kappa_M) \left(\frac{\kappa_M + \mu_M}{\kappa_I + \mu_M} \right) + (\mu_I - \mu_M) \left(\frac{2\mu_M (\kappa_M + \mu_M)}{\kappa_M \mu_M + \kappa_M \mu_I + 2\mu_M \mu_I} \right) \right) \\ &+ \nu^2 (\kappa_M + \mu_M) \left(\frac{\kappa_I - \kappa_M}{\kappa_I + \mu_M} \right)^2 \\ &+ \nu^2 (\kappa_M + \mu_M) \frac{4\mu_M (\mu_I - \mu_M)^2 \left(\mu_M + \kappa_M \left(1 + 4 \sum_{l=1}^{\infty} \pi^2 l \coth(\pi l) \operatorname{csch}^2(\pi l) \right) \right)}{(\kappa_M \mu_M + \kappa_M \mu_I + 2\mu_M \mu_I)^2}, \end{aligned} \tag{4.4.16}$$

$$\begin{aligned} c^{22}_{\text{eff},11} = c^{11}_{\text{eff},22} = \lambda_M &+ \nu \left((\kappa_I - \kappa_M) \left(\frac{\kappa_M + \mu_M}{\kappa_I + \mu_M} \right) - (\mu_I - \mu_M) \left(\frac{2\mu_M (\kappa_M + \mu_M)}{\kappa_M \mu_M + \kappa_M \mu_I + 2\mu_M \mu_I} \right) \right) \\ &+ \nu^2 (\kappa_M + \mu_M) \left(\frac{\kappa_I - \kappa_M}{\kappa_I + \mu_M} \right)^2 \\ &- \nu^2 (\kappa_M + \mu_M) \frac{4\mu_M (\mu_I - \mu_M)^2 \left(\mu_M + \kappa_M \left(1 + 4 \sum_{l=1}^{\infty} \pi^2 l \coth(\pi l) \operatorname{csch}^2(\pi l) \right) \right)}{(\kappa_M \mu_M + \kappa_M \mu_I + 2\mu_M \mu_I)^2}, \end{aligned} \tag{4.4.17}$$

$$\begin{aligned} c^{33}_{\text{eff},11} = c^{33}_{\text{eff},22} = c^{11}_{\text{eff},33} = c^{22}_{\text{eff},33} \\ = \lambda_M + \nu \left((\lambda_I - \lambda_M) \left(\frac{\kappa_M + \mu_M}{\kappa_I + \mu_M} \right) \right) + \nu^2 \left((\lambda_I - \lambda_M) \left(\frac{(\kappa_I - \kappa_M)(\kappa_M + \mu_M)}{(\kappa_I + \mu_M)^2} \right) \right), \end{aligned} \tag{4.4.18}$$

$$\begin{aligned} c^{33}_{\text{eff},33} = (\lambda_M + 2\mu_M) &+ \nu \left(\frac{(\kappa_M + \mu_I)(\lambda_I - \lambda_M)}{\kappa_I + \mu_M} + 2(\mu_I - \mu_M) \right) \\ &+ \nu^2 \left(\frac{(\kappa_M + \mu_M)(\lambda_I - \lambda_M)^2}{(\kappa_I + \mu_M)^2} \right), \end{aligned} \tag{4.4.19}$$

$$c^{13}_{\text{eff},13} = c^{23}_{\text{eff},23} = \mu_M + \nu \left(\frac{2\mu_M \left((e_{51})^2 S_p + (\epsilon^S_{I,11} + \epsilon^S_{M,11})(\mu_I - \mu_M) \right)}{(e_{51})^2 S_p + \epsilon^S_{I,11}(\mu_I + \mu_M) + \epsilon^S_{M,11}(\mu_I + \mu_M)} \right)$$
$$+ \nu^2 \left(\frac{2\mu_M \left((e_{51})^4 (S_p)^2 + 2 (e_{51})^2 S_p \mu_I (\epsilon^S_{I,11} + \epsilon^S_{M,11}) \right)}{\left((e_{51})^2 S_p + (\epsilon^S_{I,11} + \epsilon^S_{M,11})(\mu_I + \mu_M) \right)^2} \right)$$
$$+ \nu^2 \left(\frac{2\mu_M \left(-2 (e_{51})^2 S_p \mu_M (\epsilon^S_{I,11} + 3\epsilon^S_{M,11}) + (\epsilon^S_{I,11} + \epsilon^S_{M,11})^2 (\mu_I - \mu_M)^2 \right)}{\left((e_{51})^2 S_p + (\epsilon^S_{I,11} + \epsilon^S_{M,11})(\mu_I + \mu_M) \right)^2} \right), \tag{4.4.20}$$

$$c^{12}_{\text{eff},12} = \mu_M + \nu \left(2(\mu_I - \mu_M) \frac{\mu_M(\kappa_M + \mu_M)}{\kappa_M(\mu_I + \mu_M) + 2\mu_I\mu_M} \right)$$
$$+ \nu^2 \left(\frac{4(\mu_I - \mu_M)^2 \left(\mu_M + \kappa_M \left(1 + 2\sum_{l=1}^{\infty} \pi^2 l \coth(\pi l) \operatorname{csch}^2(\pi l) \right) \right)}{\kappa_M(\mu_I + \mu_M) + 2\mu_I\mu_M} \right). \tag{4.4.21}$$

The remaining coefficients are all equal to zero.

4.4.2.2 Effective electromechanical tensor coefficients

We will make use of (4.4.13) along with the solutions found in subsections §4.3.3.1-§4.3.3.3 to determine the effective electromechanical tensor coefficient. We note from Appendix E that the effective electromechanical tensor $\boldsymbol{e}_{\text{eff}}$ satisfies

$$e^k_{\text{eff},ij} = e^k_{\text{eff},ji}, \tag{4.4.22}$$

for all $i, j, k \in \{1, 2, 3\}$. Thus

$$e^3_{\text{eff},11} = e^3_{\text{eff},22} = \nu \left(e_{13} \left(\frac{\kappa_M + \mu_M}{\kappa_I + \mu_M} \right) \right) - \nu^2 \left(e_{13} \left(\frac{(\kappa_I - \kappa_M)(\kappa_M + \mu_M)}{(\kappa_I + \mu_M)^2} \right) \right) \tag{4.4.23}$$

$$e^3_{\text{eff},33} = \nu \left(e_{33} - e_{13} \left(\frac{\lambda_I - \lambda_M}{\kappa_I + \mu_M} \right) \right) + \nu^2 \left(e_{13} \left(\frac{(\kappa_M + \mu_M)(\lambda_I - \lambda_M)}{(\kappa_I + \mu_M)^2} \right) \right), \tag{4.4.24}$$

$$e^2_{\text{eff},23} = e^1_{\text{eff},13} = \nu \left(\frac{4e_{51}\epsilon^S_{M,11}\mu_M}{(e_{51})^2 S_p + \epsilon^S_{I,11}(\mu_I + \mu_M) + \epsilon^S_{M,11}(\mu_I + \mu_M)} \right)$$
$$+ \nu^2 \left(\frac{8e_{51}\epsilon^S_{M,11}\mu_M \left((e_{51})^2 S_p + \epsilon^S_{I,11}\mu_I - \epsilon^S_{M,11}\mu_M \right)}{\left((e_{51})^2 S_p + (\epsilon^S_{I,11} + \epsilon^S_{M,11})(\mu_I + \mu_M) \right)^2} \right). \tag{4.4.25}$$

All other coefficients are equal to zero.

4.4.2.3 Effective dielectric tensor coefficients

We make use of (4.4.14), along with the solutions found in subsections §4.3.3.1-§4.3.3.3, to determine the effective dielectric tensor coefficients, and find that

$$\begin{aligned}\epsilon_{\text{eff}1}^{S1} = \epsilon_{\text{eff}2}^{S2} = \epsilon_{M,11}^{S} + \nu \left(\frac{2\epsilon_{M,11}^{S} \left((e_{51})^2 S_p + (\epsilon_{I,11} - \epsilon_{M,11}) (\mu_I + \mu_M) \right)}{(e_{51})^2 S_p + \epsilon_{I,11}^{S}(\mu_I + \mu_M) + \epsilon_{M,11}^{S}(\mu_I + \mu_M)} \right) \\ + \nu^2 \left(\frac{2\epsilon_{M,11}^{S} \left((e_{51})^4 S_p^2 + 2 (e_{51})^2 S_p \epsilon_{I,11}^{S}(\mu_I + \mu_M) \right)}{\left((e_{51})^2 S_p + (\epsilon_{I,11}^{S} + \epsilon_{M,11}^{S})(\mu_I + \mu_M) \right)^2} \right) \\ + \nu^2 \left(\frac{2\epsilon_{M,11}^{S} \left(-2 (e_{51})^2 S_p \epsilon_{M,11}^{S}(\mu_I + 3\mu_M) + (\epsilon_{I,11} - \epsilon_{M,11})^2 (\mu_I + \mu_M)^2 \right)}{\left((e_{51})^2 S_p + (\epsilon_{I,11}^{S} + \epsilon_{M,11}^{S})(\mu_I + \mu_M) \right)^2} \right),\end{aligned} \tag{4.4.26}$$

$$\epsilon_{\text{eff},3}^{S3} = \epsilon_{M,11}^{S} + \nu \left(\frac{(e_{13})^2 S_p}{\kappa_I + \mu_M} + \left(\epsilon_{I,11}^{S} - \epsilon_{M,11}^{S} \right) \right) - \nu^2 \left(\frac{(e_{13})^2 S_p (\kappa_M + \mu_M)}{(\kappa_I + \mu_M)^2} \right). \tag{4.4.27}$$

All other dielectric tensor coefficients, namely the non-diagonal coefficients, are equal to zero.

4.5 Comparison of the AHM low volume fraction polynomials and the full numerical solution

In this subsection, we will compare the low volume fraction polynomials against the full numerical solution. Once again, we will use Stycast as the polymer material and PTZA5 as the inclusion material. The material properties in both phases is set out in Table 2.1.

We start by comparing the two sets of results for the effective bulk modulus κ_{eff}.

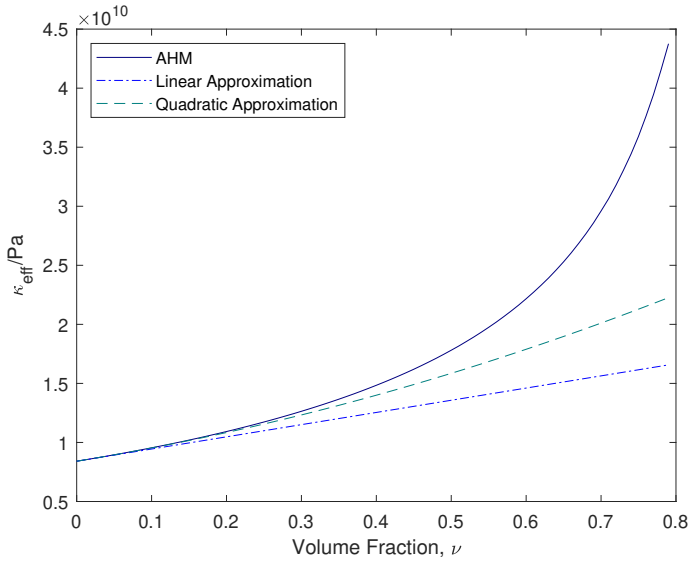


Figure 4.4: Comparison between κ_{eff} found using FEM and that found using the low volume fraction polynomials. The AHM curve is computed using the framework established in Chapter 2, while the linear and quadratic approximations are computed using equations (4.4.16), (4.4.17) and (3.2.1).

As shown in Figure 4.4, the linear approximation agrees well with the numerical results for volume fractions up to roughly 20%, while the quadratic polynomial agrees well with such results up to approximately 30%. Note that this means that for most sensors with this geometry of inclusions we can use the low volume fraction method, instead of the AHM as described in Chapter 2, to predict κ_{eff}, as typically the volume fraction of the inclusions for these is below 30%.

We now compare the two methodologies for the effective shear modulus μ_{eff}.

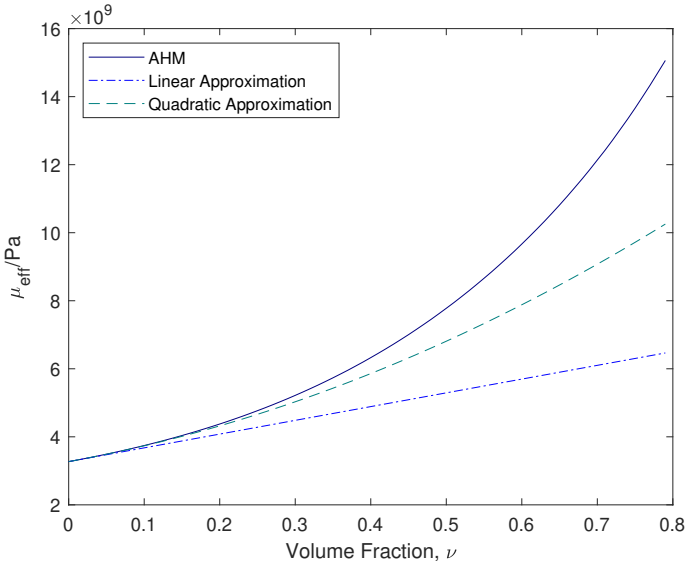


Figure 4.5: Comparison between μ_{eff} found using FEM and that found using the low volume fraction polynomials. The AHM curve is computed using the framework established in Chapter 2, while the linear and quadratic approximations are computed using equations (4.4.16), (4.4.17) and (3.2.2).

As shown in Figure 4.5, the linear approximation agrees well with the numerical results for volume fractions up to roughly 15%, while the quadratic polynomial agrees well up to approximately 30%. As before, this approximation will therefore be useful when designing most sensors.

We now compare the two methodologies for the effective electromechanical coefficient $-e_{\text{eff},13}$.

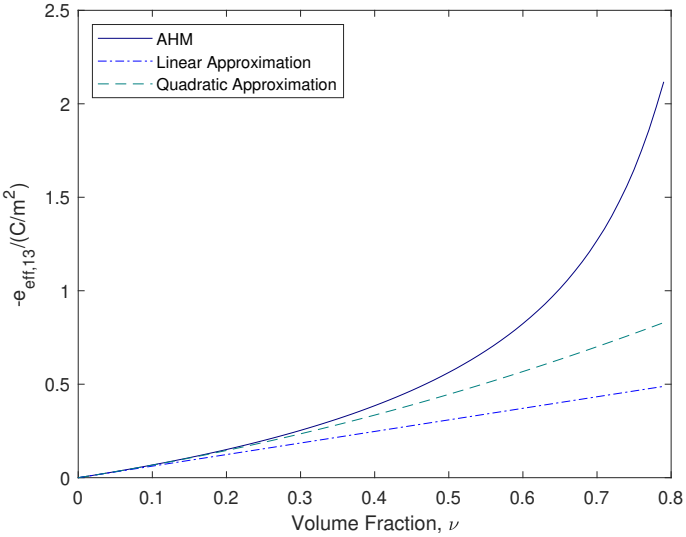


Figure 4.6: Comparison between effective $-e_{\text{eff},13}$ found using FEM and that found using the low volume fraction polynomials. The AHM curve is computed using the framework established in Chapter 2, while the linear and quadratic approximations are computed using (4.4.23).

As shown in Figure 4.6, the linear approximation agrees well with the numerical results for volume fractions up to roughly 20%, while the quadratic polynomial agrees well up to approximately 30%. Once again, this approximation will therefore be useful when designing most sensors.

We now compare the two methodologies for the effective electromechanical coefficient $e_{\text{eff},33}$.

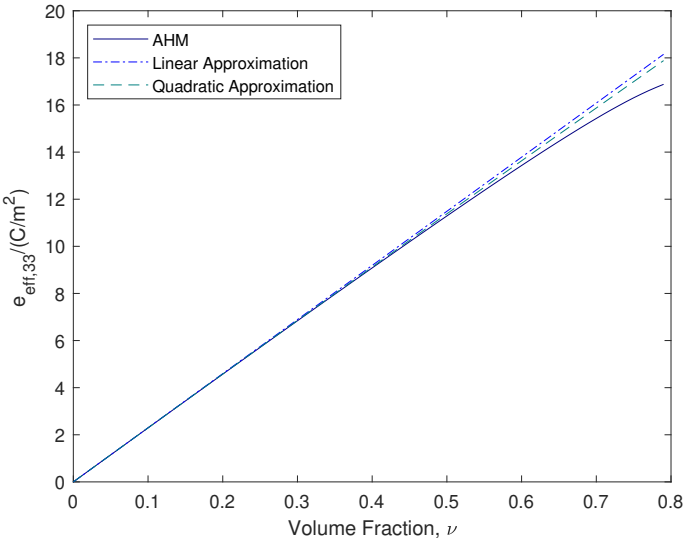


Figure 4.7: Comparison between effective $e_{\text{eff},33}$ found using FEM and that found using the low volume fraction polynomials. The AHM curve is computed using the framework established in Chapter 2, while the linear and quadratic approximations are computed using (4.4.24).

As shown in Figure 4.7, the linear and quadratic approximations both agree well with the numerical results for volume fractions up to roughly 60%. This approximation will therefore be very useful as both the linear and quadratic approximations agree with the numerical data.

We now compare the two methodologies for the effective dielectric coefficient $\epsilon^S_{\text{eff},33}$.

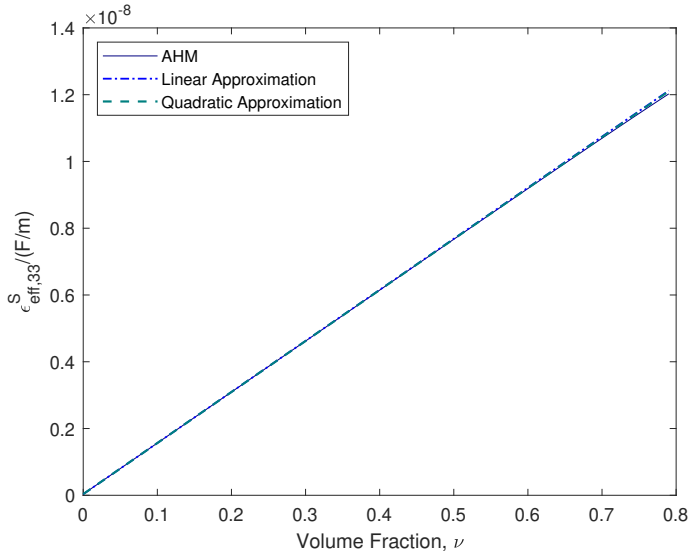


Figure 4.8: Comparison between effective $\epsilon^S_{\text{eff},33}$ found using FEM and that found using the low volume fraction polynomials. The AHM curve is computed using the framework established in Chapter 2, while the linear and quadratic approximations are computed using (4.4.27).

As shown in Figure 4.8, both the linear and quadratic approximations agree perfectly with the numerical results for volume fractions all the way up to close packing, which makes these approximations very useful for approximating this effective coefficient in particular.

4.6 Low Volume fraction approximations for the Differential Effective Medium method

Having derived low volume fraction asymptotic formulae for the AHM, we now derive similar formulae for the DEM and the MoM methods. This will allow us to compare coefficients, to determine the accuracy of these methods in the low volume fraction regime. We begin with the Differential Effective Medium method.

We postulate the asymptotic expansions for κ_{eff} and μ_{eff}

$$\kappa_{\text{eff}}(\nu) \sim \sum_{n=0}^{\infty} \kappa_n \nu^n, \tag{4.6.1}$$

$$\mu_{\text{eff}}(\nu) \sim \sum_{n=0}^{\infty} \mu_n \nu^n, \tag{4.6.2}$$

and assume that the asymptotic expansions for $d\kappa_{\text{eff}}/d\nu$ and $d\mu_{\text{eff}}/d\nu$ are obtained by term-wise differentiation of (4.6.1)-(4.6.2). The initial conditions (3.3.3)-(3.3.4) tell us that $\kappa_0 = \kappa_M$, $\mu_0 = \mu_M$. Substituting (4.6.1)-(4.6.2) into (3.3.1)-(3.3.2) gives the equations

$$\kappa_1 + 2\kappa_2\nu + O(\nu^2) = \frac{(\kappa_I - \kappa_M)(\kappa_M + \mu_M)}{\kappa_I + \mu_M} + C_1\nu + O(\nu^2), \tag{4.6.3}$$

$$\mu_1 + 2\mu_2\nu + O(\nu^2) = \frac{2\mu_M(\kappa_M + \mu_M)(\mu_I - \mu_M)}{\kappa_M(\mu_I + \mu_M) + 2\mu_I\mu_M} - C_2\nu + O(\nu^2), \tag{4.6.4}$$

where

$$\begin{aligned} C_1 = & \frac{\kappa_1(\kappa_I + \mu_M)(\kappa_I - 2\kappa_M - \mu_M)}{(\kappa_I + \mu_M)^2}, \\ & + \frac{(\kappa_I - \kappa_M)\left(\kappa_I(\kappa_M + \mu_1 + \mu_M) - \kappa_M\mu_1 + \kappa_M\mu_M + \mu_M^2\right)}{(\kappa_I + \mu_M)^2}, \end{aligned} \tag{4.6.5}$$

$$\begin{aligned} C_2 = & \frac{2\left((\mu_I - \mu_M)\mu_M\left(\kappa_M + \mu_M\right)\left(\kappa_M\mu_1 + 2\mu_1\mu_I + \kappa_1\left(\mu_I + \mu_M\right)\right)\right)}{\left(\kappa_M(\mu_I + \mu_M) + 2\mu_I\mu_M\right)^2} \\ & - \frac{2\left(\left(\kappa_1 + \mu_1\right)\left(\mu_I - \mu_M\right)\mu_M - \left(\kappa_M + \mu_M\right)\left(-\mu_1\mu_I + 2\mu_1\mu_M - \mu_I\mu_M + \mu_M^2\right)\right)}{\kappa_M(\mu_I + \mu_M) + 2\mu_I\mu_M}. \end{aligned} \tag{4.6.6}$$

If we collect like terms, then using Mathematica we deduce that

$$\kappa_1 = \frac{(\kappa_I - \kappa_M)(\kappa_M + \mu_M)}{\kappa_I + \mu_M}, \tag{4.6.7}$$

$$\kappa_2 = \frac{(\kappa_I - \kappa_M)^2(\kappa_M + \mu_M)(\kappa_M(\mu_I + \mu_M) + \mu_M(3\mu_I - \mu_M))}{(\kappa_I + \mu_M)^2(\kappa_M(\mu_I + \mu_M) + 2\mu_I\mu_M)}, \tag{4.6.8}$$

$$\mu_1 = \frac{2\mu_M(\kappa_M + \mu_M)(\mu_I - \mu_M)}{\kappa_M(\mu_I + \mu_M) + 2\mu_I\mu_M}, \tag{4.6.9}$$

$$\begin{aligned} \mu_2 = & \frac{\mu_M(\kappa_M + \mu_M)(\mu_I - \mu_M)^2\kappa_I\left(\kappa_M^2(3\mu_I + \mu_M) + \kappa_M\mu_M(9\mu_I + 5\mu_M) + 10\mu_I\mu_M^2\right)}{(\kappa_I + \mu_M)(\kappa_M(\mu_I + \mu_M) + 2\mu_I\mu_M)^3} \\ & + \frac{2\mu_M^2(\kappa_M + \mu_M)(\mu_I - \mu_M)^2\left(\kappa_M^2\mu_I + \kappa_M\mu_M(3\mu_I + 2\mu_M) + 4\mu_I\mu_M^2\right)}{(\kappa_I + \mu_M)(\kappa_M(\mu_I + \mu_M) + 2\mu_I\mu_M)^3}. \end{aligned} \tag{4.6.10}$$

From (4.6.7)-(4.6.10) and the initial conditions, we see that the three-term expansion

for κ_{eff} and μ_{eff} are given by

$$\begin{aligned}\kappa_{\text{eff}}(\nu) \sim\ & \kappa_M + \frac{(\kappa_I - \kappa_M)(\kappa_M + \mu_M)}{\kappa_I + \mu_M}\nu \\ &+ \frac{(\kappa_I - \kappa_M)^2\left(\kappa_M^2(\mu_I + \mu_M) + \kappa_M\mu_M(3\mu_I + \mu_M) + \mu_M(2\mu_I\mu_M + \mu_I - \mu_M)\right)}{(\kappa_I + \mu_M)^2(\kappa_M(\mu_I + \mu_M) + 2\mu_I\mu_M)}\nu^2,\end{aligned} \tag{4.6.11}$$

$$\begin{aligned}\mu_{\text{eff}}(\nu) \sim\ & \mu_M + \frac{2\mu_M(\kappa_M + \mu_M)(\mu_I - \mu_M)}{\kappa_M(\mu_I + \mu_M) + 2\mu_I\mu_M}\nu \\ &+ \frac{\mu_M(\kappa_M + \mu_M)(\mu_I - \mu_M)^2\kappa_I\left(\kappa_M^2(3\mu_I + \mu_M) + \kappa_M\mu_M(9\mu_I + 5\mu_M) + 10\mu_I\mu_M^2\right)}{(\kappa_I + \mu_M)(\kappa_M(\mu_I + \mu_M) + 2\mu_I\mu_M)^3}\nu^2 \\ &+ \frac{2\mu_M^2(\kappa_M + \mu_M)(\mu_I - \mu_M)^2\left(\kappa_M^2\mu_I + \kappa_M\mu_M(3\mu_I + 2\mu_M) + 4\mu_I\mu_M^2\right)}{(\kappa_I + \mu_M)(\kappa_M(\mu_I + \mu_M) + 2\mu_I\mu_M)^3}\nu^2.\end{aligned} \tag{4.6.12}$$

Using the expansion in (4.6.11) along with (3.3.5), we get the two-term expansion for p, which is given by

$$p(\nu) \sim \frac{\kappa_M + \mu_M}{\kappa_I + \mu_M} + \frac{(\kappa_I - \kappa_M)(\kappa_M + \mu_M)(\kappa_M(\mu_I + \mu_M) + \mu_M(3\mu_I - \mu_M))}{(\kappa_I + \mu_M)^2(\kappa_M(\mu_I + \mu_M) + 2\mu_I\mu_M)}\nu. \tag{4.6.13}$$

Using (4.6.13) along with (3.3.6)-(3.3.8) yields

$$\begin{aligned}e_{\text{eff},13} \sim\ & \nu e_{13}\frac{\kappa_M + \mu_M}{\kappa_I + \mu_M} \\ &+ \frac{e_{13}(\kappa_I - \kappa_M)(\kappa_M + \mu_M)(\kappa_M(\mu_I + \mu_M) + \mu_M(3\mu_I - \mu_M))}{(\kappa_I + \mu_M)^2(\kappa_M(\mu_I + \mu_M) + 2\mu_I\mu_M)}\nu^2,\end{aligned} \tag{4.6.14}$$

$$\begin{aligned}e_{\text{eff},33} \sim\ & \left(\frac{e_{13}S_p(\lambda_M - \lambda_I)}{\kappa_I + \mu_M} + e_{33}\right)\nu \\ &+ \frac{e_{13}S_p(\kappa_M + \mu_M)\left(\lambda_I - \lambda_M\right)\left(\kappa_M(\mu_I + \mu_M) + \mu_M(3\mu_I - \mu_M)\right)}{(\kappa_I + \mu_M)^2(\kappa_M(\mu_I + \mu_M) + 2\mu_I\mu_M)}\nu^2,\end{aligned} \tag{4.6.15}$$

$$\begin{aligned}\epsilon^S_{\text{eff},33} \sim\ & \epsilon^S_{M,11} + \left(\frac{(e_{13})^2 S_p}{\kappa_I + \mu_M} + \epsilon^S_{I-M,11}\right)\nu \\ &- \frac{(e_{13})^2 S_p(\kappa_M + \mu_M)(\kappa_M(\mu_I + \mu_M) + \mu_M(3\mu_I - \mu_M))}{(\kappa_I + \mu_M)^2(\kappa_M(\mu_I + \mu_M) + 2\mu_I\mu_M)}\nu^2.\end{aligned} \tag{4.6.16}$$

Having established the low volume fraction approximations for the DEM method, we will now turn our attention to the low volume fraction approximations for the coefficients derived under the MoM approach by [53].

4.7 Low Volume fraction approximations for Method of Mixtures approach

Taylor expanding (3.4.1)-(3.4.4) around $\nu = 0$ yields

$$\kappa_{\text{eff}} = \kappa_M + \frac{\kappa_M(\kappa_I - \kappa_M)}{\kappa_I}\nu + \frac{\kappa_M(\kappa_I - \kappa_M)^2}{(\kappa_I)^2}\nu^2, \tag{4.7.1}$$

$$e_{\text{eff},13} = \frac{e_{13}\kappa_M}{\kappa_I}\nu + \frac{e_{13}\kappa_M(\kappa_I - \kappa_M)}{(\kappa_I)^2}\nu^2, \tag{4.7.2}$$

$$e_{\text{eff},33} = \nu\left(e_{33} - \frac{e_{13}(\lambda_I - \lambda_M)}{\kappa_I}\right) + \frac{e_{13}\kappa_M(\lambda_I - \lambda_M)}{(\kappa_I)^2}\nu^2, \tag{4.7.3}$$

$$\epsilon^S_{\text{eff},33} = \epsilon^S_{M,11} + \frac{(e_{13})^2 S_p}{\kappa_I}\nu - \frac{(e_{13})^2 \kappa_M S_p}{(\kappa_I)^2}\nu^2. \tag{4.7.4}$$

4.8 Comparison between approaches

In this subsection, we will compare the low volume fraction polynomials that arise from the methodologies derived by the DEM method (from (4.6.11)-(4.6.12), (4.6.14)-(4.6.16)) and the MoM approach (from (4.7.1)-(4.7.4)) against the low volume fraction polynomials derived by the AHM (from (4.4.16)-(4.4.21), (4.4.23)-(4.4.25) and (4.4.26)-(4.4.27)).

We will use Stycast as the polymer material and PTZA5 as the inclusion material. The material properties in both phases is set out in Table 2.1. We start by comparing the three methodologies for the effective bulk modulus κ_{eff}.

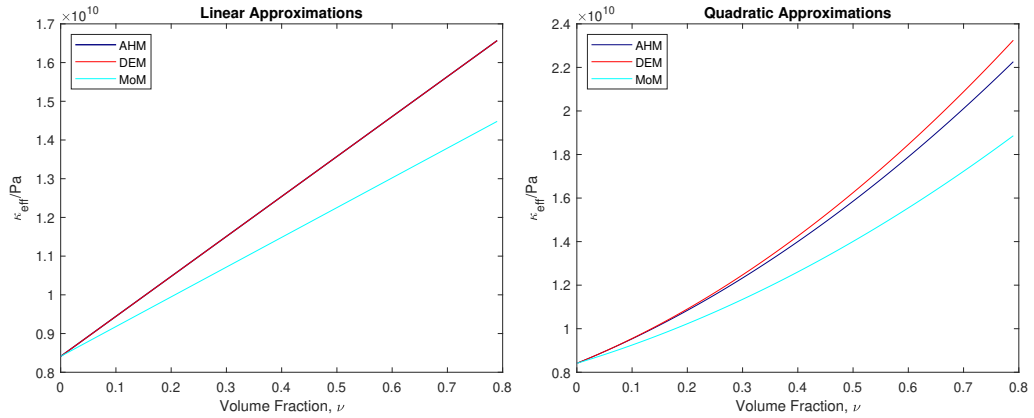


Figure 4.9: Comparison between the low volume fraction polynomials for effective bulk modulus κ_{eff} found using the AHM, the DEM and the MoM approaches. The results were computed using (4.4.16), (4.4.17) together with (3.2.1), equation (4.6.11), and equation (4.7.1) respectively. In the left pane, the AHM curve lies underneath the DEM curve.

From Figure 4.9, we see that the linear approximation for the DEM approach agrees with the linear approximation for the AHM, but the quadratic approximations disagree, as shown on the graph in Figure 4.9 on the right. On both graphs in Figure 4.9, we see that the MoM approach only agrees with the AHM up to $O(1)$, since the $O(\nu)$ terms disagree. Note that when $0 < \frac{\mu_M}{\kappa_M}, \frac{\mu_M}{\kappa_I} \ll 1$, matrix shear effects vanish and the $O(\nu)$ term predicted by both the AHM and the DEM approaches (namely, $\frac{(\kappa_I-\kappa_M)(\kappa_M+\mu_M)}{\kappa_I+\mu_M}$) tends towards the $O(\nu)$ term predicted by the MoM approach (namely, $\frac{\kappa_M(\kappa_I-\kappa_M)}{\kappa_I}$). This shows that when matrix shear effects are negligible, the predictions of κ_{eff} by the AHM and the DEM methods match the predictions of κ_{eff} under the MoM approach.

We now compare the three methodologies for the effective shear modulus μ_{eff}.

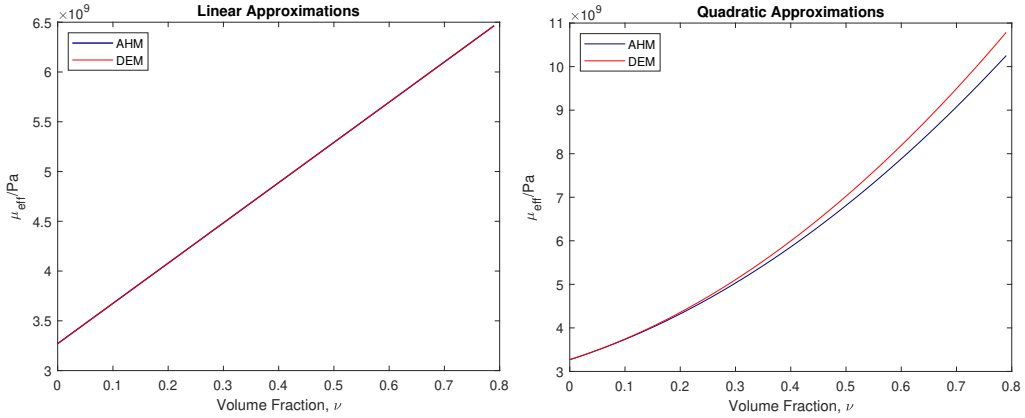


Figure 4.10: Comparison between the low volume fraction polynomials for effective shear modulus μ_{eff} found using the AHM and DEM method. Note that the MoM [53] approach does not contain a formula for μ_{eff}. The results were computed using (4.4.16), (4.4.17) together with (3.2.2), and equation (4.6.12), respectively. In the left pane, the AHM curve lies underneath the DEM curve.

From Figure 4.10, we see that once again the linear approximation for the DEM approach agrees with the linear approximation for the AHM, but the quadratic approximations disagree.

We now compare the three methodologies for the effective electromechanical coefficient $-e_{\text{eff},13}$.

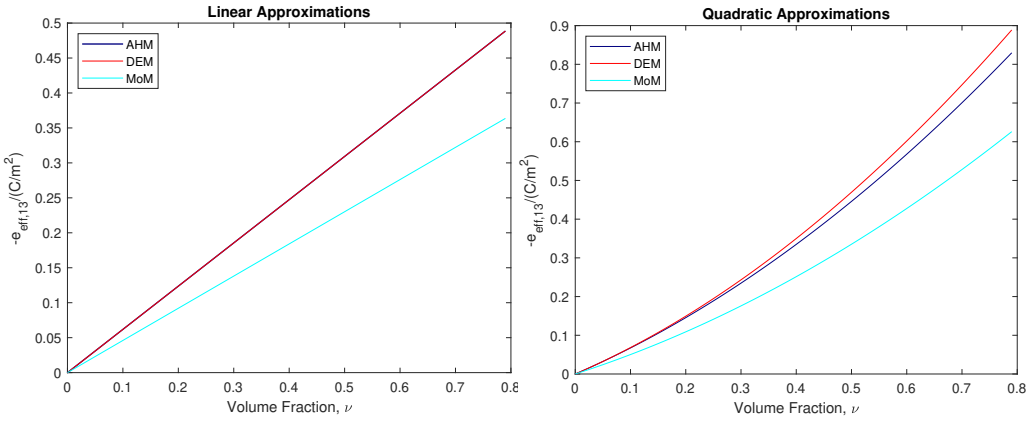


Figure 4.11: Comparison between low volume fraction polynomials for the effective electromechanical stress coefficient $-e_{\text{eff},13}$ found using the AHM, the DEM and the MoM approaches. The results were computed using (4.4.23), (4.6.14), and (4.7.2), respectively. In the left pane, the AHM curve lies underneath the DEM curve.

As shown in Figure 4.11, once again the linear approximation for the DEM approach agrees with the linear approximation for the AHM, but the quadratic approximations disagree. As before the MoM formulae only agree with the AHM approximation to leading-order. Once again, when $0 < \frac{\mu_M}{\kappa_M}, \frac{\mu_M}{\kappa_I} \ll 1$, matrix shear effects vanish and the $O(\nu)$ term predicted by both the AHM and the DEM methods (namely, $e_{13}\frac{\kappa_M+\mu_M}{\kappa_I+\mu_M}$) tends towards the $O(\nu)$ term predicted by the MoM approach (namely, $\frac{e_{13}\kappa_M}{\kappa_I}$). This shows that when matrix shear effects are negligible, the predictions of $e_{\text{eff},13}$ by the AHM and the DEM methods match the corresponding predictions of $e_{\text{eff},13}$ under the MoM approach.

We now compare the three methodologies for the effective thickness-mode electromechanical coefficient $e_{\text{eff},33}$.

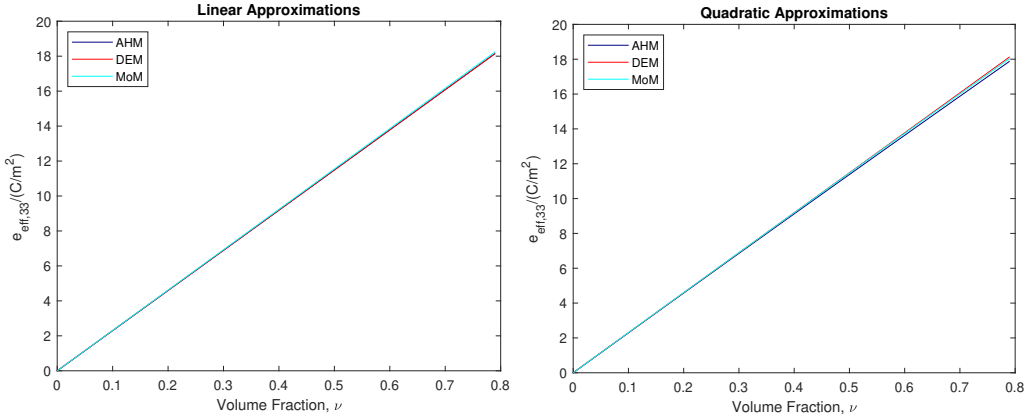


Figure 4.12: Comparison between low volume fraction polynomials for the effective thickness-mode electromechanical coefficient $e_{\text{eff},33}$ found using the AHM, the DEM and the MoM approaches. The results were computed using (4.4.24), (4.6.15), and (4.7.3), respectively. In the left pane, the AHM curve lies underneath the DEM curve.

From (4.4.24) and (4.6.15), we see that the $O(1)$ and $O(\nu)$ coefficients all agree, whereas the $O(\nu^2)$ coefficients do not. From (4.4.24) and (4.7.3), we see that the MoM coefficients only agree to $O(1)$ in general, but agree up to $O(\nu^2)$ in the limit of negligible shear effects. As shown in both graphs in Figure 4.12, the difference between the coefficients for the three methodologies is minimal for this choice of matrix and inclusion parameters.

We now compare the three methodologies for the effective thickness-mode dielectric coefficient $\epsilon^S_{\text{eff},33}$.

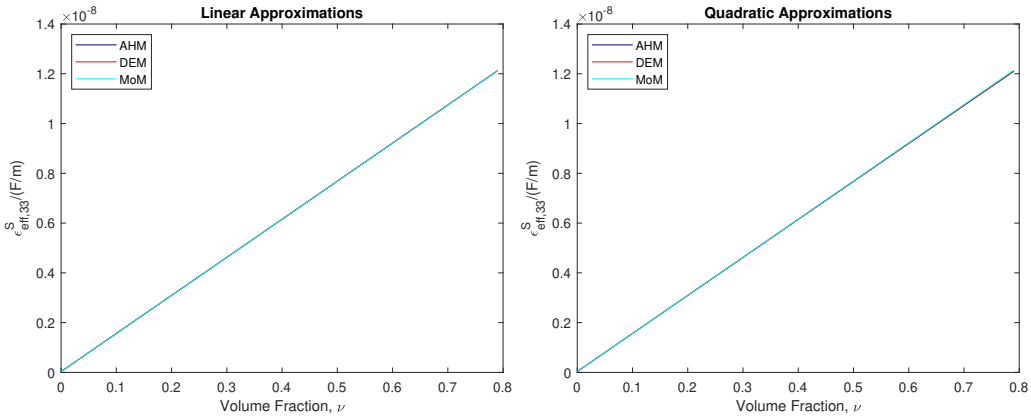


Figure 4.13: Comparison between low volume fraction polynomials for the thickness-mode dielectric coefficient $\epsilon^S_{\text{eff},33}$ found using the AHM, the DEM and the MoM approaches. The results were computed using (4.4.27), (4.6.16) and (4.7.4), respectively.

From (4.4.27) and (4.6.16), we see that the $O(1)$ and $O(\nu)$ coefficients all agree, whereas the $O(\nu^2)$ coefficients do not. From (4.4.27) and (4.7.4), we see that the

MoM coefficients only agree to $O(1)$ in general, but agree up to $O(\nu^2)$ in the limit of negligible shear effects. As shown in both graphs in Figure 4.13, the difference between the coefficients for the three methodologies is minimal for this choice of matrix and inclusion parameters.

4.9 Conclusions

Using the example of a 1-3 composite with cylindrical pillars, we have shown that the approximated coefficients calculated in the low volume fraction limit have good agreement with the results obtained under the AHM, with perfect agreement in relation to the dielectric coefficient in the thickness direction.

We calculated the low volume fraction polynomials under the DEM and the MoM approaches and compared these to the polynomials obtained under the AHM. We noted that the polynomials derived under the DEM method agree to $\mathcal{O}(\nu)$ for all the effective coefficients. In relation to the MoM approach, we showed that the low volume fraction polynomials agreed to $\mathcal{O}(1)$ in general. However, we discovered that in the limit of negligible shear effects, the low volume fraction polynomial coefficients under the AHM converged to those predicted under the MoM approach.

Overall, the DEM method appears to provide more accurate predictions than the MoM approach. However, in the thickness direction, our results show that the MoM and DEM approaches have very close agreement with the AHM results, while the MoM approach uses a simpler formulation than the DEM method. For real-world composites with volume fractions up to approximately 20-30%, the low volume fraction method is more computationally efficient than using AHM, thus making it particularly useful for sensor design.

Chapter 5

Modelling of Bulk Piezoelectric Sensors

5.1 Introduction

Sensors generate an electrical charge when mechanically stressed, due to the direct piezoelectric effect, providing a fast and highly sensitive response. They can be either passive or active. Passive sensors simply react to changes in surrounding temperature, pressure, strain, or stress. On the other hand, active sensors send out and receive signals to determine distance, position, or other properties of a target or surrounding medium.

It is worth noting that, in practice, many piezoelectric devices use the same piezoelectric material to perform both sensor and actuator functions. Piezoelectric sensors are used extensively in modern technology. They play an important role in applications involving dynamic loading, vibration, and acoustic wave propagation. They are widely used in systems such as sonar or ultrasound imaging, as well as vibration-based modelling and non-destructive inspection of structures including bridges, pipelines and offshore installations. Their high sensitivity and fast response are especially advantageous.

Piezoelectric sensors can detect acoustic signals propagating through the water and enable systems to locate, classify, and track objects such as submarines, map the contours of the ocean or river bed or other structures. Sonar sensors are highly sensitive and can detect sound over very large distances at low frequencies where attenuation in water is relatively weak, with ranges in some cases reaching 80 miles, depending on environmental conditions. They operate best when they are able to detect a wide range of frequencies, as this enables them to combine long-range, low-frequency detection with high-resolution and high-frequency imaging, so that they are able to determine exactly where the sound is coming from and track it.

In most cases, sensors operate in liquid or air. For this reason, we need to extend the two-scale model we developed in Chapter 2 to account for wave effects from incoming pressure waves across the relevant media and to understand how these interactions affect energy transfer.

For the purposes of modelling, there are two types of sensors: bulk sensors and thin-layer (or laminated) sensors (i.e., sensors where the thickness of the device is much smaller than its length or breadth). We will focus in this chapter on Bulk Sensors.

Building on the asymptotic homogenisation method developed in Chapter 2, we will extend the framework to model wave propagation in bulk piezoelectric sensors, allowing interactions with surrounding fluid domains to be captured.

Bulk sensors are compact, block-like, and mechanically robust, enabling them to operate in harsh environments. They are made mostly or entirely of piezoelectric composite material, which can act as both an actuator and a sensor simultaneously. They operate by generating an electrical charge when subjected to a mechanical stress, allowing them to measure pressure, force, or vibration through the voltage produced by electrodes within the device. Bulk sensors typically have high stiffness elements. Common examples of bulk sensors include pressure sensors, accelerometers, impact sensors, sonar sensors or hydrophones.

In addition to working out the effective stiffness, electromechanical coupling, and dielectric coefficients, we will need to use our model to calculate a number of other properties, including the electrical admittance per unit area, wave speed, and mechanical impedance.

5.1.1 Methods for modelling Bulk Sensors

The most widely used method for modelling bulk sensors in the material science and engineering literature is Finite Element Analysis. This method has limitations for the purposes of the design of materials, where, to optimise performance, it is necessary to have physical insights at the microscopic level.

To develop our Wave Asymptotic Homogenisation Model (WAHM), our starting point is Smith & Auld's analytic approach [53]. They study the behaviour of a 1-3 piezoelectric composite by considering the dynamics through the thickness mode (or Z- direction), and identify key properties needed for a good sensor. These help to develop intuition for the propagation of pressure waves in the transverse direction. However, this approach has two key limitations. As previously noted, the method relies on the Method of Mixtures approach, which is a physical, rather than a systematic mathematical approach. The method is also limited to 1-3 composites. Whilst

much research has been done on modelling sensors over the years, the majority of methods considered are numerical or semi-analytical rather than purely analytical and consist of micromechanical [57] and Eshelby-type models [19, 20, 48], rather than multiscale, models.

5.2 Modelling of Piezoelectric Sensors

We will first establish two idealised physical models, namely the half-space transducer and the finite-thickness transducer. These are considered because they provide very clear insights into how geometry, boundary conditions, and coupling mechanisms affect performance. These simplified cases provide a framework for analysing more complex configurations found in practice. Next, we will analyse how the effective properties of the sensor vary with volume fraction of the inclusion across five different geometries. We will then use the framework established in Chapter 2 to find solutions to the equations of motion in the solid region.

Most sensor problems involve a sound wave travelling through a fluid and then passing through a solid, as shown in Figure 5.1. In such cases, part of the incoming wave is reflected at the fluid-solid boundary and the rest passes through as a transmitted wave. To describe this situation, we first derive the linearised acoustic equations, which describe how waves travel in a fluid. Then we derive continuity conditions between the fluid and the piezoelectric solid. We will consider the situation where a pressure wave approaches the solid boundary. The model will enable us to predict and optimise the electrical output that arises from the incoming pressure wave. By convention, we will assume that the direction or poling is in the thickness (or Z-) direction.

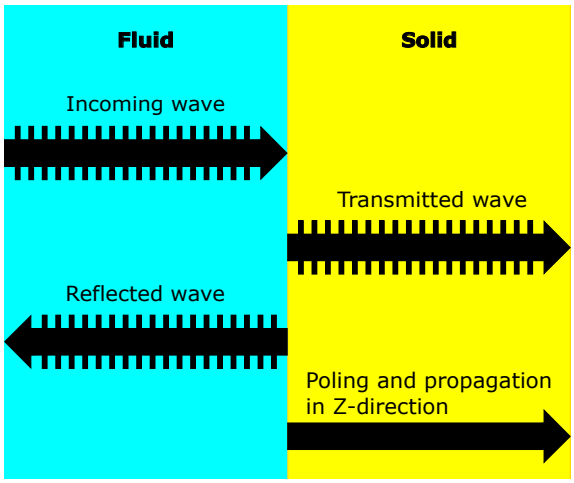


Figure 5.1: Schematic of typical sensor set-up.

5.2.1 Derivation of Linearised Equations of Acoustics

In a fluid there are three main quantities of interest, namely the fluid pressure P_f, the fluid density ρ_f and the fluid velocity $\boldsymbol{v}_f$. We assume the equilibrium pressure and density are given by P_0 and ρ_0, which are both constants. In an adiabatic process [49], the pressure P_f is assumed to be a function of the density ρ_f. When $|\rho_f - \rho_0| \ll 1$, the density can be linearised as

$$\rho_f = \frac{p_f}{A} + \rho_0, \tag{5.2.1}$$

where

$$p_f = P_f - P_0, \tag{5.2.2}$$

$$A = \left.\frac{\partial P_f}{\partial \rho}\right|_{\rho=\rho_0} > 0. \tag{5.2.3}$$

The continuity equation, which describes conservation of mass (see [55]), is given by

$$\frac{\partial \rho_f}{\partial t} + \nabla \cdot (\rho_f \boldsymbol{v}_f) = 0. \tag{5.2.4}$$

In the linear approximation, we assume that both $\rho_f - \rho_0$ and $\boldsymbol{v}_f$, together with their partial derivatives, are assumed to be small. Substituting (5.2.1) into (5.2.4) and neglecting non-linear terms, (5.2.4) reduces to

$$\frac{1}{A}\frac{\partial p_f}{\partial t} + \rho_0 \nabla \cdot \boldsymbol{v}_f = 0. \tag{5.2.5}$$

The final ingredient is Euler's equation, which describes conservation of momentum for an inviscid fluid (see [42]), given by

$$\rho_f \left(\frac{\partial \boldsymbol{v}_f}{\partial t} + (\boldsymbol{v}_f \cdot \nabla)\, \boldsymbol{v}_f \right) = -\nabla P_f. \tag{5.2.6}$$

Linearising (5.2.6) gives

$$\rho_0 \frac{\partial \boldsymbol{v}_f}{\partial t} + \nabla p_f = \boldsymbol{0}. \tag{5.2.7}$$

Combining (5.2.5) and (5.2.7) yields two equations, namely

$$\frac{1}{{c_f}^2}\frac{\partial^2 p_f}{\partial t^2} - \nabla^2 p_f = 0, \tag{5.2.8}$$

$$\frac{1}{{c_f}^2}\frac{\partial^2 \boldsymbol{v}_f}{\partial t^2} - \nabla\left(\nabla \cdot \boldsymbol{v}_f\right) = \boldsymbol{0}, \tag{5.2.9}$$

where c_f is the speed of the sound waves in the fluid, given by

$$c_f = \sqrt{A}. \tag{5.2.10}$$

Here f denotes the fluid phase and is not a summation index. Having derived the linearised equations of acoustics, we will establish equations of motion in the solid.

5.2.2 Equations of motion in the solid

Since the sensor is made from a piezoelectric composite material, the equations of motion are given by (2.4.19)-(2.4.24). After applying the homogenisation process established in Chapter 2 and re-dimensionalising, we get the following leading-order relationships

$$\rho_{\text{eff}} \frac{\partial^2 u_{s,j}}{\partial t^2} = \frac{\partial}{\partial x_i}\left(c^{kl}_{\text{eff},ij} \frac{\partial u_{s,k}}{\partial x^l} + e^{k}_{\text{eff},ij} \frac{\partial \varphi_s}{\partial x^k} \right), \tag{5.2.11}$$

$$0 = \frac{\partial}{\partial x_i}\left(e^{kl}_{\text{eff},i} \frac{\partial u_{s,k}}{\partial x^l} - \epsilon^{Sk}_{\text{eff},i} \frac{\partial \varphi_s}{\partial x^k} \right), \tag{5.2.12}$$

where s denotes the solid phase and is not a summation index. Now we have the equations of motion in each region, we proceed to establish the boundary conditions that hold at the interface between the fluid and solid. This will show how a pressure wave in the fluid will travel into the solid.

5.3 Continuity and jump conditions

In the fluid, the stress tensor[1] is given by

$$\sigma_{f,ij} = -p_f \delta_{ij}. \tag{5.3.1}$$

At the liquid-solid interface, with unit normal $\boldsymbol{n}$ pointing out of the fluid, we require that the normal stress $\boldsymbol{\sigma}_f \cdot \boldsymbol{n}$ is continuous, that is

$$n^i \sigma_{f,ij} = -p_f n_j = n^i \sigma_{s,ij} = n^i \left(c^{kl}_{\text{eff},ij} \frac{\partial u_{s,k}}{\partial x^l} + e^{k}_{\text{eff},ij} \frac{\partial \varphi_s}{\partial x^k} \right). \tag{5.3.2}$$

We also require the normal component of the velocity to be continuous, so that

$$\boldsymbol{n} \cdot \boldsymbol{v}_f = \boldsymbol{n} \cdot \frac{\partial \boldsymbol{u}_s}{\partial t} \iff n^i v_{f,i} = n^i \frac{\partial u_{s,i}}{\partial t}, \tag{5.3.3}$$

where $\boldsymbol{u}_s$ is the displacement in the solid.

[1] See [6].

Assuming no free surface charge at the interface, the normal component of the dielectric displacement vector $\boldsymbol{\mathcal{D}}\cdot\boldsymbol{n}$ is continuous across the boundary. The dielectric displacement vector $\boldsymbol{\mathcal{D}}_f$ in the fluid is given by

$$\boldsymbol{\mathcal{D}}_f = -\epsilon_f^S \nabla\varphi_f \iff \mathcal{D}_{f,i} = -\epsilon_f^S \frac{\partial\varphi_f}{\partial x^i}, \tag{5.3.4}$$

where ϵ_f^S is the dielectric permittivity of the water.

Gauss' Law [36] tells us that

$$\nabla\cdot\boldsymbol{\mathcal{D}}_f = \frac{\partial\mathcal{D}_{f,i}}{\partial x_i} = \frac{\partial}{\partial x_i}\left(-\epsilon_f^S\frac{\partial\varphi_f}{\partial x^i}\right) = 0, \tag{5.3.5}$$

in the fluid, while continuity of the normal component of $\boldsymbol{\mathcal{D}}$ at the liquid-solid interface implies

$$n^i\mathcal{D}_{f,i} = -n^i\epsilon_f^S\frac{\partial\varphi_f}{\partial x^i} = n^i\mathcal{D}_{s,i} = n^i\left(e^{kl}_{\text{eff},i}\frac{\partial u_{s,k}}{\partial x^l} - \epsilon^{Sk}_{\text{eff},i}\frac{\partial\varphi_s}{\partial x^k}\right). \tag{5.3.6}$$

Finally, due to Faraday's Law (see [36]), we require the tangential components of the electric field to be continuous, that is

$$\boldsymbol{t}\cdot\boldsymbol{E}_f = \boldsymbol{t}\cdot\boldsymbol{E}_s \iff t^k\frac{\partial\varphi_f}{\partial x^k} = t^k\frac{\partial\varphi_s}{\partial x^k}, \tag{5.3.7}$$

where $\boldsymbol{t}$ is an arbitrary vector tangent to the surface. Using (2.3.5), equation (5.3.7) implies that

$$\varphi_f = \varphi_s, \tag{5.3.8}$$

on the surface between the boundary of the fluid and the solid.

5.4 Solving physical problems

Having established the continuity and jump conditions, we will solve two sets of physical problems. We note that we will be solving for voltage output, to describe how an incoming pressure wave causes an electrical signal. We will first look at the idealised problem of a half-space transducer, a problem where the only interference is when the wave enters the solid, as shown in Figure 5.2.

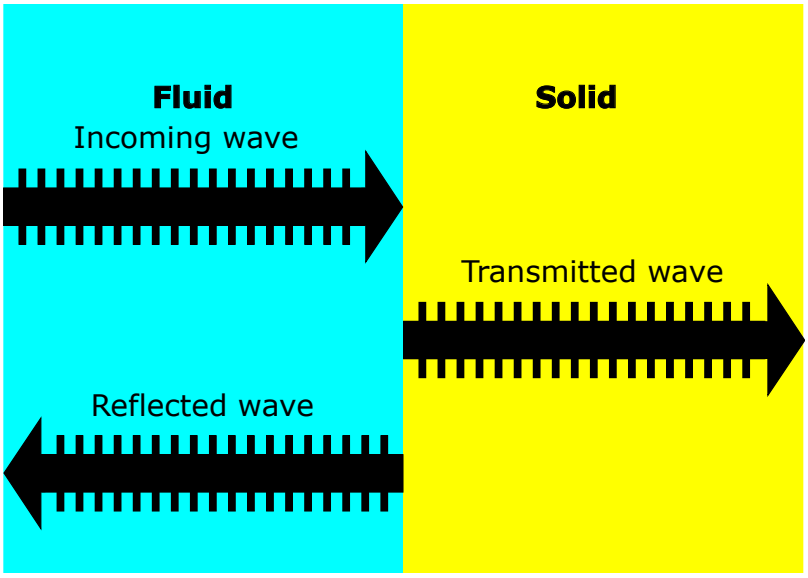


Figure 5.2: Schematic showing an half-space transducer. As the wave passes the boundary, it moves forward without reflection, at constant speed.

The second problem involves a pressure wave moving towards a finite-thickness transducer and then coming out the other side and hence into the fluid once again, as shown in Figure 5.3.

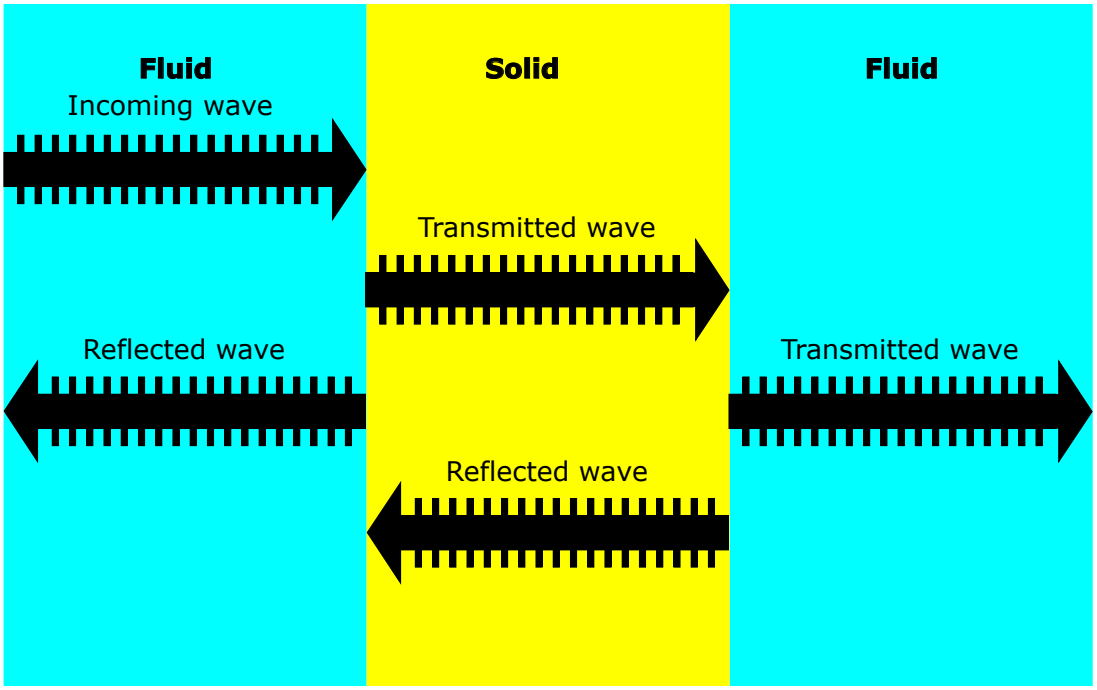


Figure 5.3: Schematic showing a finite-thickness transducer. As the wave passes the boundary at a constant speed, it partially transmits forward and partially moves backwards.

We assume that the motion is uni-directional, with variations only in the z-

direction, hence we write

$$\boldsymbol{v}_f = (0, 0, v_f(t, z)), \tag{5.4.1}$$

$$\boldsymbol{u}_s = (0, 0, u_s(t, z)), \tag{5.4.2}$$

$$\varphi_f = \varphi_f(t, z), \tag{5.4.3}$$

$$\varphi_s = \varphi_s(t, z). \tag{5.4.4}$$

5.4.1 Half-space transducer

In this scenario, we will assume that the fluid region occupies the space where $z < 0$ and the solid region (i.e., the region occupied by the sensor) is the region where $z > 0$. Thus, for $z < 0$,

$$\frac{1}{{c_f}^2}\frac{\partial^2 p_f}{\partial t^2} - \frac{\partial^2 p_f}{\partial z^2} = 0, \tag{5.4.5}$$

$$\rho_f \frac{\partial v_f}{\partial t} + \frac{\partial p_f}{\partial z} = 0, \tag{5.4.6}$$

$$\frac{\partial^2 \varphi_f}{\partial z^2} = 0, \tag{5.4.7}$$

while for $z > 0$,

$$\rho_{\text{eff}} \frac{\partial^2 u_s}{\partial t^2} = \frac{\partial}{\partial z}\left(c^{33}_{\text{eff},33}\frac{\partial u_s}{\partial z} + e^{3}_{\text{eff},33}\frac{\partial \varphi_s}{\partial z}\right), \tag{5.4.8}$$

$$0 = \frac{\partial}{\partial z}\left(e^{33}_{\text{eff},3}\frac{\partial u_s}{\partial z} - \epsilon^{S}_{\text{eff},33}\frac{\partial \varphi_s}{\partial z}\right). \tag{5.4.9}$$

Using (5.3.2), (5.3.3), (5.3.6) and (5.3.8), which all hold when $z = 0$, become

$$-p_f(t, 0) = c^{33}_{\text{eff},33}\frac{\partial u_s}{\partial z}(t, 0) + e^{3}_{\text{eff},33}\frac{\partial \varphi_s}{\partial z}(t, 0), \tag{5.4.10}$$

$$v_f(t, 0) = \frac{\partial u_s}{\partial t}(t, 0), \tag{5.4.11}$$

$$-\epsilon^{S}_{f}\frac{\partial \varphi_f}{\partial z}(t, 0) = e^{33}_{\text{eff},3}\frac{\partial u_s}{\partial z}(t, 0) - \epsilon^{S}_{\text{eff},33}\frac{\partial \varphi_s}{\partial z}(t, 0), \tag{5.4.12}$$

$$\varphi_s(t, 0) = \varphi_f(t, 0). \tag{5.4.13}$$

5.4.1.1 Wave-like solutions

Having established the model in (5.4.5)-(5.4.13) for a half-space transducer, since the system is linear, we work with complex exponents, where it is implied that we take the real part of the solution. We assume the pressure is given by

$$p_f(t, z) = P_0\left(\exp\left(\mathrm{i}\omega\left(\frac{z}{c_f} - t\right)\right) + R\exp\left(\mathrm{i}\omega\left(-\frac{z}{c_f} - t\right)\right)\right), \tag{5.4.14}$$

where ω and $P_0 \neq 0$ are the frequency and amplitude of the oscillation, which are both constants, respectively, and R is the refection coefficient.
The first term in (5.4.14) corresponds to an incoming pressure wave moving with speed c_f towards the boundary of the solid with amplitude P_0, while the second term in (5.4.14) corresponds to a reflected wave moving with speed c_f in the opposite direction, and with amplitude RP_0. Note that (5.4.14) satisfies (5.4.5).

Using (5.4.6), we deduce that

$$v_f(t,z) = \frac{P_0}{Z_f}\left(\exp\left(\mathrm{i}\omega\left(\frac{z}{c_f} - t\right)\right) - R\exp\left(\mathrm{i}\omega\left(-\frac{z}{c_f} - t\right)\right)\right), \tag{5.4.15}$$

where Z_f is the mechanical impedance of the fluid, which is given by

$$Z_f = \rho_f c_f. \tag{5.4.16}$$

We assume the solution to (5.4.7) is bounded at $z = -\infty$. This means that φ_f is only dependent on time, i.e.,

$$\varphi_f = \varphi_f(t), \tag{5.4.17}$$

which without loss of generality, we set to zero, giving

$$\varphi_f(t) = 0. \tag{5.4.18}$$

Using (5.4.9), (5.4.12), and (5.4.18), we deduce that

$$\frac{\partial \varphi_s}{\partial z}(t,z) = \frac{e^{33}_{\mathrm{eff},3}}{\epsilon^S_{\mathrm{eff},33}}\frac{\partial u_s}{\partial z}(t,z). \tag{5.4.19}$$

Substituting (5.4.19) into (5.4.8) gives

$$\rho_{\mathrm{eff}}\frac{\partial^2 u_s}{\partial t^2} = \rho_{\mathrm{eff}} c_s^2 \frac{\partial^2 u_s}{\partial z^2}, \tag{5.4.20}$$

where c_s denotes the speed of sound in the solid material, which is given by

$$c_s = \sqrt{\frac{c^{33}_{\mathrm{eff},33} + \frac{\left(e^{33}_{\mathrm{eff},3}\right)^2}{\epsilon^S_{\mathrm{eff},33}}}{\rho_{\mathrm{eff}}}} = \sqrt{\frac{c^{33}_{\mathrm{eff},33}\epsilon^S_{\mathrm{eff},33} + \left(e^{33}_{\mathrm{eff},3}\right)^2}{\rho_{\mathrm{eff}}\epsilon^S_{\mathrm{eff},33}}}. \tag{5.4.21}$$

The outgoing solution to (5.4.20) with the continuity condition (5.4.11) is given by

$$u_s(t,z) = \frac{P_0\,(1-R)}{-\mathrm{i}\omega Z_f}\exp\left(\mathrm{i}\omega\left(\frac{z}{c_s} - t\right)\right). \tag{5.4.22}$$

Now integrating (5.4.19) with respect to z and applying the continuity condition

(5.4.13) along with (5.4.18) gives

$$\begin{aligned}\varphi_s(t,z) &= \frac{e^{33}_{\text{eff},3}}{\epsilon^S_{\text{eff},33}}\left(u_s(t,z)-u_s(t,0)\right)\\ &= \frac{e^{33}_{\text{eff},3}}{\epsilon^S_{\text{eff},33}}\frac{P_0\left(1-R\right)}{-\mathrm{i}\omega Z_f}\left(\exp\left(\mathrm{i}\omega\frac{z}{c_s}\right)-1\right)\exp\left(-\mathrm{i}\omega t\right).\end{aligned} \tag{5.4.23}$$

We define the impedance of the solid material as

$$Z_s = \rho_{\text{eff}} c_s. \tag{5.4.24}$$

Applying (5.4.14), (5.4.22) and (5.4.23) to the continuity condition (5.4.10), we deduce

$$-Z_f\left(1+R\right)\exp(-\mathrm{i}\omega t) = -Z_s\left(1-R\right)\exp\left(-\mathrm{i}\omega t\right), \tag{5.4.25}$$

which we solve to find that

$$R = \frac{Z_s - Z_f}{Z_s + Z_f}. \tag{5.4.26}$$

Substituting (5.4.26) into (5.4.23) and rearranging gives

$$\varphi_s(t,z) = \frac{V_0 P_0}{-\mathrm{i}\omega}\left(\exp\left(\mathrm{i}\omega\frac{z}{c_s}\right)-1\right)\exp\left(-\mathrm{i}\omega t\right), \tag{5.4.27}$$

for $z > 0$, where V_0 is the voltage output coefficient, introduced to collect constant factors, and defined as

$$V_0 = \frac{e^{33}_{\text{eff},3}}{\epsilon^S_{\text{eff},33}}\frac{\left(1-R\right)}{Z_f} = \frac{e^{33}_{\text{eff},3}}{\epsilon^S_{\text{eff},33}}\frac{2}{Z_f+Z_s}. \tag{5.4.28}$$

Normally in wave problems we aim to minimise $|R|$ so that the transfer of mechanical energy occurs with minimal reflection. However, in this problem, we are aiming to maximise the amplitude of the electrical response instead, which occurs when V_0 is maximised, *i.e.* when $R = -1$.

5.4.2 Finite-thickness transducer

In this scenario, we will assume that the solid is in the region $(0, L)$ and that the fluid is in the regions $(-\infty, 0)$ and (L, ∞).

5.4.2.1 Solutions

As before, we assume that the pressure in $z < 0$, is given by

$$p_f(t,z) = P_0\left(\exp\left(\mathrm{i}\omega\left(\frac{z}{c_f} - t\right)\right) + R\exp\left(\mathrm{i}\omega\left(-\frac{z}{c_f} - t\right)\right)\right). \tag{5.4.29}$$

Then, using (5.4.15) and (5.4.18), we see that

$$v_f(t,z) = \frac{P_0}{Z_f}\left(\exp\left(\mathrm{i}\omega\left(\frac{z}{c_f} - t\right)\right) - R\exp\left(\mathrm{i}\omega\left(-\frac{z}{c_f} - t\right)\right)\right), \tag{5.4.30}$$

$$\varphi_f(t,z) = 0. \tag{5.4.31}$$

In the solid we assume

$$u_s(t,z) = \frac{1}{-\mathrm{i}\omega}\left(\gamma_1\exp\left(\mathrm{i}\omega\left(\frac{z}{c_s} - t\right)\right) + \gamma_2\exp\left(\mathrm{i}\omega\left(-\frac{z}{c_s} - t\right)\right)\right), \tag{5.4.32}$$

where γ_1 and γ_2 are unknown complex constants. Using (5.4.32) along with (5.4.19), we deduce that

$$\varphi_s(t,z) = \left(\frac{e^{33}_{\mathrm{eff},3}}{\epsilon^S_{\mathrm{eff},33}}\right)\left(\frac{1}{-\mathrm{i}\omega}\right)\left(\gamma_1\left(\exp\left(\mathrm{i}\omega\frac{z}{c_s}\right) - 1\right) + \gamma_2\left(\exp\left(-\mathrm{i}\omega\frac{z}{c_s}\right) - 1\right)\right) \exp\left(-\mathrm{i}\omega t\right). \tag{5.4.33}$$

Using (5.4.32) and (5.4.33) and then imposing continuity of normal stress at $z = L$, we deduce that the outgoing wave in $z > L$, is given by

$$p_f(t,z) = Z_s\left(\gamma_1\exp\left(\mathrm{i}\omega\frac{L}{c_s}\right) - \gamma_2\exp\left(-\mathrm{i}\omega\frac{L}{c_s}\right)\right)\exp\left(\mathrm{i}\omega\left(\frac{z-L}{c_f} - t\right)\right). \tag{5.4.34}$$

Using (5.4.34), along with (5.4.6), we get

$$v_f(t,z) = \frac{Z_s}{Z_f}\left(\gamma_1\exp\left(\mathrm{i}\omega\frac{L}{c_s}\right) - \gamma_2\exp\left(-\mathrm{i}\omega\frac{L}{c_s}\right)\right)\exp\left(\mathrm{i}\omega\left(\frac{z-L}{c_f} - t\right)\right). \tag{5.4.35}$$

Continuity of the normal component of the velocity at $z = L$ gives

$$\frac{Z_s}{Z_f}\left(\gamma_1\exp\left(\mathrm{i}\omega\frac{L}{c_s}\right) - \gamma_2\exp\left(-\mathrm{i}\omega\frac{L}{c_s}\right)\right) = \left(\gamma_1\exp\left(\mathrm{i}\omega\frac{L}{c_s}\right) + \gamma_2\exp\left(-\mathrm{i}\omega\frac{L}{c_s}\right)\right). \tag{5.4.36}$$

We rearrange (5.4.36) to give

$$\frac{\gamma_2}{\gamma_1} = \frac{Z_s - Z_f}{Z_s + Z_f}\exp\left(\mathrm{i}\omega\frac{2L}{c_s}\right). \tag{5.4.37}$$

Applying continuity of normal stress and velocity at $z = 0$ gives

$$-P_0\left(1+R\right) = Z_s\gamma_1\left(-1+\frac{Z_s-Z_f}{Z_s+Z_f}\exp\left(\mathrm{i}\omega\frac{2L}{c_s}\right)\right), \tag{5.4.38}$$

$$\gamma_1\left(\frac{2Z_s}{Z_s+Z_f}\right) = \frac{P_0}{Z_f}\left(1-R\right), \tag{5.4.39}$$

respectively. After solving the system defined by (5.4.38)-(5.4.39), we see that

$$\gamma_1 = \frac{-2P_0\left(Z_f+Z_s\right)}{\left(Z_f-Z_s\right)^2\exp\left(\frac{2\mathrm{i}L\omega}{c_s}\right)-\left(Z_f+Z_s\right)^2}, \tag{5.4.40}$$

$$\gamma_2 = \frac{2P_0\exp\left(\frac{2\mathrm{i}L\omega}{c_s}\right)\left(Z_f-Z_s\right)}{\left(Z_f-Z_s\right)^2\exp\left(\frac{2\mathrm{i}L\omega}{c_s}\right)-\left(Z_f+Z_s\right)^2}, \tag{5.4.41}$$

$$R = \frac{\left(1-\exp\left(\frac{2\mathrm{i}L\omega}{c_s}\right)\right)\left({Z_f}^2-{Z_s}^2\right)}{\left(Z_f-Z_s\right)^2\exp\left(\frac{2\mathrm{i}L\omega}{c_s}\right)-\left(Z_f+Z_s\right)^2}. \tag{5.4.42}$$

Using (5.4.39), we see that (5.4.33) becomes

$$\varphi_s(t,z) = \left(\frac{e^{33}_{\mathrm{eff},3}}{\epsilon^S_{\mathrm{eff},33}}\right)\left(\frac{-\mathrm{i}}{\omega}\right)\left(\frac{2P_0}{\left(Z_f-Z_s\right)^2\exp\left(\frac{2\mathrm{i}L\omega}{c_s}\right)-\left(Z_f+Z_s\right)^2}\right)$$
$$\left(\left(Z_f+Z_s\right)\left(\exp\left(\frac{\mathrm{i}\omega z}{c_s}\right)-1\right)+\exp\left(\frac{2\mathrm{i}L\omega}{c_s}\right)\left(Z_s-Z_f\right)\left(\exp\left(-\frac{\mathrm{i}\omega z}{c_s}\right)-1\right)\right)$$
$$\exp\left(-\mathrm{i}\omega t\right). \tag{5.4.43}$$

From (5.4.43), we define the voltage out coefficient for a finite-thickness case as[2]

$$V_0 = \left|\frac{e^{33}_{\mathrm{eff},3}}{\epsilon^S_{\mathrm{eff},33}}\right|\left(\frac{2\max\{Z_f,Z_s\}}{\left|\left(Z_f-Z_s\right)^2\exp\left(\frac{2\mathrm{i}L\omega}{c_s}\right)-\left(Z_f+Z_s\right)^2\right|}\right). \tag{5.4.44}$$

Note that the distributional limit of all the solutions derived in this section (as $L\to\infty$) yield the same results as given in §5.4.1.1, confirming that the behaviour of the finite-thickness transducer approaches the behaviour of the half-space transducer in the limit of infinite thickness.

Now that we have solved the equations of motion for both set-ups, we proceed to investigate how the microstructure affects the voltage output for a unit pressure wave.

[2]In (5.4.28), we defined the voltage output coefficient V_0 as being the amplitude multiplied by a factor of ω/P_0. We now define the voltage output coefficient for the finite-thickness transducer analogously.

5.5 Results

We now compare the solutions from our WAHM for half-space transducers and finite-thickness transducers made from five different types of composites, namely three types of 1-3 composites of various lattices and inclusion shapes, a 2-2 composite with plates perpendicular to the X-direction, and a 3-3 composite (also known as a Jungle Gym) with square rods arranged in a 3D grid. These are shown in Figures 5.4-5.7 and 5.9, respectively.

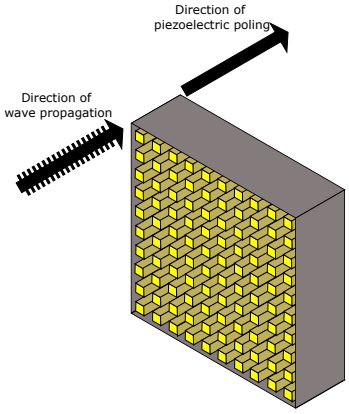


Figure 5.4: Schematic of a 1-3 composite with a square lattice and square rods.

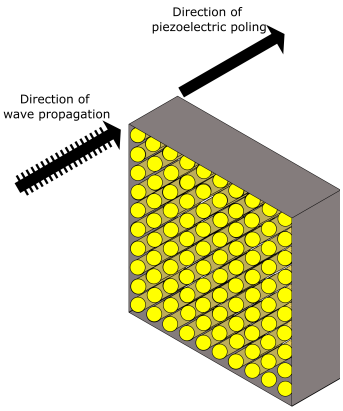


Figure 5.5: Schematic of a 1-3 composite with a square lattice and circular rods.

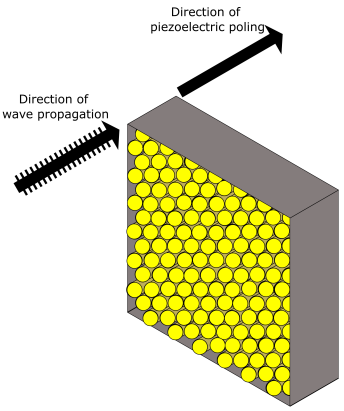


Figure 5.6: Schematic of a 1-3 composite with a hexagonal lattice and cylindrical rods.

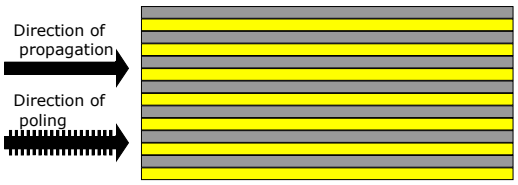


Figure 5.7: Schematic of a 2-2 composite.

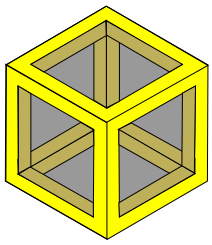


Figure 5.8: Schematic of a unit cell for a 3-3 composite (or Jungle Gym).

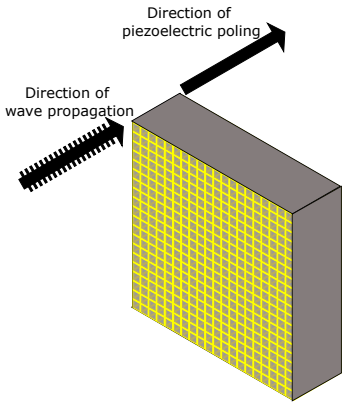


Figure 5.9: Schematic of a 3-3 sensor made up of multiple Jungle Gym cells.

With the exception of the Jungle Gym configuration, all the composites have translational symmetry in the z-direction. We will be plotting three different quantities for each geometry:

- voltage output coefficient (for both the half-space transducer and the finite-thickness transducer),
- the mechanical impedance of the solid,
- the wave speed in the solid.

Note that the mechanical impedance and wave speeds for both the half-space and finite-thickness transducers are the same, so we will only be showing one graph for those quantities instead of two. When plotting the voltage output coefficient for the finite-thickness case, we will choose ω so that $\frac{\omega L}{c_s}$ is an integer multiple of π, so that V_0 is maximised.

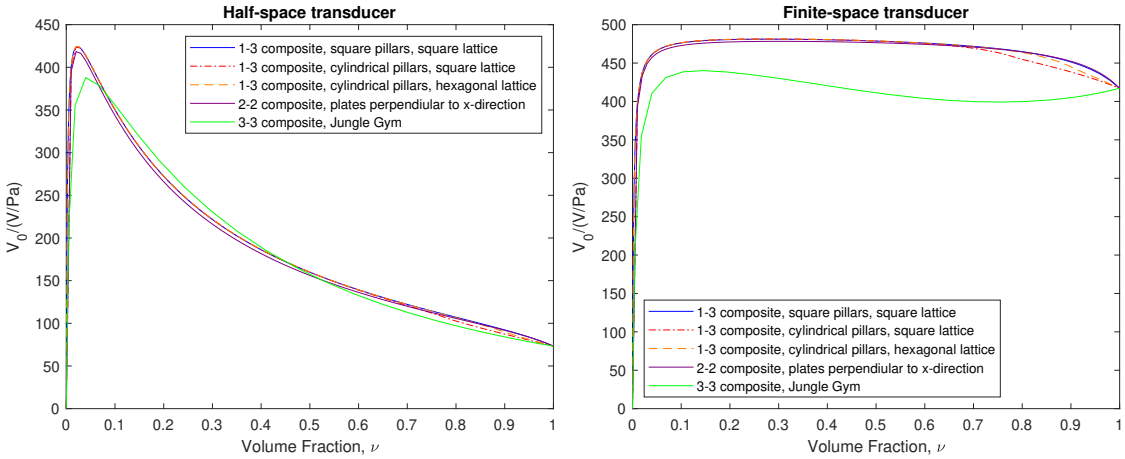


Figure 5.10: Graph comparing how the voltage output coefficient V_0 given by (5.4.28) and (5.4.44) varies with different lattices and inclusion shapes, in respect of the half-space transducer and the finite-thickness transducer.

In Figure 5.10, we see how the voltage output coefficients vary with the volume fraction of PZTA5 for the five different geometries and lattice structures for the half-space and finite-thickness transducers. We see that for the half-space transducer the voltage output coefficients rise sharply at low volume fractions, reach a maximum and then decrease monotonically. We also see that, with the exception of the Jungle Gym geometry, the curves are almost identical. For the Jungle Gym, the voltage output rapidly reaches its peak then gradually falls, but with a lower peak in voltage output compared to the other composites. For the finite-thickness transducer, we once again see that when excluding the Jungle Gym geometry, the curves are almost

identical. In this case, the Jungle Gym gives a lower piezoelectric response for all volume fractions. We also note the voltage output coefficient rises sharply at low volume fractions, as was the case for the half-space transducer, but this time the peak is much broader. This shows that adding spokes in all three directions reduces the overall piezoelectric response. The reason why the first four geometries have a higher electrical response is that in all four geometries, the piezoelectric inclusions are all aligned in the direction of poling. This makes the homogenised effective coefficients scale similarly across geometries. Furthermore, in terms of the homogenised response, piezoelectric material in the cross spokes increases the planar stiffness without contributing to the electromechanical coupling.

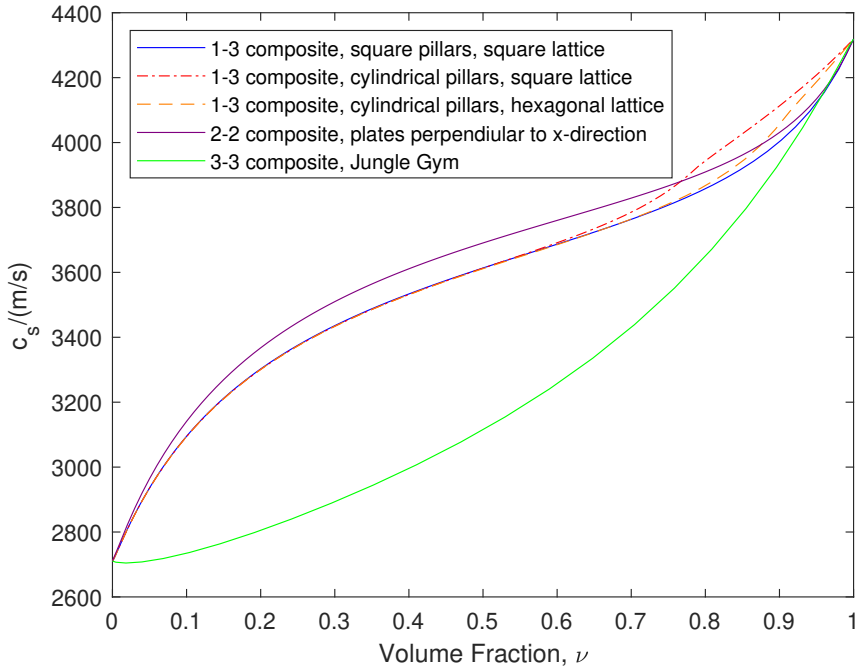


Figure 5.11: Graph comparing how the effective wave speed c_s given by (5.4.21) varies for different lattices and inclusions for a half-space transducer.

From Figure 5.11, we see how the effective wave speed varies with the volume fraction of PZTA5 for the five different geometries and lattice structures. We see that, with the exception of the Jungle Gym geometry, the results from all the geometries have similar shapes but this time with more noticeable deviations. In the Jungle Gym case, we see that the wave speed is much lower than all the other geometries for a given volume fraction. The wave speed being much lower for the Jungle Gym indicates stiffness in the thickness direction is much lower than the stiffnesses for the other geometries. This can once again be explained by the stiff piezoelectric material being wasted in the cross spokes.

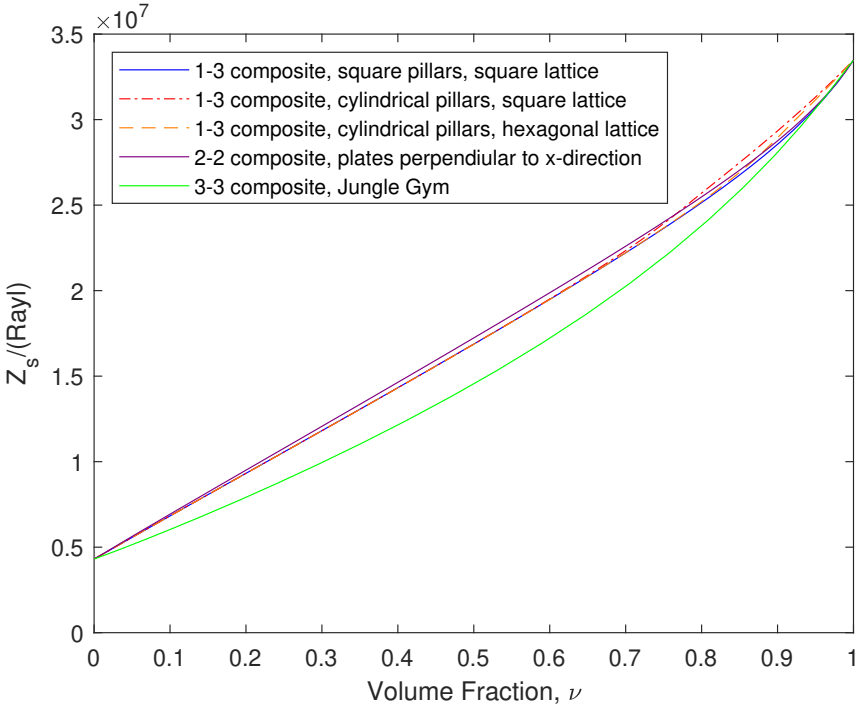


Figure 5.12: Graph comparing how the effective mechanical impedance Z_s given by using (5.4.21) and (5.4.24) varies for different lattices and inclusions for a half-space transducer.

In Figure 5.12, we see how the effective mechanical impedance varies with the volume fraction of PZTA5 for the five different geometries and lattice structures. We see that with the exception of the Jungle Gym geometry, the results for all the geometries have the same shape. In this case, we see that the mechanical impedance curve for the Jungle Gym geometry is lower than all the other curves. This is expected as the curve for the wave speed for the Jungle Gym composite was lower than all the other geometries.

5.6 Conclusions

We have shown how different composite configurations influence three key sensor performance parameters, namely the voltage output coefficent, effective mechanical impedance and wave propagation speed. Unlike other analytical or numerical methods, our asymptotic homogenisation approach is valid regardless of any inclusion shape, size, orientation or lattice structure of the composite.

The results in Figures 5.10-5.12 for the four geometries other than the Jungle Gym, the resulting voltage output coefficient, mechanical impedance and wave speed remain almost identical. This result is expected since as we showed in Chapter 3, the lattice structure and inclusion shape have minimal effect on the thickness coefficients

of the effective stiffness, electromechanical and permittivity tensors. This result is consistent with the observations of Smith & Auld [53], who showed that under a series of assumptions (including negligible in plane variation and equal lateral strains in both phases), the effective coefficients depend only on the material parameters in both phases and the inclusion volume fraction, thus showing that for a 1-3 composite, the geometry has little influence on the wave properties when these assumptions hold, which is consistent with the present results in the graphs shown above.

Our case studies further demonstrate that our asymptotic homogenisation approach is valid regardless of inclusion shape, size, orientation or lattice structure of the composite, in contrast to most analytical and numerical models.

Chapter 6

Modelling of Piezoelectric Beam Actuators

6.1 Introduction

Actuators are one of the most significant types of piezoelectric devices. They convert electrical energy into mechanical motion through the inverse piezoelectric effect. They come in two types, bulk and beam. A bulk actuator is compact, deforming when a (high) electric voltage is applied by stretching or shortening itself along the main axis. In contrast, a beam actuator is made up of flexible, slender beam-shaped piezoelectric material which deforms mainly by bending, as illustrated in Figure 6.1. Typically, beam actuators are made of thin-layers or patches of piezoelectric material bonded onto another structure, such as a metal or composite beam, so that the patch makes the beam move when voltage is applied.

Both types of actuators respond directly to voltage without the need for gears or bearings. This means they respond exceptionally fast (up to nanoseconds), as the motion comes from the change to alignment of the crystal lattice of the piezoelectric inclusion. For this reason, they are widely used in engineering, industry and defence: from sonar systems (in which they can vibrate thousands or even millions of times per second) to devices which suppress excessive vibration (e.g. on bridges) or control shape (e.g. on the wings of an aircraft). Actuators can also make very fine movements or displacements (right down to nanometres). This makes them ideal for functions such as precise positioning during manufacturing processes, focussing lenses on satellites, aligning optical fibres and regulating micro-valves.

In Figure 6.1, the length of the actuator is denoted by L and the thickness is denoted by h.

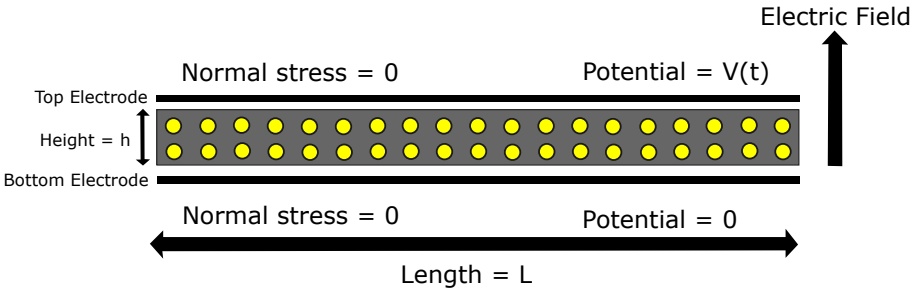


Figure 6.1: Schematic of a beam actuator.

The size of the piezoelectric inclusions is typically much smaller than L, but may be comparable to the size of h. Common applications of beam actuators include ultrasound imaging and sonar ranging devices.

6.1.1 Challenges to the modelling of Beam Actuators

Beam actuators are commonly modelled directly by computational methods such as Finite Element Analysis. However, it would be computationally prohibitive to use FEM to model the system at the microscale. This is because the spacing between neighbouring inclusions and the thickness of the piezoelectric layer are much smaller than the length of the device, meaning that there could be thousands or even millions of microscopic inclusions within the actuator. Additionally, FEA cannot readily predict effective coefficients or the impact of microstructural geometry. Furthermore, FEA does not provide the physical insights which are needed when optimising or designing piezoelectric composites.

To model a bulk actuator we can use the asymptotic homogenisation model we developed in Chapter 2, since the piezoelectric lump or stack of piezoelectric material expands or contracts as a whole.

However, to model a beam actuator, we will need to extend our methodology by incorporating aspects of Euler–Bernoulli beam theory to account for the bending effects present when the thickness of the beam is small compared to its length. Homogenisation greatly simplifies the equations to be solved but, crucially, it still retains the coupling terms between electrical field and mechanical strain at the microscale and provides other key properties.

6.1.2 Gap in literature

Despite extensive research into the modelling of piezoelectric actuators over many decades, analytical models that combine beam theory with asymptotic homogenisation are surprisingly underdeveloped. The model we will construct in this chapter,

which we shall call the Asymptotic Homogenisation Beam Model (AHBM), seeks to address this gap.

Our AHBM combines concepts from two existing analytical, beam-based methodologies. Our starting point is Ballas [5], who incorporate Euler–Bernoulli beam theory and use Lagrangian formalisms extensively, together with Hamilton's Principle, to derive the equations of motion. In that book, a number of models are developed in relation to multilayer piezoelectric composites, predicting a wide range of phenomena including: tip deflection, static displacement, resonant frequencies, electrical admittance and layer-wise performance. These are then validated by extensive experimental results. The behaviour of a combined actuator and sensor device is also modelled. Moory-Shirbani *et. al.* [47] extended Ballas' approach in relation to cantilever and multilayer actuators. The models in both [5] and [47] provide intuition on how geometry impacts actuation and give insights into the derivation of Euler–Bernoulli beam theory and equations of motion. However, a significant limitation to their studies is that they use uniform (experimentally determined) physical properties for the piezoelectric layers of the actuators. Thus they do not capture the effect of the microstructure in those layers. Additionally, their models do not include correction terms for the ansatzes assumed for the transverse displacement.

A second important inspiration for the model we will be developing is a new line of research by Zhao *et. al.* [23] which shows how to derive beam theory using a multiscale homogenisation approach. While that study is very useful, for example the method includes microstructural corrections, the model does not consider piezoelectric effects. Additionally, the model only considers cases where the microstructure is independent of the thickness (Z-) direction, where for many piezoelectric composites the variation through the thickness is key to the performance of the actuator.

6.2 Framework for Modelling Actuators

6.2.1 Introduction

In order to model beam actuators, using thin-layer theory, we will combine the asymptotic homogenisation procedure we have developed with a small-aspect-ratio expansion. We aim to accurately analyse the key properties of thin-layer composites through a wide range of lattice structures, orientations, and geometries of inclusions, so that the solutions may be obtained in a computationally efficient way.

We will start by defining the governing equations for coupled mechanical and electric fields. We will then apply our asymptotic homogenisation approach, to

derive effective beam equations at the macroscale. We will develop a macroscale model in the limit of small thickness to length ratio, defining and solving the cell functions to determine the effective stiffness and electromechanical coupling of the composite. We will then demonstrate the utility of our new AHBM by applying it to two physical situations, namely a simply supported beam and a cantilever beam. We will explore two common actuator lattice structures, namely 1-3-2 and 3-3 composites.

6.2.1.1 Derivation of Classical Beam Theory for a homogeneous material

Before we develop the asymptotic homogenised beam model, we will derive the classical Euler–Bernoulli beam equation for a homogeneous elastic material. This will provide a benchmark model and introduces the key assumptions and ideas on which we will rely. We start from the uncoupled linear elasticity equation

$$\rho \frac{\partial^2 u_j}{\partial t^2} = \frac{\partial \sigma_{ij}}{\partial x_i}, \tag{6.2.1}$$

along with the constitutive relations

$$\sigma_{ij} = c_{ij}^{kl} S_{kl}, \tag{6.2.2}$$

$$S_{ij} = \frac{1}{2}\left(\frac{\partial u_i}{\partial x^j} + \frac{\partial u_j}{\partial x^i}\right), \tag{6.2.3}$$

where the material parameters ρ and $\boldsymbol{c}$ are assumed constant. We restrict our attention to a beam and derive the corresponding reduced model. We consider the domain $\Omega = [0, L] \times [0, b] \times [0, h]$, where the beam is assumed to be slender, with aspect ratio $\frac{h}{L} \ll 1$. We further assume that

$$\boldsymbol{u} = (u_1, u_2, u_3) = (u_1(t, x, z), 0, u_3(t, x, z)) \,. \tag{6.2.4}$$

We impose traction-free boundary conditions on the upper and lower surfaces of the beam, so that the normal stress vanishes at $z = h$ and $z = 0$, i.e.,

$$n^i \sigma_{ij}\Big|_{z=h} = + \sigma_{3j}|_{z=h} = 0_j, \tag{6.2.5}$$

$$n^i \sigma_{ij}\Big|_{z=0} = - \sigma_{3j}|_{z=0} = 0_j, \tag{6.2.6}$$

where $\boldsymbol{n}$ is the unit normal vector pointing out of the device.

Using (6.2.1) along with the Neumann conditions (6.2.5)-(6.2.6), together with

the Fundamental Theorem of Calculus, we deduce the following conservation laws

$$\int_0^b \int_0^h \rho \frac{\partial^2 u_1}{\partial t^2}\, dz\, dy = \int_0^b \int_0^h \frac{\partial \sigma_{i1}}{\partial x_i}\, dz\, dy = \frac{\partial T}{\partial x}, \tag{6.2.7}$$

$$\int_0^b \int_0^h \rho \frac{\partial^2 u_3}{\partial t^2}\, dz\, dy = \int_0^b \int_0^h \frac{\partial \sigma_{i3}}{\partial x_i}\, dz\, dy = \frac{\partial N}{\partial x}, \tag{6.2.8}$$

$$\int_0^b \int_0^h \left(z - \frac{h}{2}\right) \rho \frac{\partial^2 u_1}{\partial t^2}\, dz\, dy = \int_0^b \int_0^h \left(z - \frac{h}{2}\right) \frac{\partial \sigma_{i1}}{\partial x_i}\, dz\, dy = -N + \frac{\partial M}{\partial x}, \tag{6.2.9}$$

where

$$T = \int_0^b \int_0^h \sigma_{11}\, dz\, dy, \tag{6.2.10}$$

$$N = \int_0^b \int_0^h \sigma_{13}\, dz\, dy, \tag{6.2.11}$$

$$M = \int_0^b \int_0^h \left(z - \frac{h}{2}\right) \sigma_{11}\, dz\, dy, \tag{6.2.12}$$

Following the classical Euler–Bernoulli approximation, rotary inertia is neglected. Furthermore, for slender beams undergoing predominately transverse vibration, we assume the axial inertia contribution is negligible. These assumptions lead to equations

$$\int_0^b \int_0^h \rho \frac{\partial^2 u_1}{\partial t^2}\, dz\, dy \approx 0, \tag{6.2.13}$$

$$\int_0^b \int_0^h \left(z - \frac{h}{2}\right) \rho \frac{\partial^2 u_1}{\partial t^2}\, dz\, dy \approx 0. \tag{6.2.14}$$

Substituting (6.2.9) into (6.2.8) and applying (6.2.13)-(6.2.14) reduces the system (6.2.7)-(6.2.9) to

$$0 = \frac{\partial T}{\partial x}, \tag{6.2.15}$$

$$\int_0^b \int_0^h \rho \frac{\partial^2 u_3}{\partial t^2}\, dz\, dy = \frac{\partial^2 M}{\partial x^2}. \tag{6.2.16}$$

Since the right-hand sides of (6.2.15) and (6.2.16) both depend on σ_{11}, it suffices to derive an approximation to σ_{11}. Under the Euler–Bernoulli assumptions,

$$S_{13} \ll S_{11}, S_{33}, \tag{6.2.17}$$

$$\sigma_{33} \ll \sigma_{11}. \tag{6.2.18}$$

Using (6.2.18), together with (6.2.2), we deduce

$$\sigma_{33} = c_{33}^{11} S_{11} + c_{33}^{33} S_{33} \iff S_{33} = \frac{1}{c_{33}^{33}} \left(\sigma_{33} - c_{33}^{11} S_{11} \right), \tag{6.2.19}$$

$$\sigma_{11} = c_{11}^{11} S_{11} + \frac{c_{11}^{33}}{c_{33}^{33}} \left(\sigma_{33} - c_{33}^{11} S_{11} \right) \approx E S_{11} = E \frac{\partial u_1}{\partial x}, \tag{6.2.20}$$

where $E = c_{11}^{11} - \frac{\left(c_{11}^{33}\right)^2}{c_{33}^{33}}$ is the Young's Modulus obtained after eliminating the constitutive response in the y-direction. In light of (6.2.17), we postulate the following ansatzes for u_1 and u_3

$$u_1(t, x, z) = u(t, x, z) + \hat{u}(t, x, z), \tag{6.2.21}$$

$$u_3(t, x, z) = w(t, x) + \hat{w}(t, x, z), \tag{6.2.22}$$

where u and w denote the leading-order Euler–Bernoulli displacements and $\hat{u}$ and $\hat{w}$ denote higher-order corrections. The corrections are assumed to satisfy $\hat{u} \ll u$, $\hat{w} \ll w$, together with analogous assumptions for their spatial derivatives. Substituting (6.2.21)-(6.2.22) into (6.2.17) yields

$$\frac{1}{2} \left(\frac{\partial u}{\partial z} + \frac{\partial w}{\partial x} + \frac{\partial \hat{u}}{\partial z} + \frac{\partial \hat{w}}{\partial x} \right) \ll \frac{\partial u}{\partial x} + \frac{\partial \hat{u}}{\partial x}, \frac{\partial \hat{w}}{\partial z}. \tag{6.2.23}$$

To make (6.2.23) self-consistent, we impose

$$\frac{\partial u}{\partial z} + \frac{\partial w}{\partial x} = 0, \tag{6.2.24}$$

which has the general solution

$$u(t, x, z) = u^{\dagger}(t, x) - \left(z - \frac{h}{2} \right) \frac{\partial w}{\partial x}, \tag{6.2.25}$$

where $u^{\dagger}(t, x)$ is the planar displacement at the midpoint of the beam.

Substituting (6.2.25) into (6.2.3) and (6.2.20), we deduce the following approximations

$$S_{11} = \frac{\partial u}{\partial x} \approx \frac{\partial u^{\dagger}}{\partial x} - \left(z - \frac{h}{2} \right) \frac{\partial^2 w}{\partial x^2}, \tag{6.2.26}$$

$$\sigma_{11} \approx E S_{11} \approx E \left(\frac{\partial u^{\dagger}}{\partial x} - \left(z - \frac{h}{2} \right) \frac{\partial^2 w}{\partial x^2} \right). \tag{6.2.27}$$

Substituting (6.2.27) into equations (6.2.10), (6.2.12), (6.2.15), and (6.2.16),

yields the classical Euler–Bernoulli constitutive relations and beam equations

$$T = AE\frac{\partial u^{\dagger}}{\partial x}, \tag{6.2.28}$$

$$M = -EI\frac{\partial^2 w}{\partial x^2}, \tag{6.2.29}$$

$$0 = \frac{\partial^2 u^{\dagger}}{\partial x^2} \tag{6.2.30}$$

$$\rho A\frac{\partial^2 w}{\partial t^2} = -EI\frac{\partial^4 w}{\partial x^4}, \tag{6.2.31}$$

where

$$A = bh \text{ is the cross-sectional area of the beam,} \tag{6.2.32}$$

$$I = \int_0^b \int_0^h \left(z - \frac{h}{2}\right)^2 dz\, dy \text{ is the second moment of area.} \tag{6.2.33}$$

This derivation demonstrates how the 3D elasticity equations reduce to a 1D beam model under Euler–Bernoulli assumptions. We will now adapt this method to a piezoelectric composite, using asymptotic homogenisation.

6.2.2 Equations of Motion

We consider a beam of length L, width b and height h, where these sizes are aligned with spatial coordinates x, y and z, respectively, residing in $\Omega = (0, L)\times(0, b)\times(0, h)$. We assume that the height of the beam is much smaller than the length of the beam, namely

$$\varepsilon = \frac{h}{L} \ll 1. \tag{6.2.34}$$

We assume the beam has a microstructure of typical size h and is periodic in the planar directions $\boldsymbol{e}_x = (1, 0, 0)^{\mathrm{Tr}}$ and $\boldsymbol{e}_y = (0, 1, 0)^{\mathrm{Tr}}$. We let Ω_I denote the (not necessarily connected) domain containing the piezoelectric material and let Ω_M denote the domain containing the matrix material.

In Chapter 2, we considered a linearised theory, where we implicitly linearised the Lagrangian in (A.0.6) around $\boldsymbol{u} = 0$ and $\varphi = 0$, which was valid for small strains and electric fields. However, in thin-layer actuators, a prescribed voltage produces a large transverse electric field, making the non-linear coupling due to the inverse piezoelectric effect significant. In particular, it introduces an extra mechanical stress term which leads to drifts in the natural frequencies of oscillation. We will thus need to re-derive the fundamental equations before applying the homogenisation procedure. To capture these effects while retaining a linear homogenised model,

we will now linearise around $\boldsymbol{u} = 0$ and the voltage induced electric potential profile $\varphi = V(t)z/h$. We define the term

$$\phi(t, \boldsymbol{x}) = \varphi(t, \boldsymbol{x}) - V(t)\frac{z}{h}, \tag{6.2.35}$$

where for the rest of this chapter, ϕ denotes the perturbation potential in the actuator problem and is not a cell function. Equation (A.0.6) gives the Lagrangian of our system when von-Kármán strains are assumed. Substituting (6.2.35) into (A.0.6) gives

$$\begin{aligned}\mathcal{L}_J = \frac{\rho_J}{2}\frac{\partial u_{J,j}}{\partial t}\frac{\partial u_J^j}{\partial t} - \frac{1}{2}c_{J,ij}^{kl}\left(\frac{\partial u_J^j}{\partial x_i} + \frac{1}{2}\frac{\partial u_{J,m}}{\partial x_i}\frac{\partial u_J^m}{\partial x_j}\right)\left(\frac{\partial u_{J,k}}{\partial x^l} + \frac{1}{2}\frac{\partial u_{J,n}}{\partial x^k}\frac{\partial u_J^n}{\partial x^l}\right) \\ - e_{J,ij}^k\left(\frac{\partial u_J^j}{\partial x_i} + \frac{1}{2}\frac{\partial u_{J,m}}{\partial x_i}\frac{\partial u_J^m}{\partial x_j}\right)\left(\frac{V(t)}{h}\delta_k^3 + \frac{\partial \phi_J}{\partial x^k}\right) \\ + \frac{1}{2}\epsilon_{J,i}^{Sk}\left(\frac{V(t)}{h}\delta_3^i + \frac{\partial \phi_J}{\partial x_i}\right)\left(\frac{V(t)}{h}\delta_k^3 + \frac{\partial \phi_J}{\partial x^k}\right),\end{aligned} \tag{6.2.36}$$

where δ_j^i is the Kronecker delta tensor defined in Chapter 2, and $J \in \{M, I\}$ is a phase index, with M and I denoting the matrix and inclusion phases, respectively. We assume that the mechanical displacement and electric potential gradients are sufficiently small such that all non-linear terms of cubic order or higher may be neglected. Equation (6.2.36) becomes

$$\begin{aligned}\mathcal{L}_J = \frac{\rho_J}{2}\frac{\partial u_{J,j}}{\partial t}\frac{\partial u_J^j}{\partial t} - \frac{1}{2}c_{J,ij}^{kl}\frac{\partial u_J^j}{\partial x_i}\frac{\partial u_{J,k}}{\partial x^l} \\ - e_{J,ij}^3\left(\frac{\partial u_J^j}{\partial x_i} + \frac{1}{2}\frac{\partial u_{J,m}}{\partial x_i}\frac{\partial u_J^m}{\partial x_j}\right)\frac{V(t)}{h} - e_{J,ij}^k\frac{\partial u_J^j}{\partial x_i}\frac{\partial \phi_J}{\partial x^k} \\ + \frac{1}{2}\epsilon_{J,i}^{Sk}\left(\frac{V(t)}{h}\delta_3^i + \frac{\partial \phi_J}{\partial x_i}\right)\left(\frac{V(t)}{h}\delta_k^3 + \frac{\partial \phi_J}{\partial x^k}\right).\end{aligned} \tag{6.2.37}$$

Here and throughout this chapter, Latin indices range over $\{1, 2, 3\}$, while Greek indices range over $\{1, 2\}$. By varying $\boldsymbol{u}_J \to \boldsymbol{u}_J + \delta\boldsymbol{u}_J$, $\phi_J \to \phi_J + \delta\phi_J$, we obtain

$$\begin{aligned}\delta\mathcal{L}_J = \rho_J\frac{\partial u_{J,j}}{\partial t}\frac{\partial \delta u_J^j}{\partial t} - c_{J,ij}^{kl}\frac{\partial u_{J,k}}{\partial x^l}\frac{\partial \delta u_J^j}{\partial x_i} \\ - e_{J,ij}^3\left(\frac{\partial \delta u_J^j}{\partial x_i} + \frac{\partial u_{J,m}}{\partial x_i}\frac{\partial \delta u_J^m}{\partial x_j}\right)\frac{V(t)}{h} \\ - e_{J,ij}^k\left(\frac{\partial u_J^j}{\partial x_i}\frac{\partial \delta\phi_J}{\partial x^k} + \frac{\partial \phi_J}{\partial x^k}\frac{\partial \delta u_J^j}{\partial x_i}\right) + \epsilon_{J,i}^{Sk}\left(\frac{V(t)}{h}\delta_3^i + \frac{\partial \phi_J}{\partial x_i}\right)\frac{\partial \delta\phi_J}{\partial x^k}.\end{aligned} \tag{6.2.38}$$

We define the total Lagrangian as

$$L = \int_0^{t_f} \iiint_{\Omega_M} \mathcal{L}_M \mathrm{dV}\mathrm{d}t + \int_0^{t_f} \iiint_{\Omega_I} \mathcal{L}_I \mathrm{dV}\mathrm{d}t, \tag{6.2.39}$$

where t_f is the final time. Hamilton's Principle [5] tells us that

$$\delta L = \int_0^{t_f} \iiint_{\Omega_M} \delta\mathcal{L}_M \mathrm{dV}\mathrm{d}t + \int_0^{t_f} \iiint_{\Omega_I} \delta\mathcal{L}_I \mathrm{dV}\mathrm{d}t = 0. \tag{6.2.40}$$

Substituting (6.2.38) into (6.2.40) and applying the Divergence Theorem leads to the following system of PDEs, which hold on Ω_J:

$$-\rho_J \frac{\partial^2 u_{J,j}}{\partial t^2} + \frac{\partial}{\partial x_i}\left(c^{kl}_{J,ij}\frac{\partial u_{J,k}}{\partial x^l} + e^3_{J,li}\frac{\partial u_{J,j}}{\partial x_l}\frac{V(t)}{h} + e^k_{J,ij}\frac{\partial \phi_J}{\partial x^k}\right) = 0_j, \tag{6.2.41}$$

$$\frac{\partial}{\partial x_i}\left(e^{kl}_{J,i}\frac{\partial u_{J,k}}{\partial x^l} - \epsilon^{Sk}_{J,i}\frac{\partial \phi_J}{\partial x^k}\right) = 0, \tag{6.2.42}$$

where $e^i_{J,kl} = e^{kl}_{J,i}$.
We note that the stress $\boldsymbol{\sigma}_J$ and the dielectric displacement $\boldsymbol{\mathcal{D}}_J$ are

$$\sigma_{J,ij} = c^{kl}_{J,ij}\frac{\partial u_{J,k}}{\partial x^l} + e^k_{J,ij}\left(\frac{\partial \phi_J}{\partial x^k} + \frac{V(t)}{h}\delta^3_k\right), \tag{6.2.43}$$

$$\mathcal{D}_{J,i} = e^{kl}_{J,i}\frac{\partial u_{J,k}}{\partial x^l} - \epsilon^{Sk}_{J,i}\left(\frac{\partial \phi_J}{\partial x^k} + \frac{V(t)}{h}\delta^3_k\right). \tag{6.2.44}$$

In view of Hamilton's Principle, we impose that $\boldsymbol{u}$, ϕ, $n^i\left(\sigma_{ij} + e^3_{li}\left(\partial u_j/\partial x_l\right)\left(V(t)/h\right)\right)$, and $n^i\mathcal{D}_i$ are all continuous across neighbouring phases. On the boundary $\Omega_I \cap \Omega_M$, this reads as

$$u_{M,j} = u_{I,j}, \tag{6.2.45}$$

$$\phi_M = \phi_I, \tag{6.2.46}$$

$$n^i\left(c^{kl}_{M,ij}\frac{\partial u_{M,k}}{\partial x^l}\right) = n^i\left(c^{kl}_{I,ij}\frac{\partial u_{I,k}}{\partial x^l} + e^3_{I,li}\frac{\partial u_{I,j}}{\partial x_l}\frac{V(t)}{h} + e^k_{I,ij}\left(\frac{\partial \phi_I}{\partial x^k} + \frac{V(t)}{h}\delta^3_k\right)\right), \tag{6.2.47}$$

$$n^i\left(-\epsilon^{Sk}_{M,i}\left(\frac{\partial \phi_M}{\partial x^k} + \frac{V(t)}{h}\delta^3_k\right)\right) = n^i\left(e^{kl}_{I,i}\frac{\partial u_{I,k}}{\partial x^l} - \epsilon^{Sk}_{I,i}\left(\frac{\partial \phi_I}{\partial x^k} + \frac{V(t)}{h}\delta^3_k\right)\right). \tag{6.2.48}$$

Finally, using Hamilton's Principle again, we impose the conditions that ϕ and

$$n^i\left(\sigma_{ij} + e^3_{li}\left(\partial u_j/\partial x_l\right)\left(V(t)/h\right)\right)$$

are both zero on the top and bottom surfaces, namely

$$\left(c^{kl}_{J,3j}\frac{\partial u_{J,k}}{\partial x^l}+e^3_{J,l3}\frac{\partial u_{J,j}}{\partial x_l}\frac{V(t)}{h}+e^k_{J,3j}\left(\frac{\partial \phi_J}{\partial x^k}+\frac{V(t)}{h}\delta^3_k\right)\right)\Big|_{z=h}=0, \tag{6.2.49}$$

$$\left(c^{kl}_{J,3j}\frac{\partial u_{J,k}}{\partial x^l}+e^3_{J,l3}\frac{\partial u_{J,j}}{\partial x_l}\frac{V(t)}{h}+e^k_{J,3j}\left(\frac{\partial \phi_J}{\partial x^k}+\frac{V(t)}{h}\delta^3_k\right)\right)\Big|_{z=0}=0, \tag{6.2.50}$$

$$\phi_J|_{z=h}=0, \tag{6.2.51}$$

$$\phi_J|_{z=0}=0, \tag{6.2.52}$$

which all hold on $\{(x,y,z)\in\Omega_J : z\in\{0,h\}\}$. Equations (6.2.41)-(6.2.52) show that linearising around $\boldsymbol{u}=0$ and $\varphi=V(t)\,(z/h)$ introduces extra terms in the equations of motion and the continuity and boundary conditions. These terms were not present in equations (2.4.19)-(2.4.24).

6.2.3 Non-Dimensionalisation

We use the following non-dimensionalisation

$$\begin{aligned}
&\boldsymbol{c}=c_{\text{typ}}\overline{\boldsymbol{c}},\quad \boldsymbol{e}=e_{\text{typ}}\overline{\boldsymbol{e}},\quad \boldsymbol{\epsilon}^S=\epsilon_{\text{typ}}\overline{\boldsymbol{\epsilon}}^S,\quad \rho=\rho_{\text{typ}}\overline{\rho},\\
&\boldsymbol{x}=L\overline{\boldsymbol{x}},\quad t=\frac{L}{\varepsilon}\sqrt{\frac{\rho_{\text{typ}}}{c_{\text{typ}}}}\bar{t},\quad V(t)=V_{\text{typ}}\overline{V}(\bar{t}),\quad \boldsymbol{u}=\left(\frac{e_{\text{typ}}V_{\text{typ}}}{c_{\text{typ}}\varepsilon^2}\right)\overline{\boldsymbol{u}},\\
&\phi=V_{\text{typ}}\overline{\phi},\quad \boldsymbol{\sigma}=\left(\frac{e_{\text{typ}}V_{\text{typ}}}{L\varepsilon^2}\right)\overline{\boldsymbol{\sigma}},\quad \boldsymbol{\mathcal{D}}=\left(\frac{\epsilon_{\text{typ}}V_{\text{typ}}}{L}\right)\overline{\boldsymbol{\mathcal{D}}},
\end{aligned} \tag{6.2.53}$$

where c_{typ}, e_{typ}, ϵ_{typ}, ρ_{typ} and V_{typ} are typical values of the stiffness, electromechanical, dielectric permittivity, mass density and applied potential, respectively. We define

$$\Upsilon=\frac{e_{\text{typ}}V_{\text{typ}}}{c_{\text{typ}}\varepsilon^2 h}. \tag{6.2.54}$$

We assume Υ to be independent of ε (i.e., $\mathcal{O}(1)$). Using the data provided in Tables 2.1 and 6.2, and assuming that $V_{\text{typ}}=1$ volt, we see that $\varepsilon=0.015$ and $\Upsilon=0.18$, to two significant figures, confirming that $\varepsilon\ll 1$ and $\Upsilon=\mathcal{O}(1)$).

The dimensionless versions of (6.2.41)-(6.2.42) read as

$$\varepsilon^2\overline{\rho}_J\frac{\partial^2\overline{u}_{J,j}}{\partial\bar{t}^2}=\frac{\partial}{\partial\overline{x}_i}\left(\overline{c}^{kl}_{J,ij}\frac{\partial\overline{u}_{J,k}}{\partial\overline{x}^l}+\varepsilon^2\overline{e}^k_{J,ij}\frac{\partial\overline{\phi}_J}{\partial\overline{x}^k}+\Upsilon\varepsilon^2\overline{e}^3_{J,li}\frac{\partial\overline{u}_{J,j}}{\partial\overline{x}_l}\overline{V}(\bar{t})\right), \tag{6.2.55}$$

$$0=\frac{\partial}{\partial\overline{x}_i}\left(S_p\overline{e}^{kl}_{J,i}\frac{\partial\overline{u}_{J,k}}{\partial\overline{x}^l}-\varepsilon^2\overline{\epsilon}^{Sk}_{J,i}\frac{\partial\overline{\phi}_J}{\partial\overline{x}^k}\right), \tag{6.2.56}$$

which hold for $x\in\overline{\Omega}_J=\Omega_J/L$, where S_p is defined in (2.6.22). The dimensionless

versions of the constitutive relations (6.2.43) and (6.2.44) are given by

$$\overline{\sigma}_{J,ij} = \overline{c}^{kl}_{J,ij}\frac{\partial \overline{u}_{J,k}}{\partial \overline{x}^l} + \overline{e}^{k}_{J,ij}\left(\varepsilon^2\frac{\partial \overline{\phi}_J}{\partial \overline{x}^k} + \varepsilon \overline{V}(\overline{t})\delta^3_k\right), \tag{6.2.57}$$

$$\overline{\mathcal{D}}_{J,i} = S_p\overline{e}^{kl}_{J,i}\frac{\partial \overline{u}_{J,k}}{\partial \overline{x}^l} - \overline{\epsilon}^{Sk}_{J,i}\left(\varepsilon^2\frac{\partial \overline{\phi}_J}{\partial \overline{x}^k} + \varepsilon \overline{V}(\overline{t})\delta^3_k\right). \tag{6.2.58}$$

The dimensionless versions of the boundary conditions (6.2.45)-(6.2.48), which hold on the interface between two neighbouring phases $\overline{\Omega}_M \cap \overline{\Omega}_I$, are given by

$$\overline{u}_{M,j} = \overline{u}_{I,j}, \tag{6.2.59}$$

$$\overline{\phi}_M = \overline{\phi}_I, \tag{6.2.60}$$

$$n^i\left(\overline{c}^{kl}_{M,ij}\frac{\partial \overline{u}_{M,k}}{\partial \overline{x}^l}\right) = n^i\left(\overline{c}^{kl}_{I,ij}\frac{\partial \overline{u}_{I,k}}{\partial \overline{x}^l} + \overline{e}^{k}_{I,ij}\left(\varepsilon^2\frac{\partial \overline{\phi}_I}{\partial \overline{x}^k} + \varepsilon \overline{V}(\overline{t})\delta^3_k\right) + \Upsilon\varepsilon^2\overline{e}^{3}_{I,li}\frac{\partial \overline{u}_{I,j}}{\partial \overline{x}_l}\overline{V}(\overline{t})\right), \tag{6.2.61}$$

$$n^i\left(-\overline{\epsilon}^{Sk}_{M,i}\left(\varepsilon^2\frac{\partial \overline{\phi}_M}{\partial \overline{x}^k} + \varepsilon \overline{V}(\overline{t})\delta^3_k\right)\right) = n^i\left(S_p\overline{e}^{kl}_{I,i}\frac{\partial \overline{u}_{I,k}}{\partial \overline{x}^l} - \overline{\epsilon}^{Sk}_{I,i}\left(\varepsilon^2\frac{\partial \overline{\phi}_I}{\partial \overline{x}^k} + \varepsilon \overline{V}(\overline{t})\delta^3_k\right)\right), \tag{6.2.62}$$

while (6.2.49)-(6.2.52), which now hold on $\{(\overline{x},\overline{y},\overline{z}) \in \overline{\Omega}_J : \overline{z} \in \{0,\varepsilon\}\}$, yield

$$\left(\overline{c}^{kl}_{J,3j}\frac{\partial \overline{u}_{J,k}}{\partial \overline{x}^l} + \overline{e}^{k}_{J,3j}\left(\varepsilon^2\frac{\partial \overline{\phi}_J}{\partial \overline{x}^k} + \varepsilon \overline{V}(\overline{t})\delta^3_k\right) + \Upsilon\varepsilon^2\overline{e}^{3}_{J,l3}\frac{\partial \overline{u}_{J,j}}{\partial \overline{x}_l}\overline{V}(\overline{t})\right)\Big|_{\overline{z}=\varepsilon} = 0_j, \tag{6.2.63}$$

$$\left(\overline{c}^{kl}_{J,3j}\frac{\partial \overline{u}_{J,k}}{\partial \overline{x}^l} + \overline{e}^{k}_{J,3j}\left(\varepsilon^2\frac{\partial \overline{\phi}_J}{\partial \overline{x}^k} + \varepsilon \overline{V}(\overline{t})\delta^3_k\right) + \Upsilon\varepsilon^2\overline{e}^{3}_{J,l3}\frac{\partial \overline{u}_{J,j}}{\partial \overline{x}_l}\overline{V}(\overline{t})\right)\Big|_{\overline{z}=0} = 0_j, \tag{6.2.64}$$

$$\overline{\phi}_J\Big|_{\overline{z}=\varepsilon} = 0, \tag{6.2.65}$$

$$\overline{\phi}_J\Big|_{\overline{z}=0} = 0. \tag{6.2.66}$$

This model differs from that in Chapter 2, since the boundary conditions on the top and bottom of the actuator here are relevant to the microscopic behaviour of our system. We note that the methodology in Chapter 2 assumes periodicity in all three spatial directions, whereas for actuators we can only assume periodicity in the X- and Y- directions, as the microscopic behaviour does not repeat itself in the Z-direction.

6.2.4 Establishing the Equations of Motion using asymptotic expansions

As we did in Chapter 2, we introduce microscopic variables given by

$$X^i = \frac{x^i}{\varepsilon}, \tag{6.2.67}$$

and here assume the unknowns depend on both the macroscopic variables $(x^1, x^2) \equiv (x, y)$ and the microscopic variables $(X^1, X^2, X^3) \equiv (X, Y, Z)$[1].

Furthermore, we let $\Gamma = [0,1]^3$ be the dimensionless unit cell. For each $J \in \{I, M\}$, we label each phase as $\Gamma_J \in \Gamma$, where we assume that $\Gamma_I \cup \Gamma_M = \Gamma$. Henceforth, we drop the bars from the dimensionless equations. Equations (6.2.55)-(6.2.56), which hold in each Γ_J, become

$$\begin{aligned}
\varepsilon^4 \rho_J \frac{\partial^2 u_{J,j}}{\partial t^2} = &\frac{\partial}{\partial X_i}\left(c^{kl}_{J,ij}\frac{\partial u_{J,k}}{\partial X^l} + e^k_{J,ij}\varepsilon^2\frac{\partial \phi_J}{\partial X^k}\right) \\
&+ \varepsilon\left(\frac{\partial}{\partial X_i}\left(c^{kl}_{J,ij}\frac{\partial u_{J,k}}{\partial x^l} + e^k_{J,ij}\varepsilon^2\frac{\partial \phi_J}{\partial x^k}\right) + \frac{\partial}{\partial x_i}\left(c^{kl}_{J,ij}\frac{\partial u_{J,k}}{\partial X^l} + e^k_{J,ij}\varepsilon^2\frac{\partial \phi_J}{\partial X^k}\right)\right) \\
&+ \varepsilon^2\left(\frac{\partial}{\partial x_i}\left(c^{kl}_{J,ij}\frac{\partial u_{J,k}}{\partial x^l} + e^k_{J,ij}\varepsilon^2\frac{\partial \phi_J}{\partial x^k}\right) + \frac{\partial}{\partial X_i}\left(e^3_{J,li}\Upsilon\frac{\partial u_{J,j}}{\partial X_l}\right)V(t)\right) \\
&+\varepsilon^3\Upsilon V(t)\left(\frac{\partial}{\partial x_i}\left(e^3_{J,li}\frac{\partial u_{J,j}}{\partial X_l}\right) + \frac{\partial}{\partial X_i}\left(e^3_{J,li}\frac{\partial u_{J,j}}{\partial x_l}\right)\right) + \varepsilon^4\Upsilon V(t)\frac{\partial}{\partial x_i}\left(e^3_{J,li}\frac{\partial u_{J,j}}{\partial x_l}\right),
\end{aligned} \tag{6.2.68}$$

$$\begin{aligned}
0 = &\frac{\partial}{\partial X_i}\left(S_p e^{kl}_{J,i}\frac{\partial u_{J,k}}{\partial X^l} - \epsilon^{Sk}_{J,i}\varepsilon^2\frac{\partial \phi_J}{\partial X^k}\right) \\
&+ \varepsilon\left(\frac{\partial}{\partial X_i}\left(S_p e^{kl}_{J,i}\frac{\partial u_{J,k}}{\partial x^l} - \epsilon^{Sk}_{J,i}\varepsilon^2\frac{\partial \phi_J}{\partial x^k}\right) + \frac{\partial}{\partial x_i}\left(S_p e^{kl}_{J,i}\frac{\partial u_{J,k}}{\partial X^l} - \epsilon^{Sk}_{J,i}\varepsilon^2\frac{\partial \phi_J}{\partial X^k}\right)\right) \\
&+ \varepsilon^2\left(\frac{\partial}{\partial x_i}\left(S_p e^{kl}_{J,i}\frac{\partial u_{J,k}}{\partial x^l} - \epsilon^{Sk}_{J,i}\varepsilon^2\frac{\partial \phi_J}{\partial x^k}\right)\right).
\end{aligned} \tag{6.2.69}$$

Equations (6.2.43) and (6.2.44) become

$$\sigma_{J,ij} = c^{kl}_{J,ij}\left(\frac{\partial u_{J,k}}{\partial x^l} + \varepsilon^{-1}\frac{\partial u_{J,k}}{\partial X^l}\right) + e^k_{J,ij}\left(\varepsilon^2\left(\frac{\partial \phi_J}{\partial x^k} + \varepsilon^{-1}\frac{\partial \phi_J}{\partial X^k}\right) + \varepsilon V(t)\delta^3_k\right), \tag{6.2.70}$$

$$\mathcal{D}_{J,i} = S_p e^{kl}_{J,i}\left(\frac{\partial u_{J,k}}{\partial x^l} + \varepsilon^{-1}\frac{\partial u_{J,k}}{\partial X^l}\right) - \bar{\epsilon}^{Sk}_{J,i}\left(\varepsilon^2\left(\frac{\partial \phi_J}{\partial x^k} + \varepsilon^{-1}\frac{\partial \phi_J}{\partial X^k}\right) + \varepsilon V(t)\delta^3_k\right). \tag{6.2.71}$$

Equations (6.2.59)-(6.2.62), which now hold at the dimensionless boundary between

[1] We use the notation X^i and the more usual Cartesian notation (X, Y, Z) interchangeably.

phases $\partial\Gamma_M \cap \partial\Gamma_I$, become

$$u_{M,j} = u_{I,j}, \tag{6.2.72}$$
$$\phi_M = \phi_I, \tag{6.2.73}$$

$$\begin{aligned} &n^i \left(c^{kl}_{M,ij} \frac{\partial u_{M,k}}{\partial X^l} \right) + \varepsilon n^i \left(c^{kl}_{M,ij} \frac{\partial u_{M,k}}{\partial x^l} \right) \\ &\quad = n^i \left(c^{kl}_{I,ij} \frac{\partial u_{I,k}}{\partial X^l} + e^k_{I,ij} \varepsilon^2 \frac{\partial \phi_I}{\partial X^k} \right) + \varepsilon n^i \left(c^{kl}_{I,ij} \frac{\partial u_{I,k}}{\partial x^l} + e^k_{I,ij} \varepsilon^2 \frac{\partial \phi_I}{\partial x^k} \right) \\ &\qquad + \varepsilon^2 n^i V(t) \left(e^3_{I,ij} + \Upsilon e^3_{I,li} \frac{\partial u_{I,j}}{\partial X_l} \right) + \varepsilon^3 \Upsilon V(t) n^i \left(e^3_{I,li} \frac{\partial u_{I,j}}{\partial x_l} \right), \end{aligned} \tag{6.2.74}$$

$$\begin{aligned} &n^i \left(-\epsilon^{Sk}_{M,i} \varepsilon^2 \frac{\partial \phi_M}{\partial X^k} \right) + \varepsilon n^i \left(-\epsilon^{Sk}_{M,i} \varepsilon^2 \frac{\partial \phi_M}{\partial x^k} \right) - \varepsilon^2 n^i \epsilon^{S3}_{M,i} V(t) \\ &= n^i \left(S_p e^{kl}_{I,i} \frac{\partial u_{I,k}}{\partial X^l} - \epsilon^{Sk}_{I,i} \varepsilon^2 \frac{\partial \phi_I}{\partial X^k} \right) + \varepsilon n^i \left(S_p e^{kl}_{I,i} \frac{\partial u_{I,k}}{\partial x^l} - \epsilon^{Sk}_{I,i} \varepsilon^2 \frac{\partial \phi_I}{\partial x^k} \right) - \varepsilon^2 n^i \epsilon^{S3}_{I,i} V(t). \end{aligned} \tag{6.2.75}$$

Equations (6.2.63)-(6.2.64), which now hold on $\{(X, Y, Z) \in \Gamma : Z \in \{0, 1\}\}$, become

$$\begin{aligned} &\left(c^{kl}_{J,3j} \frac{\partial u_{J,k}}{\partial X^l} + e^k_{J,3j} \varepsilon^2 \frac{\partial \phi_J}{\partial X^k} \right) \Big|_{Z=1} + \varepsilon \left(c^{kl}_{J,3j} \frac{\partial u_{J,k}}{\partial x^l} + e^k_{J,3j} \varepsilon^2 \frac{\partial \phi_J}{\partial x^k} \right) \Big|_{Z=1} \\ &\quad + \varepsilon^2 V(t) \left(e^3_{J,3j} + \Upsilon e^3_{J,l3} \frac{\partial u_{J,j}}{\partial X_l} \right) \Big|_{Z=1} + \varepsilon^3 \Upsilon V(t) \left(e^3_{J,l3} \frac{\partial u_{J,j}}{\partial x_l} \right) \Big|_{Z=1} = 0_j, \end{aligned} \tag{6.2.76}$$

$$\begin{aligned} &\left(c^{kl}_{J,3j} \frac{\partial u_{J,k}}{\partial X^l} + e^k_{J,3j} \varepsilon^2 \frac{\partial \phi_J}{\partial X^k} \right) \Big|_{Z=0} + \varepsilon \left(c^{kl}_{J,3j} \frac{\partial u_{J,k}}{\partial x^l} + e^k_{J,3j} \varepsilon^2 \frac{\partial \phi_J}{\partial x^k} \right) \Big|_{Z=0} \\ &\quad + \varepsilon^2 V(t) \left(e^3_{J,3j} + \Upsilon e^3_{J,l3} \frac{\partial u_{J,j}}{\partial X_l} \right) \Big|_{Z=0} + \varepsilon^3 \Upsilon V(t) \left(e^3_{J,l3} \frac{\partial u_{J,j}}{\partial x_l} \right) \Big|_{Z=0} = 0_j. \end{aligned} \tag{6.2.77}$$

Equations (6.2.65)-(6.2.66) remain the same, namely

$$\phi_J|_{Z=1} = 0, \tag{6.2.78}$$
$$\phi_J|_{Z=0} = 0. \tag{6.2.79}$$

Having stated the problem, we will apply our well-established homogenisation

recipe. We thus pose the following asymptotic expansions for the unknowns

$$u_j \sim \sum_{n=0}^{\infty} \varepsilon^n u_{(n)j}(t,x,y;X,Y,Z), \tag{6.2.80}$$

$$\phi \sim \sum_{n=-2}^{\infty} \varepsilon^n \phi_{(n)}(t,x,y;X,Y,Z), \tag{6.2.81}$$

and assume $\boldsymbol{u}$ and φ are 1-periodic in the variables X and Y[2].

6.2.4.1 The $\mathcal{O}(1)$ problem

We substitute (6.2.80)-(6.2.81) into (6.2.68)-(6.2.69) and (6.2.72)-(6.2.79). The $\mathcal{O}(1)$ problem reads

$$0_j = \frac{\partial}{\partial X_i}\left(c^{kl}_{J,ij}\frac{\partial u_{J,(0)k}}{\partial X^l} + e^k_{J,ij}\frac{\partial \phi_{J,(-2)}}{\partial X^k}\right), \tag{6.2.82}$$

$$0 = \frac{\partial}{\partial X_i}\left(S_p e^{kl}_{J,i}\frac{\partial u_{J,(0)k}}{\partial X^l} - \epsilon^{Sk}_{J,i}\frac{\partial \phi_{J,(-2)}}{\partial X^k}\right), \tag{6.2.83}$$

with

$$u_{M,(0)j} = u_{I,(0)j}, \tag{6.2.84}$$

$$\phi_{M,(-2)} = \phi_{I,(-2)}, \tag{6.2.85}$$

$$n^i\left(c^{kl}_{M,ij}\frac{\partial u_{M,(0)k}}{\partial X^l}\right) = n^i\left(c^{kl}_{I,ij}\frac{\partial u_{I,(0)k}}{\partial X^l} + e^k_{I,ij}\frac{\partial \phi_{I,(-2)}}{\partial X^k}\right), \tag{6.2.86}$$

$$n^i\left(-\epsilon^{Sk}_{M,i}\frac{\partial \phi_{M,(-2)}}{\partial X^k}\right) = n^i\left(S_p e^{kl}_{I,i}\frac{\partial u_{I,(0)k}}{\partial X^l} - \epsilon^{Sk}_{I,i}\frac{\partial \phi_{I,(-2)}}{\partial X^k}\right), \tag{6.2.87}$$

on $\partial\Gamma_M \cap \partial\Gamma_I$, and

$$\left(c^{kl}_{J,3j}\frac{\partial u_{J,(0)k}}{\partial X^l} + e^k_{J,3j}\frac{\partial \phi_{J,(-2)}}{\partial X^k}\right)\Big|_{Z=1} = 0_j, \tag{6.2.88}$$

$$\left(c^{kl}_{J,3j}\frac{\partial u_{J,(0)k}}{\partial X^l} + e^k_{J,3j}\frac{\partial \phi_{J,(-2)}}{\partial X^k}\right)\Big|_{Z=0} = 0_j, \tag{6.2.89}$$

$$\phi_{J,(-2)}\Big|_{Z=1} = 0, \tag{6.2.90}$$

$$\phi_{J,(-2)}\Big|_{Z=0} = 0, \tag{6.2.91}$$

on $\{(X,Y,Z) \in \Gamma : Z \in \{0,1\}\}$. Using §J.1, we find that the general solution to the

[2]Note that although we allow the expansion in ϕ to start at $\mathcal{O}\left(\varepsilon^{-2}\right)$, we will find that $\phi_{(-2)} \equiv \phi_{(-1)} \equiv 0$.

leading-order system (6.2.82)-(6.2.91) is

$$u_{J,(0)k}(t,x,y;X,Y,Z) = U_{(0)k}(t,x,y), \tag{6.2.92}$$

$$\phi_{J,(-2)} = 0. \tag{6.2.93}$$

Thus the leading-order displacement is independent of the microscale. As is common in the literature (e.g. in [23]), we assume the leading-order planar displacement is zero, and so we write

$$\begin{pmatrix} U_{(0)1}(t,x,y) \\ U_{(0)2}(t,x,y) \\ U_{(0)3}(t,x,y) \end{pmatrix} = \begin{pmatrix} 0 \\ 0 \\ w(t,x,y) \end{pmatrix}. \tag{6.2.94}$$

6.2.4.2 The $\mathcal{O}(\varepsilon)$ problem

Gathering terms of $\mathcal{O}(\varepsilon)$ from (6.2.68)-(6.2.69) and (6.2.72)-(6.2.79), we find that

$$0_j = \frac{\partial}{\partial X_i}\left(c^{kl}_{J,ij}\left(\frac{\partial u_{J,(1)k}}{\partial X^l} + \frac{\partial u_{J,(0)k}}{\partial x^l}\right) + e^k_{J,ij}\frac{\partial \phi_{J,(-1)}}{\partial X^k}\right), \tag{6.2.95}$$

$$0 = \frac{\partial}{\partial X_i}\left(S_p e^{kl}_{J,i}\left(\frac{\partial u_{J,(1)k}}{\partial X^l} + \frac{\partial u_{J,(0)k}}{\partial x^l}\right) - \epsilon^{Sk}_{J,i}\frac{\partial \phi_{J,(-1)}}{\partial X^k}\right). \tag{6.2.96}$$

The $\mathcal{O}(\varepsilon)$ versions of the boundary conditions at the interface between the materials are given by

$$u_{M,(1)j} = u_{I,(1)j}, \tag{6.2.97}$$

$$\phi_{M,(-1)} = \phi_{I,(-1)}, \tag{6.2.98}$$

$$n^i\left(c^{kl}_{M,ij}\left(\frac{\partial u_{M,(1)k}}{\partial X^l} + \frac{\partial u_{M,(0)k}}{\partial x^l}\right)\right) = n^i\left(c^{kl}_{I,ij}\left(\frac{\partial u_{I,(1)k}}{\partial X^l} + \frac{\partial u_{I,(0)k}}{\partial x^l}\right) + e^k_{I,ij}\frac{\partial \phi_{I,(-1)}}{\partial X^k}\right), \tag{6.2.99}$$

$$n^i\left(-\epsilon^{Sk}_{M,i}\frac{\partial \phi_{M,(-1)}}{\partial X^k}\right) = n^i\left(S_p e^{kl}_{I,i}\left(\frac{\partial u_{I,(1)k}}{\partial X^l} + \frac{\partial u_{I,(0)k}}{\partial x^l}\right) - \epsilon^{Sk}_{I,i}\frac{\partial \phi_{I,(-1)}}{\partial X^k}\right), \tag{6.2.100}$$

on $\Gamma_M \cap \Gamma_I$, while the $\mathcal{O}(\varepsilon)$ boundary conditions on the top and bottom surfaces are given by

$$\left(c^{kl}_{J,3j} \left(\frac{\partial u_{J,(1)k}}{\partial X^l} + \frac{\partial u_{J,(0)k}}{\partial x^l} \right) + e^k_{J,3j} \frac{\partial \phi_{J,(-1)}}{\partial X^k} \right) \Big|_{Z=1} = 0_j, \tag{6.2.101}$$

$$\left(c^{kl}_{J,3j} \left(\frac{\partial u_{J,(1)k}}{\partial X^l} + \frac{\partial u_{J,(0)k}}{\partial x^l} \right) + e^k_{J,3j} \frac{\partial \phi_{J,(-1)}}{\partial X^k} \right) \Big|_{Z=0} = 0_j, \tag{6.2.102}$$

$$\phi_{J,(-1)}\Big|_{Z=1} = 0, \tag{6.2.103}$$

$$\phi_{J,(-1)}\Big|_{Z=0} = 0, \tag{6.2.104}$$

on $\{(X,Y,Z) \in \Gamma : Z \in \{0,1\}\}$. The general solution to (6.2.95)-(6.2.104), which is derived in §J.2, is

$$u_{(1)k}(t,x,y;X,Y,Z) = U^\dagger_k(t,x,y) - \left(Z - Z^\dagger \right) \frac{\partial w}{\partial x^k}(t,x,y), \tag{6.2.105}$$

$$\phi_{(-1)}(t,x,y;X,Y,Z) = 0, \tag{6.2.106}$$

where $U^\dagger_k(t,x,y)$ is an arbitrary function that arises from integration in Z, and $Z^\dagger$ is the height of the Neutral Surface (which we will define in §6.2.4.6). We see that the $\mathcal{O}(\varepsilon)$ solutions are independent of X and Y, and we note that (6.2.94) and (6.2.105) is consistent with Kirchhoff-Love Plate Theory (see [23]), since up to $\mathcal{O}(\varepsilon)$, the displacement fields match.

6.2.4.3 The $\mathcal{O}(\varepsilon^2)$ problem

Gathering terms of $\mathcal{O}(\varepsilon^2)$ from (6.2.68)-(6.2.69) and (6.2.72)-(6.2.79) and substituting $\boldsymbol{u}_{(0)}$ and $\boldsymbol{u}_{(1)}$ from (6.2.94) and (6.2.105), we find that

$$0_j = \frac{\partial}{\partial X_i} \left(c^{kl}_{J,ij} \left(\frac{\partial u_{J,(2)k}}{\partial X^l} + \frac{\partial U^\dagger_k}{\partial x^l} - \left(Z - Z^\dagger \right) \frac{\partial^2 w}{\partial x^k \partial x^l} \right) + e^k_{J,ij} \frac{\partial \phi_{J,(0)}}{\partial X^k} \right), \tag{6.2.107}$$

$$0 = \frac{\partial}{\partial X_i} \left(S_p e^{kl}_{J,i} \left(\frac{\partial u_{J,(2)k}}{\partial X^l} + \frac{\partial U^\dagger_k}{\partial x^l} - \left(Z - Z^\dagger \right) \frac{\partial^2 w}{\partial x^k \partial x^l} \right) - \epsilon^{Sk}_{J,i} \frac{\partial \phi_{J,(0)}}{\partial X^k} \right). \tag{6.2.108}$$

The $\mathcal{O}(\varepsilon^2)$ versions of the boundary conditions at the interface are given by

$$u_{M,(2)j} = u_{I,(2)j}, \tag{6.2.109}$$

$$\phi_{M,(0)} = \phi_{I,(0)}, \tag{6.2.110}$$

$$n^i\left(c^{kl}_{M,ij}\left(\frac{\partial u_{M,(2)k}}{\partial X^l}+\frac{\partial U^\dagger_k}{\partial x^l}-\left(Z-Z^\dagger\right)\frac{\partial^2 w}{\partial x^k\partial x^l}\right)\right)$$
$$=n^i\left(c^{kl}_{I,ij}\left(\frac{\partial u_{I,(2)k}}{\partial X^l}+\frac{\partial U^\dagger_k}{\partial x^l}-\left(Z-Z^\dagger\right)\frac{\partial^2 w}{\partial x^k\partial x^l}\right)+e^k_{I,ij}\left(\frac{\partial \phi_{I,(0)}}{\partial X^k}+V(t)\delta^3_k\right)\right), \tag{6.2.111}$$

$$n^i\left(-\epsilon^{Sk}_{M,i}\left(\frac{\partial \phi_{M,(0)}}{\partial X^k}+V(t)\delta^3_k\right)\right)$$
$$=n^i\left(S_p e^{kl}_{I,i}\left(\frac{\partial u_{I,(2)k}}{\partial X^l}+\frac{\partial U^\dagger_k}{\partial x^l}-\left(Z-Z^\dagger\right)\frac{\partial^2 w}{\partial x^k\partial x^l}\right)-\epsilon^{Sk}_{I,i}\left(\frac{\partial \phi_{I,(0)}}{\partial X^k}+V(t)\delta^3_k\right)\right), \tag{6.2.112}$$

on $\Gamma_M\cap\Gamma_I$, while the $\mathcal{O}(\varepsilon^2)$ boundary conditions at the top and bottom surfaces are given by

$$\left(c^{kl}_{J,3j}\left(\frac{\partial u_{J,(2)k}}{\partial X^l}+\frac{\partial U^\dagger_k}{\partial x^l}-\left(Z-Z^\dagger\right)\frac{\partial^2 w}{\partial x^k\partial x^l}\right)\right)\Bigg|_{Z=1}$$
$$+\left(e^k_{J,3j}\left(\frac{\partial \phi_{J,(0)}}{\partial X^k}+V(t)\delta^3_k\right)\right)\Bigg|_{Z=1}=0_j, \tag{6.2.113}$$

$$\left(c^{kl}_{J,3j}\left(\frac{\partial u_{J,(2)k}}{\partial X^l}+\frac{\partial U^\dagger_k}{\partial x^l}-\left(Z-Z^\dagger\right)\frac{\partial^2 w}{\partial x^k\partial x^l}\right)\right)\Bigg|_{Z=0}$$
$$+\left(e^k_{J,3j}\left(\frac{\partial \phi_{J,(0)}}{\partial X^k}+V(t)\delta^3_k\right)\right)\Bigg|_{Z=0}=0_j, \tag{6.2.114}$$

$$\phi_{J,(0)}\Big|_{Z=1}=0, \tag{6.2.115}$$
$$\phi_{J,(0)}\Big|_{Z=0}=0, \tag{6.2.116}$$

on $\{(X,Y,Z)\in\Gamma : Z\in\{0,1\}\}$. Using the definitions in Appendix K and using the uniqueness condition derived in §J.1, we find that the general solution to (6.2.107)-

(6.2.116) is

$$u_{J,(2)k}(t,x,y;X,Y,Z) = U_k^{\dagger\dagger}(t,x,y) + \frac{\partial U_a^\dagger}{\partial x^b}(t,x,y)\Psi_{J,k}^{ab}(X,Y,Z) + \frac{\partial^2 w}{\partial x^a \partial x^b}(t,x,y)\Phi_{J,k}^{ab}(X,Y,Z) + V(t)\varsigma_{J,k}(X,Y,Z), \quad (6.2.117)$$

$$\phi_{J,(0)}(t,x,y;X,Y,Z) = \frac{\partial U_a^\dagger}{\partial x^b}(t,x,y)\psi_J^{ab}(X,Y,Z) + \frac{\partial^2 w}{\partial x^a \partial x^b}(t,x,y)\phi_J^{ab}(X,Y,Z) + V(t)\eta_J(X,Y,Z), \quad (6.2.118)$$

where we have introduced the mechanical cell functions of the first kind $\boldsymbol{\Psi}^{ab}$, ψ^{ab} (defined in §K.1.1), the mechanical cell functions of the second kind $\boldsymbol{\Phi}^{ab}$, ϕ^{ab} (defined in §K.1.2), the cell functions driven by voltage $\boldsymbol{\varsigma}$, η (defined in §K.2) and $\boldsymbol{U}^{\dagger\dagger}$, an arbitrary function independent of the microscopic variables. We note that the indices a, b denote the direction of the forcing in each cell problem.

At the two next orders we will find solvability conditions which will finally determine how the leading-order displacements vary on the macroscale. Here, our results begin to diverge from Ballas [5] and Moory-Shirbani *et. al.* [47]. This divergence stems from the fact that the contributions to the strain and electric fields from $\boldsymbol{u}_{(2)}$ and $\varphi_{(0)}$ are not present in those papers.

6.2.4.4 The $\mathcal{O}(\varepsilon^3)$ problem

From this point onwards, the only equations that will be relevant are the PDEs and the continuity and boundary conditions that involve the components of the stress tensor. Gathering terms of $\mathcal{O}(\varepsilon^3)$ in (6.2.68) yields

$$0_j = \frac{\partial \sigma_{J,(1)ij}}{\partial x_i} + \frac{\partial \sigma_{J,(2)ij}}{\partial X_i} + \Upsilon V(t)\frac{\partial}{\partial X_i}\left(e_{J,li}^3 \frac{\partial u_{J,(1)j}}{\partial X_l}\right) + \Upsilon V(t)\left(\frac{\partial}{\partial x_i}\left(e_{J,li}^3 \frac{\partial u_{J,(0)j}}{\partial X_l}\right) + \frac{\partial}{\partial X_i}\left(e_{J,li}^3 \frac{\partial u_{J,(0)j}}{\partial x_l}\right)\right). \quad (6.2.119)$$

The $\mathcal{O}(\varepsilon^3)$ terms in (6.2.74) are

$$n^i \sigma_{M,(2)ij} = n^i \sigma_{I,(2)ij} + n^i \Upsilon\left(e_{I,li}^3\left(\frac{\partial u_{I,(0)j}}{\partial x_l} + \frac{\partial u_{I,(1)j}}{\partial X_l}\right)\right) V(t), \quad (6.2.120)$$

on $\Gamma_M \cap \Gamma_I$, while the $\mathcal{O}(\varepsilon^3)$ terms in (6.2.76) and (6.2.77) read as

$$\left(\sigma_{J,(2)3j} + \Upsilon\left(e^3_{J,l3}\left(\frac{\partial u_{J,(0)j}}{\partial x_l} + \frac{\partial u_{J,(1)j}}{\partial X_l}\right)\right)V(t)\right)\Big|_{Z=1} = 0_j, \tag{6.2.121}$$

$$\left(\sigma_{J,(2)3j} + \Upsilon\left(e^3_{J,l3}\left(\frac{\partial u_{J,(0)j}}{\partial x_l} + \frac{\partial u_{J,(1)j}}{\partial X_l}\right)\right)V(t)\right)\Big|_{Z=0} = 0_j, \tag{6.2.122}$$

on $\{(X,Y,Z) \in \Gamma : Z \in \{0,1\}\}$. Introducing the notation

$$\fint\!\!\!\fint\!\!\!\fint_{\Gamma} = \frac{1}{|\Gamma|}\iiint_{\Gamma}, \tag{6.2.123}$$

to denote taking the average over the unit cell Γ, we deduce

$$0_j = \fint\!\!\!\fint\!\!\!\fint_{\Gamma} \frac{\partial \sigma_{(1)ij}}{\partial x_i} + \frac{\partial}{\partial X_i}\left(\sigma_{(2)ij} + \Upsilon\left(e^3_{li}\left(\frac{\partial u_{(0)j}}{\partial x_l} + \frac{\partial u_{(1)j}}{\partial X_l}\right)\right)V(t)\right)\mathrm{dV}, \tag{6.2.124}$$

and

$$\begin{aligned} 0_j = &\fint\!\!\!\fint\!\!\!\fint_{\Gamma}\left(Z - Z^{\dagger}\right)\frac{\partial \sigma_{(1)ij}}{\partial x_j}d\Gamma \\ &+ \fint\!\!\!\fint\!\!\!\fint_{\Gamma}\left(Z - Z^{\dagger}\right)\frac{\partial}{\partial X_i}\left(\sigma_{(2)ij} + \Upsilon\left(e^3_{li}\left(\frac{\partial u_{(0)j}}{\partial x_l} + \frac{\partial u_{(1)j}}{\partial X_l}\right)\right)V(t)\right)\mathrm{dV}. \end{aligned} \tag{6.2.125}$$

Since

$$\sigma_{(2)ij} + \Upsilon\left(e^3_{il}\left(\frac{\partial u_{(0)j}}{\partial x_l} + \frac{\partial u_{(1)j}}{\partial X_l}\right)\right)V(t),$$

is periodic on the unit cell, appealing to periodicity, using (6.2.120)-(6.2.122) and applying the Divergence Theorem to (6.2.124)-(6.2.125) gives

$$0_j = \frac{\partial T_{(1)ij}}{\partial x_i}, \tag{6.2.126}$$

$$0_j = \frac{\partial M_{(1)ij}}{\partial x_i} - \left(N_{(2)j} + \fint\!\!\!\fint\!\!\!\fint_{\Gamma}\left(\Upsilon\left(e^3_{l3}\left(\frac{\partial u_{(0)j}}{\partial x_l} + \frac{\partial u_{(1)j}}{\partial X_l}\right)\right)V(t)\right)\mathrm{dV}\right), \tag{6.2.127}$$

where $T_{(1)ij}$, $M_{(1)ij}$ and $N_{(2)j}$ are terms in the expansions of the homogenised stress, bending moment, and transverse stress tensors, which are defined as

$$T_{ij} = \fint\!\!\!\fint\!\!\!\fint_{\Gamma} \sigma_{ij}\mathrm{dV}, \tag{6.2.128}$$

$$M_{ij} = \fint\!\!\!\fint\!\!\!\fint_{\Gamma}\left(Z - Z^{\dagger}\right)\sigma_{ij}\mathrm{dV}, \tag{6.2.129}$$

$$T_{i3} = N_i = \fint\!\!\!\fint\!\!\!\fint_{\Gamma} \sigma_{i3}\mathrm{dV}, \tag{6.2.130}$$

where $i, j \in \{1, 2, 3\}$.

Using (6.2.70), (6.2.128) and (6.2.129) along with the solutions found in §6.2.4.1-§6.2.4.3, $T_{(1)ij}$, $M_{(1)ij}$ and $N_{(2)i}$ are given by

$$T_{(1)ij} = \iiint_{\Gamma} c_{ij}^{kl} \left(\frac{\partial u_{(2)k}}{\partial X^l} + \frac{\partial u_{(1)k}}{\partial x^l} \right) + e_{ij}^{k} \left(\frac{\partial \phi_{(0)}}{\partial X^k} + V(t)\delta_k^3 \right) \mathrm{dV}, \tag{6.2.131}$$

$$M_{(1)ij} = \iiint_{\Gamma} \left(Z - Z^{\dagger} \right) \left[c_{ij}^{kl} \left(\frac{\partial u_{(2)k}}{\partial X^l} + \frac{\partial u_{(1)k}}{\partial x^l} \right) + e_{ij}^{k} \left(\frac{\partial \phi_{(0)}}{\partial X^k} + V(t)\delta_k^3 \right) \right] \mathrm{dV}, \tag{6.2.132}$$

$$N_{(2)i} = \iiint_{\Gamma} c_{i3}^{kl} \left(\frac{\partial u_{(3)k}}{\partial X^l} + \frac{\partial u_{(2)k}}{\partial x^l} \right) + e_{i3}^{k} \frac{\partial \phi_{(1)}}{\partial X^k} \mathrm{dV}. \tag{6.2.133}$$

Equations (6.2.126)-(6.2.127) represent the conservation of linear planar momentum and angular momentum, respectively.

Using (6.2.117)-(6.2.118), equations (6.2.131)-(6.2.133) may be re-written as

$$T_{(1)ij} = \mathbb{A}_{ij}^{kl} \frac{\partial U_k^{\dagger}}{\partial x^l} - \mathbb{B}_{ij}^{kl} \frac{\partial^2 w}{\partial x^k \partial x^l} + \mathfrak{e}_{\mathrm{s},ij}^{3} V(t), \tag{6.2.134}$$

$$M_{(1)ij} = \mathbb{B}_{ij}^{\dagger kl} \frac{\partial U_k^{\dagger}}{\partial x^l} - \mathbb{D}_{ij}^{kl} \frac{\partial^2 w}{\partial x^k \partial x^l} + \mathfrak{e}_{\mathrm{m},ij}^{3} V(t), \tag{6.2.135}$$

$$N_{(2)i} = \frac{\partial M_{(1)ij}}{\partial x_j} + \Upsilon V(t) \left(\iiint_{\Gamma} e_{3j}^{3} \mathrm{dV} \right) \left(\delta_3^j \frac{\partial w}{\partial x^i} - \delta_i^3 \frac{\partial w}{\partial x_j} \right), \tag{6.2.136}$$

where

$$\mathbb{A}_{ij}^{kl} = \iiint_{\Gamma} c_{ij}^{k'l'} \left(\frac{\partial \Psi_{k'}^{kl}}{\partial X^{l'}} + \delta_{k'}^{k} \delta_{l'}^{l} \right) + e_{ij}^{k'} \frac{\partial \psi^{kl}}{\partial X^{k'}} \mathrm{dV}, \tag{6.2.137}$$

$$\mathbb{B}_{ij}^{kl} = \iiint_{\Gamma} c_{ij}^{k'l'} \left(-\frac{\partial \Phi_{k'}^{kl}}{\partial X^{l'}} + \left(Z - Z^{\dagger} \right) \delta_{k'}^{k} \delta_{l'}^{l} \right) - e_{ij}^{k'} \frac{\partial \phi^{kl}}{\partial X^{k'}} \mathrm{dV}, \tag{6.2.138}$$

$$\mathbb{B}_{ij}^{\dagger kl} = \iiint_{\Gamma} \left(Z - Z^{\dagger} \right) \left(c_{ij}^{k'l'} \left(\frac{\partial \Psi_{k'}^{kl}}{\partial X^{l'}} + \delta_{k'}^{k} \delta_{l'}^{l} \right) + e_{ij}^{k'} \frac{\partial \psi^{kl}}{\partial X^{k'}} \right) \mathrm{dV}, \tag{6.2.139}$$

$$\mathbb{D}_{ij}^{kl} = \iiint_{\Gamma} \left(Z - Z^{\dagger} \right) \left(-c_{ij}^{k'l'} \left(\frac{\partial \Phi_{k'}^{kl}}{\partial X^{l'}} + \left(Z - Z^{\dagger} \right) \delta_{k'}^{k} \delta_{l'}^{l} \right) - e_{ij}^{k'} \frac{\partial \phi^{kl}}{\partial X^{k'}} \right) \mathrm{dV}, \tag{6.2.140}$$

$$\mathfrak{e}_{\mathrm{s},ij}^{3} = \iiint_{\Gamma} c_{ij}^{kl} \frac{\partial \varsigma_k}{\partial X^l} + e_{ij}^{k} \left(\frac{\partial \eta}{\partial X^k} + \delta_k^3 \right) \mathrm{dV}, \tag{6.2.141}$$

$$\mathfrak{e}_{\mathrm{m},ij}^{3} = \iiint_{\Gamma} \left(Z - Z^{\dagger} \right) \left(c_{ij}^{kl} \frac{\partial \varsigma_k}{\partial X^l} + e_{ij}^{k} \left(\frac{\partial \eta}{\partial X^k} + \delta_k^3 \right) \right) \mathrm{dV}. \tag{6.2.142}$$

As in [23], $\mathbb{A}$ represents the effective planar stiffness tensor, $\mathbb{B}$ represents the effective coupling stiffness tensor, $\mathbb{D}$ represents the effective bending stiffness tensor, $\mathfrak{e}_s$ represents the effective piezoelectric stress tensor, and $\mathfrak{e}_m$ represents the effective

piezoelectric bending moment tensor. In Appendix I, we show that $\mathbb{A}$, $\mathbb{B}$, $\mathbb{D}$ have the following symmetries

$$\mathbb{A}_{ij}^{kl} = \mathbb{A}_{kl}^{ij}, \qquad \mathbb{B}_{ij}^{kl} = \mathbb{B}^{\dagger}{}_{kl}^{ij}, \qquad \mathbb{D}_{ij}^{kl} = \mathbb{D}_{kl}^{ij}. \tag{6.2.143}$$

From Appendix K, we deduce the cell functions are symmetric, namely

$$\begin{aligned} \Psi_k^{ij} &= \Psi_k^{ji}, \qquad \Phi_k^{ij} = \Phi_k^{ji}, \\ \psi^{ij} &= \psi^{ji}, \qquad \phi^{ij} = \phi^{ji}. \end{aligned} \tag{6.2.144}$$

Using the symmetries given in (2.2.3), (2.4.11), (2.4.14), and (6.2.144), we deduce the effective tensors are also symmetric, namely

$$\mathbb{A}_{ij}^{kl} = \mathbb{A}_{ji}^{kl} = \mathbb{A}_{kl}^{ij}, \tag{6.2.145}$$

$$\mathbb{B}_{ij}^{kl} = \mathbb{B}_{ji}^{kl} = \mathbb{B}_{ij}^{lk} = \mathbb{B}^{\dagger}{}_{kl}^{ij}, \tag{6.2.146}$$

$$\mathbb{D}_{ij}^{kl} = \mathbb{D}_{ji}^{kl} = \mathbb{D}_{kl}^{ij}, \tag{6.2.147}$$

$$\mathbb{e}_{\mathrm{s},ij}^{3} = \mathbb{e}_{\mathrm{s},ji}^{3}, \tag{6.2.148}$$

$$\mathbb{e}_{\mathrm{m},ij}^{3} = \mathbb{e}_{\mathrm{m},ji}^{3}. \tag{6.2.149}$$

Applying the results in §K.1.1.1 and §K.1.2.1, we deduce

$$0_{ij}^{l} = \mathbb{A}_{ij}^{3l} = \mathbb{B}^{\dagger}{}_{ij}^{3l} = \mathbb{D}_{ij}^{3l}, \tag{6.2.150}$$

$$0_{l}^{ij} = \mathbb{B}_{3l}^{ij}, \tag{6.2.151}$$

$$0_j = \mathbb{e}_{s,3j}^{3} = \mathbb{e}_{m,3j}^{3} \tag{6.2.152}$$

From (6.2.150)-(6.2.152), together with (K.2.5), (K.2.7)-(K.2.8) we deduce that

$$T_{(1)3j} = N_{(1)j} = M_{(1)3j} = 0_j. \tag{6.2.153}$$

Our system (6.2.126)-(6.2.127) is not yet closed as we still need the equations of motion governing the vertical displacement w. This will come from a solvability condition at the next order.

6.2.4.5 The $\mathcal{O}(\varepsilon^4)$ problem

Gathering terms of $\mathcal{O}(\varepsilon^4)$ in (6.2.68) yields

$$\begin{aligned} \rho_J \frac{\partial^2 u_{J,(0)j}}{\partial t^2} = \frac{\partial \sigma_{J,(2)ij}}{\partial x_i} + \frac{\partial \sigma_{J,(3)ij}}{\partial X_i} + \Upsilon V(t) \frac{\partial}{\partial X_i} \left(e_{J,li}^{3} \left(\frac{\partial u_{J,(2)j}}{\partial X_l} + \frac{\partial u_{J,(1)j}}{\partial x_l} \right) \right) \\ + \Upsilon V(t) \frac{\partial}{\partial x_i} \left(e_{J,li}^{3} \left(\frac{\partial u_{J,(1)j}}{\partial X_l} + \frac{\partial u_{J,(0)j}}{\partial x_l} \right) \right). \end{aligned} \tag{6.2.154}$$

The $\mathcal{O}(\varepsilon^4)$ terms in (6.2.74) are

$$n^i\sigma_{M,(3)ij} = n^i\left(\sigma_{I,(3)ij} + \Upsilon e^3_{I,ki}\left(\frac{\partial u_{I,(1)j}}{\partial x_k} + \frac{\partial u_{I,(2)j}}{\partial X_k}\right)V(t)\right), \tag{6.2.155}$$

on $\Gamma_M \cap \Gamma_I$, while the $\mathcal{O}(\varepsilon^4)$ terms in (6.2.76)-(6.2.77) are

$$\left(\sigma_{J,(3)3j} + \Upsilon e^3_{J,k3}\left(\frac{\partial u_{J,(1)j}}{\partial x_k} + \frac{\partial u_{J,(2)j}}{\partial X_k}\right)V(t)\right)\Big|_{Z=1} = 0_j, \tag{6.2.156}$$

$$\left(\sigma_{J,(3)3j} + \Upsilon e^3_{J,k3}\left(\frac{\partial u_{J,(1)j}}{\partial x_k} + \frac{\partial u_{J,(2)j}}{\partial X_k}\right)V(t)\right)\Big|_{Z=0} = 0_j, \tag{6.2.157}$$

on $\{(X,Y,Z) \in \Gamma : Z \in \{0,1\}\}$. We will now integrate (6.2.154) in the case where $j = 3$. Using (6.2.94), (6.2.127), (6.2.155)-(6.2.157), periodicity, and the Divergence Theorem, we deduce that

$$\rho_{\text{eff}}\frac{\partial^2 w}{\partial t^2} = \frac{\partial N_{(2)i}}{\partial x_i} + \Upsilon V(t)\left(\fint\!\!\!\fint\!\!\!\fint_{\Gamma} e^3_{ij}\mathrm{dV}\right)\frac{\partial^2 w}{\partial x_i \partial x_j}. \tag{6.2.158}$$

Using (6.2.136), we see that (6.2.158) can be rearranged to give

$$\rho_{\text{eff}}\frac{\partial^2 w}{\partial t^2} = \frac{\partial^2 M_{(1)ij}}{\partial x_i \partial x_j} + \Upsilon V(t) e^3_{\text{p},ij}\frac{\partial^2 w}{\partial x_i \partial x_j}, \tag{6.2.159}$$

where

$$e^3_{\text{p},ij} = \fint\!\!\!\fint\!\!\!\fint_{\Gamma}\left(e^3_{ij} + \delta_{ij}e^3_{33}\right)\mathrm{dV}, \tag{6.2.160}$$

$$\rho_{\text{eff}} = \fint\!\!\!\fint\!\!\!\fint_{\Gamma}\rho\mathrm{dV}. \tag{6.2.161}$$

Using (6.2.127), we rewrite (6.2.158) as

$$\rho_{\text{eff}}\frac{\partial^2 w}{\partial t^2} = \mathbb{B}^{\dagger kl}_{ij}\frac{\partial^3 U^\dagger_k}{\partial x_i \partial x_j \partial x^l} - \mathbb{D}^{kl}_{ij}\frac{\partial^4 w}{\partial x_i \partial x_j \partial x^k \partial x^l} + \Upsilon V(t) e^3_{p,ij}\frac{\partial^2 w}{\partial x_i \partial x_j}. \tag{6.2.162}$$

Let us now simplify the notation by switching back to Cartesian coordinates. We impose that to $\mathcal{O}(\varepsilon)$ there is no displacement in the y-direction. This is consistent with Euler–Bernoulli Beam Theory. The vector $\boldsymbol{U}^\dagger$ thus takes the form

$$\boldsymbol{U}^\dagger = (u^\dagger(t,x), 0, w^\dagger(t,x)), \tag{6.2.163}$$

where $u^\dagger$ represents the leading-order planar displacement and $w^\dagger$ represents the $\mathcal{O}(\varepsilon)$ correction to the vertical displacement. Substituting (6.2.163) into (6.2.131)

and (6.2.132), we deduce the following system

$$0 = \mathbb{A}_{11}^{11}\frac{\partial^2 u^\dagger}{\partial x^2} - \mathbb{B}_{11}^{11}\frac{\partial^3 w}{\partial x^3}, \tag{6.2.164}$$

$$\rho_{\text{eff}}\frac{\partial^2 w}{\partial t^2} = \mathbb{B}_{11}^{11}\frac{\partial^3 u^\dagger}{\partial x^3} - \mathbb{D}_{11}^{11}\frac{\partial^4 w}{\partial x^4} + \Upsilon V(t) e_{p,11}^3 \frac{\partial^2 w}{\partial x^2}. \tag{6.2.165}$$

Equation (6.2.164) rearranges to

$$\frac{\partial^2 u^\dagger}{\partial x^2} = \frac{\mathbb{B}_{11}^{11}}{\mathbb{A}_{11}^{11}}\frac{\partial^3 w}{\partial x^3}. \tag{6.2.166}$$

We note that (6.2.166) is well defined since $\mathbb{A}$ is positive definite as we showed in (I.0.7), and therefore $\mathbb{A}_{11}^{11} > 0$. Finally, substituting (6.2.166) into (6.2.165) gives

$$\rho_{\text{eff}}\frac{\partial^2 w}{\partial t^2} = -\hat{D}\frac{\partial^4 w}{\partial x^4} + \Upsilon V(t) e_{p,11}^3 \frac{\partial^2 w}{\partial x^2}, \tag{6.2.167}$$

where

$$\hat{D} = \mathbb{D}_{11}^{11} - \frac{\left(\mathbb{B}_{11}^{11}\right)^2}{\mathbb{A}_{11}^{11}}. \tag{6.2.168}$$

Note that, as we would expect, when there is no piezoelectricity or electric potential across the device, (6.2.167) reduces to the standard Euler-Bernoulli Beam equation (see [35]).

6.2.4.6 Neutral Surface

The neutral surface is the part of the beam where the bending stress is zero and there is zero longitudinal strain. The neutral surface separates compressive and tensile zones during bending. The location of the neutral surface depends on the stiffness distribution and is not necessarily in the centre of the beam when the material is heterogeneous. We find the neutral surface by defining the value of $Z^\dagger$ such that the $\mathbb{B}_{11}^{11}$ component of the effective coupling stiffness tensor given by (6.2.139) is zero. Thus, $Z^\dagger$ is given by

$$Z^\dagger = \frac{\fint\!\!\!\fint\!\!\!\fint_\Gamma Z\left(c_{11}^{kl}\left(\frac{\partial \Psi_k^{11}}{\partial X^l} + \delta_k^1\delta_l^1\right) + e_{11}^k\frac{\partial \psi^{11}}{\partial X^k}\right)\mathrm{dV}}{\fint\!\!\!\fint\!\!\!\fint_\Gamma \left(c_{11}^{kl}\left(\frac{\partial \Psi_k^{11}}{\partial X^l} + \delta_k^1\delta_l^1\right) + e_{11}^k\frac{\partial \psi^{11}}{\partial X^k}\right)\mathrm{dV}}. \tag{6.2.169}$$

The location of the neutral surface is given by $Z = Z^\dagger$.

Using (6.2.137), we deduce that (6.2.169) may be written as

$$Z^{\dagger} = \frac{\fint\!\!\!\fint_{\Gamma} Z\left(c_{11}^{kl}\left(\frac{\partial \Psi_k^{11}}{\partial X^l} + \delta_k^1\delta_l^1\right) + e_{11}^{k}\frac{\partial \psi^{11}}{\partial X^k}\right)\mathrm{dV}}{\mathbb{A}_{11}^{11}}. \tag{6.2.170}$$

Since $\mathbb{B}_{11}^{11} = 0$, equations (6.2.134)-(6.2.135) become

$$T_{(1)11} = \mathbb{A}_{11}^{11}\frac{\partial u^{\dagger}}{\partial x} + T_{piezo}(t), \tag{6.2.171}$$

$$M_{(1)11} = -\mathbb{D}_{11}^{11}\frac{\partial^2 w}{\partial x^2} + M_{piezo}(t), \tag{6.2.172}$$

where

$$T_{piezo}(t) = \mathbb{e}_{\mathrm{s},11}^{3}V(t), \tag{6.2.173}$$

$$M_{piezo}(t) = \mathbb{e}_{\mathrm{m},11}^{3}V(t). \tag{6.2.174}$$

Equations (6.2.164) and (6.2.165) reduce to

$$0 = \mathbb{A}_{11}^{11}\frac{\partial^2 u^{\dagger}}{\partial x^2}, \tag{6.2.175}$$

$$\rho_{\mathrm{eff}}\frac{\partial^2 w}{\partial t^2} = -\mathbb{D}_{11}^{11}\frac{\partial^4 w}{\partial x^4} + \Upsilon V(t)e_{p,11}^{3}\frac{\partial^2 w}{\partial x^2}. \tag{6.2.176}$$

Thus, we see that the equations of motion for $u^{\dagger}$ and w decouple.

6.3 Solution to Homogenised Problem

Later we will consider some specific examples of microstructural geometries, but first we find solutions to the effective equations of motion in (6.2.175) and (6.2.176) for different physical situations. The first case is the Simply Supported Beam, where the beam is supported but free to move at either end. The second case is the Cantilever Beam, where the beam is clamped at one end and there is no bending moment or shear force at the other end. For a (horizontally constrained) simply supported beam, we impose

$$u^{\dagger} = 0, \tag{6.3.1}$$

$$w = 0, \tag{6.3.2}$$

$$M_{(1)11} = -\mathbb{D}_{11}^{11}\frac{\partial^2 w}{\partial x^2} + M_{piezo}(t) = 0, \tag{6.3.3}$$

at $x = 0, 1$. For a cantilever beam, the boundary conditions at $x = 0$ are given by

$$u^{\dagger} = 0, \tag{6.3.4}$$

$$w = 0, \tag{6.3.5}$$

$$\frac{\partial w}{\partial x} = 0, \tag{6.3.6}$$

while the boundary conditions at $x = 1$ are given by

$$T_{(1)11} = \mathbb{A}_{11}^{11} \frac{\partial u^{\dagger}}{\partial x} + T_{piezo}(t) = 0, \tag{6.3.7}$$

$$M_{(1)11} = -\mathbb{D}_{11}^{11} \frac{\partial^2 w}{\partial x^2} + M_{piezo}(t) = 0, \tag{6.3.8}$$

$$\frac{\partial M_{(1)11}}{\partial x} + \Upsilon \frac{\partial w}{\partial x} e_{\mathrm{p},11}^3 V(t) = -\mathbb{D}_{11}^{11} \frac{\partial^3 w}{\partial x^3} + \Upsilon \frac{\partial w}{\partial x} e_{\mathrm{p},11}^3 V(t) = 0. \tag{6.3.9}$$

6.3.1 Rescaled Problem

We assume the potential function $V(t)$ takes the form

$$V(t) = V_{DC} + V_{AC} \cos(Kt), \tag{6.3.10}$$

where V_{DC} is the direct current and V_{AC} is the amplitude of the alternating current component, which oscillates with phase frequency K. We introduce the rescaling

$$\begin{aligned} \tau &= \sqrt{\frac{\mathbb{D}_{11}^{11}}{\rho_{\mathrm{eff}}}} t, & \tilde{u}^{\dagger}(\tau, x) &= \mathbb{A}_{11}^{11} u^{\dagger}(t, x), \\ \tilde{w}(\tau, x) &= \Upsilon w(t, x), & \tilde{K} &= K \sqrt{\frac{\rho_{\mathrm{eff}}}{\mathbb{D}_{11}^{11}}}. \end{aligned} \tag{6.3.11}$$

After dropping tildes, (6.2.175)-(6.2.176) yields

$$\frac{\partial^2 u^{\dagger}}{\partial x^2} = 0, \tag{6.3.12}$$

$$\frac{\partial^2 w}{\partial \tau^2} = -\frac{\partial^4 w}{\partial x^4} + q e_{\mathrm{p},11}^3 \frac{\partial^2 w}{\partial x^2} \left(V_{DC} + V_{AC} \cos(K\tau) \right), \tag{6.3.13}$$

where

$$q = \frac{\Upsilon}{\mathbb{D}_{11}^{11}}. \tag{6.3.14}$$

Now that we have rescaled the equations of motion and the boundary conditions, we will solve them in the limit of $q \to 0$ for the simply supported beam and cantilever beam cases. We do this because in many physical set-ups where we assume linearity,

q is small. In our analysis of both the simply supported and cantilever beams, we will assume that $e^3_{p,11} \neq 0$.

6.3.2 Simply Supported Beam Problem

In Figure 6.2 we show a simply supported beam.



Figure 6.2: Schematic of a simply supported beam.

Under the scalings given in §6.3.1, the boundary conditions in (6.3.1)-(6.3.3) are given by

$$u^{\dagger} = 0, \tag{6.3.15}$$

$$w = 0, \tag{6.3.16}$$

$$-\frac{\partial^2 w}{\partial x^2} + q\mathfrak{e}^3_{m,11}\left(V_{DC} + V_{AC}\cos\left(K\tau\right)\right) = 0. \tag{6.3.17}$$

The solution to the planar displacement (6.3.12), subject to the boundary condition (6.3.1), is given by

$$u^{\dagger}(\tau, x) = 0. \tag{6.3.18}$$

We will now solve (6.3.13), subject to boundary conditions (6.3.16)-(6.3.17). We assume that w is finite and takes the form

$$w(\tau, x) = \sum_{k=1}^{\infty} c_k(\tau)\sin(k\pi x). \tag{6.3.19}$$

Multiplying (6.3.13) by $\sin(n\pi x)$ and integrating, we deduce

$$\begin{aligned}\int_0^1 \frac{\partial^2 w}{\partial \tau^2}(\tau, x)\sin(n\pi x)\mathrm{d}x = &-\int_0^1 \frac{\partial^4 w}{\partial x^4}\sin(n\pi x)\mathrm{d}x \\ &+ qe^3_{\mathrm{p},11}\left(V_{DC} + V_{AC}\cos(K\tau)\right)\int_0^1 \frac{\partial^2 w}{\partial x^2}\sin(n\pi x)\mathrm{d}x.\end{aligned} \tag{6.3.20}$$

Substituting (6.3.19) into (6.3.20) and applying (6.3.2)-(6.3.3), we see that the ODE for the coefficients is

$$\begin{aligned}c_n{}''(\tau) = &-\left(n\pi\right)^4 c_n(\tau) - qe^3_{\mathrm{p},11}\left(V_{DC} + V_{AC}\cos(K\tau)\right)\left(n\pi\right)^2 c_n(\tau) \\ &- 2n\pi\mathfrak{e}^3_{\mathrm{m},11}q\left(V_{DC} + V_{AC}\cos(K\tau)\right)\left(1 - (-1)^n\right).\end{aligned} \tag{6.3.21}$$

In order to find solutions to (6.3.21), we must first assume a multiscale expansion. We must do this because the $-qe^3_{\mathrm{p},11}\left(V_{DC} + V_{AC}\cos(K\tau)\right)\left(n\pi\right)^2 c_n(\tau)$ term in

(6.3.13) causes a drift in the frequencies relative to their natural oscillations. We introduce the following time variables

$$\tau_0 = \tau, \qquad \tau_1 = q\tau. \tag{6.3.22}$$

We assume that the coefficients c_n have the following expansion

$$c_n \sim \sum_{m=0}^{\infty} q^m c_{n,m}(\tau_0, \tau_1). \tag{6.3.23}$$

Equation (6.3.21) gives

$$\begin{aligned}\left(\frac{\partial}{\partial\tau_0} + q\frac{\partial}{\partial\tau_1}\right)^2 c_n(\tau_0,\tau_1) = &-(n\pi)^4 c_n(\tau_0,\tau_1)\\ &- q e_{\mathrm{p},11}^3 \left(V_{DC} + V_{AC}\cos(K\tau_0)\right)(n\pi)^2 c_n(\tau_0,\tau_1)\\ &- 2n\pi \mathfrak{e}_{\mathrm{m},11}^3 q \left(V_{DC} + V_{AC}\cos(K\tau_0)\right)(1-(-1)^n).\end{aligned} \tag{6.3.24}$$

The $\mathcal{O}(1)$ version of (6.3.24) is

$$\frac{\partial^2 c_{n,0}}{\partial {\tau_0}^2} = -(n\pi)^4 c_{n,0}(\tau_0,\tau_1). \tag{6.3.25}$$

Since we are seeking real valued solutions to w, the general solution to (6.3.25) is

$$c_{n,0}(\tau_0,\tau_1) = \mathrm{Re}\left(A_{n,0}(\tau_1) e^{\mathrm{i}(n\pi)^2\tau_0}\right). \tag{6.3.26}$$

Note that

$$A_{n,0}(0) = \mathrm{Re}\left(c_n(0,0)\right) - \mathrm{i}\frac{\mathrm{Im}\left(\frac{\partial c_n}{\partial\tau_0}(0,0)\right)}{(n\pi)^2}. \tag{6.3.27}$$

The $\mathcal{O}(q)$ version of (6.3.24) gives

$$\begin{aligned}\frac{\partial^2 c_{n,1}}{\partial {\tau_0}^2} + 2\frac{\partial^2 c_{n,0}}{\partial\tau_0\partial\tau_1} = &-(n\pi)^4 c_{n,1}(\tau_0,\tau_1)\\ &- e_{\mathrm{p},11}^3 \left(V_{DC} + V_{AC}\cos(K\tau_0)\right)(n\pi)^2 c_{n,0}(\tau_0,\tau_1)\\ &- 2n\pi \mathfrak{e}_{\mathrm{m},11}^3 \left(V_{DC} + V_{AC}\cos(K\tau_0)\right)(1-(-1)^n).\end{aligned} \tag{6.3.28}$$

Using (6.3.26), we see that (6.3.28) gives

$$\frac{\partial^2 c_{n,1}}{\partial {\tau_0}^2} + 2\,\mathrm{Re}(\mathrm{i}(n\pi)^2 A_{n,0}^{'}(\tau_1)e^{\mathrm{i}(n\pi)^2\tau_0}) = -(n\pi)^4 c_{n,1}(\tau_0,\tau_1) - e_{\mathrm{p},11}^3 V_{DC}\,(n\pi)^2\,\mathrm{Re}(A_{n,0}(\tau_1)e^{\mathrm{i}(n\pi)^2\tau_0}) - \frac{e_{\mathrm{p},11}^3 V_{AC}\,(n\pi)^2}{2}\left(\mathrm{Re}\left(A_{n,0}(\tau_1)e^{\mathrm{i}\left((n\pi)^2+K\right)\tau_0}\right) + \mathrm{Re}\left(A_{n,0}(\tau_1)e^{\mathrm{i}\left((n\pi)^2-K\right)\tau_0}\right)\right) - 2n\pi\mathfrak{e}_{\mathrm{m},11}^3\left(V_{DC}+V_{AC}\cos(K\tau_0)\right)(1-(-1)^n). \quad (6.3.29)$$

In order to ensure that our expansion in (6.3.23) is a uniformly valid approximation, we need to suppress secular growth in (6.3.29). This is achieved by eliminating all terms with the same frequency as the natural frequency, which in this case are the terms with phase frequency $(n\pi)^2$. For a general forcing frequency K, the general secularity condition is

$$2\mathrm{i}(n\pi)^2 A_{n,0}^{'}(\tau_1) = -e_{\mathrm{p},11}^3 V_{DC}\,(n\pi)^2\,A_{n,0}(\tau_1) - \frac{e_{\mathrm{p},11}^3 V_{AC}\,(n\pi)^2}{2}A_{n,0}^{*}(\tau_1)\delta_{K,2(n\pi)^2} - 2n\pi\mathfrak{e}_{\mathrm{m},11}^3 V_{AC}(1-(-1)^n)\delta_{K,(n\pi)^2}, \quad (6.3.30)$$

where $*$ marks complex conjugation.

We need to consider three cases, namely

- $K = (n\pi)^2$,
- $K = 2(n\pi)^2$,
- $K \notin \{(n\pi)^2, 2(n\pi)^2\}$.

We first take the case where $K = (n\pi)^2$. From (6.3.30), we see the secularity condition for this frequency is given by

$$2\mathrm{i}(n\pi)^2 A_{n,0}^{'}(\tau_1) = -e_{\mathrm{p},11}^3 V_{DC}\,(n\pi)^2\,A_{n,0}(\tau_1) - 2n\pi\mathfrak{e}_{\mathrm{m},11}^3 V_{AC}(1-(-1)^n). \quad (6.3.31)$$

When $V_{DC} \neq 0$, the general solution to (6.3.31) is

$$A_{n,0}(\tau_1) = \left(A_{n,0}(0) + \left(\frac{2(1-(-1)^n)\mathfrak{e}_{\mathrm{m},11}^3 V_{AC}}{n\pi e_{p,11}^3 V_{DC}}\right)\right)\exp\left(\mathrm{i}\frac{e_{p,11}^3 V_{DC}}{2}\tau_1\right) - \left(\frac{2(1-(-1)^n)\mathfrak{e}_{\mathrm{m},11}^3 V_{AC}}{n\pi e_{p,11}^3 V_{DC}}\right). \quad (6.3.32)$$

We now consider the case when $K = 2(n\pi)^2$. From (6.3.30), we see that the secularity condition is given by

$$2\mathrm{i}(n\pi)^2 A'_{n,0}(\tau_1) = -e^3_{\mathrm{p},11} V_{DC} \left(n\pi\right)^2 A_{n,0}(\tau_1) - \frac{e^3_{\mathrm{p},11} V_{AC} \left(n\pi\right)^2}{2} A^*_{n,0}(\tau_1). \tag{6.3.33}$$

Equation (6.3.33) may be re-written to give

$$\frac{d}{d\tau_1}\begin{pmatrix}\mathrm{Re}\left(A_{n,0}(\tau_1)\right)\\ \mathrm{Im}\left(A_{n,0}(\tau_1)\right)\end{pmatrix} = \frac{e^3_{\mathrm{p},11}}{4}\begin{pmatrix}0 & \left(V_{AC}-2V_{DC}\right)\\ \left(V_{AC}+2V_{DC}\right) & 0\end{pmatrix}\begin{pmatrix}\mathrm{Re}\{\left(A_{n,0}\left(\tau_1\right)\right)\}\\ \mathrm{Im}\{\left(A_{n,0}\left(\tau_1\right)\right)\}\end{pmatrix}. \tag{6.3.34}$$

Equation (N.0.2) tells us that (6.3.34) has unstable solutions when

$$\left(V_{AC}\right)^2 - \left(2V_{DC}\right)^2 > 0, \tag{6.3.35}$$

and stable solutions when

$$\left(V_{AC}\right)^2 - \left(2V_{DC}\right)^2 < 0. \tag{6.3.36}$$

If $\left(V_{AC}\right)^2 - \left(2V_{DC}\right)^2 = 0$, then (6.3.34) has stable solutions if and only if

$$V_{DC} = V_{AC} = 0. \tag{6.3.37}$$

We note in passing that if $\left(V_{DC}, V_{AC}\right) \neq (0,0)$ and $\left(V_{AC}\right)^2 - \left(2V_{DC}\right)^2 = 0$, then the solution to (6.3.34) grows linearly in τ_1. Equation (6.3.36) holds provided

$$0 < |V_{AC}| < 2|V_{DC}|. \tag{6.3.38}$$

We assume that (6.3.38) holds. The general solution to (6.3.34) is

$$\begin{aligned} A_{n,0}\left(\tau_1\right) =& B_{n,+} \exp\left(\mathrm{i}\frac{e^3_{\mathrm{p},11}}{4}\sqrt{\left(2V_{DC}\right)^2 - \left(V_{AC}\right)^2}\tau_1\right) \\ &+ B_{n,-} \exp\left(-\mathrm{i}\frac{e^3_{\mathrm{p},11}}{4}\sqrt{\left(2V_{DC}\right)^2 - \left(V_{AC}\right)^2}\tau_1\right), \end{aligned} \tag{6.3.39}$$

where

$$B_{n,+} = \frac{\mathrm{Re}\left(A_{n,0}\left(0\right)\right)}{2}\left(1+\gamma\right) + \mathrm{i}\frac{\mathrm{Im}\left(A_{n,0}\left(0\right)\right)}{2}\left(1+\frac{1}{\gamma}\right), \tag{6.3.40}$$

$$B_{n,-} = \frac{\mathrm{Re}\left(A_{n,0}\left(0\right)\right)}{2}\left(1-\gamma\right) + \mathrm{i}\frac{\mathrm{Im}\left(A_{n,0}\left(0\right)\right)}{2}\left(1-\frac{1}{\gamma}\right), \tag{6.3.41}$$

$$\gamma = \frac{2V_{DC} + V_{AC}}{\sqrt{\left(2V_{DC}\right)^2 - \left(V_{AC}\right)^2}}. \tag{6.3.42}$$

We now consider the case when $K \notin \{(n\pi)^2, 2(n\pi)^2\}$. From (6.3.30) we see that

the secularity condition is

$$2\mathrm{i}(n\pi)^2 A'_{n,0}(\tau_1) = -e^3_{\mathrm{p},11} V_{DC}\,(n\pi)^2\, A_{n,0}(\tau_1), \tag{6.3.43}$$

which has a general solution

$$A_{n,0}(\tau_1) = A_{n,0}(0) e^{\frac{ie^3_{\mathrm{p},11} V_{DC}}{2}\tau_1}. \tag{6.3.44}$$

From (6.3.32), (6.3.39) and (6.3.44) we see that the presence of the oscillation term in (6.3.13) causes the frequencies of oscillation to change from their natural frequencies, regardless of the forcing frequency. When the forcing frequency matches one of the natural frequencies of oscillation, we get a non-zero steady state (i.e., independent of the timescale τ_1 amplitude). When the forcing frequency is double that of any of the natural frequencies of oscillation, our solution is conditionally stable depending on V_{DC} and V_{AC}.

Having now derived analytic formulae for the displacement, we will now demonstrate their accuracy by comparing analytical and numerical solutions. We input the dimensionless parameters in Table 6.1

Parameter	Dimensionless value
q	0.100
$e^3_{p,11}$	0.145
$\mathbb{e}^3_{\mathrm{m},11}$	0.00608
V_{DC}	1.000
V_{AC}	0.500
K	π^2

Table 6.1: Dimensionless parameters based on data from [53].

We also impose the initial conditions

$$w(0,x) = 0, \tag{6.3.45}$$

$$\frac{\partial w}{\partial \tau}(0,x) = 0. \tag{6.3.46}$$

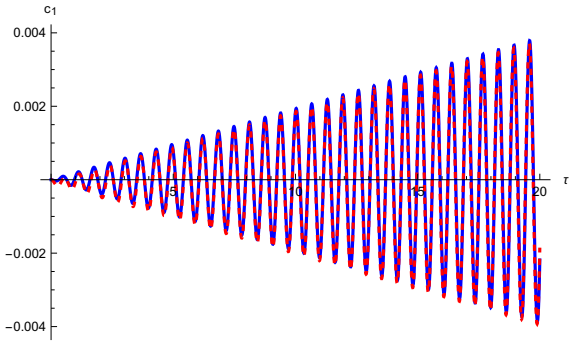


Figure 6.3: Graph showing a comparison of analytical and numerical solutions of the c_1 coefficient shown in blue and red, respectively.

As we can see from the graph in Figure 6.3, there is excellent agreement between the analytical and numerical solutions. The close agreement between the analytical and numerical solutions indicates that the mechanical response remains stable over the plotted interval. Although the oscillation amplitude increases in time, this behaviour arises because the forcing frequency matches the natural frequency. Furthermore, as shown by the leading-order solution in (6.3.32), the response remains bounded, confirming that the observed growth is not indicative of instability, but reflects enhanced transducer efficacy.

6.3.3 Cantilever Beam Problem

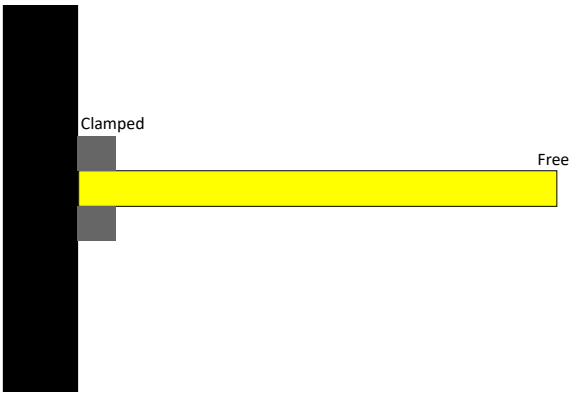


Figure 6.4: Schematic of a Cantilever Beam.

As shown in Figure 6.4, in this problem the left end is clamped and the right end is free and unsupported.

Under the scalings introduced in (6.3.11), the boundary conditions (6.3.4)-(6.3.6)

(which hold in $x = 0$) remain unchanged, reading as

$$u^{\dagger} = 0, \tag{6.3.47}$$

$$w = 0, \tag{6.3.48}$$

$$\frac{\partial w}{\partial x} = 0, \tag{6.3.49}$$

while (6.3.7)-(6.3.9) (which hold in $x = 1$) become

$$\frac{\partial u^{\dagger}}{\partial x} + \mathbb{e}^3_{\mathrm{s},11} \left(V_{DC} + V_{AC}\cos(K\tau)\right) x = 0, \tag{6.3.50}$$

$$-\frac{\partial^2 w}{\partial x^2} + q\mathbb{e}^3_{m,11} \left(V_{DC} + V_{AC}\cos\left(K\tau\right)\right) = 0, \tag{6.3.51}$$

$$-\frac{\partial^3 w}{\partial x^3} + q\frac{\partial w}{\partial x} e^3_{\mathrm{p},11} \left(V_{DC} + V_{AC}\cos(K\tau)\right) = 0. \tag{6.3.52}$$

Equation (6.2.175) with boundary conditions (6.3.4) and (6.3.7) has the solution

$$u^{\dagger} = -\mathbb{e}^3_{\mathrm{s},11} \left(V_{DC} + V_{AC}\cos(K\tau)\right) x. \tag{6.3.53}$$

We assume that w takes the form

$$w(\tau, x) = \sum_{k=1}^{\infty} c_k(\tau) X_k(x), \tag{6.3.54}$$

where $\{X_n : n \in \mathbb{Z}_{\geq 1}\}$ is the set of eigenfunctions defined in §M.2 for the cantilever beam problem.
Multiplying by X_n and integrating (6.3.13), we deduce

$$\begin{aligned}\int_0^1 \frac{\partial^2 w}{\partial \tau^2}(\tau, x) X_n(x)\mathrm{d}x = &- \int_0^1 \frac{\partial^4 w}{\partial x^4} X_n(x)\mathrm{d}x \\ &+ q e^3_{\mathrm{p},11} \left(V_{DC} + V_{AC}\cos(K\tau)\right) \int_0^1 \frac{\partial^2 w}{\partial x^2} X_n(x)\mathrm{d}x.\end{aligned} \tag{6.3.55}$$

Substituting (6.3.54) into (6.3.55) and then using (6.3.5)-(6.3.6) and (6.3.8)-(6.3.9), we find that

$$\begin{aligned}{c_n}''(\tau) = &\, q\mathbb{e}^3_{\mathrm{m},11} \left(V_{DC} + V_{AC}\cos(K\tau)\right) X_n'(1) - \left(k_n\right)^4 c_n \\ &- q e^3_{\mathrm{p},11} \left(V_{DC} + V_{AC}\cos(K\tau)\right) \sum_{j=1}^{\infty} c_j \int_0^1 X_j'(x) X_n'(x)\mathrm{d}x,\end{aligned} \tag{6.3.56}$$

where $\{k_n : n \in \mathbb{Z}_{\geq 1}\}$ are the roots of the equation $1 + \cos(k)\cosh(k) = 0$, as defined in §M.2. We once again use the time variables defined in (6.3.22) and assume the

expansion postulated in (6.3.23). Equation (6.3.56) gives

$$\left(\frac{\partial}{\partial\tau_0}+q\frac{\partial}{\partial\tau_1}\right)^2 c_n(\tau_0,\tau_1)=q\mathfrak{e}_{\mathrm{m},11}^3\left(V_{DC}+V_{AC}\cos(K\tau_0)\right)X_n^{'}(1)-\left(k_n\right)^4 c_n(\tau_0,\tau_1)$$
$$-qe_{\mathrm{p},11}^3\left(V_{DC}+V_{AC}\cos(K\tau_0)\right)\sum_{j=1}^{\infty}c_j(\tau_0,\tau_1)\int_0^1 X_j^{'}(x)X_n^{'}(x)\mathrm{d}x. \quad (6.3.57)$$

The $\mathcal{O}(1)$ version of (6.3.57) is given by

$$\frac{\partial^2 c_{n,0}}{\partial{\tau_0}^2}=-\left(k_n\right)^4 c_{n,0}(\tau_0,\tau_1), \quad (6.3.58)$$

which has the general solution

$$c_{n,0}(\tau_0,\tau_1)=\mathrm{Re}\left(A_{n,0}(\tau_1)e^{\mathrm{i}\left(k_n\right)^2\tau_0}\right). \quad (6.3.59)$$

Collecting $\mathcal{O}(q)$ terms in (6.3.57) gives

$$\frac{\partial^2 c_{n,1}}{\partial{\tau_0}^2}+2\frac{\partial^2 c_{n,0}}{\partial\tau_0\partial\tau_1}=\mathfrak{e}_{\mathrm{m},11}^3\left(V_{DC}+V_{AC}\cos(K\tau_0)\right)X_n^{'}(1)-\left(k_n\right)^4 c_{n,1}(\tau_0,\tau_1)$$
$$-e_{\mathrm{p},11}^3\left(V_{DC}+V_{AC}\cos(K\tau_0)\right)\sum_{j=1}^{\infty}c_{j,0}(\tau_0,\tau_1)\int_0^1 X_j^{'}(x)X_n^{'}(x)\mathrm{d}x. \quad (6.3.60)$$

Using (6.3.58), we see that (6.3.60) gives

$$\frac{\partial^2 c_{n,1}}{\partial{\tau_0}^2}+\mathrm{Re}\left(2\mathrm{i}\left(k_n\right)^2 A_{n,0}^{'}(\tau_1)e^{\mathrm{i}\left(k_n\right)^2\tau_0}\right)=\mathfrak{e}_{\mathrm{m},11}^3\left(V_{DC}+V_{AC}\cos(K\tau_0)\right)X_n^{'}(1)$$
$$-\left(k_n\right)^4 c_{n,1}(\tau_0,\tau_1)-e_{\mathrm{p},11}^3 V_{DC}\sum_{j=1}^{\infty}\mathrm{Re}\left(A_{j,0}(\tau_1)e^{\mathrm{i}\left(k_j\right)^2\tau_0}\right)\int_0^1 X_j^{'}(x)X_n^{'}(x)\mathrm{d}x$$
$$-\frac{e_{\mathrm{p},11}^3 V_{AC}}{2}\sum_{j=1}^{\infty}\mathrm{Re}\left(A_{j,0}(\tau_1)\left(e^{\mathrm{i}\left(\left(k_j\right)^2+K\right)\tau_0}+e^{\mathrm{i}\left(\left(k_j\right)^2-K\right)\tau_0}\right)\right)\int_0^1 X_j^{'}(x)X_n^{'}(x)\mathrm{d}x. \quad (6.3.61)$$

In order to ensure that our expansion in (6.3.23) is a uniformly valid approximation, we need to suppress secular growth in (6.3.61). This is achieved by eliminating all terms with the same frequency as the natural frequency (in this case, the terms with phase frequency $\left(k_n\right)^2$). For a general forcing frequency K, the general secularity

condition is

$$2\mathrm{i}\,(k_n)^2 A_{n,0}^{'}(\tau_1) = \mathfrak{e}_{\mathrm{m},11}^3 V_{AC}\delta_{(k_n)^2,K} X_n^{'}(1) - e_{\mathrm{p},11}^3 V_{DC} A_{n,0}(\tau_1)\int_0^1 \left(X_n^{'}(x)\right)^2 \mathrm{d}x$$
$$- \frac{e_{\mathrm{p},11}^3 V_{AC}}{2} \sum_{\substack{j\in\mathbb{Z}_{\geq 1}\\ (k_j)^2+K=(k_n)^2}} A_{j,0}(\tau_1)\int_0^1 X_j^{'}(x)X_n^{'}(x)\mathrm{d}x$$
$$- \frac{e_{\mathrm{p},11}^3 V_{AC}}{2} \sum_{\substack{j\in\mathbb{Z}_{\geq 1}\\ (k_j)^2-K=-(k_n)^2}} A_{j,0}(\tau_1)^* \int_0^1 X_j^{'}(x)X_n^{'}(x)\mathrm{d}x$$
$$- \frac{e_{\mathrm{p},11}^3 V_{AC}}{2} \sum_{\substack{j\in\mathbb{Z}_{\geq 1}\\ (k_j)^2-K=(k_n)^2}} A_{j,0}(\tau_1)\int_0^1 X_j^{'}(x)X_n^{'}(x)\mathrm{d}x. \quad (6.3.62)$$

As we did in §6.3.2, we consider three cases, namely where the forcing frequency matches one of the natural frequencies, where the forcing frequency is double a natural frequency, and where K is a general frequency. For simplicity, we will only analyse the solution to the mode corresponding to $n = 1$, which has the lowest frequency.

We now consider the case when $K = (k_1)^2$. Equation (6.3.62) becomes

$$2\mathrm{i}\,(k_1)^2 A_{1,0}^{'}(\tau_1) = \mathfrak{e}_{\mathrm{m},11}^3 V_{AC} X_1^{'}(1) - e_{\mathrm{p},11}^3 V_{DC} A_{1,0}(\tau_1)\int_0^1 \left(X_1^{'}(x)\right)^2 \mathrm{d}x. \quad (6.3.63)$$

The general solution to (6.3.63) is

$$A_{1,0}(\tau_1) = \left(A_{1,0}(0) - \left(\frac{\mathfrak{e}_{\mathrm{m},11}^3 V_{AC} X_1'(1)}{e_{p,11}^3 V_{DC}\int_0^1 \left(X_1'(x)\right)^2 dx}\right)\right)\exp\left(\mathrm{i}\frac{e_{p,11}^3 V_{DC}\int_0^1 \left(X_1'(x)\right)^2 \mathrm{d}x}{2(k_1)^2}\tau_1\right)$$
$$+ \left(\frac{\mathfrak{e}_{\mathrm{m},11}^3 V_{AC} X_1'(1)}{e_{p,11}^3 V_{DC}\int_0^1 \left(X_1'(x)\right)^2 \mathrm{d}x}\right). \quad (6.3.64)$$

Repeating the same arguments given in §6.3.2, when $e_{\mathrm{p},11}^3 V_{DC} = 0$, the solution to (6.3.63) grows linearly unless $e_{\mathrm{m},11}^3 V_{AC} = 0$. In the case where $K = 2(k_1)^2$, (6.3.62) gives

$$2\mathrm{i}\,(k_1)^2 A_{1,0}^{'}(\tau_1) = -e_{\mathrm{p},11}^3 V_{DC} A_{1,0}(\tau_1)\int_0^1 \left(X_1^{'}(x)\right)^2 \mathrm{dx}$$
$$- \frac{e_{\mathrm{p},11}^3 V_{AC}}{2} A_{1,0}(\tau_1)^* \int_0^1 \left(X_1^{'}(x)\right)^2 \mathrm{dx}. \quad (6.3.65)$$

Repeating the same arguments given in §6.3.2, we see that (6.3.65) gives stable solutions when $0 < |V_{AC}| < 2|V_{DC}|$ or $e_{\mathrm{p},11}^3 = 0$ and unstable otherwise. When

$0 < |V_{AC}| < 2|V_{DC}|$, the solution to (6.3.65) is

$$A_{1,0}(\tau_1) = B_{1,+} \exp\left(\mathrm{i}\frac{e_{\mathrm{p},11}^3 \int_0^1 (X_1'(x))^2\, dx}{4}\sqrt{(2V_{DC})^2 - (V_{AC})^2}\tau_1\right) + B_{1,-} \exp\left(-\mathrm{i}\frac{e_{\mathrm{p},11}^3 \int_0^1 (X_1'(x))^2\, dx}{4}\sqrt{(2V_{DC})^2 - (V_{AC})^2}\tau_1\right), \quad (6.3.66)$$

where $B_{1,+}$ and $B_{1,-}$ are defined analogously to (6.3.40)-(6.3.41).

We now consider the case when $K \notin \{(k_1)^2, 2(k_1)^2\}$. If we assume that none of the sets $\{(k_j)^2 + K : j \in \mathbb{Z}_{\geq 1}\}$, $\{K - (k_j)^2 : j \in \mathbb{Z}_{\geq 1}\}$ and $\{(k_j)^2 - K : j \in \mathbb{Z}_{\geq 1}\}$ contain $(k_1)^2$, then the secularity condition reads as

$$2\mathrm{i}\,(k_1)^2 A_{1,0}'(\tau_1) = -e_{\mathrm{p},11}^3 V_{DC} A_{1,0}(\tau_1) \int_0^1 \left(X_1'(x)\right)^2 \mathrm{dx}. \quad (6.3.67)$$

The general solution to (6.3.67) is

$$A_{1,0}(\tau_1) = A_{1,0}(0) \exp\left(\frac{\mathrm{i}e_{\mathrm{p},11}^3 V_{DC} \int_0^1 \left(X_1'(x)\right)^2 \mathrm{dx}}{2(k_1)^2}\tau_1\right). \quad (6.3.68)$$

If at least one of the sets $\{(k_j)^2 + K : j \in \mathbb{Z}_{\geq 1}\}$, $\{K - (k_j)^2 : j \in \mathbb{Z}_{\geq 1}\}$ and $\{(k_j)^2 - K : j \in \mathbb{Z}_{\geq 1}\}$ contains $(k_1)^2$, then the process for solving the secularity condition becomes more complex, as the amplitude function $A_{1,0}(\tau_1)$ is no longer decoupled from the other amplitude functions.

As in §6.3.2, we see that the presence of the oscillation term in (6.3.13) causes the natural frequencies of oscillation to change, regardless of the forcing frequency. Since the boundary conditions are different from the simply supported beam problem, the natural frequencies and corresponding perturbations of those frequencies are also different. When the forcing frequency matches one of the natural frequencies, assuming $V_{DC} \neq 0$ our solution has a non-zero steady state amplitude, which is independent of the timescale τ_1, but grows linearly when $V_{DC} = 0$. As for the simply supported beam case, when the forcing frequency is double that of any one of the natural frequencies, our solution is conditionally stable depending on V_{DC} and V_{AC}, with the same stability conditions established in §6.3.2.

Having now derived analytic formulae for the displacement, we will now demonstrate their accuracy by comparing analytical and numerical solutions. We input the dimensionless parameters defined in Table 6.1, with the exception of phase frequency K which we set as $(k_1)^2$, and apply the initial conditions given in (6.3.45)-(6.3.46).

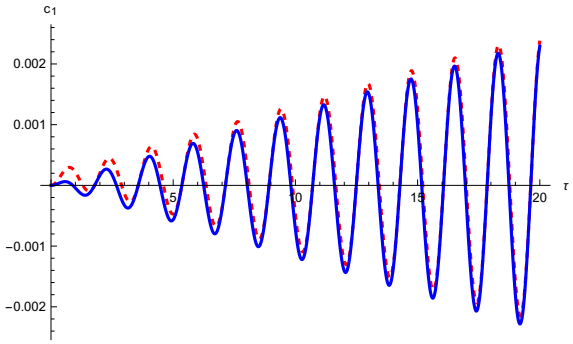


Figure 6.5: Graph showing a comparison of analytic and numerical solutions of the c_1 coefficient shown in blue and red, respectively. The numerical solution is obtained by truncating (6.3.56) so that it only includes the first five coefficients.

As we can see from the graph in Figure 6.5, there is excellent agreement between the analytical and numerical solutions. As was the case for the results shown in Figure 6.3, the close agreement between the analytical and numerical solutions indicates that the mechanical response remains stable over the plotted interval. Although the oscillation amplitude increases over time, this behaviour arises because the forcing frequency matches the natural frequency. Furthermore, as shown by the leading-order solution in (6.3.59) and the amplitude function (6.3.64), the response remains bounded, confirming that the observed growth is not indicative of instability, but reflects enhanced transducer efficacy.

6.4 Multilayer Beam

6.4.1 Introduction

For many actuators, the composite is made from multiple layers of homogeneous material, stacked over one another. Therefore, we start by solving the cell problem on the basis of N homogeneous layers. We use our framework to consider a layered geometry of thin sheets, each of which are piezoelectric and homogeneous as in Figure 6.6. In this new geometry, the microstructure is independent of the X- and Y- directions. Due to this new symmetry, we may assume that the cell functions defined in Appendix K only depend on Z. By doing this, the cell equations reduce from a system of three 3D PDEs to a system of three ODEs which only depend on Z. Once we have solved the cell problems (K.1.1)-(K.1.10), (K.1.14)-(K.1.23) and (K.2.1)-(K.2.10), and found the effective coefficients, we solve the equations of motion in (6.2.175)-(6.2.176).

We consider the case where we have N layers, each of constant thickness h_i, making up the beam, with their interfaces located at $0 = Z_0 < Z_1 < \cdots < Z_N = 1$, as shown in Figure 6.6.



Figure 6.6: Schematic of a multilayer beam comprised of homogeneous layers.

6.4.2 Adjusted coefficients

In the subsequent calculations for the effective coefficients and the neutral surface height, we find the following definitions of 'adjusted' stiffness, electromechanical and dielectric tensors for each layer $n \in \{1, 2, \cdots, N\}$ useful

$$\mathbb{Q}^{kl}_{n,ij} = c^{kl}_{n,ij} - c^{j'3}_{n,ij} c^{kl}_{n,k'3} \left(\hat{c}_n^{-1}\right)^{k'}_{j'}, \tag{6.4.1}$$

$$e^{3}_{Q,n,ij} = e^{3}_{n,ij} - c^{j'3}_{n,ij} \left(\hat{c}_n^{-1}\right)^{k'}_{j'} e^{3}_{n,3k'}, \tag{6.4.2}$$

$$\epsilon^{33}_{Q,n} = \epsilon^{S33}_{n} + S_p \left(\hat{c}_n^{-1}\right)^{kj} e^{3}_{n,j3} e^{3}_{n,k3}, \tag{6.4.3}$$

where $\hat{\boldsymbol{c}}_n$ is the tensor with components $\left(\hat{c}_n\right)^k_j = c^{k3}_{n,3j}$ and $\hat{\boldsymbol{c}}_n^{-1}$ is the matrix inverse of $\hat{\boldsymbol{c}}_n$.

6.4.3 Mechanical cell functions of the first kind

We now present simplified versions of the cell problems given in §K.1.1 in the case of N layers. Equations (K.1.1)-(K.1.2), which hold in each layer, simplify to

$$0 = \frac{d}{dZ}\left(c^{k3}_{n,3j}\frac{d\Psi^{ab}_{n,k}}{dZ} + c^{ab}_{n,3j} + e^{3}_{n,3j}\frac{d\psi^{ab}_{n}}{dZ}\right), \tag{6.4.4}$$

$$0 = \frac{d}{dZ}\left(S_p\left(e^{3}_{n,3k}\frac{d\Psi^{ab}_{n,k}}{dZ} + e^{ab}_{n,3}\right) - \epsilon^{S3}_{n,3}\frac{d\psi^{ab}_{n}}{dZ}\right), \tag{6.4.5}$$

while (K.1.3)-(K.1.6), which now hold on $Z = Z_n$, simplify to

$$\Psi^{ab}_{n,j} = \Psi^{ab}_{n+1,j}, \tag{6.4.6}$$

$$\psi^{ab}_{n} = \psi^{ab}_{n+1}, \tag{6.4.7}$$

$$\begin{aligned} &c^{k3}_{n,3j}\frac{d\Psi^{ab}_{n,k}}{dZ} + c^{ab}_{n,3j} + e^{3}_{n,3j}\frac{d\psi^{ab}_{n}} \\ &\qquad = c^{k3}_{n+1,3j}\frac{d\Psi^{ab}_{n+1,k}}{dZ} + c^{ab}_{n+1,3j} + e^{3}_{n+1,3j}\frac{d\psi^{ab}_{n+1}}{dZ}, \end{aligned} \tag{6.4.8}$$

$$\begin{aligned} &S_p\left(e^{3}_{n,k3}\frac{d\Psi^{ab}_{n,k}}{dZ} + e^{ab}_{n,3}\right) - \epsilon^{S3}_{n,3}\frac{d\psi^{ab}_{n}} \\ &\qquad = S_p\left(e^{k3}_{n+1,3}\frac{d\Psi^{ab}_{n+1,k}}{dZ} + e^{ab}_{n+1,3}\right) - \epsilon^{S3}_{n+1,3}\frac{d\psi^{ab}_{n+1}}{dZ}, \end{aligned} \tag{6.4.9}$$

and (K.1.7)-(K.1.10) simplify to

$$\left(c^{k3}_{N,3j}\frac{d\Psi^{ab}_{N,k}}{dZ} + c^{ab}_{N,3j} + e^{3}_{N,3j}\frac{d\psi^{ab}_{N}}{dZ}\right)\Bigg|_{Z=1} = 0_j, \tag{6.4.10}$$

$$\left(c^{k3}_{1,3j}\frac{d\Psi^{ab}_{1,k}}{dZ} + c^{ab}_{1,3j} + e^{3}_{1,3j}\frac{d\psi^{ab}_{1}}{dZ}\right)\Bigg|_{Z=0} = 0_j, \tag{6.4.11}$$

$$\psi^{ab}_{N}\Big|_{Z=1} = 0, \tag{6.4.12}$$

$$\psi^{ab}_{1}\Big|_{Z=0} = 0. \tag{6.4.13}$$

Using the derivation in §L.1, we find that

$$\frac{d\Psi^{ab}_{n,j}}{dZ} = -\left(\hat{c}^{-1}_{n}\right)^{k}_{j} c^{ab}_{n,3k} - \left(\hat{c}^{-1}_{n}\right)^{k}_{j}\left(\frac{S_p e^{3}_{n,3k}}{\epsilon^{33}_{Q,n}}\right)\left(e^{ab}_{Q,n,3} - \left(\frac{\left(\sum\limits_{r=1}^{N}\frac{h_r e^{ab}_{Q,r,3}}{\epsilon^{33}_{Q,r}}\right)}{\left(\sum\limits_{r=1}^{N}\frac{h_r}{\epsilon^{33}_{Q,r}}\right)}\right)\right), \tag{6.4.14}$$

$$\frac{d\psi^{ab}_{n}}{dZ} = \left(\frac{S_p}{\epsilon^{33}_{Q,n}}\right)\left(e^{ab}_{Q,n,3} - \left(\frac{\left(\sum\limits_{r=1}^{N}\frac{h_r e^{ab}_{Q,n,3}}{\epsilon^{33}_{Q,n}}\right)}{\left(\sum\limits_{r=1}^{N}\frac{h_r}{\epsilon^{33}_{Q,r}}\right)}\right)\right). \tag{6.4.15}$$

As we will see shortly, equations (6.4.14) and (6.4.15) will be used to determine the effective planar stiffness coefficient $\mathbb{A}^{11}_{11}$ (as defined in (6.2.137)), the effective piezoelectric stress coefficient $\mathfrak{e}^{3}_{s,11}$ (as defined in (6.2.141)), and the height of the neutral surface $Z^{\dagger}$ (as defined in (6.2.169)).

6.4.4 Mechanical cell functions of the second kind

We now present simplified versions of the cell problems given in §K.1.2. Equations (K.1.14)-(K.1.15), which hold in each layer, simplify to

$$0_j = \frac{d}{dZ}\left(c^{k3}_{n,3j}\frac{d\Phi^{ab}_{n,k}}{dZ} - c^{ab}_{n,3j}\left(Z - Z^\dagger\right) + e^{3j}_{n,3}\frac{d\phi^{ab}_n}{dZ}\right), \tag{6.4.16}$$

$$0 = \frac{d}{dZ}\left(S_p\left(e^{3j}_{n,3}\frac{d\Phi^{ab}_{n,j}}{dZ} - e^{ab}_{n,3}\left(Z - Z^\dagger\right)\right) - \epsilon^{S3}_{n,3}\frac{d\phi^{ab}_n}{dZ}\right), \tag{6.4.17}$$

while (K.1.16)-(K.1.19), which hold on $Z = Z_n$, simplify to

$$\Phi^{ab}_{n,j} = \Phi^{ab}_{n+1,j}, \tag{6.4.18}$$

$$\phi^{ab}_n = \phi^{ab}_{n+1}, \tag{6.4.19}$$

$$\begin{aligned} &c^{k3}_{n,3j}\frac{d\Phi^{ab}_{n,k}}{dZ} - c^{ab}_{n,3j}\left(Z - Z^\dagger\right) + e^{3}_{n,3j}\frac{d\phi^{ab}_n}{dZ} \\ &\qquad = c^{k3}_{n+1,3j}\frac{d\Phi^{ab}_{n+1,k}}{dZ} - c^{ab}_{n+1,3j}\left(Z - Z^\dagger\right) + e^{3}_{n+1,3j}\frac{d\phi^{ab}_{n+1}}{dZ}, \end{aligned} \tag{6.4.20}$$

$$\begin{aligned} &S_p e^{k3}_{n,3}\frac{d\Phi^{ab}_{n,k}}{dZ} - S_p e^{ab}_{n,3}\left(Z - Z^\dagger\right) - \epsilon^{S3}_{n,3}\frac{d\phi^{ab}_n}{dZ} \\ &\qquad = S_p e^{k3}_{n+1,3}\frac{d\Phi^{ab}_{n+1,k}}{dZ} - S_p e^{ab}_{n+1,3}\left(Z - Z^\dagger\right) - \epsilon^{S3}_{n+1,3}\frac{d\phi^{ab}_{n+1}}{dZ}, \end{aligned} \tag{6.4.21}$$

and (K.1.20)-(K.1.23) simplify to

$$\left(c^{k3}_{N,3j}\frac{d\Phi^{ab}_{N,k}}{dZ} - c^{ab}_{N,3j}\left(Z - Z^\dagger\right) + e^{3}_{N,3j}\frac{d\phi^{ab}_N}{dZ}\right)\Big|_{Z=1} = 0_j, \tag{6.4.22}$$

$$\left(c^{k3}_{1,3j}\frac{d\Phi^{ab}_{1,k}}{dZ} - c^{ab}_{1,3j}\left(Z - Z^\dagger\right) + e^{3}_{1,3j}\frac{d\phi^{ab}_1}{dZ}\right)\Big|_{Z=0} = 0_j, \tag{6.4.23}$$

$$\phi^{ab}_N\Big|_{Z=1} = 0, \tag{6.4.24}$$

$$\phi^{ab}_1\Big|_{Z=0} = 0. \tag{6.4.25}$$

As derived in §L.2, we see that

$$\frac{d\Phi_{n,j}^{ab}}{dZ} = \left(\left(\hat{c}_n^{-1}\right)_j^k c_{n,3k}^{ab} + \left(\hat{c}_n^{-1}\right)_j^k e_{n,3k}^3 \frac{S_p e_{Q,n,3}^{ab}}{\epsilon_{Q,n}^{33}} \right) (Z - Z^\dagger)$$
$$- \frac{\left(\hat{c}_n^{-1}\right)_j^k e_{n,3k}^3}{\epsilon_{Q,n}^{33}} \frac{S_p \left(\sum_{l=1}^{N} \frac{e_{Q,l,3}^{ab} \left(2h_l \sum_{k=1}^{l} h_k - (h_l)^2 \right)}{2\epsilon_{Q,n}^{33}} - Z^\dagger \sum_{l=1}^{N} \frac{e_{Q,l,3}^{ab} h_l}{\epsilon_{Q,l}^{33}} \right)}{\sum_{l=1}^{N} \left(\frac{h_l}{\epsilon_{Q,l}^{33}} \right)}, \quad (6.4.26)$$

$$\frac{d\phi_n^{ab}}{dZ} = -\frac{S_p e_{Q,n,3}^{ab} \left(Z - Z^\dagger \right)}{\epsilon_{Q,n}^{33}} + \frac{S_p \left(\sum_{l=1}^{N} \frac{e_{Q,l,3}^{ab} \left(2h_l \sum_{k=1}^{l} h_k - {h_l}^2 \right)}{2\epsilon_{Q,l}^{33}} - Z^\dagger \sum_{l=1}^{N} \frac{e_{Q,l,3}^{ab} h_l}{\epsilon_{Q,l}^{33}} \right)}{\epsilon_{Q,n}^{33} \sum_{l=1}^{N} \left(\frac{h_l}{\epsilon_{Q,l}^{33}} \right)}. \quad (6.4.27)$$

As we will see shortly, equations (6.4.26) and (6.4.27) will be used to determine the effective flexural rigidity coefficient $\mathbb{D}_{11}^{11}$ (as defined in (6.2.140)).

6.4.5 Cell functions driven by voltage

Equations (K.2.1)-(K.2.2), which hold in each layer, simplify to

$$0 = \frac{d}{dZ} \left(c_{n,3j}^{k3} \frac{d\varsigma_{n,k}}{dZ} + e_{n,3j}^3 \frac{d\eta_n}{dZ} \right), \quad (6.4.28)$$

$$0 = \frac{d}{dZ} \left(S_p e_{n,3}^{3j} \frac{d\varsigma_{n,j}}{dZ} - \epsilon_{n,3}^{S3} \frac{d\eta_n}{dZ} \right), \quad (6.4.29)$$

while (K.2.3)-(K.2.6), which hold when $Z = Z_n$, simplify to

$$\varsigma_{n,j} = \varsigma_{n+1,j}, \quad (6.4.30)$$

$$\eta_n = \eta_{n+1}, \quad (6.4.31)$$

$$c_{n,3j}^{k3} \frac{d\varsigma_{n,k}}{dZ} + e_{n,3j}^3 \left(\frac{d\eta_n}{dZ} + 1 \right) = c_{n+1,3j}^{k3} \frac{d\varsigma_{n+1,k}}{dZ} + e_{n+1,3j}^3 \left(\frac{d\eta_{n+1}}{dZ} + 1 \right), \quad (6.4.32)$$

$$S_p e_{n,3}^{3j} \frac{d\varsigma_{n,j}}{dZ} - \epsilon_{n,3}^{S3} \left(\frac{d\eta_n}{dZ} + 1 \right) = S_p e_{n+1,3}^{3j} \frac{d\varsigma_{n+1,j}}{dZ} - \epsilon_{n+1,3}^{S3} \left(\frac{d\eta_{n+1}}{dZ} + 1 \right), \quad (6.4.33)$$

and (K.2.7)-(K.2.10) simplify to

$$\left(c^{k3}_{N,3j}\frac{d\varsigma_{N,k}}{dZ}+e^{3}_{N,3j}\left(\frac{d\eta_N}{dZ}+1\right)\right)\Bigg|_{Z=1}=0, \tag{6.4.34}$$

$$\left(c^{k3}_{1,3j}\frac{d\varsigma_{1,k}}{dZ}+e^{3}_{1,3j}\left(\frac{d\eta_1}{dZ}+1\right)\right)\Bigg|_{Z=0}=0, \tag{6.4.35}$$

$$\eta_N|_{Z=1}=0, \tag{6.4.36}$$

$$\eta_1|_{Z=0}=0. \tag{6.4.37}$$

As shown in §K.2, we see that

$$\frac{d\varsigma_{n,j}}{dZ}=-\frac{\left(\hat{c}_n^{-1}\right)^k_j e^3_{n,3k}}{\epsilon^{33}_{Q,n}}\left(\frac{1}{\sum\limits_{k=1}^{N}\frac{h_k}{\epsilon^{33}_{Q,k}}}\right), \tag{6.4.38}$$

$$\frac{d\eta_n}{dZ}=\frac{1}{\epsilon^{33}_{Q,n}}\left(\frac{1}{\sum\limits_{k=1}^{N}\frac{h_k}{\epsilon^{33}_{Q,k}}}\right)-1. \tag{6.4.39}$$

As we will see shortly, equations (6.4.38) and (6.4.39) will be used to determine the effective piezoelectric stress coefficient $\mathfrak{e}^3_{s,11}$ (as defined in (6.2.141)), and the piezoelectric bending moment tensor coefficient $\mathfrak{e}^3_{m,11}$ (as defined in (6.2.142)).

6.4.6 Effective coefficients

We make use of the formulae derived in §6.4.3-§6.4.5. We start by finding $\mathbb{A}$, the effective planar stiffness tensor. We substitute (6.4.14)-(6.4.15) into (6.2.137), to find that

$$\begin{aligned}\mathbb{A}^{kl}_{ij}&=\int_0^1 c^{33}_{ij}\frac{d\Psi^{kl}_3}{dZ}+c^{kl}_{ij}+e^3_{ij}\frac{d\psi^{kl}}{dZ}\mathrm{d}Z\\&=\sum_{n=1}^{N}h_n\left(\mathbb{Q}^{kl}_{n,ij}+\left(\frac{S_p e^3_{Q,n,ij}}{\epsilon^{33}_{Q,n}}\right)\left(e^{kl}_{Q,n,3}-\frac{\sum\limits_{n=1}^{N}\frac{h_n e^{kl}_{Q,n,3}}{\epsilon^{33}_{Q,n}}}{\sum\limits_{n=1}^{N}\frac{h_n}{\epsilon^{33}_{Q,n}}}\right)\right).\end{aligned} \tag{6.4.40}$$

We now turn our attention to the neutral surface height $Z^\dagger$. We substitute (6.4.14)-(6.4.15) into (6.2.170), to find that the height of the neutral surface is

$$Z^{\dagger} = \frac{\displaystyle\sum_{n=1}^{N}\left(\frac{{Z_n}^2 - {Z_{n-1}}^2}{2}\right)\left(\mathbb{Q}^{kl}_{n,ij} + \left(\frac{S_p e^3_{Q,n,ij}}{\epsilon^{33}_{Q,n}}\right)\left(e^{kl}_{Q,n,3} - \frac{\displaystyle\sum_{n=1}^{N}\frac{h_n e^{kl}_{Q,n,3}}{\epsilon^{33}_{Q,n}}}{\displaystyle\sum_{n=1}^{N}\frac{h_n}{\epsilon^{33}_{Q,n}}}\right)\right)}{\mathbb{A}^{11}_{11}}. \quad (6.4.41)$$

Substituting (6.4.26) and (6.4.27) into (6.2.140), we find that $\mathbb{D}$, the effective bending stiffness tensor, is given by

$$\begin{aligned}\mathbb{D}^{kl}_{ij} &= \int_0^1 \left(Z - Z^{\dagger}\right)\left(-c^{33}_{ij}\frac{d\Phi^{kl}_3}{dZ} + \left(Z - Z^{\dagger}\right)c^{kl}_{ij} - e^3_{ij}\frac{d\phi^{kl}}{dZ}\right)\mathrm{d}Z \\ &= \sum_{n=1}^{N}\left(\mathbb{Q}^{kl}_{n,ij} + \frac{S_p e^3_{Q,n,ij}e^{kl}_{Q,n,3}}{\epsilon^{33}_{Q,n}}\right)\left(\frac{\hat{Z}^3_n - \hat{Z}^3_{n-1}}{3}\right) \\ &\quad - S_p\frac{\left(\displaystyle\sum_{n=1}^{N}\frac{e^3_{Q,n,ij}}{\epsilon^{33}_{Q,n}}\left(\frac{\hat{Z}^2_n - \hat{Z}^2_{n-1}}{2}\right)\right)\left(\displaystyle\sum_{n=1}^{N}\frac{e^{kl}_{Q,n,3}}{\epsilon^{33}_{Q,n}}\left(\frac{\hat{Z}^2_n - \hat{Z}^2_{n-1}}{2}\right)\right)}{\displaystyle\sum_{n=1}^{N}\left(\frac{h_n}{\epsilon^{33}_{Q,n}}\right)}, \end{aligned} \quad (6.4.42)$$

where $\hat{Z}_n = Z_n - Z^{\dagger}$ for all $n \in \{1, 2, \cdots, N\}$.

Having found the neutral surface height and relevant stiffness coefficients, we derive the piezoelectric coefficients. We start with $\mathfrak{e}^3_{\mathrm{s},ij}$, the effective piezoelectric stress tensor coefficient. Substituting (6.4.38) and (6.4.39) into (6.2.141), we find that

$$\mathfrak{e}^3_{\mathrm{s},ij} = \int_0^1 c^{33}_{ij}\frac{d\varsigma_3}{\mathrm{d}Z} + e^3_{ij}\left(\frac{d\eta}{\mathrm{d}Z} + 1\right)\mathrm{d}Z = \frac{\displaystyle\sum_{n=1}^{N}\frac{h_n e^3_{Q,n,ij}}{\epsilon^{33}_{Q,n}}}{\displaystyle\sum_{n=1}^{N}\frac{h_n}{\epsilon^{33}_{Q,n}}}. \quad (6.4.43)$$

Then we compute $\mathfrak{e}^3_{\mathrm{m},ij}$, the effective piezoelectric bending moment tensor coefficient. Substituting (6.4.38) and (6.4.39) into (6.2.142). We find that

$$\begin{aligned}\mathfrak{e}^3_{\mathrm{m},ij} &= \int_0^1 \left(Z - Z^{\dagger}\right)\left(c^{33}_{ij}\frac{d\varsigma_3}{dZ} + e^3_{33}\left(\frac{d\eta}{dZ} + 1\right)\right)\mathrm{d}Z \\ &= \frac{\displaystyle\sum_{n=1}^{N}\left(\frac{e^3_{Q,n,ij}}{\epsilon^{33}_{Q,n}}\right)\left(\frac{\hat{Z}^2_n - \hat{Z}^2_{n-1}}{2}\right)}{\displaystyle\sum_{n=1}^{N}\frac{h_n}{\epsilon^{33}_{Q,n}}}. \end{aligned} \quad (6.4.44)$$

Having found the effective coefficients in the case of multilayer beams, we will now consider the case where the beam is comprised of just one homogeneous layer.

6.4.7 Special case: Single Layer Beam

Where the beam is made from a single layer, the formulae for the effective coefficients are simpler than the formulae given in §6.4.6 for a general beam, namely

$$\mathbb{A}^{kl}_{ij} = \mathbb{Q}^{kl}_{ij}, \tag{6.4.45}$$

$$Z^{\dagger} = \frac{1}{2}, \tag{6.4.46}$$

$$\mathbb{D}^{kl}_{ij} = \frac{1}{12}\left(\mathbb{Q}^{kl}_{ij} + \frac{S_p e^3_{Q,ij} e^{kl}_{Q,3}}{\epsilon^{33}_Q}\right), \tag{6.4.47}$$

$$\mathbb{e}^3_{\mathrm{s},ij} = e^3_{Q,ij}, \tag{6.4.48}$$

$$\mathbb{e}^3_{\mathrm{m},ij} = 0. \tag{6.4.49}$$

In the absence of piezoelectric effects, as we would expect, equations (6.4.45)-(6.4.49) agree with the formulae for the coefficients derived in §6.2.1.1 (after re-dimensionalisation).

6.5 Comparison between results derived through AHBM and classical Euler–Bernoulli beam theory for a single beam using the homogenised material

For the purpose of this comparison, we will assume there is no piezoelectric coupling and that the material parameters have no dependence on the thickness coordinate Z. If we homogenise the material using the framework established in Chapter 2, then after re-dimensionalising, equations (6.4.45)-(6.4.47) become

$$\mathbb{A}^{kl}_{\mathrm{AHM},ij} = bh\mathbb{Q}^{kl}_{\mathrm{AHM},ij}, \tag{6.5.1}$$

$$Z^{\dagger} = \frac{h}{2}, \tag{6.5.2}$$

$$\mathbb{D}^{kl}_{\mathrm{AHM},ij} = \frac{bh^3}{12}\mathbb{Q}^{kl}_{\mathrm{AHM},ij}, \tag{6.5.3}$$

where

$$\mathbb{Q}^{kl}_{\mathrm{AHM},ij} = c^{kl}_{\mathrm{AHM},ij} - c^{j'3}_{\mathrm{AHM},ij} c^{kl}_{\mathrm{AHM},k'3} \left(\hat{c}^{-1}_{\mathrm{AHM}}\right)^{k'}_{j'}, \tag{6.5.4}$$

with $c^{kl}_{\mathrm{AHM},ij}$ denoting the effective stiffness coefficient found using the framework established in Chapter 2. Furthermore, $(\hat{c}_{\mathrm{AHM}})^k_j = c^{k3}_{\mathrm{AHM},3j}$ and $\hat{\boldsymbol{c}}^{-1}_{\mathrm{AHM}}$ is the inverse of $\hat{\boldsymbol{c}}_{\mathrm{AHM}}$. Substituting (6.5.1)-(6.5.3) into (6.2.134)-(6.2.135) and re-dimensionalising

yields

$$T_{\mathrm{AHM},ij} = bh\mathbb{Q}^{kl}_{\mathrm{AHM},ij}\frac{\partial U^{\dagger}_{k}}{\partial x^{l}}, \tag{6.5.5}$$

$$M_{\mathrm{AHM},ij} = -\frac{bh^{3}}{12}\mathbb{Q}^{kl}_{\mathrm{AHM},ij}\frac{\partial^{2} w}{\partial x^{k}\partial x^{l}}. \tag{6.5.6}$$

We define ℓ to be the characteristic microscopic period (i.e., the distance between neighbouring inclusions). In the limit of $0 < \frac{\ell}{h} \ll 1$ and in the absence of piezoelectric coupling, the results found in (6.5.1)-(6.5.3), and (6.5.5)-(6.5.6) converge to the results found in (6.2.137)-(6.2.140), (6.2.169) and (6.2.134)-(6.2.135).

6.6 Re-dimensionalising homogenised equations

We will shortly consider two microstructures: the Hairbrush (as shown in Figure 6.8) and the Jungle Gym (as shown in Figure 5.9). To present our results in dimensional form we first re-dimensionalise the effective coefficients. We will re-insert the overlines to show dimensionless quantities. Quantities without an overline will represent dimensional quantities. The reason we are doing this is because all the coefficients we have been using until now are dimensionless and the coefficients we will be using from now on are dimensional. Using the scalings given in §6.2, we see that

$$\overline{u}_{\alpha}(\overline{t},\overline{x},\overline{y};\overline{X},\overline{Y}) = \frac{u_{\alpha}(t,x,y)}{W} \simeq \varepsilon\overline{u}^{\dagger}_{\alpha}(\overline{t},\overline{x},\overline{y}), \tag{6.6.1}$$

$$\overline{u}_{3}(\overline{t},\overline{x},\overline{y};\overline{X},\overline{Y}) = \frac{w(t,x,y)}{W} \simeq \overline{w}(\overline{t},\overline{x},\overline{y}), \tag{6.6.2}$$

where $\alpha \in \{1,2\}$,

$$W = \frac{e_{\mathrm{typ}}V_{\mathrm{typ}}}{c_{\mathrm{typ}}\varepsilon^{2}}. \tag{6.6.3}$$

In the rest of this chapter, Greek indices are used to represent planar directions, and repeated Greek indices indicate summation over those directions. Using the displacement and potential functions derived in §6.2.4, the governing equations can then be written in a more compact form. Using the solutions to the displacement and potential functions found in §6.2.4, we see that

$$\overline{\sigma}_{ij} = \frac{\sigma_{ij}}{\sigma_{\mathrm{unit}}} \simeq \varepsilon\overline{\sigma}_{(1)ij} \iff \overline{\sigma}_{(1)ij} \simeq \frac{\sigma_{ij}}{\varepsilon\sigma_{\mathrm{unit}}}. \tag{6.6.4}$$

Using (6.6.4) along with (6.2.128) and (6.2.129), we deduce

$$\overline{T}_{ij} = \iiint_{\Gamma} \frac{\sigma_{ij}}{\sigma_{\text{unit}}} \mathrm{d}\Gamma \simeq \iiint_{\overline{\Gamma}} \varepsilon \overline{\sigma}_{(1)ij} \mathrm{d}\overline{\Gamma}, \tag{6.6.5}$$

$$\overline{M}_{ij} = \iiint_{\Gamma} \frac{Z\sigma_{ij}}{h\sigma_{\text{unit}}} \mathrm{d}\Gamma \simeq \iiint_{\overline{\Gamma}} \varepsilon \overline{Z}\overline{\sigma}_{(1)ij} \mathrm{d}\overline{\Gamma}, \tag{6.6.6}$$

where Γ is a dimensional version of the unit cell localised around an arbitrary point in $(0, L) \times (0, b) \times (0, h)$. We define the physical quantities

$$T_{ij} = \int_0^b \int_0^h \varepsilon \sigma_{\text{unit}} \overline{T}_{(1)ij} \mathrm{d}z \mathrm{d}y, \tag{6.6.7}$$

$$M_{ij} = \int_0^b \int_0^h h\varepsilon \sigma_{\text{unit}} \overline{M}_{(1)ij} \mathrm{d}z \mathrm{d}y. \tag{6.6.8}$$

Using the scalings defined in §6.2, along with (6.6.7)-(6.6.8), we deduce

$$T_{ij} = bh \left(\frac{c_{\text{typ}} W h}{L^2} \right) \left(\overline{\mathbb{A}}^{\gamma l}_{ij} \left(\frac{L}{\varepsilon W} \right) \frac{\partial u_\gamma}{\partial x^l} + \left(\frac{h \overline{\mathfrak{e}}^3_{s,ij}}{V_{\text{typ}}} \right) \left(\frac{V(t)}{h} \right) \right), \tag{6.6.9}$$

$$M_{ij} = bh \left(\frac{c_{\text{typ}} W h^2}{L^2} \right) \left(-\overline{\mathbb{D}}^{kl}_{ij} \left(\frac{L^2}{W} \right) \frac{\partial^2 w}{\partial x^k \partial x^l} + \left(\frac{h \overline{\mathfrak{e}}^3_{m,ij}}{V_{\text{typ}}} \right) \left(\frac{V(t)}{h} \right) \right). \tag{6.6.10}$$

In light of (6.6.9)-(6.6.10), we define the following dimensionalised effective tensors

$$A^{kl}_{ij} = bh \left(\frac{c_{\text{typ}} W h}{L^2} \right) \left(\frac{L}{\varepsilon W} \right) \overline{\mathbb{A}}^{kl}_{ij} = c_{\text{typ}} bh \overline{\mathbb{A}}^{kl}_{ij}, \tag{6.6.11}$$

$$e^3_{s,ij} = bh \left(\frac{c_{\text{typ}} W h}{L^2} \right) \left(\frac{1}{V_{\text{typ}}} \right) h \overline{\mathfrak{e}}^3_{s,ij} = e_{\text{typ}} bh \overline{\mathfrak{e}}^3_{s,ij}, \tag{6.6.12}$$

$$D^{kl}_{ij} = bh \left(\frac{c_{\text{typ}} W h^2}{L^2} \right) \left(\frac{L^2}{W} \right) \overline{\mathbb{D}}^{kl}_{ij} = c_{\text{typ}} bh^3 \overline{\mathbb{D}}^{kl}_{ij}, \tag{6.6.13}$$

$$e^3_{m,ij} = bh \left(\frac{c_{\text{typ}} W h^2}{L^2} \right) h \left(\frac{\overline{\mathfrak{e}}^3_{m,ij}}{V_{\text{typ}}} \right) = e_{\text{typ}} bh^2 \overline{\mathfrak{e}}^3_{m,ij}. \tag{6.6.14}$$

The neutral surface height $Z^\dagger$ is given by

$$Z^\dagger = h\overline{Z}^\dagger, \tag{6.6.15}$$

and the dimensionalised effective mass density is given by

$$\rho_{\text{eff}} = \rho_{\text{typ}} \overline{\rho}_{\text{eff}} \tag{6.6.16}$$

Note also that, after re-dimensionalising (6.4.1)-(6.4.3), we find that

$$Q^{kl}_{n,ij} = c^{kl}_{n,ij} - c^{j'3}_{n,ij} c^{kl}_{n,k'3} \left(\hat{c}^{-1}_n\right)^{k'}_{j'}, \tag{6.6.17}$$

$$e^{3}_{Q,n,ij} = e^{3}_{n,ij} - c^{j'3}_{n,ij} \left(\hat{c}^{-1}_n\right)^{k'}_{j'} e^{3}_{n,3k'}, \tag{6.6.18}$$

$$\epsilon^{33}_{Q,n} = \epsilon^{S33}_{n} + \left(\hat{c}^{-1}_n\right)^{kj} e^{3}_{n,j3} e^{3}_{n,k3}. \tag{6.6.19}$$

For the remainder of this chapter, any references to effective coefficients or frequencies should be read as references to dimensional quantities.

6.7 Simplified homogenisation method for layered composites

We may simplify the homogenisation process established in §6.2, for the special case where our beam is made up of N layers, each with 1-3 connectivity. Once we have found the effective coefficients for each layer, we may use the multilayer formulae given in §6.4 to deduce the effective coefficients of the beam. We will refer to this process, which is illustrated in Figure 6.7, as **Sequential Homogenisation**.

This approach is less computationally expensive than Standard Homogenisation, but ignores the interactions between the boundaries of neighbouring layers. Consequently, local boundary-layer effects and microscale interactions between adjacent inclusions are not fully resolved. In the configurations considered here, the distance between neighbouring inclusions is comparable to the beam height, meaning that microscale variations may be significantly influenced by the beam boundaries. If the inclusion spacing were much smaller than the beam height, one would expect the Sequential Homogenisation approach to provide improved agreement with the fully resolved model (established in §6.2.4), since the structure would appear more effectively periodic at the macroscale. Accordingly, the simplified approach substantially reduces computational cost by replacing the original three-dimensional coupled PDE system with a sequence of lower-dimensional homogenised problems.



Figure 6.7: Schematic of the Sequential Homogenisation recipe.

We use the same notation for the layers established in §6.4. For each layer, using the homogenisation method introduced in Chapter 2, we homogenise and

combine the effective coefficients in the constituent layers using the formulae found in §6.4, assuming periodicity in all three directions. We label the effective stiffness, piezoelectric and dielectric tensors in the n^{th} layer as $\boldsymbol{c}_{\text{eff},n}$, $\boldsymbol{e}_{\text{eff},n}$, $\boldsymbol{\epsilon}^{S}_{\text{eff},n}$, respectively. Once we have found these effective coefficients, we use (6.6.17)-(6.6.19) to work out the adjusted material parameters. We calculate the effective coefficients by treating the beam as a multilayer beam, using the formulae given in §6.4.

6.8 Case study of Sequential Homogenisation: The Hairbrush

We will use the Sequential Homogenisation method to find the effective coefficients for a composite with a 1-3-2 lattice structure built from a uniform layer of thickness $h\alpha_h$ underneath a layer of matrix material containing regularly spaced rectangular pillars of constant cross-section. We will then compare the results to those derived by the method in §6.2.4, which we will call **Standard Homogenisation**.

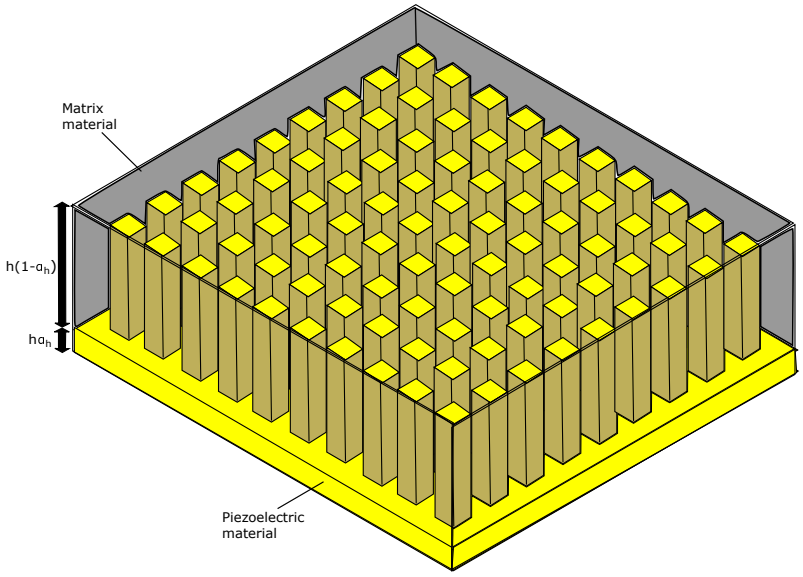


Figure 6.8: Schematic of a 1-3-2 composite, known as a Hairbrush. The base layer has height $h\alpha_h$ where $\alpha_h \in [0, 1]$.

The effective coefficients (6.4.40)-(6.4.44), found using Sequential Homogenisation, are given by

$$A_{11}^{11} = bh\alpha_h \left(Q_{1,11}^{11} + \frac{\left(e_{Q1,11}^{3}\right)^2}{\epsilon_{Q1}^{33}} \right) + bh\left(1-\alpha_h\right) \left(Q_{2,11}^{11} + \frac{\left(e_{Q2,11}^{3}\right)^2}{\epsilon_{Q2}^{33}} \right) - bh\frac{\left(\alpha_h e_{Q1,11}^{3}\epsilon_{Q2}^{33} + \left(1-\alpha_h\right)e_{Q2,11}^{3}\epsilon_{Q1}^{33}\right)^2}{\epsilon_{Q1}^{33}\epsilon_{Q2}^{33}\left(\alpha_h\epsilon_{Q2}^{33} + \left(1-\alpha_h\right)\epsilon_{Q1}^{33}\right)}, \quad (6.8.1)$$

$$D_{11}^{11} = bh^3 \left(Q_{1,11}^{11} + \frac{\left(e_{Q1,11}^{3}\right)^2}{\epsilon_{Q1}^{33}} \right) \left(\frac{\left(\alpha_h - \overline{Z}^{\dagger}\right)^3 + \overline{Z}^{\dagger 3}}{3} \right) + bh^3 \left(Q_{2,11}^{11} + \frac{\left(e_{Q2,11}^{3}\right)^2}{\epsilon_{Q2}^{33}} \right) \left(\frac{\left(1-\overline{Z}^{\dagger}\right)^3 - \left(\alpha_h - \overline{Z}^{\dagger}\right)^3}{3} \right) - bh^3 \frac{\left(\left(\frac{{\alpha_h}^2}{2} - \overline{Z}^{\dagger}\alpha_h \right) e_{Q1,11}^{3}\epsilon_{Q2}^{33} + \left(\frac{1-{\alpha_h}^2}{2} - \overline{Z}^{\dagger}\left(1-\alpha_h\right) \right) e_{Q2,11}^{3}\epsilon_{Q1}^{33} \right)^2}{\epsilon_{Q1}^{33}\epsilon_{Q2}^{33}\left(\alpha_h\epsilon_{Q2}^{33} + \left(1-\alpha_h\right)\epsilon_{Q1}^{33}\right)}, \quad (6.8.2)$$

$$e_{\mathrm{s},11}^{3} = bh\frac{\left(\frac{\alpha_h e_{Q,11}^{3}}{\epsilon_{Q1}^{33}} + \frac{(1-\alpha_h)e_{Q2,11}^{3}}{\epsilon_{Q2}^{33}} \right)}{\left(\frac{\alpha_h}{\epsilon_{Q1}^{33}} + \frac{(1-\alpha_h)}{\epsilon_{Q2}^{33}} \right)}, \quad (6.8.3)$$

$$e_{\mathrm{m},11}^{3} = bh^2\frac{\left(\left(\frac{{\alpha_h}^2}{2} - \overline{Z}^{\dagger}\alpha_h \right) \frac{e_{Q1,11}^{3}}{\epsilon_{Q1}^{33}} + \left(\frac{1-{\alpha_h}^2}{2} - \overline{Z}^{\dagger}\left(1-\alpha_h\right) \right) \frac{e_{Q2,11}^{3}}{\epsilon_{Q2}^{33}} \right)}{\left(\frac{\alpha_h}{\epsilon_{Q1}^{33}} + \frac{(1-\alpha_h)}{\epsilon_{Q2}^{33}} \right)}, \quad (6.8.4)$$

while the neutral surface height is given by

$$Z^{\dagger} = h\overline{Z}^{\dagger} = \frac{hB}{\mathbb{A}^{1111}}, \quad (6.8.5)$$

where

$$B = bh\frac{{\alpha_h}^2}{2} \left(Q_1^{1111} + \frac{\left(e_{Q1}^{113}\right)^2}{\epsilon_{Q1}^{33}} \right) + bh\left(\frac{1-{\alpha_h}^2}{2} \right) \left(Q_2^{1111} + \frac{\left(e_{Q2}^{113}\right)^2}{\epsilon_{Q2}^{33}} \right) - bh\frac{\left(\alpha_h e_{Q1,11}^{3}\epsilon_{Q2}^{33} + \left(1-\alpha_h\right)e_{Q2,11}^{3}\epsilon_{Q1}^{33}\right)\left(\alpha_h{}^2 e_{Q1,11}^{3}\epsilon_{Q2}^{33} + \left(1-\alpha_h{}^2\right)e_{Q2,11}^{3}\epsilon_{Q1}^{33}\right)}{2\epsilon_{Q1}^{33}\epsilon_{Q2}^{33}\left(\alpha_h\epsilon_{Q2}^{33} + \left(1-\alpha_h\right)\epsilon_{Q1}^{33}\right)}. \quad (6.8.6)$$

We will compare the effective coefficients for a composite comprised of PZTA5 as the piezoelectric material and Stycast as the matrix material. We will assess both

methods using three different heights for the base layer.

In Figures 6.9-6.13, we shall use the following conventions: the red curves correspond to Standard Homogenisation, the blue curves correspond to Sequential Homogenisation, and the black curve corresponds to the effective coefficients found when the base layer is purely a ceramic and the top layer is purely a polymer. This is useful because it highlights the difference in performance between pillars of a piezoelectric composite, as opposed to a homogeneous non-piezoelectric layer on the top. We assume that the base layer has height $h\alpha_h$ and that the top layer includes a square pillar, where the ratio of the length of the square pillar to the unit cell is l, and $l \in (0, 1)$. The volume fraction of the inclusion is therefore given by

$$\nu = \alpha_h + (1 - \alpha_h)\, l^2. \tag{6.8.7}$$

In the exploration that follows, we will pick $\alpha_h = 0.05,\ 0.1,\ 0.2$ and then vary l between 0 and 1. This corresponds to varying the size of the pillar. The material parameters for PZTA5 and Stycast are set out in Table 2.1. We will assume the beam will have the dimensions set out in Table 6.2.

Parameter	Size (m)
Length, L	3.00×10^{-4}
Width, b	3.00×10^{-5}
Height, h	4.63×10^{-6}

Table 6.2: Dimensions of our cantilever beam actuator, based on data from [47].

6.8.1 Results

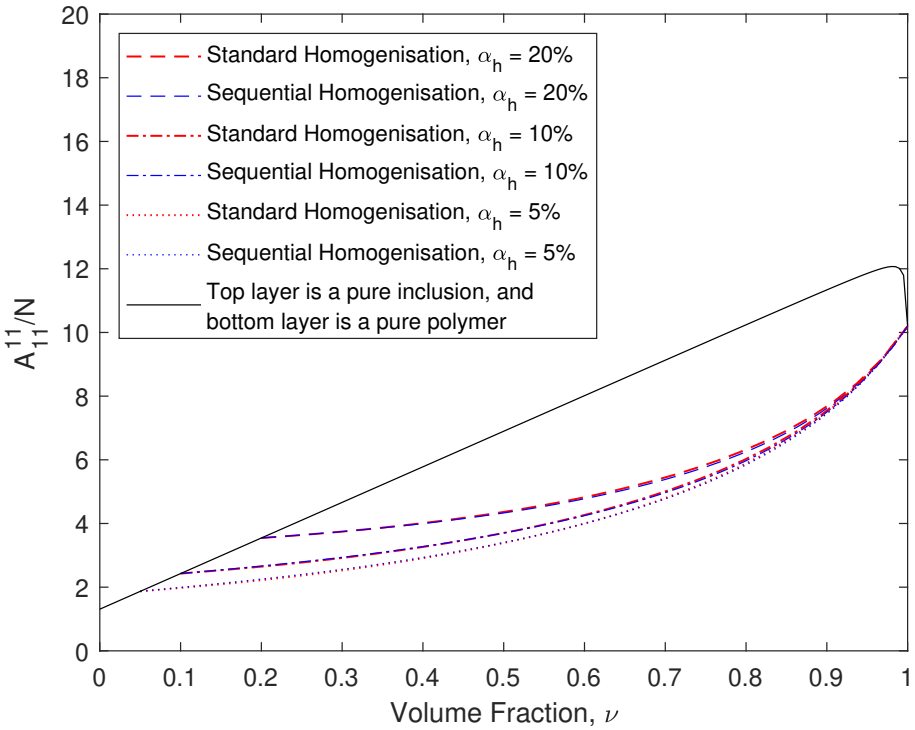


Figure 6.9: Graph showing a comparison of the effective planar stiffness coefficient A_{11}^{11} under each method. The red curves are computed using (6.2.137) and (6.6.11), while the blue curves are computed using the framework established in Chapter 2 together with (6.8.1). The black curve is computed using (6.8.1). To the extent that the red curves are not visible, they overlap with their blue counterparts.

In Figure 6.9 we see how A_{11}^{11} varies with ν. We see that both the Standard Homogenisation and Sequential Homogenisation methods agree closely for all three values of α_h. We also see that where both layers are pure, the stiffness is much stronger than that of a 1-3-2 composite. This indicates that, for a fixed volume fraction, the planar stiffness is stronger if the piezoelectric material is concentrated at the base, rather than in the pillars. We note that for each value of α_h, the volume fraction of PZTA5 cannot be smaller than α_h. This is because $\nu = \alpha_h$ corresponds to the case where both layers are pure, so the blue and red curves will always match the black curve at $\nu = \alpha_h$. We note that the rapid drop for large ν in the black curve is due to the fact that $\epsilon_{I,33} \gg \epsilon_{M,33}$.

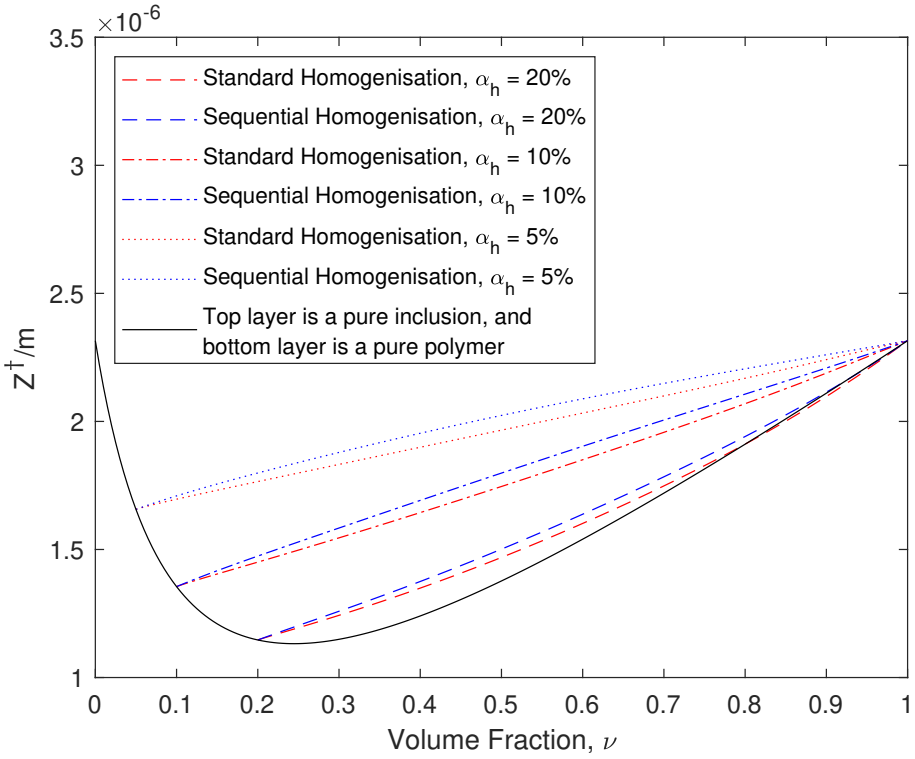


Figure 6.10: Graph showing a comparison of the heights of the neutral surface $Z^\dagger$ under each method. The red curves are computed using (6.2.170) and (6.6.15), while the blue curves are computed using the framework established in Chapter 2, together with equations (6.8.5)-(6.8.6). The black curve is computed using equations (6.8.5)-(6.8.6).

In Figure 6.10 we compare how the height of the neutral surface varies with ν. From this graph, we see that both homogenisation methods give similar results, and predict a monotonic increase as the volume fraction of the inclusion increases. This behaviour can be understood physically. Since the inclusion material has greater stiffness than the surrounding polymer material, increasing the volume fraction of the pillars causes the neutral surface to shift upward. For the case where both layers are uniform, the neutral surface height decreases until it hits a trough and then monotonically increases. This initial decrease happens because the inclusion material, which is stiffer than the matrix material, is located at the bottom of the beam, causing the stiffness distribution to be weighted more towards the base. As the volume fraction increases further, the bottom layer has a stronger influence on the overall bending response, shifting the neutral surface upward.

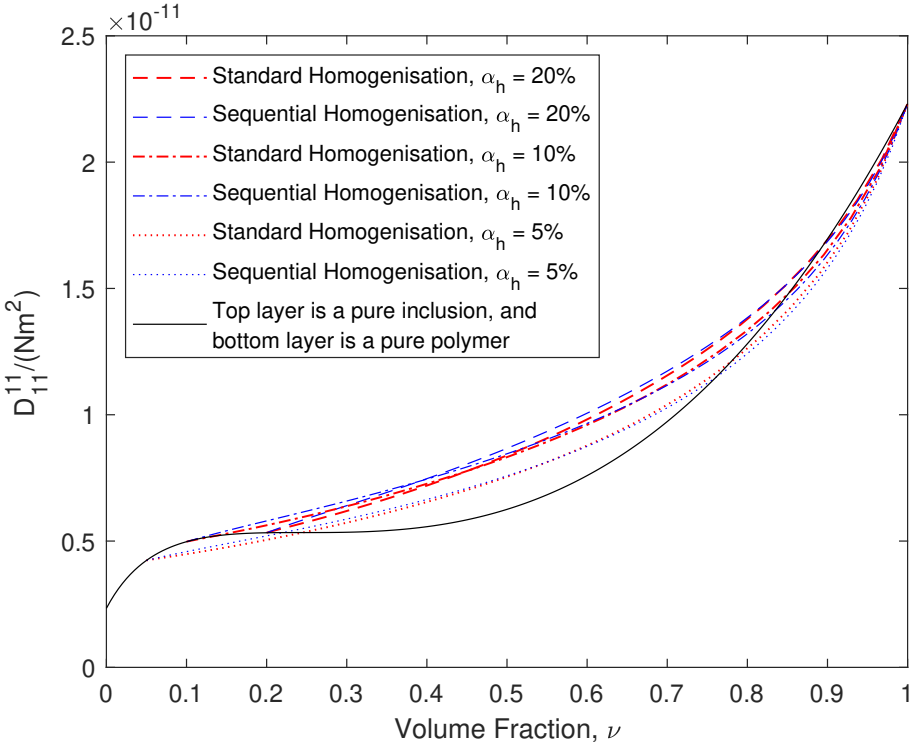


Figure 6.11: Graph showing a comparison of effective flexural rigidity D_{11}^{11} under each method. The red curves are computed using (6.2.140) and (6.6.13), while the blue curves are computed using the framework established in Chapter 2 together with (6.8.2). The black curve is computed using (6.8.2).

In Figure 6.11, we see how D_{11}^{11} varies with ν. From this graph, we see that both homogenisation methods agree very well for all three values of α_h. In the case where both layers are homogeneous (the black curve), we see that the effective flexural rigidity has a local peak near $\nu = 0.2$ and a local trough near $\nu = 0.4$, after which it increases monotonically. This pattern is caused by the shifting of the position of the neutral surface, which temporarily reduces the flexural rigidity before it begins to rise again. We note that when both the base and top materials are pure, the effective flexural rigidity is less strong than when the pillars are present, showing that the presence of the pillars enhances the rigidity.

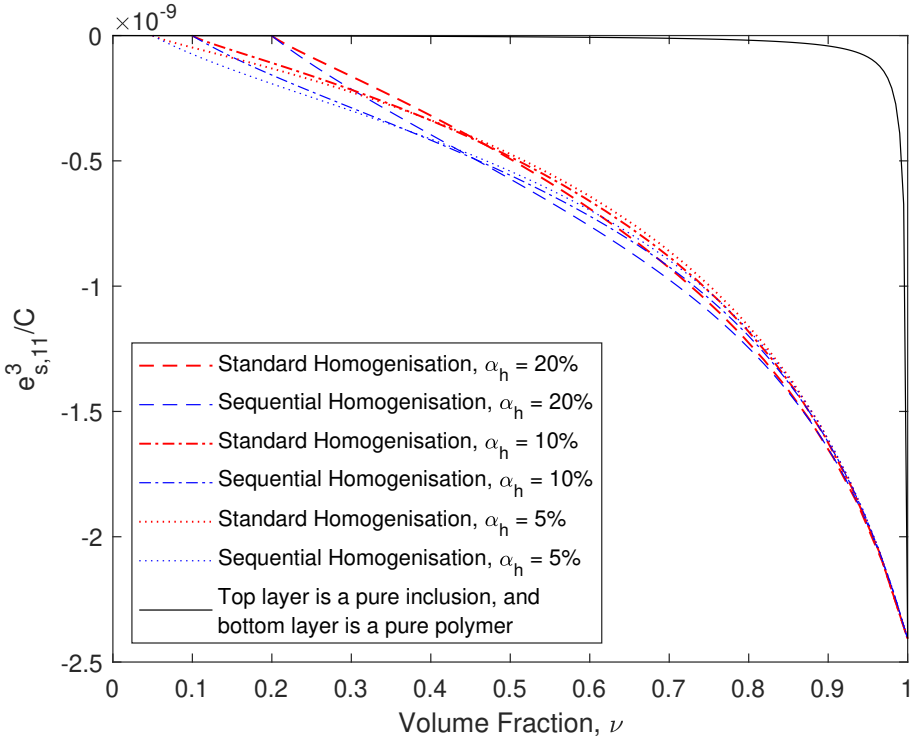


Figure 6.12: Graph showing a comparison of effective piezoelectric stress coefficient $e^3_{s,11}$ under each method. The red curves are computed using (6.2.141) and (6.6.12), while the blue curves are computed using the framework established in Chapter 2 together with (6.8.3). The black curve is computed using (6.8.3).

In Figure 6.12 we show how $e^3_{s,11}$ varies with ν. We see that there is close agreement between both homogenisation methods. Where both layers are homogeneous, we see that the piezoelectric stress coefficient is much less prominent than when there are pillars in the top layer, which is expected as the pillars make the piezoelectric response stronger.

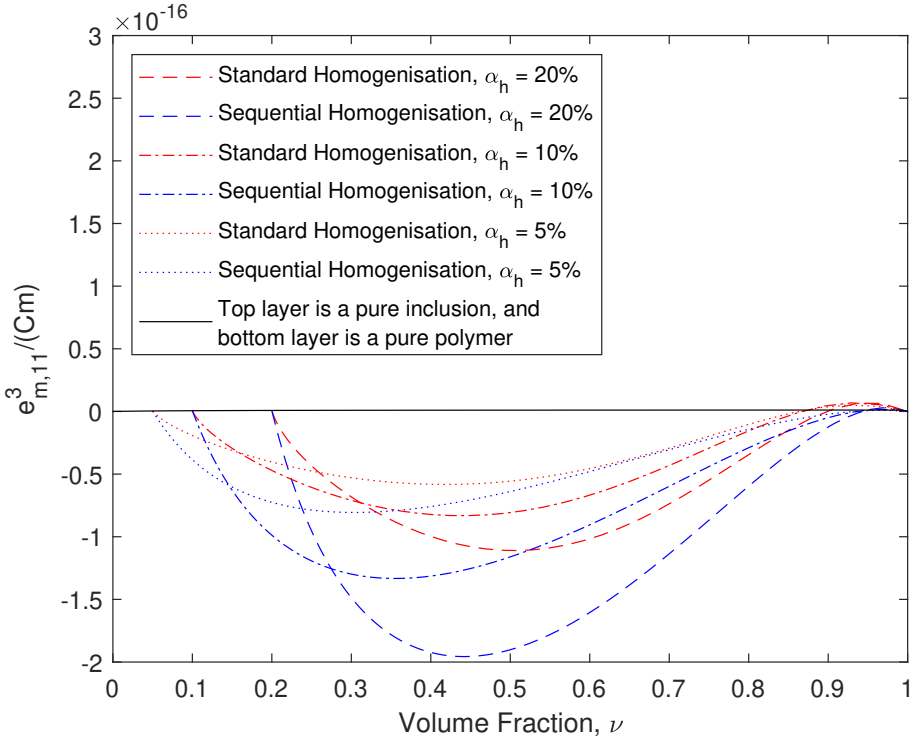


Figure 6.13: Graph showing a comparison of effective piezoelectric bending moment coefficient $e^3_{m,11}$ under each method. The red curves are computed using (6.2.142) and (6.6.14), while the blue curves are computed using the framework established in Chapter 2 together with (6.8.4). The black curve is computed using (6.8.4).

In Figure 6.13 we show how $e^3_{m,11}$ varies with ν. We see that there is a significant difference between the predictions given under the two homogenisation methods (i.e., between the red and blue curves). This suggests that when predicting effective piezoelectric bending moments, the Standard Homogenisation method should be used, as this captures the interplay between the boundaries between neighbouring layers more accurately than the Sequential Homogenisation.

It should be noted that the Sequential Homogenisation method appears to significantly overstate the piezoelectric response. This suggests that the piezoelectric bending moment is highly sensitive to the geometry of the inclusions and demonstrates that including the interactions between neighbouring layers is important when predicting the effective piezoelectric bending moment coefficient. In the case where both layers are homogeneous, we see that the effective bending moment coefficient is negligible.

We now explore how the dimensionalised frequency of the lowest mode of oscillation varies with the volume fraction of PZTA5 for the simply supported beam and cantilever beam.

Firstly we define the dimensionalised frequency coefficient ω as

$$\omega = \left(\frac{L}{\varepsilon}\sqrt{\frac{\rho_{unit}}{c_{\text{typ}}}}\right)^{-1}\sqrt{\frac{\left(\frac{D^{11}_{\text{eff},11}}{c_{\text{typ}}bh^3}\right)}{\left(\frac{\rho_{\text{eff}}}{\rho_{unit}}\right)}} = \frac{1}{L^2}\sqrt{\frac{D^{11}_{\text{eff},11}}{\rho_{\text{eff}}bh}}. \tag{6.8.8}$$

This factor gives us the timescale of the oscillations in the homogenised problem and will enable us to convert between dimensionless frequencies and dimensionalised frequencies. The frequency for the lowest mode of oscillation for the simply supported beam problem is

$$f_1 = \frac{\pi^2}{2\pi}\omega = \frac{\pi}{2L^2}\sqrt{\frac{D^{11}_{\text{eff},11}}{\rho_{\text{eff}}bh}}, \tag{6.8.9}$$

while for the cantilever beam problem, the frequency is

$$f_1 = \frac{k_1^2\omega}{2\pi} = \frac{k_1^2}{2\pi L^2}\sqrt{\frac{D^{11}_{\text{eff},11}}{\rho_{\text{eff}}bh}}. \tag{6.8.10}$$

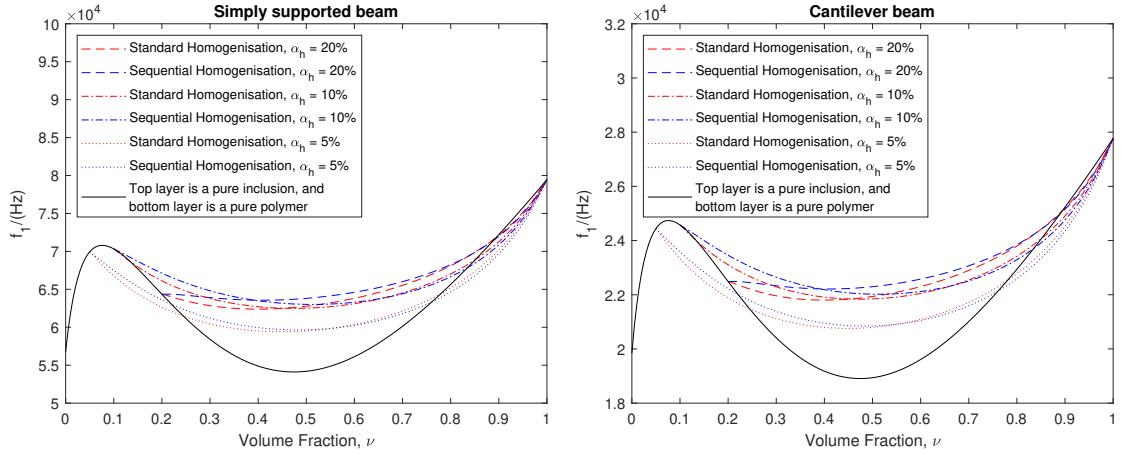


Figure 6.14: Graphs showing how the frequency of the lowest mode of oscillation f_1 varies with the volume fraction of PZTA5, in respect of boundary conditions for the simply supported beam and the cantilever beam problems. The red curves are computed using equations (6.2.140), (6.2.161), (6.6.13), (6.6.16), (6.8.9) and (6.8.10), while the blue curves are computed using the framework established in Chapter 2 together with equations (6.8.2), (6.2.161), (6.6.16), (6.8.9), and (6.8.10). The black curve is computed using equations (6.8.2), (6.2.161), (6.6.16), (6.8.9), and (6.8.10).

In Figure 6.14, we show how f_1 varies with ν for the two cases. We see that the thicker the base layer, the greater the initial deviation between the two methods for smaller values of l. We note that the red and blue curves start decreasing until reaching a trough and then monotonically increase after that. This shows that

the presence of pillars enhances the minimum frequency as well as the piezoelectric effects.

6.9 Case study of Sequential Homogenisation: Jungle Gym

We now explore how for a 3-3 composite the effective coefficients of a piezoelectric actuator vary with the volume fraction of PZTA5 under the two methods. We recall that this structure, also known as a Jungle Gym, is a 3D lattice made from rods which interconnect in three spatial directions (see Figure 5.8).

As in §6.8, we will compare results from the Standard Homogenisation and the Sequential Homogenisation methods. In the Standard Homogenisation case, we assume that the actuator is one cell high and apply the homogenisation procedure established in §6.2.4. In the Sequential Homogenisation case, we assume that the actuator is infinitely many cells high, homogenise using the method in Chapter 2, then apply the multilayer beam formulae derived in §6.4.7 to the result.

6.9.1 Standard Homogenisation set-up

The effective coefficients are computed using the notation in Figure 6.15 and the formulae given in §6.2.

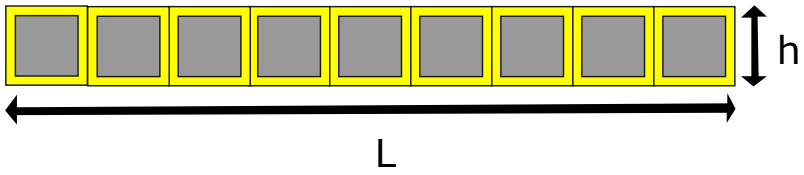


Figure 6.15: Schematic of a Jungle Gym actuator which is one cell high.

6.9.2 Sequential Homogenisation set-up

To obtain the effective coefficients, we start by calculating effective 'unadjusted' coefficients using the formulae given in §2.7.2. We then work out the 'adjusted' material coefficients using (6.4.1)-(6.4.3). Finally, we use the notation in Figure 6.16 and the formulae given in §6.4.7 to work out the effective coefficients.

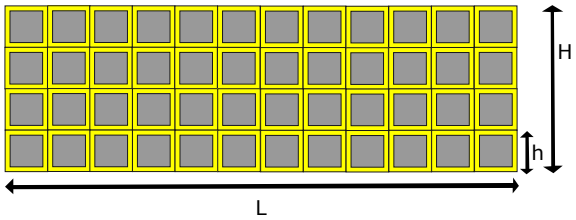


Figure 6.16: Schematic of a Jungle Gym actuator that is infinitely many cells high.

6.9.3 Results

We will compare how the effective planar stiffness coefficient A_{11}^{11}, the effective flexural rigidity D_{11}^{11}, the effective piezoelectric stress coefficient $e_{s,11}^{3}$ and the dimensionalised frequency of the lowest mode of oscillation vary with the volume fraction of PZTA5 under both homogenisation methods. Note that due to symmetry, under both methods $Z^{\dagger} = h/2$ and $e_{m,11}^{3} = 0$. For that reason, we will not investigate the neutral surface height nor the piezoelectric bending moment.

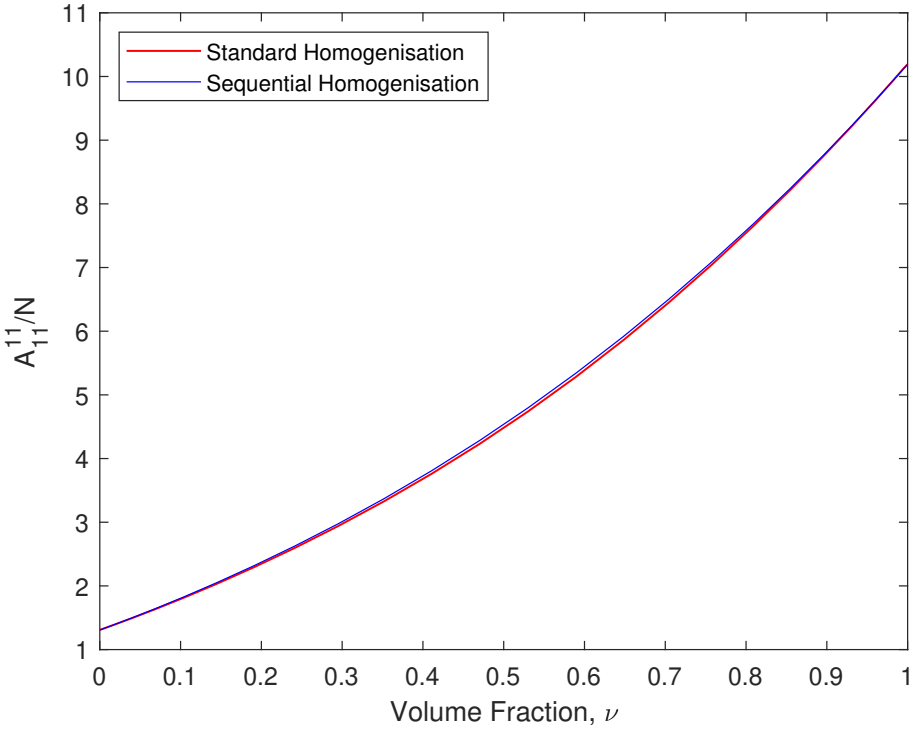


Figure 6.17: Graph showing a comparison of the effective planar stiffness coefficient A_{11}^{11} under each method. The red curves are computed using equations (6.2.137) and (6.6.11), while the blue curves are computed using the framework established in Chapter 2 together with equations (6.4.45), (6.6.11) and (6.6.17).

In Figure 6.17, we show how the effective planar stiffness coefficient varies with the volume fraction of PZTA5 under the two methods. We see that there is excellent

agreement between both approaches with the results appearing identical. We see that the effective planar stiffness coefficient increases monotonically with the volume fraction of PZTA5, as expected.

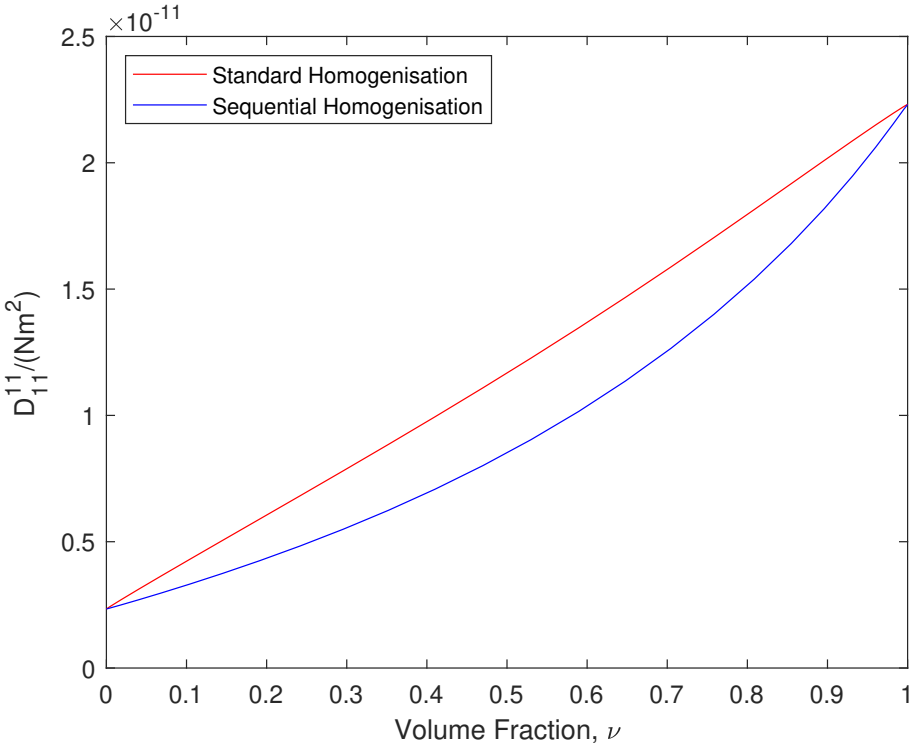


Figure 6.18: Graph showing a comparison of effective flexural rigidity D_{11}^{11}. The red curves are computed using equations (6.2.140) and (6.6.13), while the blue curves are computed using the framework established in Chapter 2, together with equations (6.4.47), (6.6.13) and (6.6.17)-(6.6.19).

In Figure 6.18, we show how the effective flexural rigidity varies with the volume fraction of PZTA5 under the two methods. We see that while both methods show a monotonic increase with the volume fraction of PZTA5, there is a significant difference between the two, with Standard Homogenisation predicting a more rigid structure than Sequential Homogenisation. This can be explained by the fact that in the 1-layer case, the highly stiff PZTA5 is concentrated away from the neutral surface, whereas in the case of infinite layers the highly stiff PZTA5 is more evenly spread out across the device, making the contributions to flexural rigidity smaller.

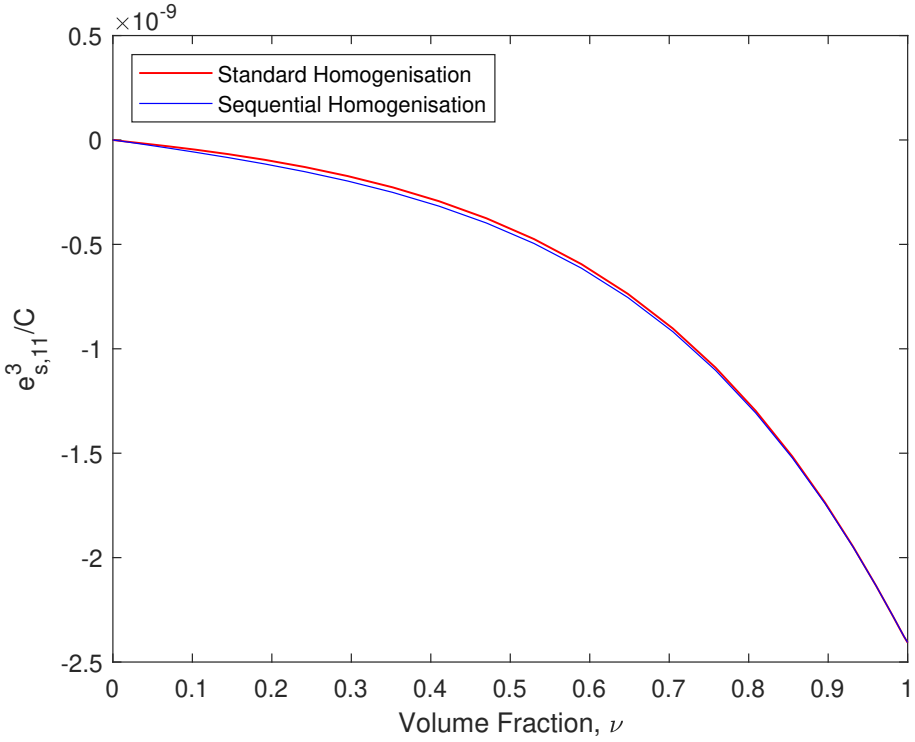


Figure 6.19: Graph showing a comparison of the effective piezoelectric stress coefficient $e^3_{s,11}$ under each method. The red curves are computed using equations (6.2.141) and (6.6.12), while the blue curves are computed using the framework established in Chapter 2 together with equations (6.4.48), (6.6.12) and (6.6.18).

In Figure 6.19, we show how the effective piezoelectric stress coefficient varies with volume fraction of PZTA5. We see that there is close agreement between the methods with the stress decreasing (i.e., becoming more negative) as the volume fraction increases.

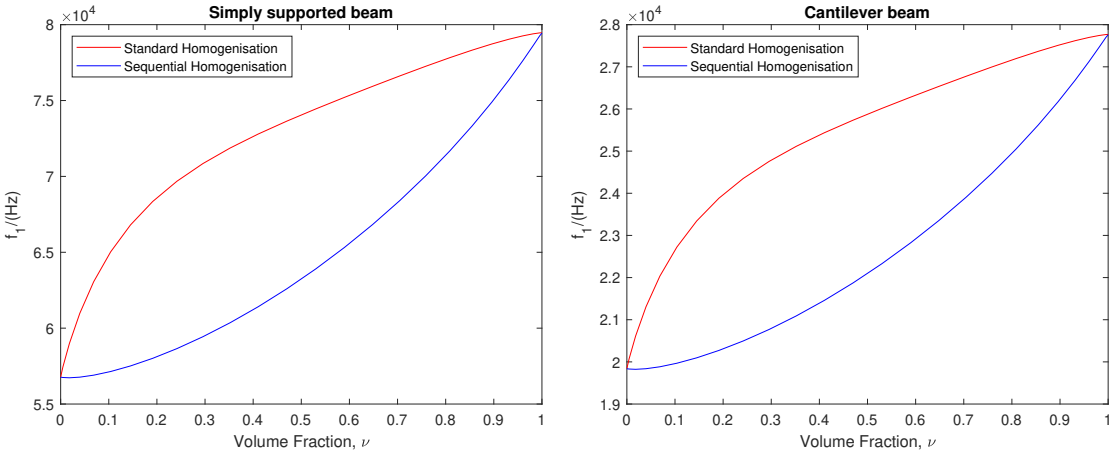


Figure 6.20: Graphs for the Simply Supported Beam and Cantilever Beam problems showing how the frequency of the lowest mode of oscillation f_1 varies between the two methods. The red curves are computed using equations (6.2.140), (6.2.161), (6.6.13), (6.6.16), (6.8.9) and (6.8.10), while the blue curves are computed using the framework established in Chapter 2 together with equations (6.2.161), (6.4.47), (6.6.13), (6.6.16), (6.8.9) and (6.8.10).

In Figure 6.20, we show how the frequencies of oscillation vary for the simply supported and cantilever beam problems under the two methods. We see that when the actuator is one cell high and the thickness is small, the frequency of oscillation is higher than when the actuator is infinitely many cells high. The higher minimal frequency is due to the fact that when the actuator is only one cell high, the material has higher flexural rigidity (as we originally showed in Figure 6.18). We note that adding infinite layers seems to have less effect on the effective flexural rigidity compared to the one-layer case. This suggests that the inclusion of more layers causes the behaviour of the materials to converge with the properties of a material with a uniform distribution of stress.

Finally, we see that the red curve is concave, while the blue curve is convex. This shows that when the beam is just one layer high, the dimensionalised frequency of the lowest mode of oscillation is highly sensitive to the length of the rods but becomes less sensitive when the rods lengthen. On the other hand, when the beam is infinitely many cells high, the dimensionalised frequency of the lowest mode of oscillation changes only slightly for small rods, but for the longer rods the averaged properties grow more rapidly, causing the convex profile.

6.10 Conclusions

We have extended our model by combining the asymptotic homogenisation framework with a small-aspect-ratio expansion.

We found that:

- The mechanical and piezoelectric bending moment tensors are dependent on the distributions of the stiffness and piezoelectric stress, respectively. Contributions to flexural rigidity and piezoelectric bending moments are stronger if they are located away from the neutral surface. This gives us insight into how the distribution of stiffness and piezoelectric stress contributes to the flexural rigidity and piezoelectric bending moments. Such insights can be used in optimising the design of piezoelectric materials.

- The alternative Sequential Homogenisation method gives reliable predictions for the stiffness coefficients but is less accurate for the piezoelectric coefficients. This suggests that piezoelectric coefficients are more sensitive to the microstructural geometry than the stiffness coefficients.

- The extra force arising from the inverse piezoelectric effect acts as an internal driving force within the beam, adding to or opposing the usual bending forces. This causes the frequencies of oscillation to shift, which in turn alters the bending path. Since the bending path and resonant behaviour are not fixed properties, they can be tuned by varying the electrical boundary conditions.

- The optimal performance of a piezoelectric transducer requires careful balancing of stiffness and geometry. Increasing the piezoelectric content strengthens electromechanical coupling, improving the conversion between electrical and mechanical energy, but also raises the effective stiffness of the structure. Excessive stiffness suppresses deformation, whereas excessive compliance weakens the force transmission. Consequently, optimal transducer performance is achieved when strong electromechanical coupling is balanced against the required level of mechanical compliance.

- The spatial placement of piezoelectric and non-piezoelectric layers, together with the stiffnesses, electromechanical couplings, permittivities and thickness ratios of each layer all affect the bending properties of a piezoelectric actuator.

The physical insights summarised above illustrate how useful asymptotic homogenisation is to manufacturers in early stage design of composites and devices. Such insights would not be available from direct FEM simulation on its own.

Chapter 7

Conclusions

7.1 Review of thesis

Asymptotic homogenisation provides a mathematically systematic process of averaging. This method is particularly useful to work out the macroscale properties of piezoelectric composites, which are otherwise difficult to model.

In this thesis, we set out to build a simple suite of models to understand the effective properties of piezoelectric composites with periodic microstructures. We then used these models to study the behaviour of piezoelectric sensors and actuators.

In Chapter 1, we presented an overview of the numerous applications of real-world piezoelectric devices. We then discussed the leading methodologies in the literature for modelling piezoelectric composites.

In Chapter 2, we established the linearised piezoelectric equations of motion which govern the behaviour of both the mechanical displacement and electric potential of the material. We then used asymptotic homogenisation to derive an approximation of the solutions to these governing equations which are valid at the macroscale. This involved introducing independent microscopic position variables and assuming that the ratio of the characteristic distance between inclusions and the length of the device, ε, is small. We then altered the partial derivatives to account for the microscopic variations arising from the microscopic variables. We introduced asymptotic expansions for the two unknowns, and assumed that they satisfied appropriate periodic boundary conditions in the microscopic variables. After equating terms with equal powers of ε, we deduced that the leading-order solutions were independent of the microscale. At the next order, we determined the 'cell problems' which describe how the microscale structure distorts the strain and electric fields locally. We solve these cell problems using the Finite Element Method. Finally, at the subsequent order, we found the effective equations which describe the behaviour of the leading-order solutions on the macroscale. These depend on the effective

stiffness, electromechanical, and dielectric tensors which may be calculated from the solutions to the cell problems. The cell functions encode the contribution of microscopic physics, arising from interactions between neighbouring phases, in the macroscopic framework.

In Chapter 3, we calculated the effective stiffness, electromechanical, and dielectric coefficients for a range of composites and compared the results derived from three other methodologies, namely the Differential Effective Medium (DEM) [4], the Method Of Mixtures (MoM) [53], and the RVE [44] approaches, with our results. We found that the results from the RVE method had the best overall agreement with our results, particularly when predicting the coefficients corresponding to the planar (X- and Y-) directions. With regards to the coefficients corresponding to the thickness (Z-) direction, both the MoM and the DEM approaches had results with excellent agreement with results from our method, with the MoM approach being less computationally demanding than the DEM and RVE methods. We found that the results from the RVE method had close agreement with our method for all coefficients and volume fractions, but with higher computational cost than DEM and MoM.

In Chapter 4, we derived polynomial approximations for the effective coefficients found in Chapter 2, when the ratio of the volume of inclusions to the composite is small. Under this method, we treat each inclusion as if it were isolated, and use the resulting inner solutions to generate periodic solutions for the outer problems. We derived low-volume-fraction approximations for the coefficients under the DEM and MoM approaches and evaluated the differences between these two approximations and those derived for our method, by comparing the coefficients in the respective expansions. We then compared the low-volume-fraction polynomials against numerical solutions to the full cell problems, observing excellent agreement when the volume fraction of inclusions was less than 30%, which validated our low-volume-fraction method.

In Chapter 5, we applied our homogenisation framework to predict the behaviour of bulk sensors, by first studying the idealised case of a half-space transducer, and then considered the more common case of a finite-thickness transducer. For the two cases, we modelled the voltage output coefficient, mechanical impedance and wave speed, noting that for 1-3 and 2-2 composites, the variation in this coefficient was minimal, which is consistent with the predictions in [53]. Similarly, in respect of the half-space transducer, we modelled mechanical impedance and wave speed and found that that for 1-3 and 2-2 composites there was negligible variation of these coefficients.

Finally, in Chapter 6, we refined the model we established in Chapter 2 in order to model a thin-layer, or beam, actuator. We did this by incorporating non-linear coupling effects. These effects arise in thin-layer actuators from the inverse piezoelectric effect where large transverse electric fields are present. By linearising around zero displacement and a linear electric potential profile, we developed an asymptotic homogenisation beam model which allowed us to analyse the properties of actuators made of plates or laminates. We subsequently derived a simplified version of this beam model, which we named Sequential Homogenisation. We compared the accuracy of Sequential Homogenisation for the following coefficients: effective planar stiffness, neutral surface height, flexural rigidity, piezoelectric stress, and bending moment. We found that:

- Multilayer structures introduce anisotropic stiffness, which can be fine-tuned by adjusting layer sequence and stiffness of the phases within the composite material.
- The spatial distribution of stiffness and piezoelectric coupling within the beam's cross-section has a significant effect on both flexural rigidity and magnitude of bending moments. This indicates that if layers or inclusions are placed away from the neutral surface, the effective rigidity will increase.
- If a significant increase in bending stiffness and actuation power is needed, strong piezoelectric layers should be placed near the outer surface of the beam, with passive layers placed near the neutral surface.
- Our simplified, Sequential Homogenisation method provides good approximations for effective planar stiffness, neutral surface height, flexural rigidities, piezoelectric stress and bending moment coefficients but less reliably predicts the piezoelectric coupling terms, showing that the latter have sensitive dependence on the geometry.
- As demonstrated by various examples, our beam model provides a powerful way of exploring bending and tip deflection across a wide range of geometries.

7.2 Concluding remarks

The asymptotic homogenisation framework we have developed provides manufacturers with a powerful and efficient way to design and optimise existing and new piezoelectric composites and devices to achieve desired properties, such as efficiency of actuation, resonance frequencies, sensitivity, and bandwidth.

The strength of the two-scale homogenisation approach lies in separating the analysis of the composite material at the microscale from the simulation of the device at the macroscale (see [1] and [8]). As there is a clear separation of scales, iterating over new material geometries requires modification of the microscale problem only, without the need to repeatedly solve over the device as a whole for each iteration. As a result, the iterative design process becomes computationally feasible, and vastly more efficient than direct numerical simulation of the full microstructure within the device, where the latter require solving millions of coupled equations.

Using our framework, researchers can easily explore a wide range of possible geometries at the unit cell level. Our method is efficient as it enables manufacturers to rapidly explore multiple options, allowing them to only carry out full FEM simulations and fabrication of prototypes for the most promising configurations, thereby speeding up the design process, reducing the reliance on trial and error, minimising computational costs and experimental resources.

7.3 Future work

Our suggestions for further work include:

- Validation of our models

  It would be valuable to validate our models computationally (ideally through specialised FEM software used in industry such as ABAQUS or COMSOL), or experimentally.

- Optimisation of material properties and device operation

  To further illustrate the utility of the proposed framework, it would be useful to investigate the optimisation of piezoelectric composite materials by systematically varying microstructural parameters, exploring how changes in inclusion geometry and lattice structure influence strain and electrical fields at the microstructure, and hence the macroscopic performance of the device. Such investigations would demonstrate how the framework may be used to design and optimise the performance of existing and new materials, allowing the tailoring of composite microstructures to achieve the macroscopic behaviour and operational performance of the device.

- Modelling of thin-layer sensors

  In Chapters 5 and 6, we explored how to model bulk sensors and thin-layer actuators, by considering aspects of wave and beam theory, respectively. It

would be valuable to extend the model to cover thin-layer sensors. To take into account phenomena present in such sensors, including wave propagation, bending, and interactions between the fluid and solid regions, a combination of aspects of wave and beam theory would need to be incorporated into our model.

- Where analysis of macroscopic boundary effects is needed

  Our homogenisation framework relies on the assumption of separation of scales, and is therefore valid in the interior of the domain. As a result, our models do not explicitly account for any boundary layer effects which may arise near the macroscopic boundaries of the device. In order to establish the precise behaviour of the system near the macroscopic boundaries, boundary layer theory would need to be incorporated into our model.

- Modelling sensors with short wavelengths

  Classical homogenisation begins to fail for sensors for which the excitation wavelength is of a similar size to the distance between neighbouring inclusions. To address this, the Bloch Wave homogenisation framework (see [2]) could be used instead. This framework uses an ansatz that incorporates both the periodicity and wave-like nature of the solution in the governing piezoelectric equations (2.4.15)-(2.4.16).

- Frequency-dependent parameters

  Since our leading-order AHM assumes that the material parameters are piecewise constant, our models cannot capture frequency-dependent material properties, and may miss resonant shifts or damping behaviour. To address this, the governing equations could be modified by making the microscale material parameters frequency-dependent, and the homogenisation process could be used to see how the frequency dependency manifests in the microscale equations.

- Where microstructure is not fully periodic or bonding is imperfect

  Our models assume fully periodic microstructure and perfect bonding between phases. However in the real-world, due to fabrication processes, materials designed to be periodic can be somewhat irregular or random in structure and the interfaces can be imperfect. In order to address this, our framework could be developed to incorporate random effects using more sophisticated methods, such as Stochastic Homogenisation.

- Where system has small non-linear effects

  All our models are linearised, which makes the homogenisation process more convenient but limits its applicability to cases where the strains (and sometimes also the strain gradients) are small. For small non-linear effects, solutions may be found by introducing higher-order correction terms, or by using a two-parameter asymptotic expansion.

- Exotic geometries

  A key strength of our homogenisation framework is that its applicability is not restricted to any specific inclusion shape, size, orientation or lattice structure. This is not the case for most of the analytical models in the literature which only work for particular, conventional, geometries. It would be valuable in future work to study more exotic geometries. There is an increasing demand for such geometries due to technological advances, and developments in the fabrication process (including 3D printing).

Chapter 8

Bibliography

[1] Grégoire Allaire. Homogenization and two-scale convergence. *SIAM Journal on Mathematical Analysis*, 23(6):1482–1518, 1992.

[2] Grégoire Allaire and Carlos Conca. Bloch wave homogenization and spectral asymptotic analysis. *Journal de Mathématiques Pures et Appliquées*, 77:153–208, 1998.

[3] Igor V. Andrianov, Vladyslav V. Danishevskyy, Alain Guillet, and Philippe Pareige. Effective properties and micro-mechanical response of filamentary composite wires under longitudinal shear. *European Journal of Mechanics A-solids*, 24:195–206, 2005.

[4] Marco Avellaneda and Pieter Swart. Calculating the performance of 1–3 piezoelectric composites for hydrophone applications: An effective medium approach. *Journal of the Acoustical Society of America*, 103:1449–1467, 1998.

[5] Rüdiger G. Ballas. *Piezoelectric Multilayer Beam-Bending Actuators: Static and Dynamic Behavior and Aspects of Sensor Integration (Microtechnology and MEMS)*. Springer, 2007.

[6] G. K. Batchelor. *An Introduction to Fluid Dynamics*. Cambridge University Press, Cambridge, UK, 2000.

[7] Carl M Bender and Steven A. Orszag. *Advanced Mathematical Methods For Scientists And Engineers*. McGraw-Hill, 1979.

[8] Alain Bensoussan, Jacques-Louis Lions, and George Papanicolaou. *Asymptotic Analysis for Periodic Structures*. North-Holland Publishing Company, Amsterdam, 1978.

[9] H. Berger, Sreedhar Kari, Ulrich Gabbert, Reinaldo Rodríguez-Ramos, Julián Bravo-Castillero, and Raúl Guinovart-Díaz. Calculation of effective coefficients for piezoelectric fiber composites based on a general numerical homogenization technique. *Composite Structures*, 71:397–400, 2005.

[10] Harald Berger, Sreedhar Kari, Ulrich Gabbert, Reinaldo Rodriguez-Ramos, Raul Guinovart, Jose A. Otero, and Julian Bravo-Castillero. An analytical and numerical approach for calculating effective material coefficients of piezoelectric fiber composites. *International Journal of Solids and Structures*, 42(21):5692–5714, 2005.

[11] Renald Brenner. Numerical computation of the response of piezoelectric composites using Fourier transform. *Physical Review B*, 79:184106, 2009.

[12] Wenwu Cao and Wenkang Qi. Plane wave propagation in finite 2-2 composites. *Journal of Applied Physics*, 78:4627–4632, 1995.

[13] Julián Bravo Castillero, José A. Otero, R. R. Ramos, and Alain Bourgeat. Asymptotic homogenization of laminated piezocomposite materials. *International Journal of Solids and Structures*, 35:527–541, 1998.

[14] K.S. Challagulla and T.A. Venkatesh. Electromechanical response of 2-2 layered piezoelectric composites: A micromechanical model based on the asymptotic homogenization method. *Philosophical Magazine*, 89(14):1197–1222, 2009.

[15] H. L. W. Chan. *Piezoelectric ceramic/polymer 1–3 composites for ultrasonic transducer applications*. PhD thesis, Macquarie University, Sydney, Australia, 1987.

[16] H. L. W. Chan and J. Unsworth. Simple model for piezoelectric ceramic/polymer 1–3 composites used in ultrasonic transducer applications. *IEEE Transactions on Ultrasonics, Ferroelectrics, and Frequency Control*, 36(4):434–441, 1989.

[17] Philippe G. Ciarlet. *Mathematical Elasticity, Volume I: Three-Dimensional Elasticity*. North-Holland, Amsterdam, 1988.

[18] Jacques Curie and Pierre Curie. Développement par pression de l'électricité polaire dans les cristaux hémièdres à faces inclinées. *Comptes Rendus de l'Académie des Sciences*, 91:294–297, 1880.

[19] Martin L. Dunn and Minoru Taya. An analysis of piezoelectric composite materials containing ellipsoidal inhomogeneities. *Proceedings of the Royal Society of London. Series A: Mathematical and Physical Sciences*, 443:265 – 287, 1993.

[20] Martin L. Dunn and Minoru Taya. Electromechanical properties of porous piezoelectric ceramics. *Journal of the American Ceramic Society*, 76(7):1697–1706, 1993.

[21] John Douglas Eshelby. The determination of the elastic field of an ellipsoidal inclusion, and related problems. *Proceedings of the Royal Society of London. Series A, Mathematical and physical sciences*, 241(1226):376–396, August 1957.

[22] Lawrence C. Evans. *Partial Differential Equations, Second edition.* American Mathematical Society, 2010.

[23] Xue feng Zhao and Yichao Zhu. A general leading-order asymptotic theory of thin microstructural plates and uncertainty quantification of the elastic performance of composite laminates. *Journal of Composite Materials*, 57:3145 – 3171, 2023.

[24] Pedro M. Ferreira, Miguel A Machado, Catarina Vidal, and Marta S. Carvalho. Modelling electro-mechanical behaviour in piezoelectric composites: Current status and perspectives on homogenisation. *Adv. Eng. Softw.*, 193:103651, 2024.

[25] Raúl Guinovart-Díaz, Julián Bravo-Castillero, Reinaldo Rodríguez-Ramos, Federico J. Sabina, and R. Martinez-Rosado. Overall properties of piezocomposite materials 1–3. *Materials Letters*, 48:93–98, 2001.

[26] T. R. Gururaja. *Piezoelectric Composite Materials for Ultrasonic Transducer Applications.* PhD thesis, The Pennsylvania State University, University Park, PA, USA, May 1984.

[27] T. R. Gururaja, W. A. Schulze, L. E. Cross, B. A. Auld, Y. A. Shih, and Y. Wang. Resonant modes of vibration in piezoelectric PZT–polymer composites with two-dimensional periodicity. *IEEE Transactions on Ultrasonics, Ferroelectrics, and Frequency Control*, 34(2):183–186, 1984.

[28] T. R. Gururaja, W. A. Schulze, L. E. Cross, R. E. Newnham, B. A. Auld, and Y. Wang. Resonant modes in piezoelectric PZT rod–polymer composite materials. In *Proceedings of the IEEE Ultrasonics Symposium*, pages 523–527, 1984.

[29] T. R. Gururaja, W. A. Schulze, L. E. Cross, R. E. Newnham, B. A. Auld, and Y. J. Wang. Piezoelectric composite materials for ultrasonic transducer applications. Part I: Resonant modes. *IEEE Transactions on Sonics and Ultrasonics*, SU-32(4):481–498, 1985.

[30] Ouassim Hamdi, Frej Mighri, and Denis Rodrigue. *Piezoelectric polymer films: synthesis, applications, and modeling*, pages 79–101. Woodhead Publishing Series in Composites Science and Engineering. Woodhead Publishing, 2020.

[31] Zvi Hashin. Analysis of composite materials—a survey. *Journal of Applied Mechanics*, 50:481–505, 1983.

[32] E M Hassan, A L Kalamkarov, A V Georgiades, and K S Challagulla. An asymptotic homogenization model for smart 3d grid-reinforced composite structures with generally orthotropic constituents. *Smart Materials and Structures*, 18(7):075006, June 2009.

[33] Johan Helsing. An integral equation method for elastostatics of periodic composites. *Journal of The Mechanics and Physics of Solids*, 43:815–828, 1995.

[34] Rodney Hill. A self-consistent mechanics of composite materials. *Journal of The Mechanics and Physics of Solids*, 13:213–222, 1965.

[35] Peter D. Howell, Gregory Kozyreff, and John R. Ockendon. *Applied Solid Mechanics*. Cambridge University Press, 2009.

[36] John David Jackson. *Classical Electrodynamics*. Wiley, New York, 3 edition, 1998.

[37] E Jacquet, F Trivaudey, and D Varchon. Calculation of the transverse modulus of a unidirectional composite material and of the modulus of an aggregate. Application of the rule of mixtures. *Composites Science and Technology*, 60(3):345–350, 2000.

[38] B. Jaffe, W. R. Cook, and H. Jaffe. *Piezoelectric Ceramics*. Academic Press, London, 1971.

[39] Alexander L. Kalamkarov and Marcelo Amorim Savi. Micromechanical modeling and effective properties of the smart grid-reinforced composites. *Journal of The Brazilian Society of Mechanical Sciences and Engineering*, 34:343–351, 2012.

[40] Ronit Kar-Gupta and T. A. Venkatesh. Electromechanical response of 1-3 piezoelectric composites: Effect of poling characteristics. *Journal of Applied Physics*, 98:054102, 2005.

[41] Ronit Kar-Gupta and T. A. Venkatesh. Electromechanical response of 1–3 piezoelectric composites: An analytical model. *Acta Materialia*, 55:1093–1108, 2007.

[42] L. D. Landau and E. M. Lifshitz. *Fluid Mechanics*, volume 6 of *Course of Theoretical Physics*. Butterworth-Heinemann, Oxford, 2 edition, 1987.

[43] Hongliang Li, Pingbing Ming, and Huiyu Wang. H2- Korn's Inequality and the Nonconforming Elements for The Strain Gradient Elastic Model. *J. Sci. Comput.*, 88:78, 2021.

[44] Yan Li, H T Zheng, Shi-guo Long, and Liang Wu. Effects of the piezoelectric phase's geometric properties on effective coefficients of 1–3 piezoelectric composites. *Computational Materials Science*, 50:2135–2141, 2011.

[45] Mohammad Ali Mangi, Hassan Elahi, Ahsan Ali, Hamid Jabbar, Anas Bin Aqeel, Aasia Farrukh, Saira Bibi, Wael A. Altabey, Sallam A. Kouritem, and Mohammad Noori. Applications of piezoelectric-based sensors, actuators, and energy harvesters. *Sensors and Actuators Reports*, 9:100302, 2025.

[46] Suvrajyoti Mishra, Lakshmi Unnikrishnan, Sanjay Nayak, and Smita Mohanty. Advances in piezoelectric polymer composites for energy harvesting applications: A systematic review. *Macromolecular Materials and Engineering*, 304, 11 2018.

[47] Meisam Moory-Shirbani, Hamid M. Sedighi, Hassen M. Ouakad, and F. Najar. Experimental and mathematical analysis of a piezoelectrically actuated multilayered imperfect microbeam subjected to applied electric potential. *Composite Structures*, 184:950–960, 2018.

[48] Trevor A. Mori and K . Tanaka. Average stress in matrix and average elastic energy of materials with misfitting inclusions. *Acta Metallurgica*, 21:571–574, 1973.

[49] A. Morro and G. Caviglia. Chapter 14 - conservation laws and variational conditions for wave propagation in plaknarly stratified media. In Stanislaw Sieniutycz and Henrik Farkas, editors, *Variational and Extremum Principles in Macroscopic Systems*, pages 293–313. Elsevier, Oxford, 2005.

[50] Houssein Nasser, Sandra Porn, Yao Koutsawa, Gaetano Genta, and Salim Belouettar. Optimal design of a multilayered piezoelectric transducer based on a special unit cell homogenization method. *Acta Mechanica*, 227:1837–1847, 2016.

[51] Robert E. Newnham, Doyle P. Skinner, and Leslie Eric Cross. Connectivity and piezoelectric-pyroelectric composites. *Materials Research Bulletin*, 13:525–536, 1978.

[52] PIEZO Technologies, Inc. Piezoelectric material properties data sheet. `https://info.piezo.com/hubfs/Data-Sheets/piezo-material-properties-data-sheet-20201112.pdf`, 2020. Typical values for PZT piezoceramics including dielectric, piezoelectric, and density data.

[53] Wallace Arden Smith and Bert A. Auld. Modeling 1-3 composite piezoelectrics: thickness-mode oscillations. *IEEE Transactions on Ultrasonics, Ferroelectrics and Frequency Control*, 38:40–47, 1991.

[54] Salvatore Torquato. Random heterogeneous media: Microstructure and improved bounds on effective properties. *Applied Mechanics Reviews*, 44:37–76, 1991.

[55] Essam Moustafa Wahba. Derivation of the differential continuity equation in an introductory engineering fluid mechanics course. *Article (available on ResearchGate)*, 2021. Accessed via ResearchGate, August 7, 2025.

[56] Fidéle Léopold Hanse Wampo, Richard Ntenga, Joseph Yves Effa, Yuri Lapusta, Guy Edgar Ntamack, and Pierre Maréchal. Generalized homogenization model of piezoelectric materials for ultrasonic transducer applications. *Journal of Composite Materials*, 56(5):713–726, 2022.

[57] Ken ya Hashimoto and Masahiro Yamaguchi. Elastic, piezoelectric and dielectric properties of composite materials. In *Proceedings of the IEEE 1986 Ultrasonics Symposium*, pages 697–702, New York, 1986. IEEE.

[58] Peng Yan and C. P. Jiang. An eigenfunction expansion-variational method based on a unit cell in analysis of a generally doubly periodic array of cracks. *Acta Mechanica*, 210:117–134, 2010.

Appendix A

Lagrangian formulation of piezoelectric problem

We define the Kinetic energy as

$$T = \iiint_{\Omega} \frac{\rho}{2} \frac{\partial u_i}{\partial t} \frac{\partial u^i}{\partial t} d\Omega. \tag{A.0.1}$$

We define the von-Kármán strains as

$$\hat{S}_{ij} = \frac{1}{2} \left(\frac{\partial u_i}{\partial x^j} + \frac{\partial u_i}{\partial x^j} + \frac{\partial u_k}{\partial x^i} \frac{\partial u^k}{\partial x^j} \right). \tag{A.0.2}$$

We define the piezoelectric strain energy as

$$U = \iiint_{\Omega} \frac{1}{2} c^{ijkl} \hat{S}_{ij} \hat{S}_{kl} - e^{ijk} \hat{S}_{ij} E_k - \frac{1}{2} \epsilon^{Sik} E_i E_k d\Omega. \tag{A.0.3}$$

If we define $L = T - U$, then by Hamilton's Principle [5], the equations of motion satisfy

$$\int_0^{t_f} \delta L \mathrm{d}t = 0. \tag{A.0.4}$$

where t_f is the final time. We define the Lagrangian density as

$$\begin{aligned} \mathcal{L} &= \frac{\rho}{2} \frac{\partial u_i}{\partial t} \frac{\partial u^i}{\partial t} - \left(\frac{1}{2} c^{ijkl} \hat{S}_{ij} \hat{S}_{kl} - e^{ijk} \hat{S}_{ij} E_k - \frac{1}{2} \epsilon^{Sik} E_i E_k \right) \\ &= \frac{\rho}{2} \frac{\partial u_i}{\partial t} \frac{\partial u^i}{\partial t} - \frac{1}{2} c^{ijkl} \hat{S}_{ij} \hat{S}_{kl} + e^{ijk} \hat{S}_{ij} E_k + \frac{1}{2} \epsilon^{Sik} E_i E_k. \end{aligned} \tag{A.0.5}$$

Using the definitions for the electric fields and strains, (A.0.5) reduces to

$$\begin{aligned} \mathcal{L} = \frac{\rho}{2} \frac{\partial u_i}{\partial t} \frac{\partial u^i}{\partial t} - \frac{1}{2} c^{ijkl} \left(\frac{\partial u_i}{\partial x^j} + \frac{1}{2} \frac{\partial u_m}{\partial x^i} \frac{\partial u^m}{\partial x^j} \right) \left(\frac{\partial u_k}{\partial x^l} + \frac{1}{2} \frac{\partial u_n}{\partial x^k} \frac{\partial u^n}{\partial x^l} \right) \\ - e^{ijk} \left(\frac{\partial u_i}{\partial x^j} + \frac{1}{2} \frac{\partial u_m}{\partial x^i} \frac{\partial u^m}{\partial x^j} \right) \frac{\partial \varphi}{\partial x^k} + \frac{1}{2} \epsilon^{Sik} \frac{\partial \varphi}{\partial x^i} \frac{\partial \varphi}{\partial x^k}. \end{aligned} \tag{A.0.6}$$

To get the equations of motion, we simply integrate (A.0.6) in both the spatial and temporal directions, then apply (A.0.4) to deduce the Euler-Lagrange equations of motion along with the appropriate boundary conditions. If we linearise our system around $\boldsymbol{u} = 0$, $\varphi = 0$ (i.e., we assume the partial derivatives of $\boldsymbol{u}$ and φ are small and we ignore all terms that are cubic or higher order), then we obtain (2.4.19)-(2.4.24).

Appendix B

Definitions of Uniform Ellipticity

We impose the following conditions on $\boldsymbol{c}$ for all (0, 2)-tensors $\boldsymbol{A}$ and $\boldsymbol{B}$ and all $X \in \mathbb{T}^n$

i.

$$A_{ij}c^{ijkl}(\boldsymbol{X})A_{kl} \geq \Gamma_1 \sum_{ij} \left| \frac{A_{ij} + A_{ji}}{2} \right|^2, \tag{B.0.1}$$

ii.

$$A_{ij}c^{ijkl}(\boldsymbol{X})B_{kl} \leq \Gamma_2 \left(\sum_{ij} \left| \frac{A_{ij} + A_{ji}}{2} \right|^2 \right)^{0.5} \left(\sum_{ij} \left| \frac{B_{ij} + B_{ji}}{2} \right|^2 \right)^{0.5}, \tag{B.0.2}$$

where Γ_1 and Γ_2 are both positive real numbers and $c_{ij}^{kl} = c^{ijkl}$.
We impose the following conditions on ϵ^S for all vectors $\vec{a}$ and $\vec{b}$ and all $\boldsymbol{X} \in \boldsymbol{T}^n$

i.

$$a_i \epsilon^{Sij}(\boldsymbol{X}) a_j \geq \Lambda_1 \|\vec{a}\|^2, \tag{B.0.3}$$

ii.

$$a_i \epsilon^{Sij}(\boldsymbol{X}) b_j \leq \Lambda_2 \|\vec{a}\| \|\vec{b}\|, \tag{B.0.4}$$

where $\|.\|$ denotes the Euclidean norm on $\mathbb{R}^n$ and $\epsilon_j^{Si} = \epsilon^{Sij}$. Once again Λ_1 and Λ_2 are both positive real numbers. We note that the conditions given by (B.0.1) and (B.0.2) are referred to as uniform (pseudo-)ellipticity of $\boldsymbol{c}$, while the conditions given in (B.0.3) and (B.0.4) are referred to as uniform ellipticity of ϵ^S. If conditions (B.0.1)-(B.0.4) all hold, then the solutions to the cell problems described by (2.7.51)-(2.7.58) and (2.7.63)-(2.7.70) are unique up to an additive constant.

Appendix C

Weak formulations and numerical solutions to cell equations arising from our homogenisation model

To find weak formulations, we first define the piece-wise constant functions

$$c(\boldsymbol{X}) = \begin{cases} c_M & \text{if } X \in M \\ c_I & \text{if } X \in I \end{cases}, \tag{C.0.1}$$

$$e(\boldsymbol{X}) = \begin{cases} 0 & \text{if } X \in M \\ e_I & \text{if } X \in I \end{cases}, \tag{C.0.2}$$

$$\epsilon^S(\boldsymbol{X}) = \begin{cases} \epsilon^S_M & \text{if } X \in M \\ \epsilon^S_I & \text{if } X \in I \end{cases}. \tag{C.0.3}$$

From cell equations (2.7.51)-(2.7.54), along with continuity conditions (2.7.55)-(2.7.58), we deduce that

$$\frac{\partial}{\partial X_i}\left(c^{kl}_{ij}\left(\frac{\partial \Psi^{ab}_k}{\partial X^l} + \delta^a_k\delta^b_l\right) + e^k_{ij}\frac{\partial \psi^{ab}}{\partial X^k}\right) = 0, \tag{C.0.4}$$

$$\frac{\partial}{\partial X_i}\left(S_p e^{kl}_i\left(\frac{\partial \Psi^{ab}_k}{\partial X^l} + \delta^a_k\delta^b_l\right) - \epsilon^{Sk}_i\frac{\partial \psi^{ab}}{\partial X^k}\right) = 0. \tag{C.0.5}$$

From cell equations (2.7.63)-(2.7.66), along with continuity conditions (2.7.67)-(2.7.70), we deduce that

$$\frac{\partial}{\partial X_i}\left(c^{kl}_{ij}\frac{\partial \Phi^f_k}{\partial X^l} + e^k_{ij}\left(\frac{\partial \phi^f}{\partial X^k} + \delta^f_k\right)\right) = 0, \tag{C.0.6}$$

$$\frac{\partial}{\partial X_i}\left(S_p e^{kl}_i\frac{\partial \Phi^f_k}{\partial X^l} - \epsilon^{Sk}_i\left(\frac{\partial \phi^f}{\partial X^k} + \delta^f_k\right)\right) = 0. \tag{C.0.7}$$

We let $\boldsymbol{\sigma}$ be a $(1,2)$-tensor and $\boldsymbol{\tau}$ be a $(1,1)$-tensor with all the entries being

functions of $\boldsymbol{x}$ and $\boldsymbol{X}$ such that for a fixed value of $\boldsymbol{x}$, each entry is in $C^\infty(\mathbb{T}^3)$, meaning every entry is smooth and 1-periodic in each Cartesian variable of $\boldsymbol{X}$. We let $\boldsymbol{\chi}$ be a $(0,2)$-tensor and $\boldsymbol{\omega}$ be a $(0,1)$-tensor with all the entries being functions of $\boldsymbol{x}$ and $\boldsymbol{X}$, such that for a fixed value of $\boldsymbol{x}$ each entry is in $C^\infty(\mathbb{T}^3)$. We multiply (C.0.4) by σ^j_{ab}, then multiply (C.0.5) by χ_{ab}, we then multiply (C.0.6) by τ^j_f, and finally multiply (C.0.7) by ω_f. Adding these expressions together, then integrating over the unit cell give

$$\begin{aligned}
&\iiint_{\mathbb{T}^3} \frac{\partial}{\partial X_i}\left(c^{kl}_{ij}\left(\frac{\partial \Psi^{ab}_k}{\partial X^l}+\delta^a_k\delta^b_l\right)+e^k_{ij}\frac{\partial \psi^{ab}}{\partial X^k}\right)\sigma^j_{ab}\mathrm{d}V\\
&\quad+\iiint_{\mathbb{T}^3}\frac{\partial}{\partial X_i}\left(S_p e^{kl}_i\left(\frac{\partial \Psi^{ab}_k}{\partial X^l}+\delta^a_k\delta^b_l\right)-\epsilon^{Sk}_i\frac{\partial \psi^{ab}}{\partial X^k}\right)\chi_{ab}\mathrm{d}V\\
&\quad+\iiint_{\mathbb{T}^3}\frac{\partial}{\partial X_i}\left(c^{kl}_{ij}\frac{\partial \Phi^f_k}{\partial X^l}+e^k_{ij}\left(\frac{\partial \phi^f}{\partial X^k}+\delta^f_k\right)\right)\tau^j_f\mathrm{d}V\\
&\quad+\iiint_{\mathbb{T}^3}\frac{\partial}{\partial X_i}\left(S_p e^{kl}_i\frac{\partial \Phi^f_k}{\partial X^l}-\epsilon^{Sk}_i\left(\frac{\partial \phi^f}{\partial X^k}+\delta^f_k\right)\right)\omega_f\mathrm{d}V=0, \quad \text{(C.0.8)}
\end{aligned}$$

for all $\sigma^j_{ab},\tau^j_f\in C^\infty(\mathbb{T}^3)$ and all $\chi_{ab},\omega_f\in C^\infty(\mathbb{T}^3)$. Using the Divergence Theorem and the periodic boundary conditions, we deduce

$$\begin{aligned}
&\iiint_{\mathbb{T}^3}\left(c^{kl}_{ij}\left(\frac{\partial \Psi^{ab}_k}{\partial X^l}+\delta^a_k\delta^b_l\right)+e^k_{ij}\frac{\partial \psi^{ab}}{\partial X^k}\right)\frac{\partial \sigma^j_{ab}}{\partial X_i}\mathrm{d}V\\
&\quad+\iiint_{\mathbb{T}^3}\left(S_p e^{kl}_i\left(\frac{\partial \Psi^{ab}_k}{\partial X^l}+\delta^a_k\delta^b_l\right)-\epsilon^{Sk}_i\frac{\partial \psi^{ab}}{\partial X^k}\right)\frac{\partial \chi_{ab}}{\partial X_i}\mathrm{d}V\\
&\quad+\iiint_{\mathbb{T}^3}\left(c^{kl}_{ij}\frac{\partial \Phi^f_k}{\partial X^l}+e^k_{ij}\left(\frac{\partial \phi^f}{\partial X^k}+\delta^f_k\right)\right)\frac{\partial \tau^j_f}{\partial X_i}\mathrm{d}V\\
&\quad+\iiint_{\mathbb{T}^3}\left(S_p e^{kl}_i\frac{\partial \Phi^f_k}{\partial X^l}-\epsilon^{Sk}_i\left(\frac{\partial \phi^f}{\partial X^k}+\delta^f_k\right)\right)\frac{\partial \omega_f}{\partial X_i}\mathrm{d}V=0. \quad \text{(C.0.9)}
\end{aligned}$$

We assume that $\boldsymbol{c}_I$ and $\boldsymbol{c}_M$ are uniformly (pseudo-)elliptic and $\boldsymbol{\epsilon}^S_M$ and $\boldsymbol{\epsilon}^S_I$ are uniformly elliptic. If we impose $\Psi^{ij}_k,\psi^{ij},\Phi^i_k\ \phi^i\in H^1(\mathbb{T}^3)$ [1] for all relevant i,j,k, then the weak formulation specified in (C.0.9) is well-defined. Using standard density results we deduce that the weak formulation above holds for all (1,2)-tensors $\boldsymbol{\sigma}$, all (1, 1)-tensors $\boldsymbol{\tau}$, all (0, 2)-tensors χ and all vector fields ω, where all of the entries are elements in $H^1(\mathbb{T}^3)$.

[1] The Sobolev space of functions that are: square integrable and weakly differentiable with a weak derivative that is also square integrable, and 1-periodic in each Cartesian variable.

We impose that

$$\sigma_{ab}^{j} = \overline{\sigma}^{j}, \tag{C.0.10}$$

$$\tau_{f}^{j} = \overline{\tau}^{j}, \tag{C.0.11}$$

$$\chi_{ab} = \frac{1}{Sp}\overline{\chi}, \tag{C.0.12}$$

$$\omega_{f} = \frac{1}{Sp}\overline{\omega}. \tag{C.0.13}$$

After some rearranging, (C.0.9) yields

$$\begin{aligned}
&\iiint_{\mathbb{T}^3}\left(c_{ij}^{kl}\frac{\partial\Psi_{k}^{ab}}{\partial X^{l}}+e_{ij}^{k}\frac{\partial\psi^{ab}}{\partial X^{k}}\right)\frac{\partial\overline{\sigma}^{j}}{\partial X_{i}}\mathrm{d}V\\
&\qquad+\frac{1}{Sp}\iiint_{\mathbb{T}^3}\left(S_{p}e_{i}^{kl}\frac{\partial\Psi_{k}^{ab}}{\partial X^{l}}-\epsilon_{i}^{Sk}\frac{\partial\psi^{ab}}{\partial X^{k}}\right)\frac{\partial\overline{\chi}}{\partial X_{i}}\mathrm{d}V\\
&\qquad\quad+\iiint_{\mathbb{T}^3}\left(c_{ij}^{kl}\frac{\partial\Phi_{k}^{f}}{\partial X^{l}}+e_{ij}^{k}\frac{\partial\phi^{f}}{\partial X^{k}}\right)\frac{\partial\overline{\tau}^{j}}{\partial X_{i}}\mathrm{d}V\\
&\qquad+\frac{1}{Sp}\iiint_{\mathbb{T}^3}\left(S_{p}e_{i}^{kl}\frac{\partial\Phi_{k}^{f}}{\partial X^{l}}-\epsilon_{i}^{Sk}\frac{\partial\phi^{f}}{\partial X^{k}}\right)\frac{\partial\overline{\omega}}{\partial X_{i}}\mathrm{d}V\\
&\qquad\quad=-\iiint_{\mathbb{T}^3}\left(c_{ij}^{ab}\frac{\partial\overline{\sigma}^{j}}{\partial X_{i}}+e_{i}^{ab}\frac{\partial\overline{\chi}}{\partial X_{i}}\right)\mathrm{d}V\\
&\qquad\qquad-\frac{1}{S_{p}}\iiint_{\mathbb{T}^3}\left(S_{p}e_{ij}^{f}\frac{\partial\overline{\tau}^{j}}{\partial X_{i}}-\epsilon_{i}^{Sf}\frac{\partial\overline{\omega}}{\partial X_{i}}\right)dV,
\end{aligned} \tag{C.0.14}$$

for all $\overline{\sigma}^{j},\overline{\tau}^{j},\overline{\chi}$ and $\overline{\omega}\in H^{1}\left(\mathbb{T}^{3}\right)$ and all relevant j. Since $\overline{\boldsymbol{\sigma}},\overline{\boldsymbol{\tau}}$ and $\overline{\chi}$, $\overline{\omega}$ can be independently set to zero, we deduce the following weak formulations

$$\begin{aligned}
&\iiint_{\mathbb{T}^3}\left(c_{ij}^{kl}\frac{\partial\Psi_{k}^{ab}}{\partial X^{l}}+e_{ij}^{k}\frac{\partial\psi^{ab}}{\partial X^{k}}\right)\frac{\partial\sigma^{j}}{\partial X_{i}}\mathrm{d}V\\
&\qquad+\frac{1}{Sp}\iiint_{\mathbb{T}^3}\left(S_{p}e_{i}^{kl}\frac{\partial\Psi_{k}^{ab}}{\partial X^{l}}-\epsilon_{i}^{Sk}\frac{\partial\psi^{ab}}{\partial X^{k}}\right)\frac{\partial\chi}{\partial X_{i}}\mathrm{d}V\\
&\qquad\quad=-\iiint_{\mathbb{T}^3}\left(c_{ij}^{ab}\frac{\partial\sigma^{j}}{\partial X_{i}}+e_{i}^{ab}\frac{\partial\chi}{\partial X_{i}}\right)\mathrm{d}V,
\end{aligned} \tag{C.0.15}$$

$$\begin{aligned}
&\iiint_{\mathbb{T}^3}\left(c_{ij}^{kl}\frac{\partial\Phi_{k}^{f}}{\partial X^{l}}+e_{ij}^{k}\frac{\partial\phi^{f}}{\partial X^{k}}\right)\frac{\partial\tau^{j}}{\partial X_{i}}\mathrm{d}V\\
&\qquad+\frac{1}{S_{p}}\iiint_{\mathbb{T}^3}\left(S_{p}e_{i}^{kl}\frac{\partial\Phi_{k}^{f}}{\partial X^{l}}-\epsilon_{i}^{Sk}\frac{\partial\phi^{f}}{\partial X^{k}}\right)\frac{\partial\omega}{\partial X_{i}}\mathrm{d}V\\
&\qquad\quad=-\frac{1}{S_{p}}\iiint_{\mathbb{T}^3}\left(S_{p}e_{ij}^{f}\frac{\partial\tau^{j}}{\partial X_{i}}-\epsilon_{i}^{Sf}\frac{\partial\omega}{\partial X_{i}}\right)\mathrm{d}V.
\end{aligned} \tag{C.0.16}$$

The weak formulations in (C.0.15) and (C.0.16) must hold for all $\sigma, \tau \in H^1(\mathbb{T}^3; \mathbb{R}^3)$, all $\chi, \omega \in H^1(\mathbb{T}^3)$ and all a, b, f. In order to solve the cell problems (C.0.15) and (C.0.16), we use the finite element solver FEniCS and treat Ψ^{ab} as a vector field for each a and b, where the k^{th} element is Ψ^{ab}_k. We treat Φ^f as a vector field for each f, where the k^{th} element is Φ^f_k. We treat ψ^{ab} and ϕ^f as scalars for each a, b and f. We use the weak formulations (C.0.15) and (C.0.16) in the programming.

Since c is uniformly (pseudo-)elliptic and ϵ^S is uniformly elliptic, if we impose that the components of Ψ, ψ, Φ and ϕ have a mean value of 0 in $\mathbb{T}^3$ then the conditions of the Lax-Milgram Theorem are met (see [22]). Therefore, we can use the finite element approximation to find a numerical solution to the cell problem with ease. Furthermore, our solutions to the cell problems are smooth inside Λ_I and Λ_M and thus the finite element solution will converge to the actual solution if we use progressively finer meshes.

Equations (C.0.15) and (C.0.16) give a weak formulation of (C.0.4) and (C.0.5) for each value of $a, b \in \{1, 2, 3\}$. These indices represent the direction of the forcing. This give $3 \times 3 = 9$ cell problems from (C.0.15) as there are three choices for a and b. However, the RHS of (C.0.15) is symmetric when switching a and b around and therefore $\Psi^{ab} = \Psi^{ba}$ and $\psi^{ab} = \psi^{ba}$ for all $a, b \in \{1, 2, 3\}$. This reduces the number of cell problems in (C.0.15) from 9 to 6. Equation (C.0.16) give a weak formulation of (C.0.6) and (C.0.7) for each value of $f \in \{1, 2, 3\}$. This weak formulation give 3 cell problems, and therefore we need to solve a total of 9 systems of coupled cell equations. Throughout the thesis, the linear system defined by (C.0.15) and (C.0.16) were solved using the GMRES iterative solver implemented in FEniCS. Convergence was determined using the default solver tolerances. The finite element discretisation of the solutions introduces degrees of freedom corresponding to the nodal values of the solutions to the cell functions on the mesh. The mesh resolution was varied depending on the geometry of the inclusions, and solutions were verified to be insensitive to further mesh refinement. Since the solutions of (C.0.15) and (C.0.16) are unique up to additive constants, we may enforce uniqueness by imposing that the average values of the solutions on the unit cell are zero.

Appendix D

Isotropy

D.1 Mechanical isotropy

We say a material is mechanically isotropic if the stiffness tensor c is invariant under rotations and translations. The general form of the stiffness tensor for an isotropic material is given by

$$c_{ij}^{kl} = \lambda \delta_{ij} \delta^{kl} + \mu \left(\delta_i^k \delta_j^l + \delta_i^l \delta_j^k \right), \tag{D.1.1}$$

where λ and μ are constants, which are called the Lamê parameters.

D.2 Piezoelectric isotropy

We say a material is piezoelectrically isotropic, with respect to Z-axis, if the piezoelectric strain tensor remains invariant under rotations about the Z-axis and translations. The general form for the piezoelectric strain tensor is given by

$$\begin{aligned} e_{ij}^k = e_{13} \left(\delta_i^1 \delta_j^1 + \delta_i^2 \delta_j^2 \right) \delta_3^k + e_{33} \delta_i^3 \delta_j^3 \delta_3^k \\ + e_{51} \left(\left(\delta_i^1 \delta_1^k + \delta_i^2 \delta_2^k \right) \delta_j^3 + \left(\delta_j^1 \delta_1^k + \delta_j^2 \delta_2^k \right) \delta_i^3 \right), \end{aligned} \tag{D.2.1}$$

where e_{13}, e_{33} and e_{51} are constant.

D.3 Dielectrical isotropy

We say that a material is dielectrically isotropic if it remains invariant under rotations and translations. The general form for the piezoelectric strain tensor is given by

$$\epsilon_i^{Sk} = \epsilon^S \delta_i^k, \tag{D.3.1}$$

where ϵ^S is a constant.

Appendix E

Symmetry relations for homogenisation of bulk materials

In this chapter, we will prove that given (2.2.3) and (2.3.2) hold, then

$$c^{ijkl}_{\text{eff}} = c^{klij}_{\text{eff}}, \qquad e^{ijk}_{\text{eff}} = h^{ijk}, \qquad \epsilon^{Sik}_{\text{eff}} = \epsilon^{Ski}_{\text{eff}}. \tag{E.0.1}$$

Note that $c^{ijkl}_{\text{eff}} = c^{kl}_{\text{eff},ij}$, $e^{ijk}_{\text{eff}} = e^{k}_{\text{eff},ij}$, $h^{ijk} = h^{ij}_{k}$ and $\epsilon^{Sik}_{\text{eff}} = \epsilon^{Sk}_{\text{eff},i}$. We write the indices on top for convenience. We will start by proving $c^{ijkl}_{\text{eff}} = c^{klij}_{\text{eff}}$.

Proof. We consider the quantity

$$\begin{aligned} I_1^{ijkl} = &\iiint_{\Gamma_M} c_M^{i'j'k'l'} \left(\delta^i_{i'}\delta^j_{j'} + \frac{\partial \Psi^{ij}_{M,i'}}{\partial X^{j'}}\right)\left(\delta^k_{k'}\delta^l_{l'} + \frac{\partial \Psi^{kl}_{M,k'}}{\partial X^{l'}}\right) \mathrm{d}V \\ &+ \iiint_{\Gamma_I} c_I^{i'j'k'l'} \left(\delta^i_{i'}\delta^j_{j'} + \frac{\partial \Psi^{ij}_{I,i'}}{\partial X^{j'}}\right)\left(\delta^k_{k'}\delta^l_{l'} + \frac{\partial \Psi^{kl}_{I,k'}}{\partial X^{l'}}\right) \mathrm{d}V \\ &+ \iiint_{\Gamma_M} -\frac{1}{S_p}\epsilon_M^{Si'k'}\frac{\partial \psi^{ij}_M}{\partial X^{i'}}\frac{\partial \psi^{kl}_M}{\partial X^{k'}}\mathrm{d}V \\ &+ \iiint_{\Gamma_I} 2e^{i'j'k'}\left(\delta^i_{i'}\delta^j_{j'} + \frac{\partial \Psi^{ij}_{I,i'}}{\partial X^{j'}}\right)\frac{\partial \psi^{kl}_I}{\partial X^{k'}} - \frac{1}{S_p}\epsilon_I^{Si'k'}\frac{\partial \psi^{ij}_I}{\partial X^{i'}}\frac{\partial \psi^{kl}_I}{\partial X^{k'}}\mathrm{d}V. \end{aligned} \tag{E.0.2}$$

Using (2.7.51)-(2.7.54) along with (2.7.55)-(2.7.58) and periodicity, we deduce that

$$\begin{aligned} &\iiint_{\Gamma_M}\left(c_M^{i'j'k'l'}\left(\delta^i_{k'}\delta^j_{l'} + \frac{\partial \Psi^{ij}_{M,k'}}{\partial X^{l'}}\right)\right)\frac{\partial \Psi^{kl}_{M,i'}}{\partial X^{j'}}\mathrm{d}V \\ &\quad + \iiint_{\Gamma_I}\left(c_I^{i'j'k'l'}\left(\delta^i_{k'}\delta^j_{l'} + \frac{\partial \Psi^{ij}_{I,k'}}{\partial X^{l'}}\right) + e^{i'j'k'}\frac{\partial \psi^{ij}_I}{\partial X^{k'}}\right)\frac{\partial \Psi^{kl}_{I,i'}}{\partial X^{j'}}\mathrm{d}V = 0, \end{aligned} \tag{E.0.3}$$

$$\iiint_{\Gamma_M}\left(-\epsilon_M^{Sk'i'}\frac{\partial\psi_M^{ij}}{\partial X^{i'}}\right)\frac{\partial\psi_M^{kl}}{\partial X^{k'}}\mathrm{d}V + \iiint_{\Gamma_I}\left(S_p e^{i'j'k'}\left(\delta^i_{i'}\delta^j_{j'}+\frac{\partial\Psi^{ij}_{I,i'}}{\partial X^{j'}}\right)-\epsilon_I^{Sk'i'}\frac{\partial\psi_I^{ij}}{\partial X^{i'}}\right)\frac{\partial\psi_I^{kl}}{\partial X^{k'}}=0. \quad \text{(E.0.4)}$$

Using (E.0.2) and (E.0.3), we deduce the following identities

$$\begin{aligned} I_1^{ijkl} = &\iiint_{\Gamma_M} c_M^{i'j'k'l'}\left(\delta^i_{i'}\delta^j_{j'}+\frac{\partial\Psi^{ij}_{M,i'}}{\partial X^{j'}}\right)\left(\delta^k_{k'}\delta^l_{l'}+\frac{\partial\Psi^{kl}_{M,k'}}{\partial X^{l'}}\right)\mathrm{d}V \\ &+\iiint_{\Gamma_I} c_I^{i'j'k'l'}\left(\delta^i_{i'}\delta^j_{j'}+\frac{\partial\Psi^{ij}_{I,i'}}{\partial X^{j'}}\right)\left(\delta^k_{k'}\delta^l_{l'}+\frac{\partial\Psi^{kl}_{I,k'}}{\partial X^{l'}}\right)\mathrm{d}V \\ &+\frac{1}{S_p}\left(\iiint_{\Gamma_M}\epsilon_M^{Si'k'}\frac{\partial\psi_M^{ij}}{\partial X^{i'}}\frac{\partial\psi_M^{kl}}{\partial X^{k'}}\mathrm{d}V+\iiint_{\Gamma_I}\epsilon_I^{Si'k'}\frac{\partial\psi_I^{ij}}{\partial X^{i'}}\frac{\partial\psi_I^{kl}}{\partial X^{k'}}\mathrm{d}V\right), \end{aligned} \quad \text{(E.0.5)}$$

$$\begin{aligned} I_1^{ijkl} = &\iiint_{\Gamma_M} c_M^{i'j'k'l'}\left(\delta^i_{i'}\delta^j_{j'}+\frac{\partial\Psi^{ij}_{M,i'}}{\partial X^{j'}}\right)\left(\delta^k_{k'}\delta^l_{l'}+\frac{\partial\Psi^{kl}_{M,k'}}{\partial X^{l'}}\right)\mathrm{d}V \\ &+\iiint_{\Omega_I} c_I^{i'j'k'l'}\left(\delta^i_{i'}\delta^j_{j'}+\frac{\partial\Psi^{ij}_{I,i'}}{\partial X^{j'}}\right)\left(\delta^k_{k'}\delta^l_{l'}+\frac{\partial\Psi^{kl}_{I,k'}}{\partial X^{l'}}\right)\mathrm{d}V \\ &+\iiint_{\Gamma_I} e^{i'j'k'}\left(\delta^i_{i'}\delta^j_{j'}+\frac{\partial\Psi^{ij}_{I,i'}}{\partial X^{j'}}\right)\frac{\partial\psi_I^{kl}}{\partial X^{k'}}\mathrm{d}V. \end{aligned} \quad \text{(E.0.6)}$$

Using (E.0.5) along with (2.2.3) and (2.3.2), we deduce that

$$I_1^{ijkl} = I_1^{klij}. \quad \text{(E.0.7)}$$

Using (E.0.3) and (2.7.85), (E.0.6) reduces to

$$\iiint_{\Gamma_M} c_M^{ijk'l'}\left(\delta^k_{k'}\delta^l_{l'}+\frac{\partial\Psi^{kl}_{M,k'}}{\partial X^{l'}}\right)\mathrm{d}V + \iiint_{\Gamma_I} c_I^{ijk'l'}\left(\delta^k_{k'}\delta^l_{l'}+\frac{\partial\Psi^{kl}_{I,k'}}{\partial X^{l'}}\right)\mathrm{d}V+\iiint_{\Gamma_I} e^{ijk'}\frac{\partial\psi_I^{kl}}{\partial X^{k'}}\mathrm{d}V = c_{\text{eff}}^{ijkl}. \quad \text{(E.0.8)}$$

This completes the proof. □

We will now prove $e_{\text{eff}}^{ijk} = h^{ijk}$.

Proof. We consider the quantity

$$
\begin{aligned}
I_2^{ijk} = \iiint_{\Gamma_M} c_M^{i'j'k'l'} \left(\delta^i_{i'}\delta^j_{j'} + \frac{\partial \Psi^{ij}_{M,i'}}{\partial X^{j'}}\right) \frac{\partial \Phi^k_{M,k'}}{\partial X^{l'}} \mathrm{d}V \\
+ \iiint_{\Gamma_I} c_I^{i'j'k'l'} \left(\delta^i_{i'}\delta^j_{j'} + \frac{\partial \Psi^{ij}_{I,i'}}{\partial X^{j'}}\right) \frac{\partial \Phi^k_{I,k'}}{\partial X^{l'}} \mathrm{d}V \\
+ \iiint_{\Gamma_I} e^{i'j'k'} \left(\frac{\partial \psi^{ij}_I}{\partial X^{k'}} \frac{\partial \Phi^k_{I,i'}}{\partial X^{j'}} + \left(\delta^i_{i'}\delta^j_{j'} + \frac{\partial \Psi^{ij}_{I,i'}}{\partial X^{j'}}\right)\left(\delta^k_{k'} + \frac{\partial \phi^k_I}{\partial X^{k'}}\right)\right) \mathrm{d}V \\
- \frac{1}{S_p}\left(\iiint_{\Gamma_M} \epsilon_M^{Si'k'} \frac{\partial \psi^{ij}_M}{\partial X^{i'}} \left(\delta^k_{k'} + \frac{\partial \phi^k_M}{\partial X^{k'}}\right) \mathrm{d}V \right) \\
- \frac{1}{S_p}\left(\iiint_{\Gamma_I} \epsilon_I^{Si'k'} \frac{\partial \psi^{ij}_I}{\partial X^{i'}} \left(\delta^k_{k'} + \frac{\partial \phi^k_I}{\partial X^{k'}}\right) \mathrm{d}V \right). \quad \text{(E.0.9)}
\end{aligned}
$$

Using (2.7.51) and (2.7.53) along with (2.7.57), (2.7.67) and periodicity, we deduce that

$$
\begin{aligned}
\iiint_{\Gamma_M} \left(c_M^{i'j'k'l'} \left(\delta^i_{k'}\delta^j_{l'} + \frac{\partial \Psi^{ij}_{M,k'}}{\partial X^{l'}}\right)\right) \frac{\partial \Phi^k_{M,j'}}{\partial X^{i'}} \mathrm{d}V \\
+ \iiint_{\Gamma_I} \left(c_I^{i'j'k'l'} \left(\delta^i_{k'}\delta^j_{l'} + \frac{\partial \Psi^{ij}_{I,k'}}{\partial X^{l'}}\right) + e^{i'j'k'} \frac{\partial \psi^{ij}_I}{\partial X^{k'}} \right) \frac{\partial \Phi^k_{I,j'}}{\partial X^{i'}} \mathrm{d}V = 0. \quad \text{(E.0.10)}
\end{aligned}
$$

Using (2.7.63) and (2.7.65) along with (2.7.69), (2.7.55) and periodicity, we deduce that

$$
\begin{aligned}
\iiint_{\Gamma_M} \left(c_M^{i'j'k'l'} \frac{\partial \Phi^k_{M,k'}}{\partial X^{l'}} \right) \frac{\partial \Psi^{ij}_{M,j'}}{\partial X^{i'}} \mathrm{d}V \\
+ \iiint_{\Gamma_I} \left(c_I^{i'j'k'l'} \frac{\partial \Phi^k_{I,k'}}{\partial X^{l'}} + e^{i'j'k'} \left(\delta^k_{k'} + \frac{\partial \phi^k_I}{\partial X^{k'}}\right)\right) \frac{\partial \Psi^{ij}_{I,j'}}{\partial X^{i'}} \mathrm{d}V = 0. \quad \text{(E.0.11)}
\end{aligned}
$$

Using (E.0.10)-(E.0.11), we deduce the following identities

$$
\begin{aligned}
I_2^{ijk} = \iiint_{\Gamma_M} c_M^{ijk'l'} \frac{\partial \Phi^k_{M,k'}}{\partial X^{l'}} \mathrm{d}V + \iiint_{\Gamma_I} c_I^{ijk'l'} \frac{\partial \Phi^k_{I,k'}}{\partial X^{l'}} \mathrm{d}V \\
+ \iiint_{\Gamma_I} e^{i'j'k'} \left(\frac{\partial \psi^{ij}_I}{\partial X^{k'}} \frac{\partial \Phi^k_{I,i'}}{\partial X^{j'}} + \left(\delta^i_{i'}\delta^j_{j'}\right)\left(\delta^k_{k'} + \frac{\partial \phi^k_I}{\partial X^{k'}}\right)\right) \mathrm{d}V \\
- \frac{1}{S_p}\left(\iiint_{\Gamma_M} \epsilon_M^{Si'k'} \frac{\partial \psi^{ij}_M}{\partial X^{i'}} \left(\delta^k_{k'} + \frac{\partial \phi^k_M}{\partial X^{k'}}\right) \mathrm{d}V \right) \\
- \frac{1}{S_p}\left(\iiint_{\Gamma_I} \epsilon_I^{Si'k'} \frac{\partial \psi^{ij}_I}{\partial X^{i'}} \left(\delta^k_{k'} + \frac{\partial \phi^k_I}{\partial X^{k'}}\right) \mathrm{d}V \right), \quad \text{(E.0.12)}
\end{aligned}
$$

$$I_2^{ijk} = \iiint_{\Gamma_I} e^{i'j'k'} \left(\left(\delta^i_{i'} \delta^j_{j'} + \frac{\partial \Psi^{ij}_{I,i'}}{\partial X^{j'}} \right) \left(\delta^k_{k'} + \frac{\partial \phi^k_I}{\partial X^{k'}} \right) \right) \mathrm{d}V$$
$$- \frac{1}{S_p} \left(\iiint_{\Gamma_M} \epsilon_M^{Si'k'} \frac{\partial \psi^{ij}_M}{\partial X^{i'}} \left(\delta^k_{k'} + \frac{\partial \phi^k_M}{\partial X^{k'}} \right) \mathrm{d}V \right)$$
$$- \frac{1}{S_p} \left(\iiint_{\Gamma_I} \epsilon_I^{Si'k'} \frac{\partial \psi^{ij}_I}{\partial X^{i'}} \left(\delta^k_{k'} + \frac{\partial \phi^k_I}{\partial X^{k'}} \right) \mathrm{d}V \right). \quad \text{(E.0.13)}$$

Using (2.7.64) and (2.7.66) along with (2.7.56), (2.7.70) and periodicity we deduce that

$$\iiint_{\Gamma_M} \left(-\epsilon_M^{Si'k'} \left(\frac{\partial \phi^k_M}{\partial X^{k'}} + \delta^k_{k'} \right) \right) \frac{\partial \psi^{ij}_M}{\partial X^{i'}} \mathrm{d}V$$
$$+ \iiint_{\Gamma_I} \left(S_p e^{k'l'i'} \frac{\partial \Phi^k_{I,k'}}{\partial X^{l'}} - \epsilon_I^{Si'k'} \left(\frac{\partial \phi^k_I}{\partial X^{k'}} + \delta^k_{k'} \right) \right) \frac{\partial \psi^{ij}_I}{\partial X^{i'}} \mathrm{d}V = 0. \quad \text{(E.0.14)}$$

Using (2.7.52) and (2.7.54) along with (2.7.58), (2.7.68) and periodicity we deduce that

$$\iiint_{\Gamma_M} \left(-\epsilon_M^{Si'k'} \left(\frac{\partial \psi^{ij}_M}{\partial X^{k'}} + \delta^k_{k'} \right) \right) \frac{\partial \phi^k_M}{\partial X^{i'}} \mathrm{d}V$$
$$+ \iiint_{\Gamma_I} \left(S_p e^{k'l'i} \frac{\partial \Psi^{ij}_{I,k'}}{\partial X^{l'}} - \epsilon_I^{Si'k'} \left(\frac{\partial \psi^{ij}_I}{\partial X^{k'}} + \delta^k_{k'} \right) \right) \frac{\partial \phi^k_I}{\partial X^{i'}} \mathrm{d}V = 0. \quad \text{(E.0.15)}$$

Using (E.0.14)-(E.0.15) and (2.7.86)-(2.7.87), we deduce from (E.0.12)-(E.0.13) that

$$I_2^{ijk} = \iiint_{\Gamma_I} e^{i'j'k} \left(\delta^i_{i'} \delta^j_{j'} + \frac{\partial \Psi^{ij}_{I,i'}}{\partial X^{j'}} \right) \mathrm{d}V$$
$$- \frac{1}{S_p} \left(\iiint_{\Gamma_M} \epsilon_M^{Si'k} \frac{\partial \psi^{ij}_M}{\partial X^{i'}} \mathrm{d}V + \iiint_{\Gamma_I} \epsilon_I^{Si'k} \frac{\partial \psi^{ij}_I}{\partial X^{i'}} \mathrm{d}V \right) = h^{ijk}, \quad \text{(E.0.16)}$$

$$I_2^{ijk} = \iiint_{\Gamma_M} c_M^{ijk'l'} \frac{\partial \Phi^k_{M,k'}}{\partial X^{l'}} \mathrm{d}V$$
$$+ \iiint_{\Gamma_I} c_I^{ijk'l'} \frac{\partial \Phi^k_{I,k'}}{\partial X^{l'}} + e^{ijk'} \left(\delta^k_{k'} + \frac{\partial \phi^k_I}{\partial X^{k'}} \right) \mathrm{d}V = e^{ijk}_{\text{eff}}. \quad \text{(E.0.17)}$$

This completes the proof. □

Note that $e^{ijk}_{\text{eff}} = h^{ijk}$ even when (2.2.3) and (2.3.2) do not hold.

We proceed to prove $\epsilon^{Sik}_{\text{eff}} = \epsilon^{Ski}_{\text{eff}}$.

Proof. We consider the quantity

$$I_3^{ik} = \iiint_{\Gamma_M} c_M^{i'j'k'l'} \frac{\partial \Phi_{M,i'}^i}{\partial X^{j'}} \frac{\partial \Phi_{M,k'}^k}{\partial X^{l'}} \mathrm{d}V + \iiint_{\Gamma_I} c_I^{i'j'k'l'} \frac{\partial \Phi_{I,i'}^i}{\partial X^{j'}} \frac{\partial \Phi_{I,k'}^k}{\partial X^{l'}} \mathrm{d}V$$
$$+ \iiint_{\Gamma_I} 2e^{i'j'k'} \frac{\partial \Phi_{I,i'}^i}{\partial X^{j'}} \left(\delta_{k'}^k + \frac{\partial \phi_I^k}{\partial X^{k'}} \right) \mathrm{d}V$$
$$- \frac{1}{S_p} \left(\iiint_{\Gamma_M} \epsilon_M^{Si'k'} \left(\delta_{i'}^i + \frac{\partial \phi_M^i}{\partial X^{i'}} \right) \left(\delta_{k'}^k + \frac{\partial \phi_M^k}{\partial X^{k'}} \right) \mathrm{d}V \right)$$
$$- \frac{1}{S_p} \left(\iiint_{\Gamma_I} \epsilon_I^{Si'k'} \left(\delta_{i'}^i + \frac{\partial \phi_I^i}{\partial X^{i'}} \right) \left(\delta_{k'}^k + \frac{\partial \phi_I^k}{\partial X^{k'}} \right) \mathrm{d}V \right). \quad \text{(E.0.18)}$$

Using (2.7.63)-(2.7.66), (2.7.67)-(2.7.70) and periodicity, we deduce that

$$\iiint_{\Gamma_M} c_M^{i'j'k'l'} \frac{\partial \Phi_{M,i'}^i}{\partial X^{j'}} \frac{\partial \Phi_{M,k'}^k}{\partial X^{l'}} \mathrm{d}V + \iiint_{\Gamma_I} c_I^{i'j'k'l'} \frac{\partial \Phi_{I,i'}^i}{\partial X^{j'}} \frac{\partial \Phi_{I,k'}^k}{\partial X^{l'}} \mathrm{d}V$$
$$+ \iiint_{\Gamma_I} e^{i'j'k'} \frac{\partial \Phi_{I,i'}^i}{\partial X^{j'}} \left(\delta_{k'}^k + \frac{\partial \phi_I^k}{\partial X^{k'}} \right) \mathrm{d}V = 0, \quad \text{(E.0.19)}$$

$$\iiint_{\Gamma_I} S_p e^{i'j'k'} \frac{\partial \Phi_{I,i'}^i}{\partial X^{j'}} \frac{\partial \phi_I^k}{\partial X^{k'}} \mathrm{d}V$$
$$- \left(\iiint_{\Gamma_M} \epsilon_M^{Si'k'} \left(\delta_{i'}^i + \frac{\partial \phi_M^i}{\partial X^{i'}} \right) \frac{\partial \phi_M^k}{\partial X^{k'}} \mathrm{d}V + \iiint_{\Gamma_I} \epsilon_I^{Si'k'} \left(\delta_{i'}^i + \frac{\partial \phi_I^i}{\partial X^{i'}} \right) \frac{\partial \phi_I^k}{\partial X^{k'}} \mathrm{d}V \right) = 0. \quad \text{(E.0.20)}$$

Using (E.0.19)-(E.0.20), we deduce from (E.0.18) that

$$I_3^{ik} = \iiint_{\Gamma_I} e^{i'j'k'} \frac{\partial \Phi_{I,i'}^i}{\partial X^{j'}} \left(\delta_{k'}^k + \frac{\partial \phi_I^k}{\partial X^{k'}} \right) \mathrm{d}V$$
$$- \frac{1}{S_p} \left(\iiint_{\Gamma_M} \epsilon_M^{Si'k'} \left(\delta_{i'}^i + \frac{\partial \phi_M^i}{\partial X^{i'}} \right) \left(\delta_{k'}^k + \frac{\partial \phi_M^k}{\partial X^{k'}} \right) \mathrm{d}V \right)$$
$$- \frac{1}{S_p} \left(\iiint_{\Gamma_I} \epsilon_I^{Si'k'} \left(\delta_{i'}^i + \frac{\partial \phi_I^i}{\partial X^{i'}} \right) \left(\delta_{k'}^k + \frac{\partial \phi_I^k}{\partial X^{k'}} \right) \mathrm{d}V \right), \quad \text{(E.0.21)}$$

$$I_3^{ik} = \iiint_{\Gamma_M} c_M^{i'j'k'l'} \frac{\partial \Phi_{M,i'}^i}{\partial X^{j'}} \frac{\partial \Phi_{M,k'}^k}{\partial X^{l'}} \mathrm{d}V + \iiint_{\Gamma_I} c_I^{i'j'k'l'} \frac{\partial \Phi_{I,i'}^i}{\partial X^{j'}} \frac{\partial \Phi_{I,k'}^k}{\partial X^{l'}} \mathrm{d}V$$
$$+ \frac{1}{S_p} \left(\iiint_{\Gamma_M} \epsilon_M^{Si'k'} \left(\delta_{i'}^i + \frac{\partial \phi_M^i}{\partial X^{i'}} \right) \left(\delta_{k'}^k + \frac{\partial \phi_M^k}{\partial X^{k'}} \right) \mathrm{d}V \right)$$
$$+ \frac{1}{S_p} \left(\iiint_{\Gamma_I} \epsilon_I^{Si'k'} \left(\delta_{i'}^i + \frac{\partial \phi_I^i}{\partial X^{i'}} \right) \left(\delta_{k'}^k + \frac{\partial \phi_I^k}{\partial X^{k'}} \right) \mathrm{d}V \right). \quad \text{(E.0.22)}$$

Using (E.0.20) and (2.7.88), we see that (E.0.21) reduces to

$$I_3^{ik} = \iiint_{\Gamma_I} e^{i'j'k} \frac{\partial \Phi^i_{I,i'}}{\partial X^{j'}} \mathrm{d}V \\ - \frac{1}{S_p} \left(\iiint_{\Gamma_M} \epsilon_M^{Si'k} \left(\delta^i_{i'} + \frac{\partial \phi^i_M}{\partial X^{i'}} \right) \mathrm{d}V + \iiint_{\Gamma_I} \epsilon_I^{Si'k} \left(\delta^i_{i'} + \frac{\partial \phi^i_I}{\partial X^{i'}} \right) \mathrm{d}V \right) = \epsilon^{Ski}. \tag{E.0.23}$$

This completes the proof. □

Note that in Appendix C, we showed that

$$\mathbf{\Psi}^{ab} = \mathbf{\Psi}^{ba} \text{ and } \psi^{ab} = \psi^{ba}. \tag{E.0.24}$$

Using (E.0.24), we conclude that

$$c^{kl}_{\text{eff},ij} = c^{kl}_{\text{eff},ji} = c^{lk}_{\text{eff},ij} = c^{ij}_{\text{eff},kl}, \tag{E.0.25}$$
$$e^{k}_{\text{eff},ij} = h^{k}_{ij}, \tag{E.0.26}$$
$$e^{ij}_{\text{eff},k} = h^{ij}_{k}, \tag{E.0.27}$$
$$e^{ij}_{\text{eff},k} = e^{ji}_{\text{eff},k}, \tag{E.0.28}$$
$$\epsilon^{Sk}_{\text{eff},i} = \epsilon^{Si}_{\text{eff},k}. \tag{E.0.29}$$

Appendix F

Cell problems for a bulk device made of a 1-3 composite

F.1 Assumptions about the tensors in each phase

In a 1-3 composite, the inclusions are aligned so there is translational symmetry in the Z-axis. This ensures that the solutions to the cell problems are independent of the Z-coordinate. When dealing with 1-3 composites, we assume the following properties

i.
$$c_{\alpha\beta}^{\gamma 3} = c_{\alpha\beta}^{3\gamma} = c_{\gamma 3}^{\alpha\beta} = c_{3\gamma}^{\alpha\beta} = 0, \tag{F.1.1}$$

ii.
$$c_{\alpha 3}^{33} = c_{3\alpha}^{33} = c_{33}^{\alpha 3} = c_{33}^{3\alpha} = 0, \tag{F.1.2}$$

iii.
$$e_{\alpha\beta}^{\gamma} = 0, \tag{F.1.3}$$

iv.
$$e_{33}^{\gamma} = 0, \tag{F.1.4}$$

v.
$$\epsilon_{\alpha}^{S3} = \epsilon_{3}^{S\alpha} = 0, \tag{F.1.5}$$

where $\alpha, \beta, \gamma \in \{1, 2\}$. These are true for fully isotropic materials (see Appendix D).

We will use the convention that Greek indices and summation of Greek indices refer to planar directions only.

As we will see shortly, (F.1.1)-(F.1.5), together with the assumption that the cell functions do not depend on Z, ensure that for each cell problem the planar displacement decouples from the vertical displacement and the scalar potential.

F.2 Mechanical cell problems

Under the assumptions set out in §F.1, (2.7.51)-(2.7.54) reduce to

$$\frac{\partial}{\partial X_\alpha}\left(c^{\gamma\eta}_{M,\alpha\beta}\frac{\partial \Psi^{ab}_{M,\gamma}}{\partial X^\eta}\right) = 0_\beta, \tag{F.2.1}$$

$$\frac{\partial}{\partial X_\alpha}\left(c^{3\beta}_{M,\alpha 3}\frac{\partial \Psi^{ab}_{M,3}}{\partial X^\beta}\right) = 0, \tag{F.2.2}$$

$$\frac{\partial}{\partial X_\alpha}\left(-\epsilon^{S\beta}_{M,\alpha}\frac{\partial \psi^{ab}_{M}}{\partial X^\beta}\right) = 0, \tag{F.2.3}$$

in the matrix phase, and

$$\frac{\partial}{\partial X_\alpha}\left(c^{\gamma\eta}_{I,\alpha\beta}\frac{\partial \Psi^{ab}_{I,\gamma}}{\partial X^\eta}\right) = 0_\beta, \tag{F.2.4}$$

$$\frac{\partial}{\partial X_\alpha}\left(c^{3\beta}_{I,\alpha 3}\frac{\partial \Psi^{ab}_{I,3}}{\partial X^\beta} + e^{\beta}_{\alpha 3}\frac{\partial \psi^{ab}_{I}}{\partial X^\beta}\right) = 0, \tag{F.2.5}$$

$$\frac{\partial}{\partial X_\alpha}\left(S_p e^{3\beta}_{\alpha}\frac{\partial \Psi^{ab}_{I,3}}{\partial X^\beta} - \epsilon^{S\beta}_{I,\alpha}\frac{\partial \psi^{ab}_{I}}{\partial X^\beta}\right) = 0, \tag{F.2.6}$$

in the inclusion phase, while satisfying the continuity conditions

$$\Psi^{ab}_{M,\alpha} = \Psi^{ab}_{I,\alpha}, \tag{F.2.7}$$

$$\Psi^{ab}_{M,3} = \Psi^{ab}_{I,3}, \tag{F.2.8}$$

$$\psi^{ab}_{M} = \psi^{ab}_{I}, \tag{F.2.9}$$

and the jump conditions

$$n^\alpha\left[c^{\gamma\eta}_{M,\alpha\beta}\frac{\partial \Psi^{ab}_{M,\gamma}}{\partial X^\eta} - c^{\gamma\eta}_{I,\alpha\beta}\frac{\partial \Psi^{ab}_{I,\gamma}}{\partial X^\eta}\right] = n^\alpha\left[c^{ab}_{I,\alpha\beta} - c^{ab}_{M,\alpha\beta}\right], \tag{F.2.10}$$

$$n^\alpha\left[c^{3\beta}_{M,\alpha 3}\frac{\partial \Psi^{ab}_{M,3}}{\partial X^\beta} - \left(c^{3\beta}_{I,\alpha 3}\frac{\partial \Psi^{ab}_{I,3}}{\partial X^\beta} + e^{\beta}_{\alpha 3}\frac{\partial \psi^{ab}_{I}}{\partial X^\beta}\right)\right] = n^\alpha\left[c^{ab}_{I,\alpha 3} - c^{ab}_{M,\alpha 3}\right], \tag{F.2.11}$$

$$n^\alpha\left[\left(-\epsilon^{S\beta}_{M,\alpha}\frac{\partial \psi^{ab}_{M}}{\partial X^\beta}\right) - \left(S_p e^{3\beta}_{\alpha}\frac{\partial \Psi^{ab}_{I,3}}{\partial X^\beta} - \epsilon^{S\beta}_{I,\alpha}\frac{\partial \psi^{ab}_{I}}{\partial X^\beta}\right)\right] = n^\alpha S_p e^{ab}_{\alpha}, \tag{F.2.12}$$

which hold on the boundary $\partial\Gamma_I \cap \partial\Gamma_M$. Note that because the inclusions are aligned so that there is translational symmetry in the Z-axis, the vertical component of the unit normal $\boldsymbol{n}$ is zero, namely $n^3 = 0$. If the RHS of (F.2.10) is zero for some $a, b \in \{1, 2, 3\}$, then $\Psi^{ab}_{\alpha} = 0_\alpha$. Similarly, if the RHS of both (F.2.11) and (F.2.12) are zero for some $a, b \in \{1, 2, 3\}$, then $\Psi^{ab}_{3} = \psi^{ab} = 0$.

F.3 Electrical cell problems

Under the assumptions set out in §F.1, (2.7.63)-(2.7.66) reduce to

$$\frac{\partial}{\partial X_\alpha}\left(c^{\gamma\eta}_{M,\alpha\beta}\frac{\partial \Phi^f_{M,\gamma}}{\partial X^\eta}\right) = 0_\beta, \tag{F.3.1}$$

$$\frac{\partial}{\partial X_\alpha}\left(c^{3\beta}_{M,\alpha 3}\frac{\partial \Phi^f_{M,3}}{\partial X^\beta}\right) = 0, \tag{F.3.2}$$

$$\frac{\partial}{\partial X_\alpha}\left(-\epsilon^{S\beta}_{M,\alpha}\frac{\partial \phi^f_M}{\partial X^\beta}\right) = 0, \tag{F.3.3}$$

in the matrix phase, and

$$\frac{\partial}{\partial X_\alpha}\left(c^{\gamma\eta}_{I,\alpha\beta}\frac{\partial \Phi^f_{I,\gamma}}{\partial X^\eta}\right) = 0_\beta, \tag{F.3.4}$$

$$\frac{\partial}{\partial X_\alpha}\left(c^{3\beta}_{I,\alpha 3}\frac{\partial \Phi^f_{I,3}}{\partial X^\beta} + e^{\beta}_{\alpha 3}\frac{\partial \phi^f_I}{\partial X^\beta}\right) = 0, \tag{F.3.5}$$

$$\frac{\partial}{\partial X_\alpha}\left(S_p e^{3\beta}_{\alpha}\frac{\partial \Phi^f_{I,3}}{\partial X^\beta} - \epsilon^{S\beta}_{I,\alpha}\frac{\partial \phi^f_I}{\partial X^\beta}\right) = 0, \tag{F.3.6}$$

in the inclusion phase, while satisfying the continuity conditions

$$\Phi^f_{M,\alpha} = \Phi^f_{I,\alpha}, \tag{F.3.7}$$

$$\Phi^f_{M,3} = \Phi^f_{I,3}, \tag{F.3.8}$$

$$\phi^f_M = \phi^f_I, \tag{F.3.9}$$

and the jump conditions

$$n^\alpha\left[c^{\gamma\eta}_{M,\alpha\beta}\frac{\partial \Phi^f_{M,\gamma}}{\partial X^\eta} - c^{\gamma\eta}_{I,\alpha\beta}\frac{\partial \Phi^f_{I,\gamma}}{\partial X^\eta}\right] = n^\alpha e^f_{\alpha\beta}, \tag{F.3.10}$$

$$n^\alpha\left[c^{3\beta}_{M,\alpha 3}\frac{\partial \Phi^f_{M,3}}{\partial X^\beta} - \left(c^{3\beta}_{I,\alpha 3}\frac{\partial \Phi^f_{I,3}}{\partial X^\beta} + e^{\beta}_{\alpha 3}\frac{\partial \phi^f_I}{\partial X^\beta}\right)\right] = n^\alpha e^f_{\alpha 3}, \tag{F.3.11}$$

$$n^\alpha\left[\left(-\epsilon^{S\beta}_{M,\alpha}\frac{\partial \phi^f_M}{\partial X^\beta}\right) - \left(S_p e^{3\beta}_{\alpha}\frac{\partial \Phi^f_{I,3}}{\partial X^\beta} - \epsilon^{S\beta}_{I,\alpha}\frac{\partial \phi^f_I}{\partial X^\beta}\right)\right] = n^\alpha\left[\epsilon^{Sf}_{M,\alpha} - \epsilon^{Sf}_{I,\alpha}\right], \tag{F.3.12}$$

which hold on the boundary $\partial\Gamma_I \cap \partial\Gamma_M$. Once again, because the inclusions are aligned so there is translational symmetry in the Z-axis, the vertical component of the unit normal $\boldsymbol{n}$ is zero, namely $n^3 = 0$. If the RHS of (F.3.10) is zero for some $f \in \{1,2,3\}$, then $\Phi^f_\alpha = 0_\alpha$. Similarly, if the RHS of both (F.3.11) and (F.3.12) are zero for some $f \in \{1,2,3\}$, then $\Phi^f_3 = \phi^f = 0$.

F.4 Cell functions that are zero

We will now use the boundary conditions established in §F.2-F.3, along with the assumptions established in (F.1.1)-(F.1.5), to determine which cell functions are zero [1]. This will reduce the number of unknowns we need to solve for analytically or numerically, as appropriate. Using (F.1.1)-(F.1.3) and (F.2.7)-(F.2.12), we see that

$$\Psi_3^{\alpha\beta} = \psi^{\alpha\beta} = 0, \tag{F.4.1}$$

$$\Psi_3^{33} = \psi^{33} = 0 \tag{F.4.2}$$

$$\Psi_\beta^{\alpha 3} = 0_\beta. \tag{F.4.3}$$

Using (F.1.3)-(F.1.5) and (F.3.7)-(F.3.12), we see that

$$\Phi_\beta^\alpha = 0_\beta, \tag{F.4.4}$$

$$\Phi_3^3 = \phi^3 = 0. \tag{F.4.5}$$

F.5 Effective coefficients

F.5.1 Stiffness coefficients

Using (F.4.1)-(F.4.3) along with (2.7.85), we deduce that

$$\begin{aligned} c^{\gamma\eta}_{\text{eff},\alpha\beta} &= \iiint_{\Gamma_M} c^{\alpha'\beta'}_{M,\alpha\beta}\frac{\partial \Psi^{\gamma\eta}_{M,\alpha'}}{\partial X^{\beta'}}\mathrm{d}V + \iiint_{\Gamma_I} c^{\alpha'\beta'}_{I,\alpha\beta}\frac{\partial \Psi^{\gamma\eta}_{I,\alpha'}}{\partial X^{\beta'}}\mathrm{d}V \\ &\quad + (1-\nu)c^{\gamma\eta}_{M,\alpha\beta} + \nu c^{\gamma\eta}_{I,\alpha\beta}, \end{aligned} \tag{F.5.1}$$

$$c^{\gamma 3}_{\text{eff},\alpha\beta} = c^{\alpha\beta}_{\text{eff},\gamma 3} = (1-\nu)c^{\gamma 3}_{M,\alpha\beta} + \nu c^{\gamma 3}_{I,\alpha\beta} = 0, \tag{F.5.2}$$

$$\begin{aligned} c^{\beta 3}_{\text{eff},\alpha 3} &= \iiint_{\Gamma_M} c^{3\gamma}_{M,\alpha 3}\frac{\partial \Psi^{\beta 3}_{M,3}}{\partial X^{\gamma}}\mathrm{d}V + \iiint_{\Gamma_I} c^{3\gamma}_{I,\alpha 3}\frac{\partial \Psi^{\beta 3}_{I,3}}{\partial X^{\gamma}} + e^{\gamma}_{\alpha 3}\frac{\partial \psi^{\beta 3}_I}{\partial X^\gamma}\mathrm{d}V \\ &\quad + (1-\nu)c^{\beta 3}_{M,\alpha 3} + \nu c^{\beta 3}_{I,\alpha 3}, \end{aligned} \tag{F.5.3}$$

$$c^{\gamma 3}_{\text{eff},33} = c^{33}_{\text{eff},\gamma 3} = (1-\nu)c^{\gamma 3}_{M,33} + \nu c^{\gamma 3}_{I,33} = 0, \tag{F.5.4}$$

$$\begin{aligned} c^{33}_{\text{eff},\alpha\beta} = c^{\alpha\beta}_{\text{eff},33} &= \iiint_{\Gamma_M} c^{\gamma\eta}_{M,\alpha\beta}\frac{\partial \Psi^{33}_{M,\gamma}}{\partial X^{\eta}}\mathrm{d}V + \iiint_{\Gamma_I} c^{\gamma\eta}_{I,\alpha\beta}\frac{\partial \Psi^{33}_{I,\gamma}}{\partial X^{\eta}}\mathrm{d}V \\ &\quad + (1-\nu)c^{33}_{M,\alpha\beta} + \nu c^{33}_{I,\alpha\beta}, \end{aligned} \tag{F.5.5}$$

$$\begin{aligned} c^{33}_{\text{eff},33} &= \iiint_{\Gamma_M} c^{\alpha\beta}_{M,33}\frac{\partial \Psi^{33}_{M,\alpha}}{\partial X^{\beta}}\mathrm{d}V + \iiint_{\Gamma_I} c^{\alpha\beta}_{I,33}\frac{\partial \Psi^{33}_{I,\alpha}}{\partial X^{\beta}}\mathrm{d}V + (1-\nu)c^{33}_{M,33} \\ &\quad + \nu c^{33}_{I,33}. \end{aligned} \tag{F.5.6}$$

[1] To be precise, we will determine which of the cell functions are constant. These functions are set to zero when the zero-mean condition is imposed for uniqueness.

F.5.2 Electromechanical coefficients

Using (F.4.4)-(F.4.5) along with (2.7.86), we deduce that

$$e^{\gamma}_{\text{eff},\alpha\beta} = \nu e^{\gamma}_{\alpha\beta} = 0, \tag{F.5.7}$$

$$e^{3}_{\text{eff},\alpha\beta} = \iiint_{\Gamma_M} c^{\gamma\eta}_{M,\alpha\beta}\frac{\partial \Phi^{3}_{M,\gamma}}{\partial X^{\eta}}\mathrm{d}V + \iiint_{\Gamma_I} c^{\gamma\eta}_{I,\alpha\beta}\frac{\partial \Phi^{3}_{I,\gamma}}{\partial X^{\eta}}\mathrm{d}V + \nu e^{3}_{\alpha\beta}, \tag{F.5.8}$$

$$e^{\beta}_{\text{eff},\alpha 3} = \iiint_{\Gamma_M} c^{3\gamma}_{M,\alpha 3}\frac{\partial \Phi^{\beta}_{M,3}}{\partial X^{\gamma}}\mathrm{d}V + \iiint_{\Gamma_I} c^{3\gamma}_{I,\alpha 3}\frac{\partial \Phi^{\beta}_{I,3}}{\partial X^{\gamma}} + e^{\gamma}_{\alpha 3}\frac{\partial \phi^{\beta}_{I}}{\partial X^{\gamma}}\mathrm{d}V + \nu e^{\beta}_{\alpha 3}, \tag{F.5.9}$$

$$e^{3}_{\text{eff},\alpha 3} = \nu e^{3}_{\alpha 3} = 0, \tag{F.5.10}$$

$$e^{\alpha}_{\text{eff},33} = \nu e^{\alpha}_{33} = 0, \tag{F.5.11}$$

$$e^{3}_{\text{eff},33} = \iiint_{\Gamma_M} c^{\alpha\beta}_{M,33}\frac{\partial \Phi^{3}_{M,\alpha}}{\partial X^{\beta}}\mathrm{d}V + \iiint_{\Gamma_I} c^{\alpha\beta}_{I,33}\frac{\partial \Phi^{3}_{I,\alpha}}{\partial X^{\beta}}\mathrm{d}V + \nu e^{3}_{33}. \tag{F.5.12}$$

F.5.3 Dielectric coefficients

Using (F.4.4)-(F.4.5) along with (2.7.88), we deduce that

$$\begin{aligned}\epsilon^{S\beta}_{\text{eff},\alpha} = &\iiint_{\Gamma_M} \epsilon^{S\gamma}_{M,\alpha}\frac{\partial \phi^{\beta}_{M}}{\partial X^{\gamma}}\mathrm{d}V + \iiint_{\Gamma_I} -S_p e^{3\gamma}_{\alpha}\frac{\partial \Phi^{\beta}_{I,3}}{\partial X^{\gamma}} + \epsilon^{S\gamma}_{I,\alpha}\frac{\partial \phi^{\beta}_{I}}{\partial X^{\gamma}}\mathrm{d}V \\ &+ (1-\nu)\epsilon^{S\beta}_{M,\alpha} + \nu\epsilon^{S\beta}_{I,\alpha},\end{aligned} \tag{F.5.13}$$

$$\epsilon^{S3}_{\text{eff},\alpha} = \epsilon^{S\alpha}_{\text{eff},3} = (1-\nu)\epsilon^{S3}_{M,\alpha} + \nu\epsilon^{S3}_{I,\alpha} = 0, \tag{F.5.14}$$

$$\epsilon^{S3}_{\text{eff},3} = \iiint_{\Gamma_I} -S_p e^{\alpha\beta}_{3}\frac{\partial \Phi^{3}_{I,\alpha}}{\partial X^{\beta}}\mathrm{d}V + (1-\nu)\epsilon^{S3}_{M,3} + \nu\epsilon^{S3}_{I,3}. \tag{F.5.15}$$

Appendix G

Definitions of lattice sums

We will use the convention that $\sum_{l=-\infty}^{\infty}\sum_{k=-\infty}^{\infty}$ denotes a sum taken first with respect to k and then with respect to l. Similarly, $\sum_{k=-\infty}^{\infty}\sum_{l=-\infty}^{\infty}$ will denote a sum taken first with respect to l, then with respect to k. Note that in Chapter 4, for the x coordinate, we will first sum with respect to k and then with respect to l, while for the y coordinate we will sum with respect to l, then k. Additionally, we will use the convention that a prime on a double sum indicates that the origin term has been omitted. If f_{kl} is a map from $\mathbb{Z}\times\mathbb{Z}/\{(0,0)\}$ to $\mathbb{R}$, then we define

$$\begin{aligned}\sum_{l=-\infty}^{\infty}\sum_{k=-\infty}^{\infty}{}' f_{kl} &= \sum_{l=1}^{\infty}\sum_{k=1}^{\infty}\left(f_{-k,-l}+f_{k,-l}+f_{-k,l}+f_{k,l}\right)\\ &\quad+\sum_{k=1}^{\infty}\left(f_{0,-k}+f_{-k,0}+f_{k,0}+f_{0,k}\right), \qquad \text{(G.0.1)}\\ \sum_{k=-\infty}^{\infty}\sum_{l=-\infty}^{\infty}{}' f_{kl} &= \sum_{k=1}^{\infty}\sum_{l=1}^{\infty}\left(f_{-k,-l}+f_{k,-l}+f_{-k,l}+f_{k,l}\right)\\ &\quad+\sum_{k=1}^{\infty}\left(f_{0,-k}+f_{-k,0}+f_{k,0}+f_{0,k}\right). \qquad \text{(G.0.2)}\end{aligned}$$

Appendix H

Taylor expansions of lattice sums computations

In this section of the Appendix, we will derive the Taylor expansions of some of the common functions that show up in Chapter 4.

We first note that

$$\sum_{l=-\infty}^{\infty}\sum_{k=-\infty}^{\infty}\frac{X-k}{(X-k)^2+(Y-l)^2} = \frac{X}{X^2+Y^2}+\sum_{l=-\infty}^{\infty}\sum_{k=-\infty}^{\infty}{}'\frac{X-k}{(X-k)^2+(Y-l)^2}. \tag{H.0.1}$$

If we assume term wise differentiation, then we get

$$\sum_{l=-\infty}^{\infty}\sum_{k=-\infty}^{\infty}\frac{X-k}{(X-k)^2+(Y-l)^2} \sim \frac{X}{X^2+Y^2}+X\left(\sum_{l=-\infty}^{\infty}\sum_{k=-\infty}^{\infty}{}'\frac{l^2-k^2}{(k^2+l^2)^2}\right) - Y\left(\sum_{l=-\infty}^{\infty}\sum_{k=-\infty}^{\infty}{}'\frac{2kl}{(k^2+l^2)^2}\right)+O\left(X^2+Y^2\right). \tag{H.0.2}$$

Using the definitions (G.0.1)-(G.0.2) and the help of Mathematica, we compute the following lattice sums

$$\sum_{l=-\infty}^{\infty}\sum_{k=-\infty}^{\infty}{}'\frac{l^2-k^2}{(k^2+l^2)^2} = \sum_{l=1}^{\infty}\sum_{k=1}^{\infty}4\frac{l^2-k^2}{(k^2+l^2)^2}+\sum_{k=1}^{\infty}\left(\frac{1}{k^2}-\frac{1}{k^2}-\frac{1}{k^2}+\frac{1}{k^2}\right) = 4\sum_{l=1}^{\infty}\sum_{k=1}^{\infty}\frac{l^2-k^2}{(k^2+l^2)^2}=-\pi, \tag{H.0.3}$$

$$\sum_{l=-\infty}^{\infty}\sum_{k=-\infty}^{\infty}{}' \frac{2kl}{(k^2+l^2)^2}$$
$$= \sum_{l=1}^{\infty}\sum_{k=1}^{\infty}\left(\frac{2kl}{(k^2+l^2)^2} - \frac{2kl}{(k^2+l^2)^2} + \frac{2kl}{(k^2+l^2)^2} - \frac{2kl}{(k^2+l^2)^2}\right)$$
$$+ \sum_{k=1}^{\infty}(0+0+0+0) = 0. \quad \text{(H.0.4)}$$

Substituting (H.0.3)-(H.0.4), we deduce

$$\sum_{l=-\infty}^{\infty}\sum_{k=-\infty}^{\infty}\frac{X-k}{(X-k)^2+(Y-l)^2} \sim \frac{X}{X^2+Y^2} - \pi X + O\left(X^2+Y^2\right). \quad \text{(H.0.5)}$$

The function $\sum_{k=-\infty}^{\infty}\sum_{l=-\infty}^{\infty}\frac{Y-l}{(X-k)^2+(Y-l)^2}$ is similar to $\sum_{l=-\infty}^{\infty}\sum_{k=-\infty}^{\infty}\frac{X-k}{(X-k)^2+(Y-l)^2}$ except with the X and Y coordinates switched. Using (H.0.5) we deduce

$$\sum_{k=-\infty}^{\infty}\sum_{l=-\infty}^{\infty}\frac{Y-l}{(X-k)^2+(Y-l)^2} \sim \frac{Y}{X^2+Y^2} - \pi Y + O\left(X^2+Y^2\right). \quad \text{(H.0.6)}$$

We will now derive the Taylor expansions of the functions $\sum_{l=-\infty}^{\infty}\sum_{k=-\infty}^{\infty}\frac{(X-k)((Y-l)^2-(X-k)^2)}{((X-k)^2+(Y-l)^2)^2}$ and $\sum_{k=-\infty}^{\infty}\sum_{l=-\infty}^{\infty}\frac{(Y-l)((Y-l)^2-(X-k)^2)}{((X-k)^2+(Y-l)^2)^2}$. We first start by deriving the Taylor series for $\sum_{l=-\infty}^{\infty}\sum_{k=-\infty}^{\infty}\frac{X-k}{(X-k)^2+(Y-l)^2}$. We first note that

$$\sum_{l=-\infty}^{\infty}\sum_{k=-\infty}^{\infty}\frac{(X-k)((Y-l)^2-(X-k)^2)}{((X-k)^2+(Y-l)^2)^2}$$
$$\sim \frac{X(Y^2-X^2)}{(X^2+Y^2)^2} + \sum_{l=-\infty}^{\infty}\sum_{k=-\infty}^{\infty}{}'\frac{(X-k)((Y-l)^2-(X-k)^2)}{((X-k)^2+(Y-l)^2)^2}. \quad \text{(H.0.7)}$$

If we assume term wise differentiation, then we get

$$\sum_{l=-\infty}^{\infty}\sum_{k=-\infty}^{\infty}\frac{(X-k)((Y-l)^2-(X-k)^2)}{((X-k)^2+(Y-l)^2)^2} \sim \frac{X(Y^2-X^2)}{(X^2+Y^2)^2}$$
$$+X\left(\sum_{l=-\infty}^{\infty}\sum_{k=-\infty}^{\infty}{}'\frac{k^4-6k^2l^2+l^4}{(k^2+l^2)^3}\right) - Y\left(\sum_{l=-\infty}^{\infty}\sum_{k=-\infty}^{\infty}{}'\frac{6k^3l-2kl^3}{(k^2+l^2)^3}\right) + O\left(X^2+Y^2\right). \quad \text{(H.0.8)}$$

Using the definitions (G.0.1)-(G.0.2) and the help of Mathematica, we compute the

following lattice sums

$$\sum_{l=-\infty}^{\infty}\sum_{k=-\infty}^{\infty}{}' \frac{k^4-6k^2l^2+l^4}{\left(k^2+l^2\right)^3} = \sum_{l=1}^{\infty}\sum_{k=1}^{\infty}{}' 4\frac{k^4-6k^2l^2+l^4}{\left(k^2+l^2\right)^3} + \sum_{k=1}^{\infty} 4\frac{k^4}{\left(k^2\right)^3}$$
$$= \pi\left(1+4\sum_{l=1}^{\infty}\pi^2 l\coth(l\pi)\operatorname{csch}(l\pi)^2\right), \quad \text{(H.0.9)}$$

$$\sum_{l=-\infty}^{\infty}\sum_{k=-\infty}^{\infty}{}' \frac{6k^3l-2kl^3}{\left(k^2+l^2\right)^3}$$
$$= \sum_{l=1}^{\infty}\sum_{k=1}^{\infty}\left(\frac{6k^3l-2kl^3}{\left(k^2+l^2\right)^3} - \frac{6k^3l-2kl^3}{\left(k^2+l^2\right)^3} + \frac{6k^3l-2kl^3}{\left(k^2+l^2\right)^3} - \frac{6k^3l-2kl^3}{\left(k^2+l^2\right)^3}\right)$$
$$+ \sum_{k=1}^{\infty}(0+0+0+0) = 0. \quad \text{(H.0.10)}$$

Substituting (H.0.9)-(H.0.10), we deduce

$$\sum_{l=-\infty}^{\infty}\sum_{k=-\infty}^{\infty}\frac{(X-k)((Y-l)^2-(X-k)^2)}{((X-k)^2+(Y-l)^2)^2}$$
$$\sim \frac{X(Y^2-X^2)}{(X^2+Y^2)^2} + \pi\left(1+4\sum_{l=1}^{\infty}\pi^2 l\coth(l\pi)\operatorname{csch}(l\pi)^2\right)X + O\left(X^2+Y^2\right). \quad \text{(H.0.11)}$$

The function $\sum_{k=-\infty}^{\infty}\sum_{l=-\infty}^{\infty}\frac{(Y-l)((Y-l)^2-(X-k)^2)}{((X-k)^2+(Y-l)^2)^2}$ is similar to $\sum_{l=-\infty}^{\infty}\sum_{k=-\infty}^{\infty}\frac{(X-k)((Y-l)^2-(X-k)^2)}{((X-k)^2+(Y-l)^2)^2}$ except with the X and Y coordinates switched and the output multiplied by -1. Using (H.0.11) we deduce

$$\sum_{k=-\infty}^{\infty}\sum_{l=-\infty}^{\infty}\frac{(Y-l)((Y-l)^2-(X-k)^2)}{((X-k)^2+(Y-l)^2)^2}$$
$$\sim \frac{Y(Y^2-X^2)}{(X^2+Y^2)^2} - \pi\left(1+4\sum_{l=1}^{\infty}\pi^2 l\coth(l\pi)\operatorname{csch}(l\pi)^2\right)Y + O\left(X^2+Y^2\right). \quad \text{(H.0.12)}$$

Appendix I

Symmetry relations for actuator problem

In this section, we will prove the following symmetry relations

$$\mathbb{A}^{ijkl} = \mathbb{A}^{klij}, \qquad \mathbb{B}^{ijkl} = \mathbb{B}^{\dagger klij}, \qquad \mathbb{D}^{ijkl} = \mathbb{D}^{klij}. \tag{I.0.1}$$

We will start by proving $\mathbb{A}^{ijkl} = \mathbb{A}^{klij}$.

Proof. Using (6.2.137), we deduce

$$\mathbb{A}^{ijkl} = \fint\!\!\!\fint_{\Gamma} \delta^i_{i'}\delta^j_{j'} \left(c^{i'j'k'l'} \left(\frac{\partial \Psi^{kl}_{k'}}{\partial X^{l'}} + \delta^k_{k'}\delta^l_{l'} \right) + e^{ijk'} \frac{\partial \psi^{kl}}{\partial X^{k'}} \right) d\Gamma. \tag{I.0.2}$$

Applying the Divergence Theorem and (K.1.1)-(K.1.10), we deduce

$$\fint\!\!\!\fint_{\Gamma} \left(c^{i'j'k'l'} \left(\frac{\partial \Psi^{kl}_{k'}}{\partial X^{l'}} + \delta^k_{k'}\delta^l_{l'} \right) + e^{i'j'k'} \frac{\partial \psi^{kl}}{\partial X^{k'}} \right) \frac{\partial \Psi^{ij}_{i'}}{\partial X^{j'}} d\Gamma = 0. \tag{I.0.3}$$

From (I.0.2)-(I.0.3), we deduce

$$\mathbb{A}^{ijkl} = \fint\!\!\!\fint_{\Gamma} \left(c^{i'j'k'l'} \left(\frac{\partial \Psi^{kl}_{k'}}{\partial X^{l'}} + \delta^k_{k'}\delta^l_{l'} \right) + e^{i'j'k'} \frac{\partial \psi^{kl}}{\partial X^{k'}} \right) \left(\frac{\partial \Psi^{ij}_{i'}}{\partial X^{j'}} + \delta^i_{i'}\delta^j_{j'} \right) d\Gamma. \tag{I.0.4}$$

Equation (I.0.4) rearranges to

$$\mathbb{A}^{ijkl} = \fint\!\!\!\fint_{\Gamma} c^{i'j'k'l'} \left(\frac{\partial \Psi^{kl}_{k'}}{\partial X^{l'}} + \delta^k_{k'}\delta^l_{l'} \right) \left(\frac{\partial \Psi^{ij}_{i'}}{\partial X^{j'}} + \delta^i_{i'}\delta^j_{j'} \right) + e^{k'l'i'} \left(\frac{\partial \Psi^{ij}_{k'}}{\partial X^{l'}} + \delta^i_{k'}\delta^j_{l'} \right) \frac{\partial \psi^{kl}}{\partial X^{i'}} d\Gamma. \tag{I.0.5}$$

Using the Divergence Theorem and (K.1.1)-(K.1.10), we deduce

$$\fint\!\!\!\fint_{\Gamma} \left(e^{k'l'i'} \left(\frac{\partial \Psi^{ij}_{k'}}{\partial X^{l'}} + \delta^i_{k'}\delta^j_{l'} \right) - \frac{1}{S_p} \epsilon^{Si'k'} \frac{\partial \psi^{ij}}{\partial X^{k'}} \right) \frac{\partial \psi^{kl}}{\partial X^{i'}} d\Gamma = 0. \tag{I.0.6}$$

Applying (I.0.6), (I.0.5) yields

$$\mathbb{A}^{ijkl} = \iiint_{\Gamma} c^{i'j'k'l'} \left(\frac{\partial \Psi^{ij}_{i'}}{\partial X^{j'}} + \delta^i_{i'} \delta^j_{j'} \right) \left(\frac{\partial \Psi^{kl}_{k'}}{\partial X^{l'}} + \delta^k_{k'} \delta^l_{l'} \right) + \frac{1}{S_p} \epsilon^{Si'k'} \frac{\partial \psi^{ij}}{\partial X^{i'}} \frac{\partial \psi^{kl}}{\partial X^{k'}} d\Gamma. \quad \text{(I.0.7)}$$

From (I.0.7) along with (2.2.3) and (2.4.11), we deduce

$$\mathbb{A}^{ijkl} = \mathbb{A}^{klij}. \quad \text{(I.0.8)}$$

This completes the proof. □

We will now prove $\mathbb{B}^{ijkl} = \mathbb{B}^{\dagger klij}$.

Proof. Using (6.2.138)-(6.2.139), we see that

$$\mathbb{B}^{ijkl} = -\iiint_{\Gamma} \left(c^{i'j'k'l'} \left(\frac{\partial \Phi^{kl}_{k'}}{\partial X^{l'}} - \left(Z - Z^{\dagger} \right) \delta^k_{k'} \delta^l_{l'} \right) + e^{ijk'} \frac{\partial \phi^{kl}}{\partial X^{k'}} \right) \delta^i_{i'} \delta^j_{j'} d\Gamma, \quad \text{(I.0.9)}$$

$$\mathbb{B}^{\dagger ijkl} = \iiint_{\Gamma} \left(Z - Z^{\dagger} \right) \left(c^{i'j'k'l'} \left(\frac{\partial \Psi^{kl}_{k'}}{\partial X^{l'}} + \delta^k_{k'} \delta^l_{l'} \right) + e^{i'j'k'} \frac{\partial \psi^{kl}}{\partial X^{k'}} \right) \delta^i_{i'} \delta^j_{j'} d\Gamma. \quad \text{(I.0.10)}$$

Applying the Divergence Theorem and (K.1.14)-(K.1.23), we deduce

$$\iiint_{\Gamma} \left(c^{i'j'k'l'} \left(\frac{\partial \Phi^{kl}_{k'}}{\partial X^{l'}} - \left(Z - Z^{\dagger} \right) \delta^k_{k'} \delta^l_{l'} \right) + e^{i'j'k'} \frac{\partial \phi^{kl}}{\partial X^{k'}} \right) \frac{\partial \Psi^{ij}_{i'}}{\partial X^{j'}} d\Gamma = 0, \quad \text{(I.0.11)}$$

$$\iiint_{\Gamma} \left(c^{i'j'k'l'} \left(\frac{\partial \Psi^{kl}_{k'}}{\partial X^{l'}} + \delta^k_{k'} \delta^l_{l'} \right) + e^{i'j'k'} \frac{\partial \psi^{kl}}{\partial X^{k'}} \right) \frac{\partial \Phi^{ij}_{i'}}{\partial X^{j'}} d\Gamma = 0. \quad \text{(I.0.12)}$$

From (I.0.9)-(I.0.12), we deduce

$$\mathbb{B}^{ijkl} = -\iiint_{\Gamma} \left(c^{i'j'k'l'} \left(\frac{\partial \Phi^{kl}_{k'}}{\partial X^{l'}} - \left(Z - Z^{\dagger} \right) \delta^k_{k'} \delta^l_{l'} \right) + e^{i'j'k'} \frac{\partial \phi^{kl}}{\partial X^{k'}} \right) \left(\delta^i_{i'} \delta^j_{j'} + \frac{\partial \Psi^{ij}_{i'}}{\partial X^{j'}} \right) d\Gamma, \quad \text{(I.0.13)}$$

$$\mathbb{B}^{\dagger ijkl} = -\iiint_{\Gamma} \left(c^{i'j'k'l'} \left(\frac{\partial \Psi^{kl}_{k'}}{\partial X^{l'}} + \delta^k_{k'} \delta^l_{l'} \right) + e^{i'j'k'} \frac{\partial \psi^{kl}}{\partial X^{k'}} \right) \left(\frac{\partial \Phi^{ij}_{i'}}{\partial X^{j'}} - \left(Z - Z^{\dagger} \right) \delta^i_{i'} \delta^j_{j'} \right) d\Gamma. \quad \text{(I.0.14)}$$

Equations (I.0.13)-(I.0.14) rearrange to

$$\mathbb{B}^{ijkl} = -\iiint_{\Gamma} c^{i'j'k'l'} \left(\frac{\partial \Phi^{kl}_{k'}}{\partial X^{l'}} - \left(Z - Z^{\dagger} \right) \delta^k_{k'} \delta^l_{l'} \right) \left(\delta^i_{i'} \delta^j_{j'} + \frac{\partial \Psi^{ij}_{i'}}{\partial X^{j'}} \right) d\Gamma$$
$$- \iiint_{\Gamma} e^{i'j'k'} \frac{\partial \phi^{kl}}{\partial X^{k'}} \left(\delta^i_{i'} \delta^j_{j'} + \frac{\partial \Psi^{ij}_{i'}}{\partial X^{j'}} \right) d\Gamma, \quad \text{(I.0.15)}$$

$$\mathbb{B}^{\dagger ijkl} = -\iiint_{\Gamma} c^{i'j'k'l'} \left(\frac{\partial \Psi^{kl}_{k'}}{\partial X^{l'}} + \delta^k_{k'}\delta^l_{l'}\right)\left(\frac{\partial \Phi^{ij}_{i'}}{\partial X^{j'}} - \left(Z - Z^\dagger\right)\delta^i_{i'}\delta^j_{j'}\right) d\Gamma$$
$$- \iiint_{\Gamma} e^{i'j'k'} \frac{\partial \psi^{kl}}{\partial X^{k'}}\left(\frac{\partial \Phi^{ij}_{i'}}{\partial X^{j'}} - \left(Z - Z^\dagger\right)\delta^i_{i'}\delta^j_{j'}\right) d\Gamma. \quad \text{(I.0.16)}$$

Using the Divergence Theorem and (K.1.1)-(K.1.10), we deduce

$$\iiint_{\Gamma}\left(e^{i'j'k'}\left(\frac{\partial \Psi^{ij}_{i'}}{\partial X^{j'}} + \delta^i_{i'}\delta^j_{j'}\right) - \frac{1}{S_p}\epsilon^{Sk'i'}\frac{\partial \psi^{ij}}{\partial X^{i'}}\right)\frac{\partial \phi^{kl}}{\partial X^{k'}} d\Gamma = 0, \quad \text{(I.0.17)}$$
$$\iiint_{\Gamma}\left(e^{i'j'k'}\left(\frac{\partial \Phi^{ij}_{i'}}{\partial X^{j'}} - (Z - Z^\dagger)\delta^i_{i'}\delta^j_{j'}\right) - \frac{1}{S_p}\epsilon^{Sk'i'}\frac{\partial \phi^{ij}}{\partial X^{i'}}\right)\frac{\partial \psi^{kl}}{\partial X^{k'}} d\Gamma = 0. \quad \text{(I.0.18)}$$

Applying (I.0.15)-(I.0.18), (I.0.13)-(I.0.14) reduce to

$$\mathbb{B}^{ijkl} = -\iiint_{\Gamma} c^{i'j'k'l'}\left(\delta^i_{i'}\delta^j_{j'} + \frac{\partial \Psi^{ij}_{i'}}{\partial X^{j'}}\right)\left(\frac{\partial \Phi^{kl}_{k'}}{\partial X^{l'}} - \left(Z - Z^\dagger\right)\delta^k_{k'}\delta^l_{l'}\right) + \frac{1}{S_p}\epsilon^{Sk'i'}\frac{\partial \psi^{ij}}{\partial X^{k'}}\frac{\partial \phi^{kl}}{\partial X^{i'}} d\Gamma, \quad \text{(I.0.19)}$$

$$\mathbb{B}^{\dagger ijkl} = -\iiint_{\Gamma} c^{i'j'k'l'}\left(\frac{\partial \Phi^{ij}_{i'}}{\partial X^{j'}} - \left(Z - Z^\dagger\right)\delta^i_{i'}\delta^j_{j'}\right)\left(\frac{\partial \Psi^{kl}_{k'}}{\partial X^{l'}} + \delta^k_{k'}\delta^l_{l'}\right) + \frac{1}{S_p}\epsilon^{Sk'i'}\frac{\partial \phi^{ij}}{\partial X^{k}}\frac{\partial \psi^{kl}}{\partial X^{i}} d\Gamma. \quad \text{(I.0.20)}$$

From (I.0.19)-(I.0.20) we deduce

$$\mathbb{B}^{ijkl} = \mathbb{B}^{\dagger klij}. \quad \text{(I.0.21)}$$

This completes the proof. □

We will now prove $\mathbb{D}^{ijkl} = \mathbb{D}^{klij}$.

Proof. Using (6.2.137), we deduce

$$\mathbb{D}^{ijkl} = \iiint_{\Gamma}\left(c^{i'j'k'l'}\left(\frac{\partial \Phi^{kl}_{k'}}{\partial X^{l'}} - \left(Z - Z^\dagger\right)\delta^k_{k'}\delta^l_{l'}\right) + e^{i'j'k'}\frac{\partial \phi^{kl}}{\partial X^{k'}}\right)\left(-\left(Z - Z^\dagger\right)\delta^i_{i'}\delta^j_{j'}\right) d\Gamma. \quad \text{(I.0.22)}$$

Applying the Divergence Theorem and (K.1.1)-(K.1.10), we deduce

$$\iiint_{\Gamma}\left(c^{i'j'k'l'}\left(\frac{\partial \Phi^{kl}_{k'}}{\partial X^{l'}} - \left(Z - Z^\dagger\right)\delta^k_{k'}\delta^l_{l'}\right) + e^{i'j'k'}\frac{\partial \phi^{kl}}{\partial X^{k'}}\right)\frac{\partial \Phi^{ij}_{i'}}{\partial X^{j'}} d\Gamma = 0. \quad \text{(I.0.23)}$$

From (I.0.22)-(I.0.23), we deduce

$$\mathbb{D}^{ijkl} = \iiint_{\Gamma}\left(c^{i'j'k'l'}\left(\frac{\partial \Phi^{kl}_{k'}}{\partial X^{l'}} - \left(Z - Z^\dagger\right)\delta^k_{k'}\delta^l_{l'}\right) + e^{i'j'k'}\frac{\partial \phi^{kl}}{\partial X^{k'}}\right)\left(\frac{\partial \Phi^{ij}_{i'}}{\partial X^{j'}} - \left(Z - Z^\dagger\right)\delta^i_{i'}\delta^j_{j'}\right) d\Gamma. \quad \text{(I.0.24)}$$

Equation (I.0.24) rearranges to

$$\mathbb{D}^{ijkl} = \iiint_{\Gamma} c^{i'j'k'l'} \left(\frac{\partial \Phi^{ij}_{i'}}{\partial X^{j'}} - \left(Z - Z^{\dagger} \right) \delta^{i}_{i'} \delta^{j}_{j'} \right) \left(\frac{\partial \Phi^{kl}_{k'}}{\partial X^{l'}} - \left(Z - Z^{\dagger} \right) \delta^{k}_{k'} \delta^{l}_{l'} \right) d\Gamma$$
$$+ \iiint_{\Gamma} e^{i'j'k'} \left(\frac{\partial \Phi^{ij}_{i'}}{\partial X^{j'}} - \left(Z - Z^{\dagger} \right) \delta^{i}_{i'} \delta^{j}_{j'} \right) \frac{\partial \phi^{kl}}{\partial X^{k'}} d\Gamma. \quad \text{(I.0.25)}$$

Using the Divergence Theorem and (K.1.1)-(K.1.10), we deduce

$$\iiint_{\Gamma} \left(e^{i'j'k'} \left(\frac{\partial \Phi^{ij}_{i'}}{\partial X^{j'}} - (Z - Z^{\dagger}) \delta^{i}_{i'} \delta^{j}_{j'} \right) - \frac{1}{S_p} \epsilon^{Sk'i'} \frac{\partial \phi^{ij}}{\partial X^{i'}} \right) \frac{\partial \phi^{kl}}{\partial X^{k'}} d\Gamma = 0. \quad \text{(I.0.26)}$$

Applying (I.0.26), (I.0.25) yields

$$\mathbb{D}^{ijkl} = \iiint_{\Gamma} c^{i'j'k'l'} \left(\frac{\partial \Phi^{ij}_{i'}}{\partial X^{j'}} - \left(Z - Z^{\dagger} \right) \delta^{i}_{i'} \delta^{j}_{j'} \right) \left(\frac{\partial \Phi^{kl}_{k'}}{\partial X^{l'}} - \left(Z - Z^{\dagger} \right) \delta^{k}_{k'} \delta^{l}_{l'} \right) d\Gamma$$
$$+ \iiint_{\Gamma} \frac{1}{S_p} \epsilon^{Sk'i'} \frac{\partial \phi^{ij}}{\partial X^{k'}} \frac{\partial \phi^{kl}}{\partial X^{i'}} d\Gamma. \quad \text{(I.0.27)}$$

From (I.0.27) along with (2.2.3) and (2.4.11), we deduce

$$\mathbb{D}^{ijkl} = \mathbb{D}^{klij}. \quad \text{(I.0.28)}$$

This completes the proof. □

Appendix J

Solving the time-independent piezoelectric problem on the unit cell with actuator boundary conditions

J.1 Case with no forcing

We define Γ and Γ_J , J $\in \{M, I\}$ as in §6.2.4. We impose the PDEs (which hold on Γ_J)

$$\frac{\partial}{\partial X^i}\left(c_J^{ijkl}\frac{\partial U_{J,k}}{\partial X^l} + e_J^{ijk}\frac{\partial \varphi_J}{\partial X^k}\right) = 0^j, \tag{J.1.1}$$

$$\frac{\partial}{\partial X^i}\left(e_J^{kli}\frac{\partial U_{J,k}}{\partial X^l} - \frac{1}{S_p}\epsilon_J^{Sik}\frac{\partial \varphi_J}{\partial X^k}\right) = 0, \tag{J.1.2}$$

we then impose continuity and jump conditions (which hold on $\partial\Gamma_M \cup \partial\Gamma_I$)

$$U_{M,j} = U_{I,j}, \tag{J.1.3}$$

$$\varphi_M = \varphi_I, \tag{J.1.4}$$

$$n_i\left(c_M^{ijkl}\frac{\partial U_{M,k}}{\partial X^l} + e_M^{ijk}\frac{\partial \varphi_M}{\partial X^k}\right) = n^i\left(c_I^{ijkl}\frac{\partial U_{I,k}}{\partial X^l} + e_I^{ijk}\frac{\partial \varphi_I}{\partial X^k}\right), \tag{J.1.5}$$

$$n_i\left(S_p e_M^{kli}\frac{\partial U_{M,k}}{\partial X^l} - \epsilon_M^{Sik}\frac{\partial \varphi_M}{\partial X^k}\right) = n_i\left(S_p e_I^{kli}\frac{\partial U_{I,k}}{\partial X^l} - \epsilon_I^{Sik}\frac{\partial \varphi_I}{\partial X^k}\right), \tag{J.1.6}$$

and finally impose the boundary conditions (which hold on $\{(X,Y,Z) \in \partial\Gamma : Z \in \{0,1\}\}$)

$$\left[c_J^{3jkl}\frac{\partial U_{J,k}}{\partial X^l} + e_J^{3jk}\frac{\partial \varphi_J}{\partial X^k}\right]_{Z=1} = 0^j, \tag{J.1.7}$$

$$\left[c_J^{3jkl}\frac{\partial U_{J,k}}{\partial X^l} + e_J^{3jk}\frac{\partial \varphi_J}{\partial X^k}\right]_{Z=0} = 0^j, \tag{J.1.8}$$

$$\varphi_J|_{Z=1} = 0, \tag{J.1.9}$$

$$\varphi_J|_{Z=0} = 0. \tag{J.1.10}$$

We let $\delta\boldsymbol{U}$ and $\delta\varphi$ be small variations of $\boldsymbol{U}$ and φ which both satisfy periodic boundary conditions on Γ (in the planar directions only). In light of (J.1.9)-(J.1.10), we impose the following condition on $\delta\varphi$ (which hold on $\{(X,Y,Z) \in \partial\Gamma : Z \in \{0,1\}\}$)

$$\delta\varphi_J|_{Z=1} = 0, \tag{J.1.11}$$

$$\delta\varphi_J|_{Z=0} = 0. \tag{J.1.12}$$

Using (J.1.1)-(J.1.2) along with D'Alembert's principle (see [5]), we deduce that

$$\iiint_\Gamma \frac{\partial}{\partial X^i}\left(c^{ijkl}\frac{\partial U_k}{\partial X^l} + e^{ijk}\frac{\partial \varphi}{\partial X^k}\right)\delta U_j + \frac{\partial}{\partial X^i}\left(e^{kli}\frac{\partial U_k}{\partial X^l} - \frac{1}{S_p}\epsilon^{Sik}\frac{\partial \varphi}{\partial X^k}\right)\delta\varphi d\Gamma = 0. \tag{J.1.13}$$

Applying integration by parts, (J.1.13) yields

$$\begin{aligned}&\frac{1}{|\Gamma|}\iint_{\partial\Gamma} n_i\left(c^{ijkl}\frac{\partial U_k}{\partial X^l} + e^{ijk}\frac{\partial \varphi}{\partial X^k}\right)\delta U_j + n_i\left(e^{kli}\frac{\partial U_k}{\partial X^l} - \frac{1}{S_p}\epsilon^{Sik}\frac{\partial \varphi}{\partial X^k}\right)\delta\varphi d\partial\Gamma \\ &-\iiint_\Gamma \left(c^{ijkl}\frac{\partial U_k}{\partial X^l} + e^{ijk}\frac{\partial \varphi}{\partial X^k}\right)\left(\frac{\partial\left(\delta U_j\right)}{\partial X^i}\right) + \left(e^{kli}\frac{\partial U_k}{\partial X^l} - \frac{1}{S_p}\epsilon^{Sik}\frac{\partial \varphi}{\partial X^k}\right)\left(\frac{\partial(\delta\varphi)}{\partial X^i}\right) d\Gamma = 0.\end{aligned} \tag{J.1.14}$$

From the periodic boundary conditions and also the stress conditions (J.1.7)-(J.1.8), (J.1.14) yields

$$-\iiint_\Gamma \left(c_{ij}^{kl}\frac{\partial U_k}{\partial X^l} + e_{ij}^{k}\frac{\partial \varphi}{\partial X^k}\right)\left(\frac{\partial\left(\delta U_j\right)}{\partial X_i}\right) + \left(e_i^{kl}\frac{\partial U_k}{\partial X^l} - \frac{1}{S_p}\epsilon^{Sik}\frac{\partial \varphi}{\partial X^k}\right)\left(\frac{\partial(\delta\varphi)}{\partial X_i}\right) d\Gamma = 0. \tag{J.1.15}$$

If we set $\delta U_j = -U_j$ and $\delta\varphi = \varphi$, (J.1.14) yields

$$\iiint_\Gamma c_{ij}^{kl}\frac{\partial U_k}{\partial X^l}\frac{\partial U_j}{\partial X_i} + \frac{1}{S_p}\epsilon^{Sik}\frac{\partial \varphi}{\partial X^k}\frac{\partial \varphi}{\partial X_i} d\Gamma = 0. \tag{J.1.16}$$

Because of the uniform ellipticity of the elasticity and dielectric tensors (see Appendix B, (J.1.16) implies

$$\frac{\partial U_i}{\partial X^j} + \frac{\partial U_j}{\partial X^i} = 0_{ij}, \tag{J.1.17}$$

$$\frac{\partial \varphi}{\partial X^k} = 0_k. \tag{J.1.18}$$

Using (J.1.9)-(J.1.10), we see that (J.1.18) implies

$$\varphi = 0. \tag{J.1.19}$$

Equation (J.1.17) implies

$$\frac{\partial U_\alpha}{\partial X^\beta} + \frac{\partial U_\beta}{\partial X^\alpha} = 0_{\alpha\beta}, \tag{J.1.20}$$

$$\frac{\partial U_3}{\partial X^\alpha} + \frac{\partial U_\alpha}{\partial Z} = 0_\alpha, \tag{J.1.21}$$

$$2\frac{\partial U_3}{\partial Z} = 0. \tag{J.1.22}$$

From Korn's inequality (see [43]) we see that (J.1.20) implies that U_α is independent of X and Y, namely

$$U_\alpha = U_\alpha(Z). \tag{J.1.23}$$

Equation (J.1.22) implies U_3 is independent of Z, namely

$$U_3 = U_3(X, Y). \tag{J.1.24}$$

Using (J.1.23)-(J.1.24), (J.1.21) can be re-written as

$$\frac{\partial U_3}{\partial X^\alpha}(X, Y) + \frac{dU_\alpha}{dZ}(Z) = 0_\alpha. \tag{J.1.25}$$

From (J.1.25), we see that $\frac{\partial U_3}{\partial X^\alpha}(X, Y)$ is independent of both X and Y, which implies that $U_3(X, Y)$ is linear in both X and Y. Since U_3 must satisfy periodic boundary conditions, it follows that

$$\frac{\partial U_3}{\partial X^\alpha}(X, Y) = 0 \iff U_3 \text{ is a constant}, \tag{J.1.26}$$

$$\frac{dU_\alpha}{dZ}(Z) = 0 \iff U_\alpha \text{ is a constant}. \tag{J.1.27}$$

Therefore, if the right hand sides of (J.1.1)-(J.1.10) are non-zero, and a solution exists, $\boldsymbol{U}$ is unique up to an additive constant (or a function independent of X, Y and Z) while φ is uniquely determined.

J.2 Solution to $O(\varepsilon)$ problem for time-dependent problem

From §J.1 and §K.1, we assume that

$$\varphi_{(1)}(t,x,y;X,Y,Z)=0, \tag{J.2.1}$$

and that $\boldsymbol{u}_{(1)}$ satisfies the following system

$$\left(\frac{\partial u_{J(1)k}}{\partial X^l}+\frac{\partial u_{J(1)l}}{\partial X^k}\right)+\left(\frac{\partial u_{J(0)k}}{\partial x^l}+\frac{\partial u_{J(0)l}}{\partial x^k}\right)=0_{kl}. \tag{J.2.2}$$

Equation (J.2.2) implies

$$\frac{\partial u_{J(1)\alpha}}{\partial X^\beta}+\frac{\partial u_{J(1)\beta}}{\partial X^\alpha}=0_{\alpha\beta}, \tag{J.2.3}$$

$$\frac{\partial u_{J(1)3}}{\partial X^\alpha}+\frac{\partial u_{J(1)\alpha}}{\partial Z}+\frac{\partial w}{\partial x^\alpha}=0_\alpha, \tag{J.2.4}$$

$$2\frac{\partial u_{J(1)3}}{\partial Z}=0. \tag{J.2.5}$$

Applying a similar argument to that used in §J.1, we see that (J.2.3) & (J.2.5) imply

$$u_{J(1)\alpha}=u_{J(1)\alpha}(t,x,y;Z), \tag{J.2.6}$$

$$u_{J(1)3}=u_{J(1)3}(t,x,y;X,Y), \tag{J.2.7}$$

and (J.2.4) can be re-written as

$$\frac{\partial u_{J(1)3}}{\partial X^\alpha}(t,x,y;X,Y)+\frac{\partial u_{J(1)\alpha}}{\partial Z}(t,x,y;Z)+\frac{\partial w}{\partial x^\alpha}(t,x,y)=0_\alpha. \tag{J.2.8}$$

Repeating the argument used in §J.1, we see that $u_{J(1)3}$ is linear in both X and Y, thus must be independent of both X and Y by periodicity, i.e.

$$u_{J(1)3}=u_{J(1)3}(t,x,y). \tag{J.2.9}$$

(J.2.8) then reduces to

$$\frac{\partial u_{J(1)\alpha}}{\partial Z}(t,x,y;Z)=-\frac{\partial w}{\partial x^\alpha}(t,x,y). \tag{J.2.10}$$

Integrating (J.2.10) with respect to Z give

$$u_{(1)\alpha}(t,x,y;Z)=U^\dagger_\alpha(t,x,y)-\left(Z-Z^\dagger\right)\frac{\partial w}{\partial x^\alpha}(t,x,y), \tag{J.2.11}$$

where $U_\alpha^\dagger(t, x, y)$ is an arbitrary function of (t, x, y) that arises from integration with respect to Z and $Z^\dagger$ is the height of the Neutral Surface, which is defined in §6.2.4.6.

Appendix K

Cell functions for the actuator problem

K.1 Mechanically driven cell functions

K.1.1 Cell functions of the first kind

We define Γ and Γ_J as in §6.2.4. We define the functions $\mathbf{\Psi}^{ab}$ and ψ^{ab} as being solutions to the following PDEs on Γ_J

$$0^j = \frac{\partial}{\partial X^i}\left(c_J^{ijkl}\frac{\partial \Psi_{J,k}^{ab}}{\partial X^l} + e_J^{ijk}\frac{\partial \psi_J^{ab}}{\partial X^k}\right), \tag{K.1.1}$$

$$0 = \frac{\partial}{\partial X^i}\left(S_p e_J^{kli}\frac{\partial \Psi_{J,k}^{ab}}{\partial X^l} - \epsilon_J^{Sik}\frac{\partial \psi_J^{ab}}{\partial X^k}\right), \tag{K.1.2}$$

subject to the following continuity conditions on $\Gamma_J \cap \Gamma_K$

$$\Psi_{J,j}^{ab} = \Psi_{K,j}^{ab}, \tag{K.1.3}$$

$$\psi_J^{ab} = \psi_K^{ab}, \tag{K.1.4}$$

$$n_i\left(c_J^{ijkl}\left(\frac{\partial \Psi_{J,k}^{ab}}{\partial X^l} + \delta_k^a\delta_l^b\right) + e_J^{ijk}\frac{\partial \psi_J^{ab}}{\partial X^k}\right) = n_i\left(c_K^{ijkl}\left(\frac{\partial \Psi_{K,k}^{ab}}{\partial X^l} + \delta_k^a\delta_l^b\right) + e_K^{ijk}\frac{\partial \psi_K^{ab}}{\partial X^k}\right), \tag{K.1.5}$$

$$n_i\left(S_p e_J^{kli}\left(\frac{\partial \Psi_{J,k}^{ab}}{\partial X^l} + \delta_k^a\delta_l^b\right) - \epsilon_J^{Sik}\frac{\partial \psi_J^{ab}}{\partial X^k}\right) = n_i\left(S_p e^{kli}\left(\frac{\partial \Psi_{K,k}^{ab}}{\partial X^l} + \delta_k^a\delta_l^b\right) - \epsilon_K^{Sik}\frac{\partial \psi_K^{ab}}{\partial X^k}\right), \tag{K.1.6}$$

and the following boundary conditions on $\{(X,Y,Z) \in \partial\Gamma : Z \in \{0,1\}\}$

$$\left[c_J^{3jkl}\left(\frac{\partial \Psi_{J,k}^{ab}}{\partial X^l} + \delta_k^a\delta_l^b\right) + e_J^{3jk}\frac{\partial \psi_J^{ab}}{\partial X^k}\right]_{Z=1} = 0^j, \tag{K.1.7}$$

$$\left[c_J^{3jkl}\left(\frac{\partial \Psi_{J,k}^{ab}}{\partial X^l} + \delta_k^a\delta_l^b\right) + e_J^{3jk}\frac{\partial \psi_J^{ab}}{\partial X^k}\right]_{Z=0} = 0, \tag{K.1.8}$$

$$\psi_J^{ab}\Big|_{Z=1} = 0, \tag{K.1.9}$$

$$\psi_J^{ab}\Big|_{Z=0} = 0. \tag{K.1.10}$$

K.1.1.1 Solution to vertical strain functions

We let $a \in \{1,2,3\}$, $b = 3$. If we assume that

$$\frac{\partial \Psi_{J,k}^{a3}}{\partial X^l} + \delta_k^a\delta_l^3 = 0_{kl}, \tag{K.1.11}$$

$$\psi_J^{a3} = 0, \tag{K.1.12}$$

then (K.1.1)-(K.1.2) and (K.1.5)-(K.1.10) are all satisfied. After integrating with respect to Z, (K.1.11)-(K.1.12) yield

$$\Psi_{J,k}^{a3} = -Z\delta_k^a. \tag{K.1.13}$$

Equations (K.1.12)-(K.1.13) satisfy (K.1.1)-(K.1.10). It follows that (K.1.13) is uniquely determined up to an additive constant, while (K.1.12) is uniquely determined.

K.1.2 Cell functions of the second kind

We define the functions $\mathbf{\Phi}^{ab}$ and ϕ^{ab} as being solutions to the following PDEs on Γ_J

$$0^j = \frac{\partial}{\partial X^i}\left(c_J^{ijkl}\left(\frac{\partial \Phi_{J,k}^{ab}}{\partial X^l} - (Z - Z^\dagger)\delta_k^a\delta_l^b\right) + e_J^{ijk}\frac{\partial \phi_J^{ab}}{\partial X^k}\right), \tag{K.1.14}$$

$$0 = \frac{\partial}{\partial X^i}\left(S_p e_J^{kli}\left(\frac{\partial \Phi_{J,k}^{ab}}{\partial X^l} - (Z - Z^\dagger)\delta_k^a\delta_l^b\right) - \epsilon_J^{Sik}\frac{\partial \phi_J^{ab}}{\partial X^k}\right), \tag{K.1.15}$$

subject to the following continuity conditions on $\Gamma_J \cap \Gamma_K$

$$\Phi_{J,j}^{ab} = \Phi_{K,j}^{ab}, \tag{K.1.16}$$

$$\phi_J^{ab} = \phi_K^{ab}, \tag{K.1.17}$$

$$n_i \left(c_J^{ijkl} \left(\frac{\partial \Phi_{J,k}^{ab}}{\partial X^l} - (Z - Z^\dagger)\delta_k^a \delta_l^b \right) + e_J^{ijk} \frac{\partial \phi_J^{ab}}{\partial X^k} \right) = n_i \left(c_K^{ijkl} \left(\frac{\partial \Phi_{K,k}^{ab}}{\partial X^l} - (Z - Z^\dagger)\delta_k^a \delta_l^b \right) + e_K^{ijk} \frac{\partial \phi_K^{ab}}{\partial X^k} \right), \quad \text{(K.1.18)}$$

$$n_i \left(S_p e_J^{kli} \left(\frac{\partial \Phi_{J,k}^{ab}}{\partial X^l} - (Z - Z^\dagger)\delta_k^a \delta_l^b \right) - \epsilon_J^{Sik} \frac{\partial \phi_J^{ab}}{\partial X^k} \right) = n_i \left(S_p e_K^{kli} \left(\frac{\partial \Phi_{K,k}^{ab}}{\partial X^l} - (Z - Z^\dagger)\delta_k^a \delta_l^b \right) - \epsilon_K^{Ski} \frac{\partial \phi_K^{ab}}{\partial X^k} \right), \quad \text{(K.1.19)}$$

and the following boundary conditions on $\{(X, Y, Z) \in \partial\Gamma : Z \in \{0, 1\}\}$

$$\left[c_J^{3jkl} \left(\frac{\partial \Phi_{J,k}^{ab}}{\partial X^l} - (Z - Z^\dagger)\delta_k^a \delta_l^b \right) + e_J^{3jk} \frac{\partial \phi_J^{ab}}{\partial X^k} \right] |_{Z=1} = 0^j, \quad \text{(K.1.20)}$$

$$\left[c_J^{3jkl} \left(\frac{\partial \Phi_{J,k}^{ab}}{\partial X^l} - (Z - Z^\dagger)\delta_k^a \delta_l^b \right) + e_J^{3jk} \frac{\partial \phi_J^{ab}}{\partial X^k} \right] |_{Z=0} = 0^j, \quad \text{(K.1.21)}$$

$$\phi_J^{ab}|_{Z=1} = 0, \quad \text{(K.1.22)}$$

$$\phi_J^{ab}|_{Z=0} = 0. \quad \text{(K.1.23)}$$

K.1.2.1 Solution to vertical strain functions

We let $a \in \{1, 2, 3\}$, $b = 3$. Repeating the argument given in §K.1.1.1, we deduce

$$\Phi_{J,k}^{a3} = \frac{\left(Z - Z^\dagger\right)^2}{2} \delta_k^a, \quad \text{(K.1.24)}$$

$$\phi_J^{a3} = 0. \quad \text{(K.1.25)}$$

It follows that (K.1.24) is uniquely determined up to an additive constant, while (K.1.25) is uniquely determined.

K.2 Cell functions driven by voltage

We define the functions ς and η as being solutions to the following PDEs on Γ_J

$$0^j = \frac{\partial}{\partial X^i} \left(c_J^{ijkl} \frac{\partial \varsigma_{J,k}}{\partial X^l} + e_J^{ijk} \left(\frac{\partial \eta_J}{\partial X^k} + \delta_k^3 \right) \right), \quad \text{(K.2.1)}$$

$$0 = \frac{\partial}{\partial X^i} \left(S_p e_J^{kli} \frac{\partial \varsigma_{J,k}}{\partial X^l} - \epsilon_J^{Sik} \left(\frac{\partial \eta_J}{\partial X^k} + \delta_k^3 \right) \right), \quad \text{(K.2.2)}$$

subject to the following continuity conditions on $\Gamma_J \cap \Gamma_K$

$$\varsigma_{J,j}{=}\varsigma_{K,j}, \tag{K.2.3}$$
$$\eta_J{=}\eta_K, \tag{K.2.4}$$

$$n_i\left(c_J^{ijkl}\frac{\partial\varsigma_{J,k}}{\partial X^l}+e_J^{ijk}\left(\frac{\partial\eta_J}{\partial X^k}+\delta_k^3\right)\right)=n_i\left(c_K^{ijkl}\frac{\partial\varsigma_{K,k}}{\partial X^l}+e_K^{ijk}\left(\frac{\partial\eta_K}{\partial X^k}+\delta_k^3\right)\right), \tag{K.2.5}$$

$$n_i\left(S_p e_J^{kli}\frac{\partial\varsigma_{J,k}}{\partial X^l}-\epsilon_J^{Sik}\left(\frac{\partial\eta_J}{\partial X^k}+\delta_k^3\right)\right)=n_i\left(S_p e_K^{kli}\frac{\partial\varsigma_{K,k}}{\partial X^l}-\epsilon_K^{Sik}\left(\frac{\partial\eta_K}{\partial X^k}+\delta_k^3\right)\right), \tag{K.2.6}$$

and the following boundary conditions on $\{(X,Y,Z)\in\partial\Gamma : Z\in\{0,1\}\}$

$$\left[c_J^{3jkl}\frac{\partial\varsigma_{J,k}}{\partial X^l}+e_J^{3jk}\left(\frac{\partial\eta_J}{\partial X^k}+\delta_k^3\right)\right]_{Z=1}=0^j, \tag{K.2.7}$$
$$\left[c_J^{3jkl}\frac{\partial\varsigma_{J,k}}{\partial X^l}+e_J^{3jk}\left(\frac{\partial\eta_J}{\partial X^k}+\delta_k^3\right)\right]_{Z=0}=0^j, \tag{K.2.8}$$

$$\eta_J|_{Z=1}=0, \tag{K.2.9}$$
$$\eta_J|_{Z=0}=0. \tag{K.2.10}$$

Then η is uniquely determined while $\boldsymbol{\varsigma}$ is uniquely determined up to an additive constant.

Appendix L

Multilayer beam derivations

L.1 Cell functions of the first kind

Equations (6.4.4)-(6.4.11) imply the following relationships, which holds when $Z \in (Z_{n-1}, Z_n)$

$$c^{k3}_{n,3j}\frac{d\Psi^{ab}_{n,k}}{dZ} + c^{ab}_{n,3j} + e^{3}_{n,3j}\frac{d\psi^{ab}_{n}}{dZ} = 0_j, \tag{L.1.1}$$

$$S_p\left(e^{k3}_{n,3}\frac{d\Psi^{ab}_{n,k}}{dZ} + e^{ab}_{n,3}\right) - \epsilon^{S33}_{n}\frac{d\psi^{ab}_{n}}{dZ} = D^{ab}, \tag{L.1.2}$$

where D^{ab} is an unknown constant, and $n \in \{1, 2, \cdots, N\}$, where N is the number of layers. Note that in (L.1.2), repeated indices imply summation, except for the layer index n, for which summation is only taken if its explicitly indicated by a summation sign. This convention will be used for the rest of this appendix chapter. By inspection, we see that $\mathbf{\Psi}^{ab}_{n}$, ψ^{ab}_{n} are all linear terms, which means that their first-order derivatives with respect to Z are all constant. Using (6.4.12)-(6.4.13) and the Fundamental Theorem of Calculus, we deduce

$$\sum_{n=1}^{N} h_n \frac{d\psi^{ab}_{n}}{dZ} = 0. \tag{L.1.3}$$

From (L.1.1)-(L.1.2), we deduce the following relationship, which holds when $Z \in (Z_{n-1}, Z_n)$

$$\frac{d\Psi^{ab}_{n,j}}{dZ} = -\left(\hat{c}^{-1}_{n}\right)^{k}_{j}\left(c^{ab}_{n,3k} + e^{3}_{n,3k}\frac{d\psi^{ab}_{n}}{dZ}\right), \tag{L.1.4}$$

where $\hat{c}_n$ is the matrix defined as

$$(\hat{c}_n)^{k}_{j} = (c_n)^{3k}_{3j}\,. \tag{L.1.5}$$

Substituting (L.1.4) into (L.1.1)-(L.1.2) gives

$$\begin{aligned}
&S_p\left(e^{k3}_{n,3}\frac{d\Psi^{ab}_{n,k}}{dZ}+e^{ab}_{n,3}\right)-\epsilon^{S33}_n\frac{d\psi^{ab}_n}{dZ}\\
=&S_p\left(e^{k3}_{n,3}\left(-\left(\hat{c}^{-1}_n\right)^j_k\left(c^{ab}_{n,3j}+e^3_{n,3j}\frac{d\psi^{ab}_n}{dZ}\right)\right)+e^{ab}_{n,3}\right)-\epsilon^{S33}_n\frac{d\psi^{ab}_n}{dZ}\\
=&S_p\left(-\left(\hat{c}^{-1}_n\right)^j_k c^{ab}_{n,3j}e^{k3}_{n,3}-\left(\hat{c}^{-1}_n\right)^j_k e^3_{n,3j}e^{k3}_{n,3}\frac{d\psi^{ab}_n}{dZ}+e^{ab}_{n,3}\right)-\epsilon^{S33}_n\frac{d\psi^{ab}_n}{dZ}\\
=&S_p\left(e^{ab}_{n,3}-\left(\hat{c}^{-1}_n\right)^j_k c^{ab}_{n,3j}e^{k3}_{n,3}\right)\\
&\qquad-\left(\epsilon^{S33}_n+S_p\left(\hat{c}^{-1}_n\right)^j_k e^3_{n,3j}e^{k3}_{n,3}\right)\frac{d\psi^{ab}_n}{dZ}=D^{ab}. \qquad \text{(L.1.6)}
\end{aligned}$$

For each $n\in\{1,2,\cdots,N\}$, we define the following quantities

$$\mathbb{Q}^{kl}_{n,ij}=c^{kl}_{n,ij}-c^{j'3}_{n,ij}c^{kl}_{n,k'3}\left(\hat{c}^{-1}_n\right)^{k'}_{j'}, \qquad \text{(L.1.7)}$$

$$e^{ab}_{Q,n,3}=e^{ab}_{n,3}-c^{ab}_{n,j3}\left(\hat{c}^{-1}_n\right)^j_k e^{3k}_{n,3}, \qquad \text{(L.1.8)}$$

$$\epsilon^{33}_{Q,n}=\epsilon^{S33}_n+S_p\left(\hat{c}^{-1}_n\right)^j_k e^3_{n,3j}e^{k3}_{n,3}. \qquad \text{(L.1.9)}$$

Substituting (L.1.8)-(L.1.9) and (L.1.3) into (L.1.6) gives

$$S_p e^{ab}_{Q,n,3}-\epsilon^{33}_{Q,n}\frac{d\psi^{ab}_n}{dZ}=D^{ab}. \qquad \text{(L.1.10)}$$

Rearranging (L.1.10) gives

$$\frac{S_p e^{ab}_{Q,n,3}-D^{ab}}{\epsilon^{33}_{Q,n}}=\frac{d\psi^{ab}_n}{dZ}. \qquad \text{(L.1.11)}$$

Using (L.1.3) and (L.1.11), we deduce

$$\begin{aligned}
\sum_{n=1}^N h_n\left(\frac{S_p e^{ab}_{Q,n,3}-D^{ab}}{\epsilon^{33}_{Q,n}}\right)&=S_p\left(\sum_{n=1}^N\frac{h_n e^{ab}_{Q,n,3}}{\epsilon^{33}_{Q,n}}\right)-D^{ab}\left(\sum_{n=1}^N\frac{h_n}{\epsilon^{33}_{Q,n}}\right)\\
&=\sum_{n=1}^N h_n\frac{d\psi^{ab}_n}{dZ}=0. \qquad \text{(L.1.12)}
\end{aligned}$$

Equation (L.1.12) rearranges to

$$D^{ab}=\frac{S_p\left(\sum\limits_{n=1}^N\frac{h_n e^{ab}_{Q,n,3}}{\epsilon^{33}_{Q,n}}\right)}{\left(\sum\limits_{n=1}^N\frac{h_n}{\epsilon^{33}_{Q,n}}\right)}. \qquad \text{(L.1.13)}$$

Using (L.1.13) along with (L.1.11) and (L.1.4), we deduce the following equations, which holds on for $Z \in (Z_{n-1}, Z_n)$

$$\frac{d\psi_n^{ab}}{dZ} = \frac{S_p e_{Q,n,3}^{ab} - D^{ab}}{\epsilon_{Q,n}^{33}} = \frac{S_p e_{Q,n,3}^{ab} - \left(\frac{S_p \left(\sum_{n'=1}^{N} \frac{h_{n'} e_{Q,n',3}^{ab}}{\epsilon_{Q,n'}^{33}} \right)}{\left(\sum_{n'=1}^{N} \frac{h_{n'}}{\epsilon_{Q,n'}^{33}} \right)} \right)}{\epsilon_{Q,n}^{33}}$$
$$= \left(\frac{S_p}{\epsilon_{Q,n}^{33}} \right) \left(e_{Q,n,3}^{ab} - \left(\frac{\left(\sum_{n'=1}^{N} \frac{h_{n'} e_{Q,n',3}^{ab}}{\epsilon_{Q,n'}^{33}} \right)}{\left(\sum_{n'=1}^{N} \frac{h_{n'}}{\epsilon_{Q,n'}^{33}} \right)} \right) \right), \tag{L.1.14}$$

$$\frac{d\Psi_{n,j}^{ab}}{dZ} = -\left(\hat{c}_n^{-1}\right)_j^k c_{n,3k}^{ab} - \left(\hat{c}_n^{-1}\right)_j^k \left(\frac{S_p e_{n,3k}^3}{\epsilon_{Q,n}^{33}} \right) \left(e_{Q,n,3}^{ab} - \left(\frac{\left(\sum_{n'=1}^{N} \frac{h_{n'} e_{Q,n',3}^{ab}}{\epsilon_{Q,n'}^{33}} \right)}{\left(\sum_{n'=1}^{N} \frac{h_{n'}}{\epsilon_{Q,n'}^{33}} \right)} \right) \right). \tag{L.1.15}$$

L.2 Cell functions of the second kind

Equations (6.4.16)-(6.4.25) imply the following relationships (which hold when $Z \in (Z_{n-1}, Z_n)$)

$$c_{n,3j}^{k3} \frac{d\Phi_{n,k}^{ab}}{dZ} - c_{n,3j}^{ab} \left(Z - Z^{\dagger} \right) + e_{n,3j}^3 \frac{d\phi_n^{ab}}{dZ} = 0_j, \tag{L.2.1}$$

$$S_p \left(e_{n,3j}^3 \frac{d\Phi_{n,j}^{ab}}{dZ} - e_{n,3}^{ab} \left(Z - Z^{\dagger} \right) \right) - \epsilon_n^{S33} \frac{d\phi_n^{ab}}{dZ} = \tilde{D}^{ab}, \tag{L.2.2}$$

where $\tilde{D}^{ab}$ is an unknown constant. By inspection, we see that $\mathbf{\Phi}_n^{ab}$, ϕ_n^{ab}, $\mathbf{\Phi}_n^{ab}$, ϕ_n^{ab} are all quadratic terms, which means that their first-order derivatives with respect to Z are all linear. Using (6.4.24)-(6.4.25) and the Fundamental Theorem of Calculus, we deduce

$$\int_0^1 \frac{d\phi^{ab}}{dZ} \mathrm{d}Z = \sum_{n=1}^{N} \int_{Z_{n-1}}^{Z_n} \frac{d\phi_n^{ab}}{dZ} \mathrm{d}Z = 0. \tag{L.2.3}$$

From (L.2.1)-(L.2.2), we deduce the following relationship, which holds when $Z \in (Z_{n-1}, Z_n)$

$$\frac{d\Phi_{n,j}^{ab}}{dZ} = \left(\hat{c}_n^{-1}\right)_j^k \left(c_{n,3k}^{ab} (Z - Z^{\dagger}) - e_{n,3k}^3 \frac{d\phi_n^{ab}}{dZ} \right), \tag{L.2.4}$$

where $\hat{c}_n$ is the matrix defined in (L.1.5). Substituting (L.2.4) into (L.2.2) gives the

following equation, which holds when $Z \in (Z_{n-1}, Z_n)$

$$\begin{aligned} &S_p\left(e^3_{n,3j}\left(\hat{c}^{-1}_n\right)^{jk}\left(c^{ab}_{n,3k}(Z-Z^\dagger)-e^3_{n,3k}\frac{d\phi^{ab}_n}{dZ}\right)-e^{ab}_{n,3}\left(Z-Z^\dagger\right)\right)-\epsilon^{S33}_n\frac{d\phi^{ab}_n}{dZ}\\ =&S_p\left(e^3_{n,3j}\left(\hat{c}^{-1}_n\right)^{kj}c^{ab}_{n,3k}-e^{ab}_{n,3}\right)(Z-Z^\dagger)-\left(\epsilon^{S33}_n+S_pe^3_{n,3j}\left(\hat{c}^{-1}_n\right)^{kj}e^3_{n,3k}\right)\frac{d\phi^{ab}_n}{dZ}=\tilde{D}^{ab}. \end{aligned} \tag{L.2.5}$$

Equation (L.2.5) rearranges to give the following equation

$$\frac{d\phi^{ab}_n}{dZ}=\frac{-S_pe^{ab}_{Q,n,3}(Z-Z^\dagger)-\tilde{D}^{ab}}{\epsilon^{33}_{Q,n}}=-\left(\frac{S_pe^{ab}_{Q,n,3}(Z-Z^\dagger)+\tilde{D}^{ab}}{\epsilon^{33}_{Q,n}}\right). \tag{L.2.6}$$

Applying (L.2.3) to (L.2.6) yields

$$\begin{aligned} &\sum_{n=1}^{N}\int_{Z_{n-1}}^{Z_n}\frac{d\phi^{ab}_n}{dZ}\mathrm{d}Z=-\sum_{n=1}^{N}\int_{Z_{n-1}}^{Z_n}\left(\frac{S_pe^{ab}_{Q,n,3}(Z-Z^\dagger)+\tilde{D}^{ab}}{\epsilon^{33}_{Q,n}}\right)\mathrm{d}Z\\ =&-\sum_{n=1}^{N}\left(\frac{S_pe^{ab}_{Q,n,3}\left(\frac{(Z_n)^2-(Z_{n-1})^2}{2}-Z^\dagger\left(Z_n-Z_{n-1}\right)\right)+\tilde{D}^{ab}\left(Z_n-Z_{n-1}\right)}{\epsilon^{33}_{Q,n}}\right)=0. \end{aligned} \tag{L.2.7}$$

Equations (L.2.7) rearranges to get

$$\begin{aligned} 0=&-\sum_{n=1}^{N}\left(\frac{S_pe^{ab}_{Q,n,3}\left(\frac{(Z_n-Z_{n-1})(Z_n+Z_{n-1})}{2}-Z^\dagger\left(Z_n-Z_{n-1}\right)\right)+\tilde{D}^{ab}\left(Z_n-Z_{n-1}\right)}{\epsilon^{33}_{Q,n}}\right)\\ =&-\sum_{n=1}^{N}\left(\frac{S_pe^{ab}_{Q,n,3}\left(\frac{Z_n+Z_{n-1}}{2}-Z^\dagger\right)+\tilde{D}^{ab}}{\epsilon^{33}_{Q,n}}\right)h_n. \end{aligned} \tag{L.2.8}$$

Using the definition of Z_n, (L.2.8) can be re-written as

$$\tilde{D}^{ab}=-\frac{S_p\left(\sum_{n=1}^{N}\frac{e^{ab}_{Q,n,3}\left(2h_n\left(\sum_{k=1}^{n}h_k\right)-(h_n)^2\right)}{2\epsilon^{33}_{Q,n}}-Z^\dagger\sum_{n=1}^{N}\frac{e^{ab}_{Q,n,3}h_n}{\epsilon^{33}_{Q,n}}\right)}{\sum_{n=1}^{N}\left(\frac{h_n}{\epsilon^{33}_{Q,n}}\right)}. \tag{L.2.9}$$

Applying (L.2.9) along with (L.2.4) and (L.2.6) yields the following equations,

which hold on $Z \in (Z_{n-1}, Z_n)$

$$\frac{d\phi_n^{ab}}{dZ} = -\frac{S_p e_{Q,n,3}^{ab}(Z - Z^\dagger)}{\epsilon_{Q,n}^{33}} - \frac{\tilde{D}^{ab}}{\epsilon_{Q,n}^{33}}$$
$$= -\frac{S_p e_{Q,n,3}^{ab}(Z - Z^\dagger)}{\epsilon_{Q,n}^{33}} + \frac{1}{\epsilon_{Q,n}^{33}} \frac{S_p \left(\sum_{n'=1}^{N} \frac{e_{Q,n',3}^{ab} \left(2h_{n'} \left(\sum_{k=1}^{n'} h_k \right) - (h_{n'})^2 \right)}{2\epsilon_{Q,n'}^{33}} - Z^\dagger \sum_{n'=1}^{N} \frac{e_{Qn',3}^{ab} h_{n'}}{\epsilon_{Q,n'}^{33}} \right)}{\sum_{n'=1}^{N} \left(\frac{h_{n'}}{\epsilon_{Q,n'}^{33}} \right)}, \tag{L.2.10}$$

$$\frac{d\Phi_{n,j}^{ab}}{dZ} = \left(\left(\hat{c}_n^{-1} \right)_j^k c_{n,3k}^{ab} + \left(\hat{c}_n^{-1} \right)_j^k e_{n,3k}^3 \frac{S_p e_{Q,n,3}^{ab}}{\epsilon_{Q,n}^{33}} \right) (Z - Z^\dagger)$$
$$- \frac{\left(\hat{c}_n^{-1} \right)_j^k e_{n,3k}^3}{\epsilon_{Q,n}^{33}} \frac{S_p \left(\sum_{n'=1}^{N} \frac{e_{Q,n',3}^{ab} \left(2h_{n'} \left(\sum_{k=1}^{n'} h_k \right) - (h_{n'})^2 \right)}{2\epsilon_{Q,n'}^{33}} - Z^\dagger \sum_{n'=1}^{N} \frac{e_{Q,n',3}^{ab} h_{n'}}{\epsilon_{Q,n'}^{33}} \right)}{\sum_{n'=1}^{N} \left(\frac{h_{n'}}{\epsilon_{Q,n'}^{33}} \right)}. \tag{L.2.11}$$

L.3 Voltage driven cell functions

Equations (6.4.28)-(6.4.35) imply the following relationships, which hold when $Z \in (Z_{n-1}, Z_n)$

$$c_{n,3j}^{k3} \frac{d\varsigma_{n,k}}{dZ} + e_{n,3j}^3 \left(\frac{d\eta_n}{dZ} + 1 \right) = 0_j, \tag{L.3.1}$$

$$S_p e_{n,3j}^3 \frac{d\varsigma_{n,j}}{dZ} - \epsilon_n^{S33} \left(\frac{d\eta_n}{dZ} + 1 \right) = \hat{D}, \tag{L.3.2}$$

where $\hat{D}$ is an unknown constant. By inspection $\boldsymbol{\varsigma}_n$, η_n, $\boldsymbol{\varsigma}_n$, η_n are all linear terms, which means their first-order derivatives with respect to Z are all constant. Using (6.4.36)-(6.4.37) and the Fundamental Theorem of Calculus, we deduce

$$\int_0^1 \frac{d\eta}{dZ} \mathrm{d}Z = \sum_{n=1}^{N} \int_{Z_{n-1}}^{Z_n} \frac{d\eta_n}{dZ} \mathrm{d}Z = 0. \tag{L.3.3}$$

Using (L.3.1), we get the following equation, which holds when $Z \in (Z_{n-1}, Z_n)$

$$\frac{d\varsigma_{n,j}}{dZ} = -\left(\hat{c}_n^{-1} \right)_j^k e_{n,3k}^3 \frac{d\eta_n}{dZ} \text{ for } Z \in (Z_{n-1}, Z_n). \tag{L.3.4}$$

Substituting (L.3.4) into (L.3.2) gives the following equation, which holds when $Z \in (Z_{n-1}, Z_n)$

$$
\begin{aligned}
&- S_p e^3_{n,3j} \left(\hat{c}_n^{-1}\right)^j_k e^{3k}_{n,3} \left(\frac{d\eta_n}{dZ} + 1\right) - \epsilon_n^{S33} \left(\frac{d\eta_n}{dZ} + 1\right) \\
&\quad = -\left(\epsilon_n^{S33} + S_p e^3_{n,3j} \left(\hat{c}_n^{-1}\right)^j_k e^{3k}_{n,3}\right) \left(\frac{d\eta_n}{dZ} + 1\right) = \hat{D} \text{ for } Z \in (Z_{n-1}, Z_n). \quad \text{(L.3.5)}
\end{aligned}
$$

Equation (L.3.5) simplifies to give

$$
-\epsilon^{33}_{Q,n} \left(\frac{d\eta_n}{dZ} + 1\right) = \hat{D} \iff \frac{d\eta_n}{dZ} = -\frac{\hat{D}}{\epsilon^{33}_{Q,n}} - 1. \quad \text{(L.3.6)}
$$

Using (L.3.3) and (L.3.6), we deduce

$$
0 = \sum_{n=1}^{N} \int_{Z_{n-1}}^{Z_n} \frac{d\eta_n}{dZ} dZ = \sum_{n=1}^{N} \int_{Z_{n-1}}^{Z_n} -\frac{\hat{D}}{\epsilon^{33}_{Q,n}} - 1 \mathrm{d}Z = -\hat{D} \left(\sum_{n=1}^{N} \int_{Z_{n-1}}^{Z_n} \frac{1}{\epsilon^{33}_{Q,n}} \mathrm{d}Z\right) - 1. \quad \text{(L.3.7)}
$$

Equation (L.3.7) rearranges to

$$
\hat{D} = \frac{-1}{\left(\sum\limits_{n=1}^{N} \frac{h_n}{\epsilon^{33}_{Q,n}}\right)}. \quad \text{(L.3.8)}
$$

Using (L.3.8) along with (L.3.4) and (L.3.6) gives the following equations, which hold when $Z \in (Z_{n-1}, Z_n)$

$$
\frac{d\eta_n}{dZ} = \frac{1}{\epsilon^{33}_{Q,n}} \left(\frac{1}{\left(\sum\limits_{n'=1}^{N} \frac{h_{n'}}{\epsilon^{33}_{Q,n'}}\right)}\right) - 1, \quad \text{(L.3.9)}
$$

$$
\frac{d\varsigma_{n,j}}{dZ} = -\frac{\left(\hat{c}_n^{-1}\right)^k_j e^3_{n,3k}}{\epsilon^{33}_{Q,n}} \left(\frac{1}{\left(\sum\limits_{n'=1}^{N} \frac{h_{n'}}{\epsilon^{33}_{Q,n'}}\right)}\right). \quad \text{(L.3.10)}
$$

Appendix M

Eigenvalues and eigenfunctions of the $\frac{d^4}{dx^4}$ operator

M.1 Simply Supported beam

The set $\{\sin(n\pi x), n \in \mathbb{Z}_{\geq 1}\}$ has the following properties

- $$\int_0^1 \sin(n\pi x)\sin(m\pi x)\mathrm{d}x = \frac{\delta_{n,m}}{2} \text{ for all } n, m \in \mathbb{Z}_{\geq 1}, \tag{M.1.1}$$
- $$\frac{d^4}{dx^4}\left(\sin(n\pi x)\right) = (n\pi)^4 \sin(n\pi x) \text{ for all } n \in \mathbb{Z}_{\geq 1}, \tag{M.1.2}$$
- $$\frac{d^2}{dx^2}\left(\sin(n\pi x)\right) = -(n\pi)^2 \sin(n\pi x) \text{ for all } n \in \mathbb{Z}_{\geq 1}, \tag{M.1.3}$$
- $$\text{span}\{\sin(n\pi x) n \in \mathbb{Z}_{\geq 1}\} \text{ is dense in } L^2(0,1). \tag{M.1.4}$$

  For each $n \in \mathbb{Z}_{\geq 1}$, $\sin(n\pi x)$ satisfies the homogeneous version of (6.3.2)-(6.3.3), namely

- $$\sin(n\pi x) = 0 \text{ for } x \in \{0, 1\}, \tag{M.1.5}$$
- $$\frac{d^2}{dx^2}\left(\sin(n\pi x)\right) = 0 \text{ for } x \in \{0, 1\}. \tag{M.1.6}$$

Using (M.1.1) and (6.3.19), we deduce

$$\int_0^1 w(\tau, x)\sin(n\pi x)\mathrm{d}x = \frac{c_n(\tau)}{2} \iff c_n(\tau) = \int_0^1 w(\tau, x)\left(2\sin(n\pi x)\right)\mathrm{d}x. \tag{M.1.7}$$

M.2 Cantilever beam

Let $L = \frac{d^4}{dx^4}$, let $X = \{f \in L^2(0,1;\mathbb{R}) \cup C^\infty(0,1;\mathbb{R}) : f(0) = f'(0) = f''(1) = f'''(1) = 0\}$. If we let $f, g \in X$, then we have

$$\begin{aligned}\int_0^1 (Lf)(x)g(x)\mathrm{d}x &= \int_0^1 f''''(x)g(x)\mathrm{d}x \\ &= \left[f'''(x)g(x)\right]_0^1 - \left[f''(x)g'(x)\right]_0^1 + \left[f'(x)g''(x)\right]_0^1 - \left[f(x)g'''(x)\right]_0^1 \\ &+ \int_0^1 f(x)g''''(x)\mathrm{d}x = \int_0^1 f(x)g''''(x)\mathrm{d}x = \int_0^1 f(x)(Lg)(x)\mathrm{d}x.\end{aligned} \tag{M.2.1}$$

From (M.2.1), we see that L is self-adjoint with respect to $L^2(0,1;\mathbb{R})$. Since X is a compact subset of $L^2(0,1;\mathbb{R})$, it follows from the Spectral Theorem that L is diagonisable with an orthonormal basis in $L^2(0,1;\mathbb{R})$ and all eigenvalues of L are real. If f is a non-trivial eigenfunction of L with eigenvalue $\lambda \in \mathbb{R}$, then we see that

$$\int_0^1 (Lf)(x)f(x)\mathrm{d}x = \lambda \int_0^1 f(x)^2\mathrm{d}x = \int_0^1 \left(f''(x)\right)^2 \mathrm{d}x > 0. \tag{M.2.2}$$

Using (M.2.2), we see that all eigenvalues must be positive.

We let $k > 0$. We seek non-trivial solutions of the equation

$$(Lf)(x) = f''''(x) = k^4 f(x), \tag{M.2.3}$$

subject to the boundary conditions

$$f(0) = 0, \tag{M.2.4}$$
$$f'(0) = 0, \tag{M.2.5}$$
$$f''(1) = 0, \tag{M.2.6}$$
$$f'''(1) = 0. \tag{M.2.7}$$

The general solution to (M.2.3) is given by

$$f(x) = A\cosh(kx) + B\cos(kx) + C\sinh(kx) + D\sin(kx). \tag{M.2.8}$$

Using (M.2.8), (M.2.4)-(M.2.7) gives

$$A + B = 0, \tag{M.2.9}$$
$$Ck + Dk = 0, \tag{M.2.10}$$
$$Ak^2\cosh(k) - Bk^2\cos(k) + Ck^2\sinh(k) - Dk^2\sin(k) = 0, \tag{M.2.11}$$
$$Ak^3\sinh(k) + Bk^3\sin(k) + Ck^3\cosh(k) - Dk^3\cos(k) = 0. \tag{M.2.12}$$

Applying (M.2.9)-(M.2.10), we deduce

$$A = -B, \tag{M.2.13}$$

$$C = -D, \tag{M.2.14}$$

$$A\left(\cosh(k) + \cos(k)\right) + C\left(\sinh(k) + \sin(k)\right) = 0, \tag{M.2.15}$$

$$A\left(\sinh(k) - \sin(k)\right) + C\left(\cosh(k) + \cos(k)\right) = 0. \tag{M.2.16}$$

From (M.2.15)-(M.2.16), we deduce non-trivial solutions exist if and only if

$$\left(\cosh(k) + \cos(k)\right)\left(\cosh(k) + \cos(k)\right) - \left(\sinh(k) + \sin(k)\right)\left(\sinh(k) - \sin(k)\right) = 0. \tag{M.2.17}$$

Equation (M.2.17) expands to give

$$\cosh(k)^2 + 2\cosh(k)\cos(k) + \cos(k)^2 - \sinh(k)^2 + \sin(k)^2 = 0. \tag{M.2.18}$$

Using standard hyperbolic and trigonometric identities, (M.2.18) reduces to give

$$1 + 2\cosh(k)\cos(k) + 1 = 2 + 2\cosh(k)\cos(k) = 0 \iff 1 + \cosh(k)\cos(k) = 0. \tag{M.2.19}$$

We define the set $K = \{k > 0 : 1 + \cosh(k)\cos(k) = 0\}$. We let $\{k_n : n \in \mathbb{Z}_{\geq 1}\}$ be the sequence of roots in K so that k_1 is the smallest and $k_{n+1} > k_n$ for all $n \in \mathbb{Z}_{\geq 1}$. We define the following constants

$$\tilde{A}_n = \sinh(k_n) + \sin(k_n), \tag{M.2.20}$$

$$\tilde{c}_n = -\left(\cosh(k_n) + \cos(k_n)\right), \tag{M.2.21}$$

$$l_n = \sqrt{\int_0^1 \left(\tilde{A}_n\left(\cosh(k_n x) - \cos(k_n x)\right) + \tilde{c}_n\left(\sinh(k_n x) - \sin(k_n x)\right)\right)^2 \mathrm{d}x}, \tag{M.2.22}$$

$$A_n = \frac{\tilde{A}_n}{l_n}, \tag{M.2.23}$$

$$C_n = \frac{\tilde{c}_n}{l_n}, \tag{M.2.24}$$

$$X_n(x) = A_n\left(\cosh(k_n x) - \cos(k_n x)\right) + c_n\left(\sinh(k_n x) - \sin(k_n x)\right). \tag{M.2.25}$$

Note that $\{X_n : n \in \mathbb{Z}_{\geq 1}\}$ is an orthonormal basis, so for all $n, m \in \mathbb{Z}_{\geq 1}$

$$\int_0^1 X_n(x) X_m(x) \mathrm{d}x = \delta_{nm}. \tag{M.2.26}$$

M.2.1 Properties

The set $\{X_n(x) : n \in \mathbb{Z}_{\geq 1}\}$, where X_n are the eigenfunctions found in §M.2 has the following properties

- $$\int_0^1 X_n(x)X_m(x) = \delta_{n,m}, \tag{M.2.27}$$
- $$\frac{d^4X_n}{dx^4} = (k_n)^4 X_n, \tag{M.2.28}$$
- $$\text{span}\{X_n(x) : n \in \mathbb{Z}_{\geq 1}\} \text{ is dense in } L^2(0,1), \tag{M.2.29}$$
- $$X_n(0) = X_n^{'}(0) = 0, \tag{M.2.30}$$
- $$X_n^{''}(1) = X_n^{'''}(1) = 0. \tag{M.2.31}$$

Appendix N

Stability analysis for case where the forcing frequency is double the natural frequency

If we define the matrix

$$A = \frac{e_{\mathrm{p},11}^3}{4}\begin{pmatrix} 0 & (V_{AC} - 2V_{DC}) \\ (V_{AC} + 2V_{DC}) & 0 \end{pmatrix}, \tag{N.0.1}$$

the characteristic equation of (N.0.1) is given by

$$\chi_A(\lambda) = \mathrm{Det}(A - \lambda I) = \lambda^2 - \left(\frac{e_{\mathrm{p},11}^3}{4}\right)^2 (V_{AC} - 2V_{DC})\,(V_{AC} + 2V_{DC}) = 0. \tag{N.0.2}$$